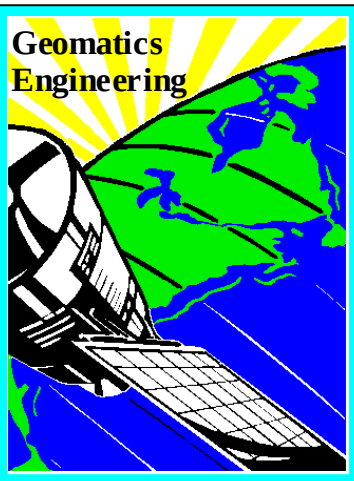

UCGE Reports
Number 20136

Department of Geomatics Engineering

Mitigation of GPS Code and Carrier Phase Multipath Effects Using a Multi-Antenna System

PhD Thesis

By

Jayanta Kumar Ray

March 2000

Calgary, Alberta, Canada

THE UNIVERSITY OF CALGARY

Mitigation of GPS Code and Carrier Phase Multipath Effects Using a Multi-Antenna System

by

Jayanta Kumar Ray

A DISSERTATION

SUBMITTED TO THE FACULTY OF GRADUATE STUDIES

IN PARTIAL FULFILMENT OF THE REQUIREMENTS FOR THE

DEGREE OF DOCTOR OF PHILOSOPHY

DEPARTMENT OF GEOMATICS ENGINEERING

CALGARY, ALBERTA

MARCH, 2000

ABSTRACT

Multipath is a major source of error in GPS code and carrier phase measurements in the differential mode of operation, which can prevent the achievement of the highest levels of accuracy. This is especially prevalent in a static receiver where multipath introduces slow varying errors in the measurements due to satellite dynamics, and which cannot be averaged out. Multipath is spatially correlated within a small area. This relationship can be exploited to mitigate multipath errors. The research aims at reducing the effect of multipath in code and carrier phase measurements in a stationary receiver using a multiple antenna/receiver approach.

A method is developed, which uses five or more antennas, spaced about 5-10 cm apart. The response of the GPS receiver code and carrier discriminator functions in the presence of a multipath signal is analyzed, and multipath errors within a small area are related to the antenna-satellite and antenna-reflector geometry using multipath and geometric parameters, such as, the reflection coefficient, multipath delay, multipath phase, as well as multipath signal azimuth and elevation. A Kalman filter is developed to use multipath-corrupted measurements from multiple closely-spaced antennas to estimate the multipath and geometric parameters, from which the multipath errors in the code and carrier measurements at each antenna can be computed. Field tests in a moderate multipath environment show a reduction in multipath errors up to 73% (average 22%) in the code and up to 52% (average 15%) in the carrier residuals. Improvements are also observed in the position domain, whereby the differential position accuracy is improved by up to 51% (average 21%) and up to 37% (average 24%) for the non-smoothed code and carrier cases respectively. A desirable characteristic of this technique is that it is more effective in a high multipath environment. This technique has potential to be used in real time in reference stations generating corrections for kinematic applications. Furthermore, this technique can be extended to other direct sequence spread spectrum communication systems employing PRN codes for signal spreading.

ACKNOWLEDGEMENTS

It is with a great deal of pleasure that I acknowledge my heartfelt thanks and gratitude to my supervisor, Dr. Elizabeth Cannon for her support, encouragement and guidance throughout my research, who was also the prime reason for me to come to Calgary for higher studies. My sincere thanks to Mr. Patrick Fenton and Mr. Waldemar Kunysz of NovAtel Inc. for the fruitful discussions as well as support, logistics and equipment. I am grateful to Dr. Gerard Lachapelle and Dr. Klaus-Peter Schwarz for valuable discussions and encouragement during the research. Others in my defense committee Dr. M. Okoniewski and Dr. M. S. Braasch are thanked for reading the dissertation and giving valuable suggestions. I also wish to thank my fellow graduate students, faculty and staff members of Geomatics Engineering for providing a pleasurable and conducive environment for studies and research. My research has been supported by funding from a variety of sources: the Nesbitt Burns Graduate Scholarship, the Canadian Natural Resources Graduate Scholarship, the UTI Graduate Fellowship, the Geomatics Canada Scholarship, the Province of Alberta Graduate Fellowship, KIS-94 Graduate Scholarship, ION Student Chapter Award and The University of Calgary.

There have been many, who have made indelible impressions in shaping my life through their love, affection and blessings. Mr. Nirod Chackroborty (my primary school teacher), Mr. Haripada Dutta (my mathematics teacher) and Dr. H. S. Jamadagni (my M.Tech. supervisor) are some of them who have gone extra miles to help me way beyond the scope of the teacher-student relationship. Accord Software and Systems at Bangalore, India, where I broached up my professional career, provided me an opportunity to work in this interesting and wonderful world of GPS. And finally, my parents, sisters, friends and well wishers were an unending source of encouragement, motivation and driving force which has made this possible.

Dedicated to my parents

TABLE OF CONTENTS

LIST OF TABLES

LIST OF FIGURES

NOTATION

LIST OF SYMBOLS

a_{0i}	Distance between A_0 and A_i
A_C	L1 quadrature-phase amplitude
a_k	Differential path delay of the *k*th reflected signal
A_P	L1 in-phase amplitude
B_P	L2 signal amplitude
c	Speed of light
c()	GPS C/A or P code
C_{XY}	Correlation coefficient between X and Y
D	Navigation data bit
D_c	Coherent code discriminator
D_{cm}	Coherent code discriminator in presence of multipath
d_{hw}	Hardware delay
d_{ion}	Ionospheric delay error
d_k	Horizontal distance between the antenna and the *k*th reflector
D_n	Non-coherent code discriminator
D_{nm}	Non-coherent code discriminator in presence of multipath
dρ	Orbital error, nominal and SA
D_r	Carrier phase discriminator
D_{rm}	Carrier phase discriminator in presence of multipath
dt	Satellite clock error, nominal and SA
dT	Receiver clock error
d_{trop}	Troptospheric delay error
$E_\perp$	Perpendicularly polarized electric field
$E_\parallel$	Parallel polarized electric field
$f_{L1,i}$	GPS L1 signal

$f_{L2,i}$	GPS L2 signal
H	Design matrix
IE	In-phase early correlation value
IL	In-phase late correlation value
IP	In-phase prompt correlation value
K	A function of correlation ratio
m_X	Mean of state variable X
m_Y	Mean of state variable Y
N	Integer cycle ambiguity
P	Measured code range/Average carrier power
Q	Proecess noise covariance
QE	Quadrature-phase early correlation value
QL	Quadrature-phase late correlation value
QP	Quadrature-phase prompt correlation value
r	Pseudorange
R	Measurement noise covariance/First Fresnel zone radius
$R_{0,i}$	SNR ratio
$R(\tau)$	Autocorrelation function
$R_{1,2}(\tau)$	Cross-correlation function
s_i	Satellite signal
s_{IE}	In-phase early signal
s_{IL}	In-phase late signal
s_{IP}	In-phase prompt signal
s_{QE}	Quadrature-phase early signal
s_{QL}	Quadrature-phase late signal
s_{QP}	Quadrature-phase prompt signal
T_c	Chip width
t_{oc}	Time to which the clock correction coefficients refer
t_{sv}	GPS time maintained and transmitted by the satellite
x	State vector

XG	C/A code
XP	P code
x_u	User co-ordinates
z	Measurement vector
α_1	Reflection coefficient
α'	Correlation ratio
γ_0	Direct signal phase
$\hat{\gamma}_c$	Receiver estimate of the incoming signal carrier phase
γ_{ij}	Multipath phase
γ_k	*k*th reflected signal phase
Δh	Mean height of irregularities within the First Fresnel ellipse
$\Delta\Psi$	Carrier phase multipath error
ε_1	Permittivity of medium 1
$\varepsilon_{M\varphi}$	Carrier phase multipath error
ε_{Mp}	Code range multipath error
ε_φ	Receiver carrier noise
ε_P	Receiver code noise
θ	Elevation of the direct satellite signal
θ_k	Elevation of the *k*th reflected signal
λ	Carrier wavelength
ν_b	Brewster angle
ν_i	Angle of incidence
ν_r	Angle of reflection
ν_t	Angle of transmission
ρ	Geometric range between the satellite and receiver antennas
φ	Azimuth of the direct satellite signal
Φ	Measured carrier phase
ϕ_{0i}	Azimuth of Antenna *i* with respect to reference antenna

φ_k	Azimuth of the *k*th reflected signal
τ_0	Satellite signal code delay
$\hat{\tau}_c$	Receiver estimate of the incoming signal code delay
τ_e	Multipath error
$\hat{\omega}_0$	Receiver's estimate of the signal carrier frequency
ω_1	L1 centre frequency
ω_2	L2 centre frequency

LIST OF ABBREVIATIONS

ADC	Analog to Digital Converter
AGC	Automatic Gain Control
C/A	Clear/Acquisition or Coarse/Acquisition
CDMA	Code Division Multiple Access
DGPS	Differential Global Positioning System
DLL	Delay Lock Loop
DSP	Digital Signal Processing
EKF	Extended Kalman Filter
FLL	Frequency Lock Loop
GPS	Global Positioning System
IE	In-phase Early
IL	In-phase Late
IP	In-phase Prompt
IF	Intermediate Frequency
LAAS	Local Area Augmentation System
LHCP	Left Hand Circularly Polarized
LNA	Low Noise Amplifier
MCS	Master Control Station
MEDLL	Multipath Estimation Delay Lock Loop
MET	Multipath Elimination Technique
MUSIC	Multiple Signal Classification
NCO	Numerically Controlled Oscillator
NDP	Navigation Data Processing
OCS	Operational Control Segment
PLL	Phase Lock Loop
PPS	Precise Positioning Services
PRN	Pseudo-random Noise
QE	Quadrature-phase Early

QL	Qaudrature-phase Late
QP	Quadrature-phase Prompt
RF	Radio Frequency
RFF	Radio Frequency Front-end
RHCP	Right Hand Circularly Polarized
RMS	Root Mean Square
SA	Selective Availability
SEP	Spherical Error Probability
SMR	Signal to Multipath Ratio
SNR	Signal to Noise Ratio
SPS	Standard Positioning Service
TCXO	Temperature Controlled Crystal Oscillator
TEM	Transverse Electromagnetic
VCXO	Voltage Controlled Crystal Oscillator

CHAPTER 1

INTRODUCTION

1.1 Background

The Global Positioning System (GPS) is revolutionizing navigation as a primary source of information (Cohen and Parkinson, 1991). The fast evolution of various GPS applications has produced a variety of performance requirements for GPS receivers (Weill, 1997). The demand for increasing accuracy has required a deeper understanding of GPS positioning error sources and methods to reduce or eliminate them.

Multipath is a significant source of error, especially for differential positioning in high accuracy applications. Multipath is the phenomenon whereby a signal is reflected or diffracted from various objects in the environment and arrives at the receiver via multiple paths (Braasch and Van Graas, 1991). A GPS receiver can not distinguish between a direct and reflected signal, and as a result, the receiver tracking loops align the locally generated code and carrier to the composite signal instead of the direct signal causing the multipath error. If the reflecting surface is smooth, then the reflected signal is deterministic in nature and is called specular multipath. On the other hand, if the GPS signal incidents on sharp edges or rough surfaces, then the reflected signal is scattered in all directions and is called diffuse multipath. Specular multipath is a more serious problem in static applications whereby the periodicity of range error induced by it can reach values in the order of one hour (Van Nee, 1992). Multipath induced errors are prevalent in both code range and carrier phase measurements in a receiver.

In GPS single point positioning, multipath is not a major problem as selective availability is generally higher (Braasch, 1998). However, in differential positioning most of the

common errors like atmospheric, orbital and satellite clock errors in the range are nearly eliminated, (except for the spatially decorrelated component), and very accurate position and velocity with respect to a reference receiver can be obtained. As a result, multipath remains the most significant error source in the range. It can be as large as several metres with currently available state-of-the-art receiver technologies, and can not be removed through differential positioning due to its highly localized nature (Braasch, 1996a).

In order to achieve position accuracies at the centimetre and metre levels using GPS carrier and code measurements respectively, the data must be used in differential mode (DGPS). However, the presence of multipath has deleterious effects on phase measurements, and limits the performance of high-end GPS receivers used for surveying, and other high precision applications. Multipath also affects the range measurements and limits the achievable performance using DGPS. The range and phase multipath errors can reach as much as 5 cm and 15 m respectively using state-of-the-art receivers. Furthermore, because differential carrier phase ambiguity resolution often uses the pseudorange for initialization, multipath corrupted pseudoranges can increase the time to resolve ambiguities (Braasch, 1996a).

Multipath is particularly a serious problem in short baseline static applications, where the antennas are stationary with respect to the surrounding environment. It has a significant effect in GPS-based networks where the reference stations in the network provide corrections for kinematic applications within the network (Raquet, 1998). Multipath also plays a crucial role in aircraft positioning during taxiing (Braasch and Van Graas, 1991). In spacecraft attitude determination system, measurements are affected by static multipath from the spacecraft body itself. Multipath accounts for 90% of the total error budget in carrier phase measurements in spacecraft attitude determination systems (Cohen and Parkinson, 1991; Lightsey, 1996). In applications such as surveying, where there are a limited number of choices of the antenna siting, static multipath could be a major source of error.

1.2 Relevant Research

Multipath effects on a Pseudo Random Noise (PRN) ranging receiver were studied by Hagerman (Hagerman, 1973) even before GPS was born. His comprehensive investigation of multipath effects on a Delay Lock Loop (DLL) was further extended by Van Nee (1992) and Braasch (1996a). Multipath was experienced by several researchers including Falkenberg et al. (1988) and Lachapelle et al. (1989) in marine DGPS experiments, and Cannon and Lachapelle (1992) in static and dynamic land experiments. Tranquilla and Carr (1991) observed multipath occuring at various locations, such as rock embankments, high-tension overhead wires, highway overhead wires, saltwater/freshwater horizon etc. Notably, Georgiadou and Kleusberg (1988) detected carrier phase multipath using dual frequency receivers. Similarly, there have been numerous publications (Braasch and Van Graas 1991; Breeuwer et al., 1992; Kee and Parkinson, 1994; Lachapelle et al., 1996; Itani et al., 1996; Mora-Castro et al., 1998) on multipath experiences in various situations.

Significant work has been done to reduce the multipath effects using various methods, which can be broadly classified as

- Antenna-based mitigation
- Improved receiver technology
- Signal and data processing

Antenna-based mitigation involves improving the antenna gain pattern to counter the effects of multipath. This method includes the use of special antennas, spatial processing with multi-antenna arrays, antenna location strategies and long-term signal observation to infer multipath parameters, facilitated by the changing reflection geometry. A choke ring with a RF absorbing ground plane has been found to be quite effective in this regard (Falkenberg et al., 1988; Lachapelle et al., 1989; Tranquilla and Karr, 1991). By designing an antenna with very low gain for left hand circularly polarized (LHCP)

signals, and using an antenna array to have a sharp cutoff below a certain elevation angle, significant improvements can be achieved (Counselman, 1998; Bartone and Van Graas, 1998). However, most of these methods are costly, and have the disadvantage of large size and weight. Most importantly, they can not effectively mitigate multipath signals arriving from above the horizontal (Weill, 1997).

A comprehensive overview of receiver technologies to mitigate multipath appears in the research of Van Dierendonck and Braasch (1997). Narrow Correlator™ (Fenton et al., 1991; Van Dierendonck et al., 1992) has a 0.1 chip spacing and a larger bandwidth at the IF and provides good long delay multipath mitigation. The Multipath Elimination Technique (MET™), is an improvement of Narrow Correlator™ with respect to multipath mitigation (Townsend and Fenton, 1994). It estimates the slope of the two sides of the autocorrelation peak as well as the amplitude, thus estimating for two lines that intersects at the peak, irrespective of the slope. Multipath Estimation Delay Lock Loop (MEDLL™), utilizes multiple narrow-spaced correlators to estimate multipath and remove it from the correlation function to provide a more pure signal correlation function (Van Nee, 1995). MEDLL™ was further extended by Townsend et al. (1995) for carrier phase multipath mitigation. Moelker (1997) described various methods to mitigate multipath effects by using the Multiple Signal Classification (MUSIC) technique with multiple antennas and an extended MEDLL™. The Edge Correlator™ technique (Garin et al., 1996) shows slightly better performance than the narrow correlator for long delay multipath. The Strobe Correlator™ and Enhanced Strobe Correlator™ (Garin and Rousseau, 1997) use the slope of multiple narrow correlators and show very good long delay multipath mitigation performance. However, in a strong and fast-changing multipath environment, they do not completely eliminate the effects. Stansell and Maenpa (1999) describe a multipath mitigation correlator-based technique called ClearTrack™, which has a maximum code multipath error equal to one quarter of the maximum error in Narrow Correlator™. These techniques, however, are not very effective for slow multipath, due to close-by reflectors. Also, one of the major problems with using receiver related techniques to mitigate multipath, is that many of the users do

not have access to the receiver hardware, and none of these techniques can be directly used with all kinds of existing receivers.

Several researchers have devised methods to counter multipath effects using measurement data and other information generated by the receiver. Code multipath can be reduced to a great extent by smoothing the pseudorange with the carrier phase (Hatch, 1982; Cannon and Lachapelle, 1992; Lachapelle et al., 1996). Another method developed by Georgiadou and Kleusberg (1988), uses L1-L2 measurements to estimate the carrier phase multipath error using the relationship between the frequency of the carrier phase multipath error and the carrier wavelength. Sennott and Pietraszewski (1987) used state variable models for the estimation of multipath in differential GPS ground stations. Axelrad et al. (1996) and Comp and Axelrad (1998) have used a Signal-to-Noise-Ratio (SNR) based technique to correct the multipath error in differential phase measurements. This technique is effective mainly when dealing with short delay or slow multipath. High frequency multipath is still a problem with this technique. Moreover, this technique requires the knowledge of the antenna gain pattern. SNR measurements are further utilized by Reichert and Axelrad (1999) to identify an effective reflector, and to generate carrier phase multipath correction profiles. The day-to-day repeatability of multipath along with SNR measurements are used by Sleewaegen (1997). The geometrical aspects of reflection in combination with a special arrangement of GPS antennas are exploited (Becker et al., 1994) to detect and track multipath in a simulated multipath environment. Raquet and Lachapelle (1996) investigated the use of multiple reference stations in order to estimate both code and carrier multipath. Bruton (1997) used adaptive filters and multiple DGPS receivers to remove multipath and other errors in kinematic positioning. Code multipath is calibrated and estimated using spherical harmonics in static applications by Kee and Parkinson (1994). Dai et al. (1997) proposes spectral decomposition based multipath mitigation technique, which combines carrier smoothing, carrier SNR and repeatability.

In general, there are more code multipath mitigation techniques compared to methods of dealing with carrier multipath. Therefore, carrier phase multipath still remains a big challenge, which is only partially addressed by some researchers. Furthermore, there is no unified technique to date, that addresses both code and carrier multipath mitigation and has potential for real time applications.

1.3 Research Objective

The primary objective of this research is to develop a technique to effectively mitigate GPS code and carrier phase multipath, which also has the potential to be used in real time applications.

Given the primary objective, there are several areas and issues that need to be addressed in the course of this research. They are:

- Analyze GPS code and carrier tracking loops and discriminator functions to characterize the responses of the loops in the presence of multipath signals and characterize the resultant code and carrier multipath errors.

- Characterize multipath errors from a geometrical perspective and analyze their behaviour in closely-spaced antennas. Identify effects of antenna-satellite and antenna-reflector geometry on multipath errors.

- Derive a multipath mitigation algorithm, which uses measurements from multiple closely-spaced antennas that can be used in real time applications. Validate the algorithm using simulations.

- Develop a multi-antenna system consisting of several closely-spaced antennas and evaluate the effectiveness of the multipath estimation algorithm for code and carrier phase multipath mitigation using real data.

1.4 Dissertation Outline

This dissertation consists of eight chapters and eight appendices.

Chapter 1 states the problem to be investigated and researched during the course of this dissertation. It describes the relevant background of the research to bring the current research topic into the right perspective, and briefly discusses some of the important relevant literature. It then describes the objective of this dissertation.

Chapter 2 briefly describes the Global Positioning System and explains its different components. It then reviews the GPS signal structure. It also discusses various error sources in GPS code and carrier measurements, and explains how these errors can be reduced by single and double differenced measurement techniques. It then identifies situations where the multipath error is a major concern.

Chapter 3 gives a brief description of electromagnetic properties of the GPS signal and how they affect the reflection of the signal from a reflector. It also describes various types of reflection and gives an account of the changes in amplitude and polarization for different components of the signal upon reflection.

Chapter 4 forms the foundation for the multipath characterization. It describes a generic GPS receiver architecture and some of its important components - in particular the code and carrier tracking loops. The correlation properties of the GPS C/A and P codes with finite bandwidth are also briefly described.

Chapter 5 describes the GPS code and carrier tracking loops in the presence of multipath signals for different types of discriminators. It characterizes multipath error in terms of its pattern, mean, standard deviation, error envelope, etc. The synergistic relationship among code, carrier and SNR is drawn. The second part of the chapter analyses multipath errors from a geometrical perspective and relates the error with antenna-satellite and antenna-

reflector geometry. Multipath frequency and spatial correlation within a small area are analyzed and shown with simulations.

Chapter 6 describes the core algorithm leading to multipath mitigation for code and carrier using multiple closely-spaced antennas. It derives the formulation of mitigation algorithm, exploiting the correlated nature of multipath within a small area using an Extended Kalman Filter. Numerous simulations are carried out and described to validate the algorithms, wherein simulated multipath errors are mitigated by using code, carrier, SNR measurements or their combinations.

Chapter 7 describes a multi-antenna system that was developed to verify the proposed code and carrier phase multipath mitigation techniques using actual data. It first describes various test strategies and data collection schemes. Some of the techniques used to identify and isolate the code and carrier multipath errors are also given. The multipath mitigation test procedures using real data are explained with flowcharts. The results of the experiments are analyzed and explained in detail; residual measurement and position domains for both code and carrier phase multipath errors are discussed.

Chapter 8 summarizes the research described in the earlier chapters of this dissertation. It makes specific conclusions from the results of the findings during the course of the work. It then identifies the drawbacks of the developed technique and presents recommendations for further research.

CHAPTER 2

GLOBAL POSITIONING SYSTEM OVERVIEW AND MEASUREMENTS

2.1 Introduction

The Global Positioning System (GPS) is a space based radio navigation system, which was originally developed as a military force enhancement system in 1973 (GPS Navstar, 1995). Though humans have long been developing ingenious methods of navigation, with the development of radios another class of navigation aids was born (Parkinson et al., 1995). Initially ground based transmitters were used for long range radio navigation which led to the development of Loran and Omega. The Transit system developed by John Hopkins Applied Physics Laboratory was the first operational navigation satellite system using artificial satellites in the 1960s (Parkinson et al., 1995). Two other major development programs appeared in the mid sixties: Timation by the Naval Research Laboratory and Program 621B by the Airforce Space and Missile Organization formally merged in 1973 to give birth of Navstar Global Positioning System (Easton, 1980). Each of these navigational techniques has expanded the horizon of its spectrum of applications and usability. Though it has taken 20 years to establish this latest system, "With the quiet revolution of NAVSTAR, it can be seen that these potential uses are only limited by our imagination" (Parkinson, 1980).

The GPS provides accurate three-dimensional position, velocity and time information to a user anywhere in the world at any time. Position determinations are based on measurements of transit time of radio signals from at least four satellites (Milliken and Zoller, 1980). The GPS system consists of three segments: space, control and user segments (Spilker and Parkinson, 1996).

2.2 Space Segment

This segment consists of 24 operational GPS satellites deployed in six planes with an inclination of 55°, with four satellites per plane, as shown in Figure 2.1. The satellites travel in nearly circular orbits with an altitude of about 20 200 km above the earth and a period of approximately 12 sidereal hours (Hofmann-Wellenhof et al., 1994).

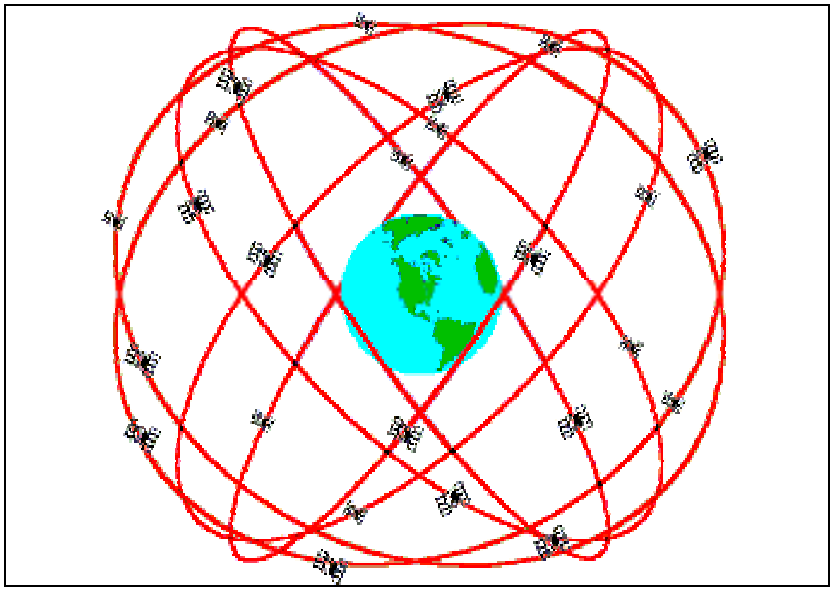

Figure 2.1: GPS satellite constellation

There are five classes of GPS satellites: Block I, II, IIA, IIR and IIF. Block I satellites were the earliest GPS satellites, which did not have intentional errors induced in the later versions and have 63° inclination as opposed to 55°, which is the inclination of the later versions. Block II satellites allow a gradual degradation of service for a period of 14 days in the event of the control segment failure. Block IIA satellites added an autonomous momentum management capability that allows them to function for a period of 180 days without ground contact. Block IIR satellites use satellite crosslinks for inter-satellite communication, which enables autonav capabilities allowing graceful degradation (16 m SEP) of navigation accuracy up to 180 days without ground contact (Aparicio et al., 1996). Block IIF satellites have yet to be launched and are expected to have a host of

other advanced functions such as new civil frequencies (Armor, 1999). Currently, there are 28 operational satellites of which 8 are Block II, 18 are Block IIA and 2 are Block IIR satellites (CANSPACE, 2000). All Block I satellites are decommissioned.

Each GPS satellite broadcasts two modulated signal carriers at L band. They are L1 = 1.57542 GHz and L2 = 1.22760 GHz (Navstar GPS, 1995). The signals carry navigation data bits, which contain information about the satellite position in terms of Keplerian orbital parameters and the satellite time correction with respect to GPS time. The time in the on-board satellite is maintained by atomic clocks, which were initially yielding a daily uncertainty of a few parts in 10^{13} (Bartholomew, 1980). Such a high frequency clock is used to control the centre radio frequency to generate GPS signals, which are transmitted to the user using a helical array antenna of optimum gain patterns.

2.3 Control Segment

This segment maintains the satellite in its orbit through commanded maneuvers, and generates satellite clock and orbit corrections. It uploads the corrections to the satellite such that they can be broadcast to the users through the navigation data (Spilker and Parkinson, 1996). The Operational Control Segment (OCS) consists of five monitor stations, four ground antenna upload stations (all monitor stations except Hawaii) and one Master Control Station (MCS) as shown in Figure 2.2.

Monitor stations continuously track the entire GPS constellation and collect navigation data from all satellites round the clock. This navigation data is used by the OCS for analyzing satellite condition and for generating high integrity navigation data set for each satellite. The generated navigation data for each satellite is uploaded using an S band telemetry channel in the upload stations. The MCS is responsible for all the OCS functions, such as navigation information processing, satellite data upload, vehicle command control and overall system management (Francisco, 1996).

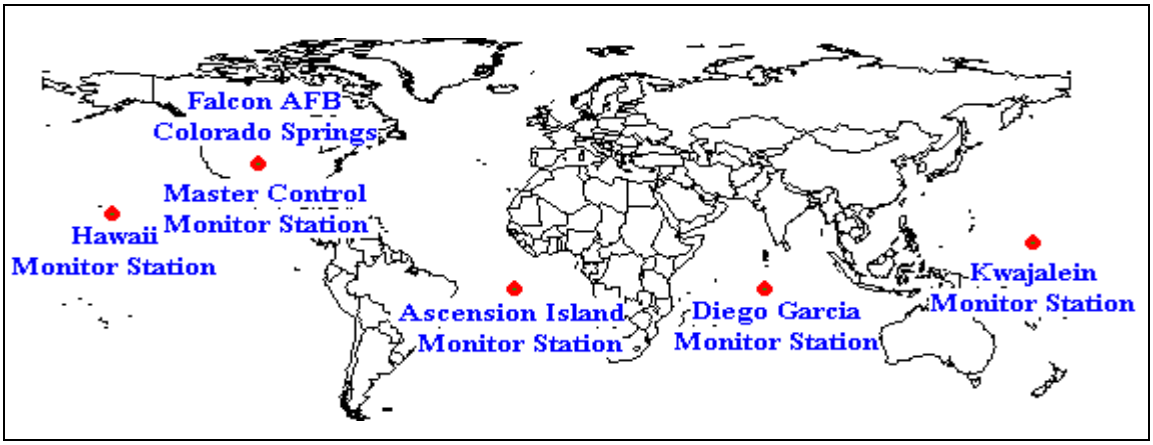

Figure 2.2: GPS control segment - master control station and monitor stations

2.4 User Segment

The GPS user segment consists of GPS receivers, which use satellite signals to determine their position, velocity and time with accuracies specified by various GPS services. A GPS receiver measures the apparent transit time of the satellite signal from the satellite to the user. This is called the pseudorange; it consists of the propagation delay and receiver clock bias. By using at least four such measurements and knowing the satellite position from the computed ephemeris data, the problem is reduced to determining four unknown parameters (receiver's three co-ordinates and clock bias) from known measurements (i.e. pseudoranges) which are related by the following non-linear equation:

$$r_i = \sqrt{(x_i - x_u)^2 + (y_i - y_u)^2 + (z_i - z_u)^2} + cT \qquad (2.1)$$

where,

i	is the satellite index
r	is the pseudorange (m)
x_i, y_i, z_i	are the co-ordinates of *i*th satellite (m, m, m)
x_u,y_u,z_u	are the co-ordinates of the user (m, m, m)
c	is the speed of light (m/s), and
T	is the clock bias (s).

By linearizing equation 2.1 with respect to some initial values and using least square or a Kalman filter algorithm, the user position and clock bias can be determined. Often, measurements are available from more than four satellites. In this case, the solution becomes over-determined and the redundant measurements improve the solution accuracy and integrity. The velocity and clock drift of the user receiver can be computed from range rate measurements using similar sets of simultaneous equations.

The user segment can be broadly classified as civilian users and military users. The civilian users are entitled to Standard Positioning Service (SPS), whereby they use a less precise ranging code compared to the military receivers. This means civilian users are susceptible to intentional accuracy degradation. The SPS positioning and timing predictable accuracy standards are (Navstar GPS, 1995):

Table 2.1: Standard Positioning Service accuracies

Item	Accuracy	Probability (%)
Horizontal position	≤ 100 m	95
Vertical position	≤ 156 m	95
Time	≤ 340 ns	95
Horizontal position	≤ 300 m	99.99
Vertical position	≤ 500 m	99.99

However, using differential code and carrier positioning techniques whereby simultaneous measurements of at least two points are made, relative position accuracies of better than a meter and a centimetre respectively are achievable.

The military users avail Precise Positioning Service (PPS), whereby they use a more precise ranging code compared to the civilian receivers. This ranging code is used for

highly accurate military positioning, velocity and timing information even without the differential technique.

Although the primary purpose of GPS was military applications, it is already being used by a significant number of people in the civilian community. Even within civilian applications, GPS receivers are used in a wide spectrum of applications, such as aircraft navigation, land mobile navigation, marine vessel navigation, spacecraft orbit determination, precise time transfer, surveying and ionospheric measurements.

2.5 GPS Satellite Signal Structure

The choice of GPS frequencies is a trade-off among ease of bandwidth allocation, smaller ionospheric delay errors, lesser space loss and availability of bandwidth for global transmission (Spilker, 1996).

The L1 in-phase component is modulated by a P (precise) code and data bits, whereas quadrature-phase component is modulated by a C/A (coarse/acquisition) code and data bits. P and C/A codes are +/-1 ranging signals having chipping rates of 10.23 MHz and 1.023 MHz respectively, whereas navigation data bits are +/-1 and have a frequency of 50 Hz. Therefore, L1 satellite signal is then expressed as (Spilker, 1996):

$$f_{L1,i}(t) = A_P XP_i(t) D_i(i) \cos(\omega_1 t + \varphi) + A_C XG_i(t) D_i(t) \sin(\omega_1 t + \gamma_1) \qquad (2.2)$$

where,

i	is the satellite index
A_P, A_C	are the in-phase and quadrature signal amplitudes respectively (volt, volt)
XP, XG	are the P and C/A code respectively
D	is the navigation data bit
ω_1	is the L1 centre frequency (rad/s), and
γ_1	is the small phase noise and oscillator drift component (rad).

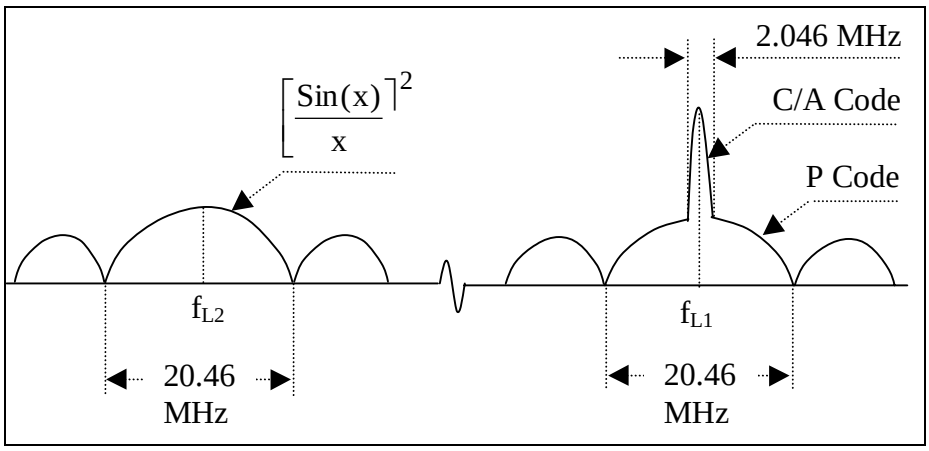

Figure 2.3: GPS signal power spectral density (Spilker, 1996)

The L2 signal is biphase modulated by either a P or a C/A code as selected by the ground command and the same data bits as in L1. Therefore the L2 satellite signal is

$$f_{L2,i}(t) = B_P XP_i(t)D_i(i)\cos(\omega_2 t + \gamma_2) \qquad (2.3)$$

where

B_P is the L2 signal amplitude (volt)

ω_2 is the L2 centre frequency (rad/s), and

γ_2 is the phase noise (rad).

The P code is replaced by the Y code when anti-spoofing (AS) is activated. Details of P, Y, C/A code and other signal characteristics are described in ICD-GPS-200 (1991) and Spilker (1996).

As the GPS signal carrier is modulated by a PRN sequence, it spreads the signal within a wide band suitable for spread spectrum communication. Spread spectrum communication of this type allows code division multiple access (CDMA), whereby each satellite transmits at the same frequency band, and simplifies the receiver front-end design

considerably. At the receiver, a replica of the PRN sequence is generated and correlated with the incoming signals from all satellites to isolate and identify each satellite signal separately for generating range and range rate measurements. Additionally, spread spectrum allows higher resistance to jamming and very good security, two characteristics which are especially important for military and critical civilian applications.

2.6 GPS Observables and Error Sources

Most high performance receivers generate range and phase measurements. The range measurement from a receiver is referred to as the pseudorange, as it denotes the receiver antenna to satellite antenna distance plus the clock bias. The range measurement from a receiver also contains various other small error components and is given by (Wells et al., 1987; Leick, 1995)

$$P = \rho + d\rho + c(dt - dT) + d_{ion} + d_{trop} + d_{hw} + \varepsilon_p + \varepsilon_{Mp} \tag{2.4}$$

where

- P is the measured code range (m)
- ρ is the geometric range between the satellite and receiver antennas (m)
- $d\rho$ is the orbital error, nominal and SA (m)
- c is the velocity of light (m/s)
- dt is the satellite clock error with respect to GPS time, nominal and SA (s)
- dT is the receiver clock error with respect to GPS time (s)
- d_{ion} is the ionospheric delay error (m)
- d_{trop} is the troptospheric delay error (m)
- d_{hw} is the hardware delay in the satellite and in the receiver (m)
- ε_{Mp} is the code range multipath error (m), and
- ε_P is the receiver code noise (m).

Similar to the code measurement, the carrier phase measurement from a receiver contains many error components and is given by (Wells et al., 1987; Leick, 1995)

$$\Phi = \rho + d\rho + c(dt - dT) + \lambda N - d_{ion} + d_{trop} + d_{hw} + \varepsilon_{\varphi} + \varepsilon_{M\varphi} \quad (2.5)$$

where

- Φ is the measured carrier phase (m)
- λ is the carrier wavelength (m)
- N is the integer cycle ambiguity (cycles)
- $\varepsilon_{M\varphi}$ is the carrier phase multipath error (m), and
- ε_{φ} is the receiver carrier noise (m).

Comparing Equations 2.4 and 2.5, it can be seen that the code range and carrier phase measurements differ in the following ways:

a) Phase measurement contains one additional term corresponding to the integer cycle ambiguity
b) The ionospheric delay error has an opposite sign in the two expressions
c) The code multipath error in Equation 2.4 is replaced by carrier multipath error in Equation 2.5
d) The code noise in Equation 2.4 is replaced by carrier noise in Equation 2.5

The nominal values of various errors in Equations 2.4 and 2.5 are given in Table 2.2 (Lachapelle, 1997).

2.6.1 Orbital Error

Orbital error occurs due to the fact that the broadcast ephemeris does not accurately represent the correct position of the satellite. The radial component of the error directly affects the range accuracy. Precise ephemeris can be used in post-mission applications, and is expected to have an accuracy of around a few decimetres (Zumberge and Bertiger, 1996). The effect of orbital error in differential mode depends upon the distance between

the two antennas (i.e. the baseline length) and is about 1 ppm for each 20 m of satellite position error (Lachapelle, 1997).

Table 2.2: GPS error sources for SPS receivers (Lachapelle, 1997)

Error source	Nominal Values (m)	Remarks
Orbit	5-10	Error in broadcast ephemeris due to residual errors in curve fitting
Clock	10	Due to satellite clock drift
SA	5-80	δ and ε components (see Section 2.6.3)
Ionosphere	2-50	Depends upon satellite elevation angle and solar activity
Troposphere	2-30	Depends upon the water vapour content in the lower part of atmosphere
Code multipath	0.2-3	Maximum 150 m using one chip correlator spacing and 15 m using 0.1 chip correlator spacing
Code noise	0.1-3	For C/A code. Depends upon receiver technology and dynamic stress
Carrier multipath	0.001-0.03	Maximum 4.75 cm for L1 carrier and 6.11 cm for L2 carrier
Carrier noise	0.0002-0.002	For L1 carrier. Depends upon receiver technology and dynamic stress

2.6.2 Clock Error

The satellite clock error is the difference between the true GPS time and the time maintained by a satellite. Though the satellite contains highly stable atomic clocks, they drift with time. This drift is closely monitored by the monitor stations. The master control

station estimates the drift and transmits clock correction parameters to the satellite for rebroadcast in the navigation message, which is used to correct the time and measurements in a receiver in the following way (Van Dierendonck et al., 1980):

$$t = t_{sv} - dt \quad (2.6a)$$

$$dt = a_0+a_1(t-t_{oc})+a_2(t-t_{oc})^2 \quad (2.6b)$$

where

t	is the true GPS time (s)
t_{sv}	is the GPS time maintained and transmitted by the satellite (s)
dt	is the satellite clock error (s)
a_0, a_1, a_2	are the satellite broadcast clock correction coefficients (s, s^{-1}, s^{-2}) respectively, and
t_{oc}	is the time to which the coefficients refer (s).

The residual clock error after the clock correction by the broadcast parameters was found to be around 11 ns (Zumberge and Bertiger, 1996) without selective availability (SA).

2.6.3 Selective Availability

SA is the intentional degradation of the GPS signal with the objective to deny full position and velocity accuracy to unauthorized users (Van Graas and Braasch, 1996). The position and time accuracy with SA turned on is given in Table 2.1. If SA is turned off, the horizontal, vertical and time accuracies are 20 m, 30 m and 40 ns respectively, 95% of the time.

The denial of full accuracy can be accomplished by i) introducing error into the satellite broadcast orbit (known as ε-process), and ii) dithering satellite clock frequency (known as δ-process). In case of the former, the calculated satellite position accuracy is degraded, resulting in a slowly varying bias-like range and user position errors. In the latter case however, the satellite clock frequency is dithered with a period of the order of several minutes, resulting in fairly fast varying errors in the pseudorange and phase measurements.

Differential position accuracy depends upon the acceleration of SA, processing time and the data link latency.

2.6.4 Ionospheric Delay Error

The ionospheric delay is the error in range and range rate due to the propagation of the GPS signal through the ionospheric medium, located 50-1000 km above the earth's surface. The lower 100 km of the ionosphere has negligible effect on the GPS signal. It is the upper part of ionosphere that has the highest variability causing potential problems to the GPS receiving systems (Klobuchar, 1996). The major effects of the ionosphere on GPS are i) group delay or pseudorange error, ii) phase advance or carrier phase error, iii) Doppler shift, iv) Faraday rotation of linearly polarized signal, v) refraction of the radio wave, vi) distortion of the pulse waveform, vii) signal amplitude fading or scintillation, and viii) signal phase scintillations (Klobuchar, 1996). The magnitude of ionospheric error is a function of the sunspot number, time of day, receiver location and satellite elevation angle.

The ionosphere is a dispersive medium, which enables dual frequency (L1-L2) receivers to take advantage of it and estimate the first order ionospheric delay error directly. However, slow varying multipath errors corrupt the L1 and L2 measurements and are hindrances to accurate estimation of ionospheric errors. The ionospheric range delay error at L1 is (Klobuchar, 1996):

$$d_{ion} = \frac{f_2^2}{f_1^2 - f_2^2}(P_1 - P_2) \tag{2.7}$$

where

f_1, f_2 are the GPS L1, L2 frequencies (Hz), and

P_1, P_2 are the GPS range measurements at L1 and L2 frequencies.

For single frequency users, the ionospheric delay error can be partially corrected, (up to 50% on an average), by utilizing the satellite broadcast ionospheric delay coefficients in the half-cosine ionospheric delay model (Klobuchar, 1987).

2.6.5 Tropospheric Delay Error

The troposphere affects the GPS L-band signal in terms of signal attenuation, scintillation and delay. The delay error is caused by wet (up to about 11 km) and dry (up to about 40 km) components of the atmosphere, and is a function of the satellite elevation and atomospheric conditions, such as temperature, pressure and relative humidity.

The dry component of the tropospheric error constitutes around 80% of the total error, and can be modelled within 2-5%. The wet component of the error is due to water vapour in the atmosphere and is more difficult to model. There are several models that estimate the tropospheric error. Saastamoinen (1972) proposed a constant lapse rate model for troposphere that estimates delay as a function of elevation. Hopfield (1963) developed separate zenith models for the dry and wet components of the troposphere. That is further extended by Black and Eisner (1984) to include elevation angle mapping function.

2.6.6 Multipath Error

Multipath effects are due to the reflection and diffraction of satellite signals off nearby objects, such as buildings or vents. They introduce significant errors in code and carrier measurements. Multipath effects are described in detail in Chapters 3, 4 and 5.

2.6.7 Receiver Noise

The receiver noise in the code measurement is due to high frequency thermal noise jitter and the effect of dynamic stress on the code tracking loop (Leva et al., 1996). Other sources of receiver error include hardware and software resolution and oscillator stability. The C/A code receiver noise is generally one order of magnitude higher compared to that

of P(Y) code, because the chip width of C/A code is ten times that of P(Y) code. It is in the order of a few decimetres in most modern receivers.

The receiver noise in the phase measurement is mainly due to thermal noise, dynamic stress and the oscillator phase noise. When a Frequency Lock Loop (FLL) is used for carrier tracking instead of a Phase Lock Loop (PLL), the phase noise is an order of magnitude higher. The Signal to Noise Ratio (SNR) of the carrier directly affects the phase measurement accuracy. The phase noise is in the order of a few millimetres in most modern receivers.

2.7 Differenced Observables and Residual Errors

Many of the errors in the observation Equations 2.4 and 2.5 are spatially correlated between receivers tracking a satellite simultaneously. This is because those errors are satellite dependent, or caused by atmospheric propagation and therefore common for two receivers on earth separated by a short distance (called the baseline). Often the degree of correlation between errors at two receivers is a function of the baseline length.

The errors that are correlated in measurements from two receivers simultaneously tracking a satellite, can be reduced by taking the single difference of the range and phase observation equations for a single satellite and two receivers and is given by (Wells et al, 1987)

$$\Delta P = \Delta\rho + \Delta d\rho + c\Delta dT + \Delta d_{ion} + \Delta d_{trop} + \Delta d_{hw} + \Delta\varepsilon_{p} + \Delta\varepsilon_{Mp} \quad (2.8)$$

$$\Delta\Phi = \Delta\rho + \Delta d\rho + c\Delta dT + \lambda\Delta N - \Delta d_{ion} + \Delta d_{trop} + \Delta d_{hw} + \Delta\varepsilon_{\Phi} + \Delta\varepsilon_{M\Phi} \quad (2.9)$$

where Δ represents a *between-receiver single difference*.

In Equations 2.8 and 2.9, the satellite clock error term has disappeared, as it is the same for the two receivers at a particular time epoch. Other errors have now become the difference of errors in the two receivers. As a result, a high degree of correlation of errors

in the two receivers results in cancellation of the error in the differenced equation. For a short baseline, the orbital error, ionospheric delay error and the tropospheric delay error are highly correlated, such that the residual error can be assumed to be very small. The receiver clock bias, integer ambiguity, multipath and receiver noise, however, do not cancel. The hardware delay error, which is completely receiver dependent, is likely to be cancelled if both the receivers are of the same type, and from the same manufacturer. Under these circumstances, multipath error is perhaps the most dominant source of error in the single differenced measurements. For a long baseline, however, the residual orbital, ionospheric, and tropospheric errors become significant compared to multipath errors.

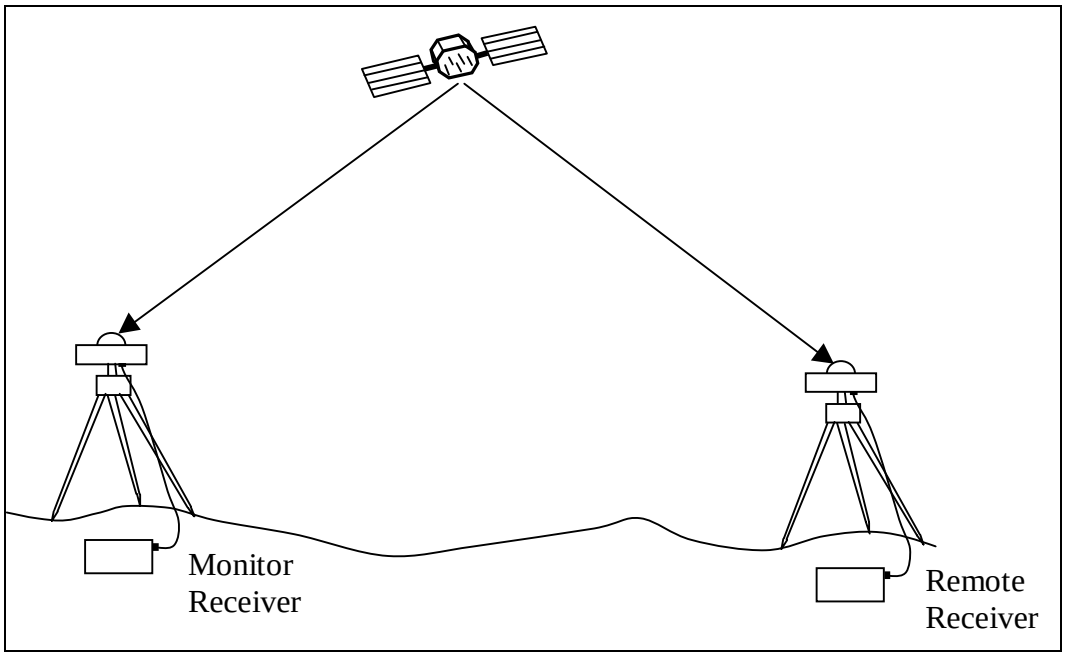

Figure 2.4: Between-receiver single differencing

The difference in the true range term ($\Delta\rho$) now refers to the difference in distances, where the first distance is between receiver 1 and the satellite, and the second distance is between receiver 2 and the satellite. If the satellite position and one of the receiver's positions are known, the position of the other receiver can be determined. This is the concept of *differential positioning*.

By a subsequent differencing of the between-receiver *single difference* across two different satellites, a between-receiver-between-satellite *double difference* can be obtained and given by (Wells et al., 1987)

$$\Delta\nabla P = \Delta\nabla\rho + \Delta\nabla d\rho + \Delta\nabla d_{ion} + \Delta\nabla d_{trop} + \Delta\nabla\varepsilon_{p} + \Delta\nabla\varepsilon_{Mp} \quad (2.10)$$

$$\Delta\nabla\Phi = \Delta\nabla\rho + \Delta\nabla d\rho + \lambda\Delta\nabla N - \Delta\nabla d_{ion} + \Delta\nabla d_{trop} + \Delta\nabla\varepsilon_{\Phi} + \Delta\nabla\varepsilon_{M\Phi} \quad (2.11)$$

where ∇ represents a *between-satellite signal difference*.

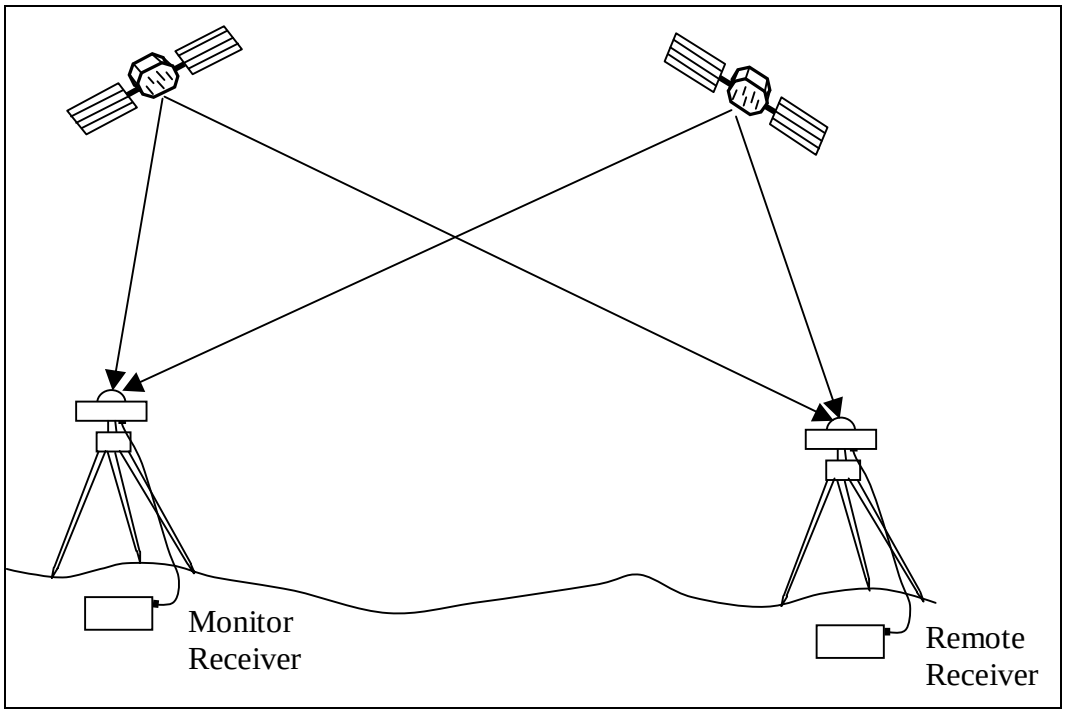

Figure 2.5: Between-receiver and between-satellite double differencing

In Equations 2.10 and 2.11, the receiver clock error and hardware bias terms have disappeared, as they are the same for the two satellites observed at the same time. For a short baseline, the residual orbital, ionospheric and tropospheric errors are very small, causing multipath to be the dominant source of error in the double differenced measurements. However, similar to the single differenced measurement, for a long baseline the residual orbital, ionospheric, and tropospheric errors become significant over

multipath. There is statistically twice as much receiver noise in this case as there is in a single measurement.

The advantage of the double differenced observable is that the receiver clock error term is eliminated. As a result, if the residual errors are small, the double differenced ambiguity term can be resolved to an integer value. The number of double differenced ambiguities is equal to the number of satellites tracked, less one. While forming double differenced measurements between satellite pairs, one of the satellites is kept common in all the pairs. That satellite is called the *base satellite*, which is generally the satellite with highest elevation, as the highest elevation satellite is likely to have least amount of multipath, atmospheric delay errors and phase noise.

In general, pseudorange measurements are used in single differenced form, while carrier phase measurements are used in double differenced form. The advantage of removing the receiver clock error by double differencing for pseudorange is eclipsed by the growth of measurement noise. In the case of carrier phase measurements, it is difficult to separate the initial clock bias from the ambiguity term, and only after the clock bias is removed can the integer nature of ambiguity be exploited.

The residual errors in the double differenced measurements, (namely, the orbital, ionospheric, and tropospheric errors), contribute to the total error depending upon the separation between the receivers. See Parkinson and Enge (1996) for details on differential positioning using GPS.

Multipath errors, however, are not spatially correlated (except a very short baseline) and do not get any better by differencing techniques. In kinematic situations, multipath errors are more random in nature, and contribute towards increasing the receiver noise. In static situations, however, they may be very slowly varying, causing bias like errors during the observation period.

Antennas (receivers), which are static with respect to the surrounding environment and used in short baseline applications, are severely affected by multipath. Even in long baseline applications, where the residual errors are compensated by appropriate modelling or additional measurement aid, multipath errors cause major concerns. In spacecraft attitude determination system, measurements are affected by static multipath from the spacecraft body itself. In applications such as surveying, where there are a limited number of choices of the antenna siting, static multipath could be a major source of error. In such applications, mitigation of code and carrier multipath errors poses a major challenge.

CHAPTER 3

THEORY OF MULTIPATH

3.1 Introduction

Multipath is the phenomenon whereby a signal arrives at a receiver via multiple paths attributable to reflection and diffraction (Braasch, 1996a). To understand the behaviour of multipath effects, it is important to understand the electromagnetic properties of the GPS signal and the changes that take place during reflection and diffraction.

This chapter gives a brief description of electromagnetic properties of the GPS signal. It then describes various types of reflection and gives an account of the changes in amplitude and polarization for different components of the signal upon reflection from a plane surface.

3.2 Electromagnetic Properties of the GPS Signal

The electric and the magnetic fields of an electromagnetic wave are interdependent while propagating through a space. During the wave propagation, the time-varying magnetic and time-varying electric field generates each other and propagates through the empty space at the velocity of light (Kraus and Carver, 1973).

Figure 3.1 shows a plane travelling wave wherein the electric field (E) and the magnetic field (H) are perpendicular to each other everywhere. Together they propagate in a direction perpendicular to the plane of the electric and magnetic field vectors. Such a wave, where the E and the H fields are perpendicular on a plane and the direction of

propagation is transverse to that plane is called a Transverse Electromagnetic (TEM) wave.

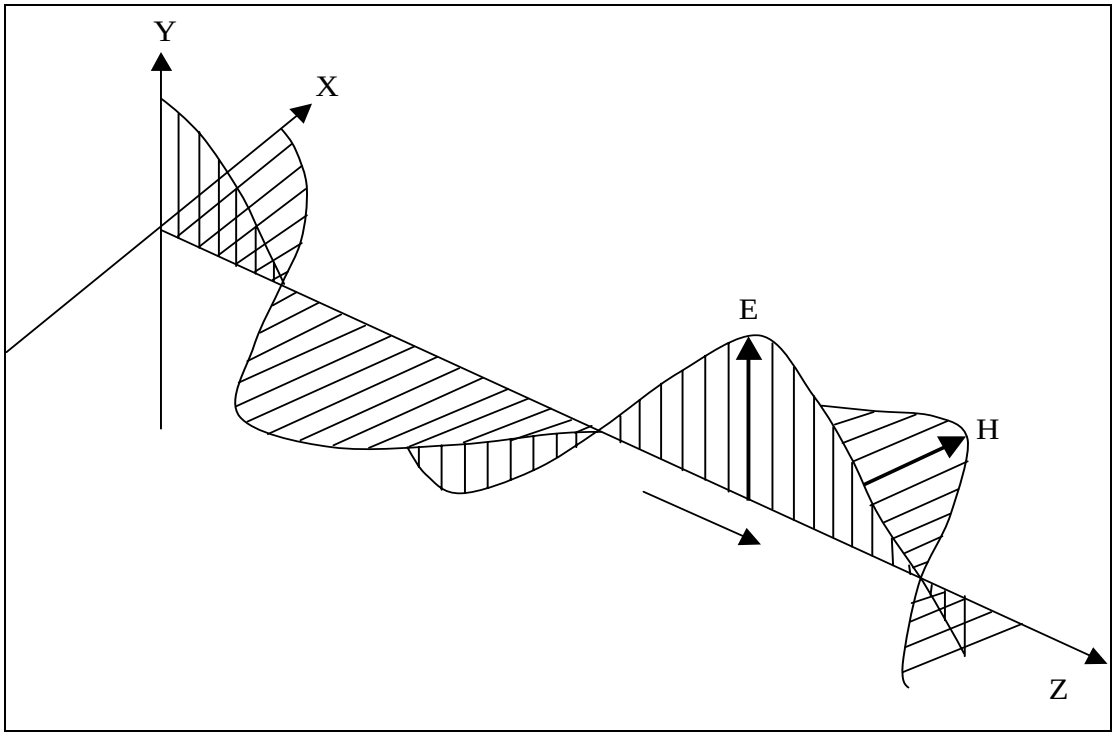

Figure 3.1: Plane travelling wave with E and H vectors perpendicular to each other and on a plane perpendicular to the direction of propagation

The polarization of a propagating electromagnetic wave is decided by the time-varying nature of the electric field component. If the direction of the electric field remains unchanged over time, with respect to the direction of propagation, then it is a linearly polarized wave. If, however, the electric field vector rotates as a function of time, then the tip of the vector describes the polarization to be either elliptical or circular depending upon the shape of the curve traced by the tip. The elliptical polarization is the most generalized form, which in two extreme cases turns out to be either linear or circular polarized signal. If the direction of rotation of the electric vector is clockwise, as viewed from the origin towards the direction of propagation, then it is right-hand polarized signal. Figure 3.2 shows different types of polarization as the curve traced by the electric field vector.

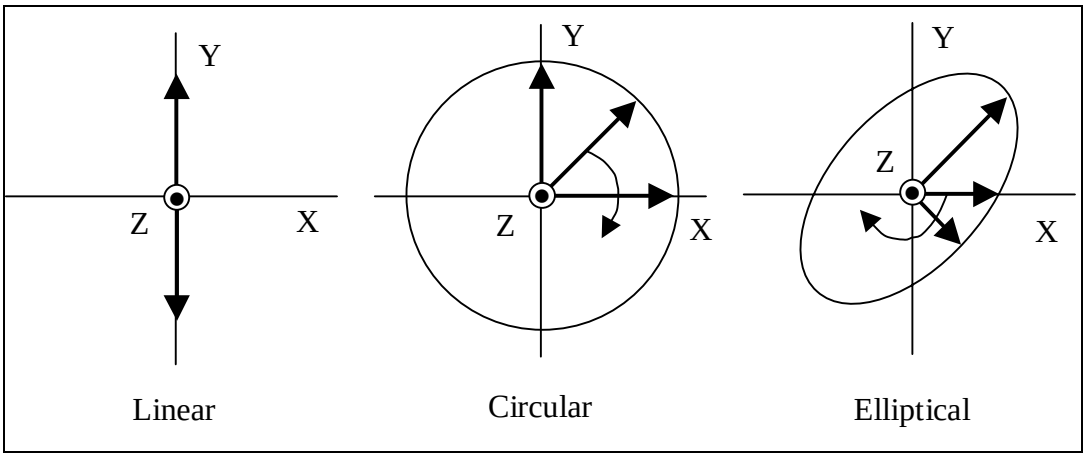

Figure 3.2: Linear, Circular and Elliptical polarization

GPS is a right-hand circularly polarized Transverse Electromagnetic (TEM) wave. Satellite signals are in general circularly polarized, because a linearly polarized signal while travelling through the ionosphere undergoes changes in its polarization. This phenomenon is known as *Faraday rotation*. As the amount of change or rotation is fluctuating, it is difficult to receive it through an antenna, which needs to have the same polarization as the incoming signal. GPS avoids this problem by sending the signal as circularly polarized.

3.3 Reflection of a Electromagnetic wave

The reflection and scattering of the signal from a surface has two components: the specular and the diffuse components. Specular reflection occurs when the electromagnetic wave is reflected by a smooth surface. The reflected wave is the result of the radiation of the points on the Fresnel ellipse (described later). The resultant wave has very little fluctuation of phase and amplitude and therefore is more deterministic than the other type of reflection. If on the other hand, the surface is rough, then the reflected signals are diffuse (Beckmann and Spizzichino, 1963).

Rayleigh quantifies the roughness of a surface through a simple expression, known as the *Rayleigh criterion*. According to this criterion, a surface is smooth if,

$$\Delta h < \frac{1}{8}\frac{\lambda}{\sin\theta} \tag{3.1}$$

where

Δh is the mean height of irregularities within the First Fresnel ellipse (m)

λ is the wavelength of the signal (m), and

θ is the grazing angle or elevation angle of the signal (rad).

Equation 3.1 is just an indicator of the smoothness and can be modified by changing the factor $\frac{1}{8}$ by $\frac{1}{16}$ or $\frac{1}{32}$. Figure 3.3 shows the reflection from a surface. It is easy to see from Figure 3.3 that the differential path delay is equal to $2\Delta h\sin\theta$. For a smooth surface, the differential path delay should be smaller than a fraction of a wavelength. For example, if the differential path delay to be less than one-fourth of a wavelength, then,

$$2\Delta h\sin\theta < \frac{\lambda}{4} \tag{3.2}$$

From Equation 3.2, *Rayleigh criterion* can be easily derived.

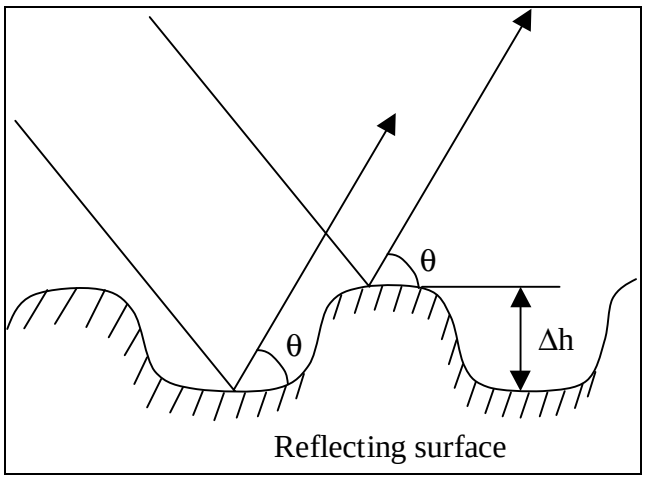

Figure 3.3: Electromagnetic wave reflection from a surface

3.3.1 Specular Reflection

The incident signal induces surface currents on the reflecting plane, which radiates a secondary or reflected field. The locus of all points on the plane, from which the secondary radiation arrives at the image receiver (image of the actual receiver with respect to the reflecting plane) with a constant phase difference of $\frac{\lambda}{2}$ with respect to the direct line-of-sight is called the *First Fresnel zone*. This has the shape of an ellipse as shown in Figure 3.4. If the phase difference is increased in steps of $\frac{\lambda}{2}$, a family of ellipses on the plane will result.

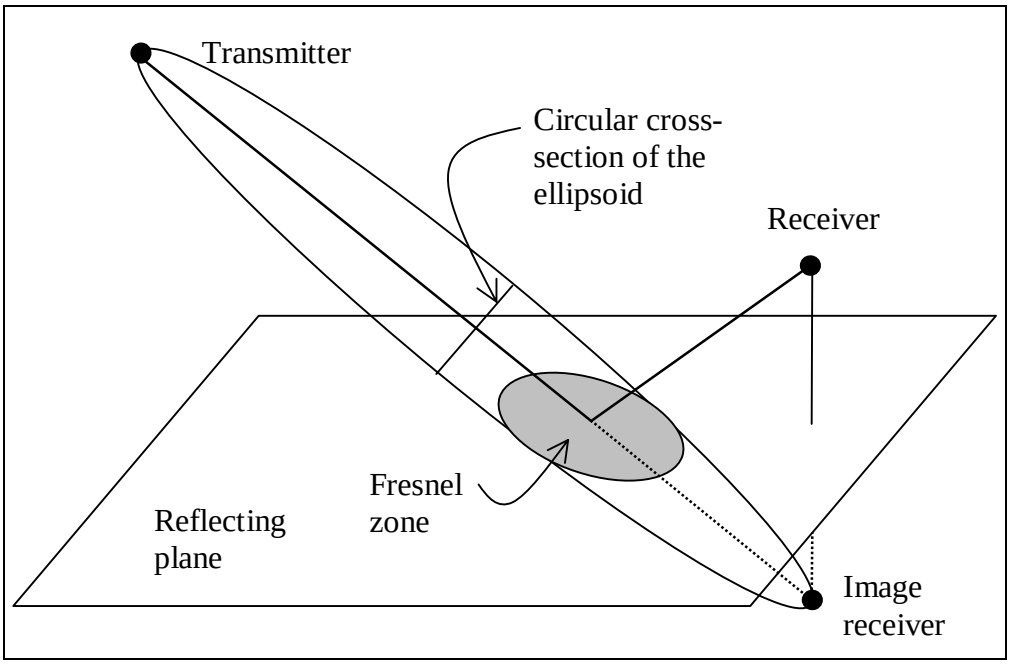

Figure 3.4: Fresnel zone on a reflecting plane

Since successive zones are in phase opposition, the sum of adjacent zones will tend to cancel. However, as the amplitude of excitation decreases slowly from zone to zone, the total sum of the radiation is approximately equivalent to that of half the First Fresnel zone (Beckmann and Spizzichino, 1963).

The Fresnel zone is quantified by a Fresnel zone radius. It is the radius of the circular cross-section of the ellipsoidal Fresnel reflection region, which is orthogonal to the transmitter to the image-receiver line-of-sight as shown in Figure 3.4. For the n^{th} Fresnel region for a reflecting plane at the far field, the radius is given by (Braasch, 1998):

$$R = \sqrt{n\lambda \frac{l_1 l_2}{l_1 + l_2}} \tag{3.3}$$

where

l_1 is the distance between the cross-section and the transmitter (m), and

l_2 is the distance between the cross-section and the receiver (m).

If l_1 is much higher than l_2, as in the case of GPS, Equation 3.3 reduces to,

$$R = \sqrt{n\lambda l_2} \tag{3.4}$$

The footprint of the ellipsoid on the plane of reflection is of the form of an ellipse, the semi-major axis of which can be approximated as:

$$a = \frac{R}{\sin\theta} \tag{3.5}$$

From Equation 3.5 it is clear that for a low elevation angle, the semi-major axis is large. Then the ellipse becomes prolonged, getting longer and narrower with decreasing elevation angle. As a result, the smaller the elevation angle, the larger the semi-major axis and the area of the ellipse. Which means that a large size reflector is needed for a low elevation satellite to reflect the same amount of energy that is reflected by a small size reflector for a high elevation satellite.

Oblique Incidence of a Plane Wave on a Smooth Surface

Let a plane wave be obliquely incident on the boundary between two media as shown in Figure 3.5. The incident wave makes an angle ν_i with respect to the y axis (incident angle) and the reflected wave makes an angle ν_r with respect to the same axis (angle of

reflection) and the transmitted wave makes an angle ν_t with respect to the negative y axis (angle of refraction).

The incident wave has two components of electric fields: *perpendicularly polarized* ($E_\perp$) and *parallel polarized* ($E_\parallel$) components. The suffix 'i', 'r' and 't' of the electric field vector refer to the incident, reflected and the refracted (or transmitted) components respectively. The perpendicularly polarized component is normal to the plane of incident (i.e. X-Y plane in Figure 3.5) and the parallel polarized component is parallel to the plane of incident. The behaviour of the reflector and thereby the reflected signal properties depend upon the polarization (perpendicular or parallel) of the incident signal.

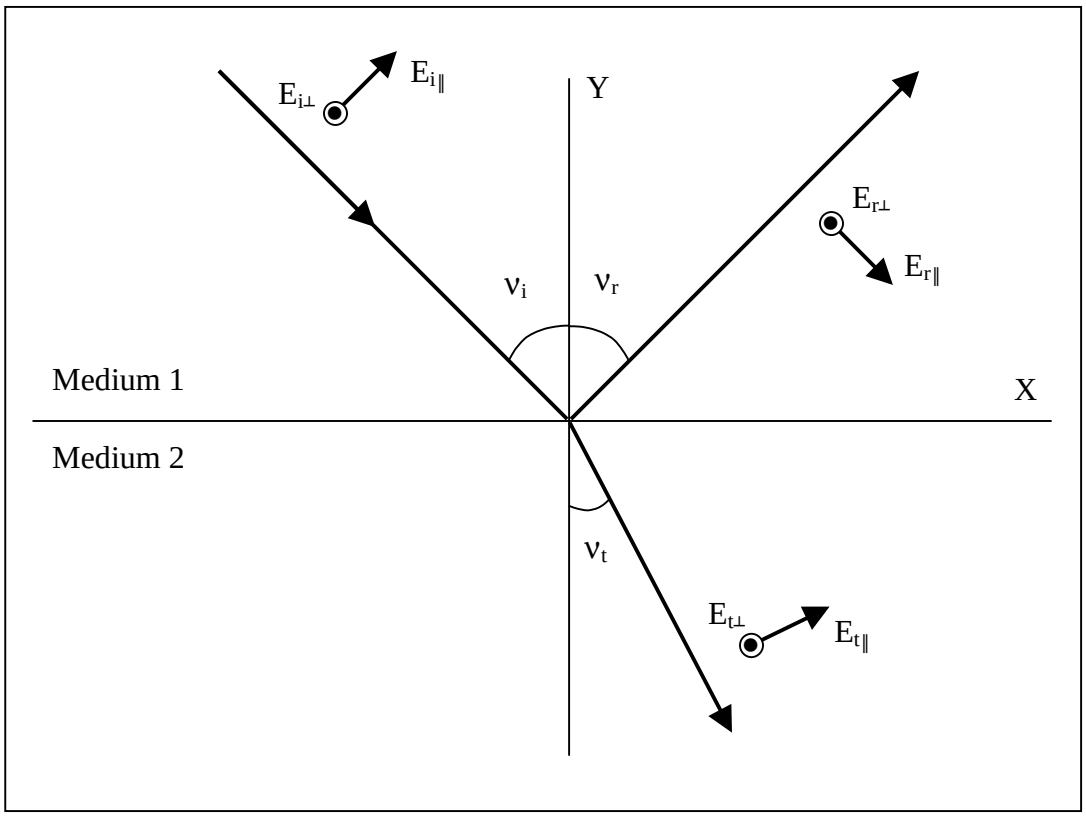

Figure 3.5: Reflection of a circularly polarized wave obliquely incident on a plane surface

The reflected wave undergoes changes in its amplitude and phase after reflection from a plane surface. Therefore, the reflection coefficient has a magnitude and a phase, which is different for a perpendicularly and a parallel polarized signal.

In the case of a perpendicularly polarized wave, the magnitude of the coefficient gradually increases up to 1, as the angle of incident increases up to 90 degrees. The signal however undergoes about 180 degrees phase change during reflection. The amplitude and the phase are a function of the permittivity and conductivity of the reflective plane.

In the case of a parallel polarized wave, the magnitude of the coefficient generally remains constant for all incident angles, except that, it has a sharp dip at a high incident angle and after that the magnitude rapidly increases up to 1 for an incident angle of 90 degrees. The phase of the coefficient is 180 degrees till near high incident angles, but decreases rapidly to 0 degrees at high incident angles.

Brewster Angle

When a parallel polarized wave is incident on a surface with zero conductivity, there is an incident angle at which the reflection coefficient becomes zero. This angle is known as *Brewster angle* and is given by the following expression (in radians):

$$\nu_b = \sqrt{\frac{\varepsilon_2}{\varepsilon_1}} \tag{3.6}$$

where

νb is the Brewster angle (rad)

ε_1 is the permittivity of medium 1 (F/m), and

ε_2 is the permittivity of medium 2 (F/m).

The Brewster angle is also known as the Polarization angle, since a wave composed of both perpendicularly and parallel polarized components incident at the Brewster angle produces a reflected wave with only a perpendicular component. Thus a circularly polarized wave incident at the Brewster angle becomes linearly polarized on reflection. In general, a circularly polarized wave becomes an elliptically polarized wave after reflection. See Kraus and Carver (1973) for more details on wave reflection.

In general, most GPS antennas have a 5-10 dB attenuation for an opposite polarized wave. But if the wave is reflected with a high incident angle (higher than the Brewster angle), then the parallel polarized component of the wave will not undergo a sign reversal and therefore will not be rejected or attenuated by the antenna. For a good conductor the Brewster angle is around 90 degrees and for dry soil it is around 80 degrees (Breeuwer, 1991).

3.3.2 Diffuse Scattering

Diffuse scattering occurs when the electromagnetic wave is reflected by a rough surface. It takes place over a much larger area of the surface than the first Fresnel zone. Its phase is non-coherent and its fluctuations have a large amplitude. It is equivalent to the sum total of many reflections with different amplitudes and phases, depending upon the irregularities on the surface and the surface structure. Because of such a nature, it follows a Rayleigh distribution (Beckmann and Spizzichino, 1963). The diffuse reflection is difficult to model due to its random behaviour and therefore, is treated like noise in many practical situations.

3.4 Diffraction

Diffraction occurs when the electromagnetic wave hits on the edge of an object or a curved surface-like cylinder causing Edge diffraction and Creeping-wave diffraction, respectively (Kraus and Carver, 1973).

One example of diffraction in the case of GPS is that, when the surface reflections hit the edge of a ground plane without a choke-ring, then edge diffraction takes place and some of the diffracted signals reach the antenna. This is similar to diffuse reflection, and has many components and is therefore difficult to model.

CHAPTER 4

GPS RECEIVER TRACKING LOOPS

4.1 Introduction

The GPS user segment consists of GPS receivers, which are used to determine the user position, velocity, and precise time from the satellite signal. As the satellites are always in motion, the receiver has to continuously track the satellite signal to generate an uninterrupted solution, as desired in most applications. GPS signal code and carrier tracking loops in a receiver form the core of the signal processing and they continuously track the incoming satellite signal to generate pseudorange and carrier phase measurements.

In this chapter, a generic GPS receiver is briefly described, and its various physical and functional elements are identified. Different types of code and carrier tracking loops used in the receiver are described and their behaviours are analyzed. The correlation properties of GPS P and C/A codes are also described under ideal and band limited situations.

4.2 Receiver Architecture

A GPS receiver is a spread spectrum receiver, requiring several essential parts for acquisition, tracking and extracting useful information from the incoming satellite signal. It can be broadly divided into three sections: the RF Front-end (RFF), Digital Signal Processing (DSP) and the Navigation Data Processing (NDP) (Accord, 1993). The functions of the RFF section are generally the same in all receivers, as are the functions of the DSP section. But the functions of the NDP section are often custom defined, and depend upon the type of application in which the receiver is intended to be used. Figure

4.1 shows a simple block diagram of a typical single frequency GPS receiver with major interfaces and input/output signals of the essential blocks.

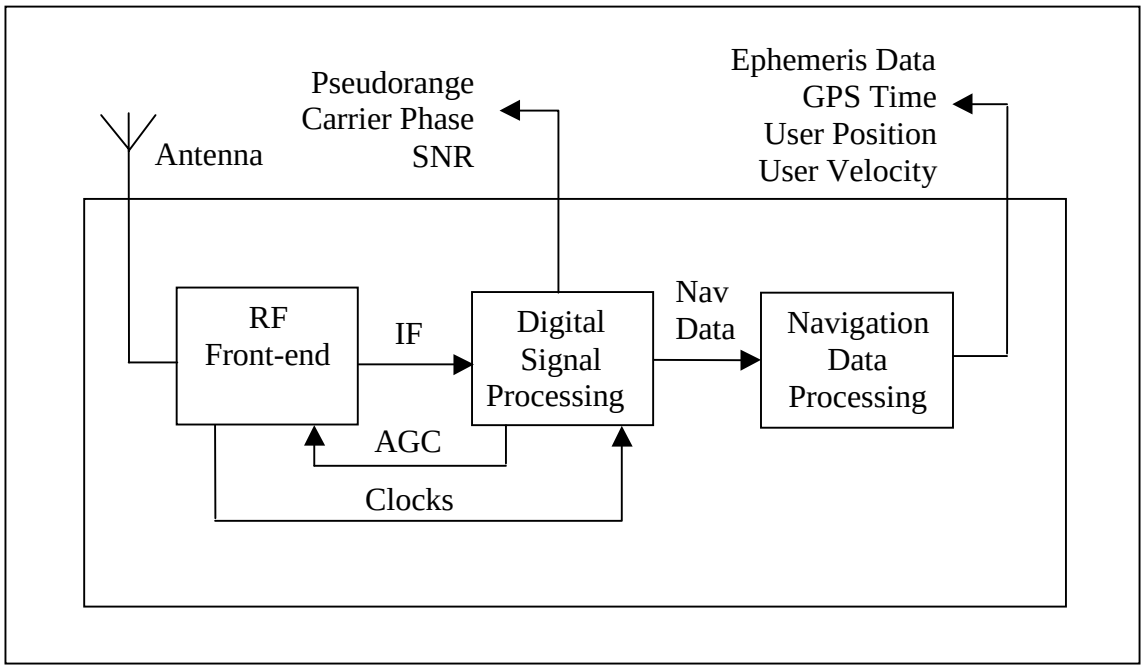

Figure 4.1: Block diagram of a generic GPS receiver

Table 4.1 shows various physical and functional elements of a typical GPS receiver. The RFF and the DSP sections generally consist of various hardware modules, whereas the NDP section is implemented using software. However, in some modern receivers, the DSP section is also implemented in software (Shenoy et al., 1999). A brief description of each of these functional modules is given below.

4.2.1 RF Front-end

The RF Front-end receives GPS spread spectrum signals, generally at L1 and L2 frequencies, using an omni-directional, broad band, Right Hand Circularly Polarized (RHCP) antenna, as GPS signals are RHCP. Use of a linear antenna instead of an RHCP antenna would cause an attenuation of 3 dB.

Table 4.1: Various physical and functional elements of a generic GPS receiver (Accord, 1993; Van Dierendonck, 1996; GEC Plessey, 1996)

Item	RFF	DSP	NDP
Physical components	1. Antenna and cable 2. Low Noise Amplifier (LNA) 3. Mixers and Local Oscillators 4. Amplifiers and Filters 5. Frequency synthesizer 6. Clock/oscillator 7. Automatic Gain Control (AGC) 8. Analog to Digital Converter (ADC)	Parallel channels for each satellite. Each channel consists of, 1. Numerically Controlled Oscillators (NCO) 2. Code generator 3. Delay Lock Loop (DLL) 4. Costas Loop	Software Algorithms
Functions	1. Signal reception 2. Amplification 3. Out-of-band noise rejection 4. Automatic gain control 5. Analog to digital conversion 6. Clock to DSP	1. Signal acquisition 2. Code tracking 3. Carrier tracking 4. Code, carrier measurements generation 5. C/N_0 computation 6. Data extraction	1. Data bit synchronization 2. Data sub-frame synchronization 3. Data base management 4. User position, velocity, clock offset computation 5. Custom functions

Furthermore, if an active antenna is used, the received signal is amplified by a Low Noise Amplifier (LNA) before it is fed to the antenna cable. This LNA reduces the overall noise figure of the RF down conversion, rejects out-of-band interference and compensates for the cable loss (Van Dierendonck, 1996). The GPS signal is then down converted from the radio frequency (RF) to an intermediate frequency (IF) by one or multiple stages.

The RFF has several stages of down converters, and consist of mixers, local oscillators and band pass filters. The RFF has a frequency synthesizer, which generates all the clocks used in the RFF as well as DSP sections of the receiver from a stable oscillator, which is generally a TCXO (Temperature controlled crystal oscillator), VCXO (Voltage controlled crystal oscillator) or Rubidium. The down converters reduce the GPS carrier frequency from GHz to a couple of MHz. The last stage of the RFF is an Analog to Digital Converter (ADC), which samples the down converted GPS signal using a suitable sampling frequency. This results in one, two or three bit(s) digital GPS signals, which can be processed in the digital domain. Intermediate bandpass filters are used to disallow image frequencies. An AGC maintains the signal level before the ADC within a reasonable range by increasing or decreasing the gains of the intermediate amplifiers, depending upon the signal strength. Until this point, the GPS signal is a mixture of all the visible satellite signals, which are offset in frequency by only the dopplers of individual satellites.

4.2.2 Digital Signal Processing

The Digital Signal Processing section is the core of a GPS receiver, and performs several functions in real time. The satellite signal is processed in multiple (usually 8 to 12) parallel channels, whereby each channel is dedicated to acquire and dynamically track one visible satellite. Each channel consists of, (among other things), code and carrier tracking loops and associated hardware and software. The code tracking loop is generally a Delay Lock Loop (DLL) and the carrier tracking loop is a Costas Loop.

The tracking loops generally work together. The DLL uses local code generators, correlators, a code discriminator and a loop filter, and aligns the locally generated code with the incoming code. On the other hand, the Costas Loop uses the in-phase and quadrature-phase versions of the locally generated carrier, carrier discriminator, and loop filter, and matches the locally generated carrier with the incoming satellite signal carrier. The phase error of the carrier discriminator function is used for navigation data transition detection. The pseudorange measurements, carrier phase measurements, and Signal to Noise Ratio (SNR) are generated as by-products of the signal tracking.

4.2.3 Navigation Data Processing

The Navigation Data processing generally refers to the GPS receiver functions that involve navigation data extraction and utilization. Navigation data consists of 50 Hz data bits transmitted from the satellite in terms of frames and sub-frames. The data bit modulates the carrier and causes a 180° phase shift of the carrier at data bit transitions. In a receiver, the carrier lock loop discriminator calculates the difference between the incoming and the local carrier phase, and detects the data bit transition, whenever there is a 180° phase shift of the incoming signal.

The data bit streams are collected and compared, with respect to the known 8-bit preamble, which is transmitted at the beginning of each sub-frame. The preamble signifies the sub-frame beginning, and subsequent synchronization of data bits. From the sub-frame ID in the navigation data, the frame synchronization can then be achieved.

Each satellite sends its own position, in terms of ephemeris data consisting of Keplerian orbital parameters. After the sub-frame synchronization is achieved, the navigation data bit is decoded to extract the orbital parameters for the satellite position computation. The navigation data is decoded to obtain the GPS time, clock correction, ionospheric delay error correction, etc. That extracted information is used to determine the receiver position, velocity, and precise time. It is also used for various user specific applications.

4.3 Receiver Tracking Loops

Figure 4.2 shows a block diagram of typical GPS receiver tracking loops, which consist of a DLL for code tracking and a Costas Loop for carrier tracking (Ward, 1996; GEC Plessey, 1996). In practice, the DLL in a GPS receiver generally has a non-coherent type of discriminator (see Holmes, 1982 for various code discriminators; and Haykin, 1989 for coherent and non-coherent techniques). An *n* parallel channel receiver will have *n* such sets of blocks corresponding to each independent tracking loop.

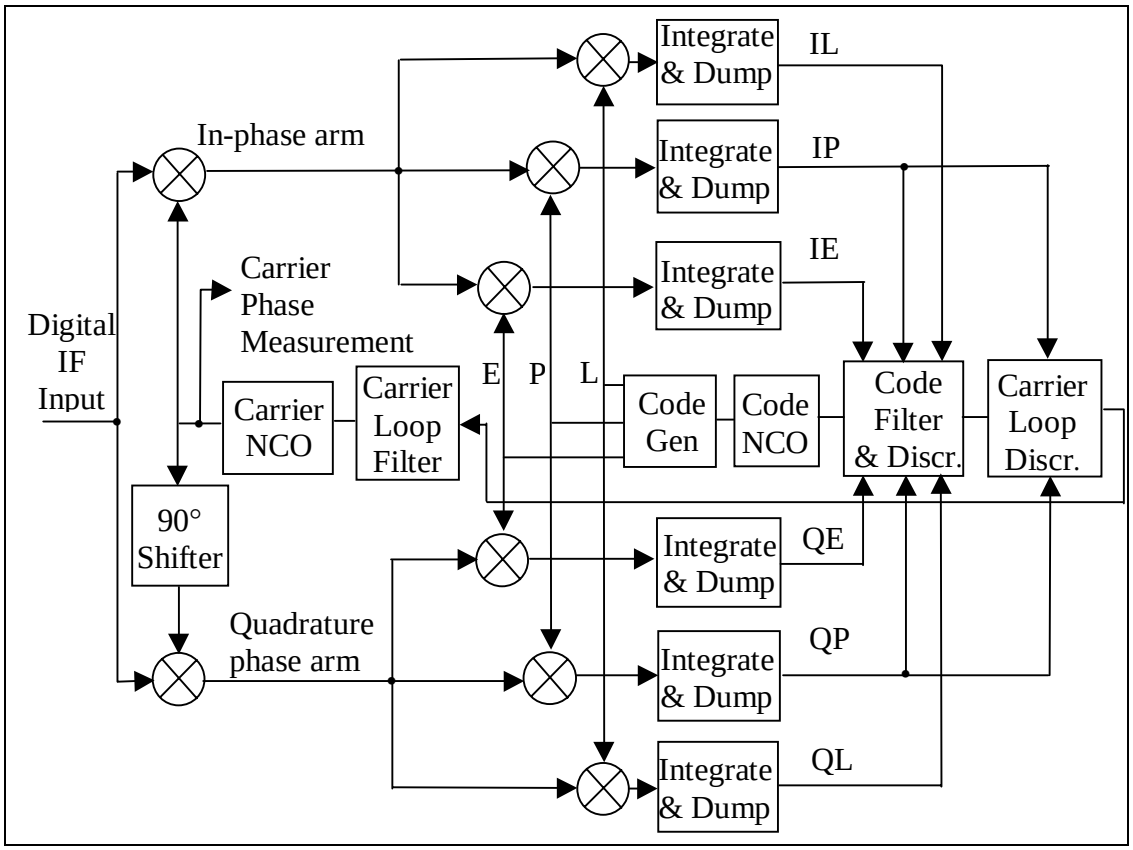

Figure 4.2: Typical GPS receiver code and carrier tracking loops (Ward, 1996, GEC Plessy, 1996)

In a receiver, the digitized IF signal is input to each of these parallel channels. The input signal is beat with the locally generated in-phase and quadrature-phase replicas of the carrier. The signal is then correlated with the prompt (P), early (E) and late (L) versions

of the locally generated code, and the correlation values are integrated for a pre-detection integration period. The early and late correlation values in the in-phase and quadrature-phase arms (IE, IL, QE, QL) are generally used for code tracking, whereas the prompt correlation values (IP, QP) are used for carrier tracking. Some code discriminators, such as the dot-product type, use prompt correlation values as well. For analysis of the effects of multipath on GPS code and carrier measurements, the behaviours of code and carrier discriminator functions in the presence of multipath need to be analyzed. However, prior to that, the behaviours of code and carrier discriminator functions in the absence of multipath are to be understood.

In an ideal case, a GPS receiver receives only the direct signal from the satellite. Assuming that the signal has the C/A or the P code only, after neglecting the navigation data bit, the direct (input) signal at the receiver may be simplified from Equation 2.1 as:

$$s_i(t) = Ac(t - \tau_0)\cos(\omega_0 t + \gamma_0) \tag{4.1}$$

where,

- A is the satellite signal carrier amplitude (volt)
- c() is the GPS C/A or P code
- τ_0 is the satellite signal code delay (s)
- ω_0 is the satellite signal carrier frequency (rad/s), and
- γ_0 is the satellite signal carrier phase (rad).

The local replica of the carrier has frequency and phase equal to the receiver's estimate of the incoming satellite signal frequency and phase. Similarly, the locally generated prompt code has a delay equal to the receiver's estimate of the incoming signal code delay. The locally generated signal, combining code and carrier, in the in-phase arm for the prompt correlator then can be expressed as:

$$s_{IP}(t) = c(t - \hat{\tau}_0)\cos(\hat{\omega}_0 t + \hat{\gamma}_0) \tag{4.2a}$$

where,

$\hat{\tau}_0$ is the receiver's estimate of the direct signal code delay (s)

$\hat{\omega}_0$ is the receiver's estimate of the signal carrier frequency (rad/s), and

$\hat{\gamma}_0$ is the receiver's estimate of the signal carrier phase (rad).

Similarly, the locally generated signal, combining code and carrier, in the quadrature-arm for the prompt correlator can be expressed as:

$$s_{QP}(t) = c(t - \hat{\tau}_0)\sin(\hat{\omega}_0 t + \hat{\gamma}_0) \tag{4.2b}$$

Then, the in-phase prompt correlation value, assuming that the incoming and the locally generated carrier frequencies are the same, is given by:

$$\begin{aligned} IP = \overline{s_i(t)s_{IP}(t)} &= \int_0^{T_P} Ac(t - \tau_0)c(t - \hat{\tau}_0)\cos(\omega_0 t + \gamma_0)\cos(\hat{\omega}_0 t + \hat{\gamma}_0) \\ &\approx \frac{A}{2} R(\hat{\tau}_0 - \tau_0)\cos(\gamma_0 + \hat{\gamma}_0) \end{aligned} \tag{4.3a}$$

where,

T_P is the pre-detection integration period (s)

R() is the correlation function, a detailed discussion of which is given in section 4.4

Similarly, the in-phase early (IE), in-phase late (IL), quadrature-phase prompt (QP), quadrature-phase early (QE) and quadrature-phase late (QL) correlation values are respectively:

$$\begin{aligned} IE &= \overline{s_i(t)s_{IE}(t)} \approx \frac{A}{2} R(\hat{\tau}_0 - \tau_0 + T_d)\cos(\gamma_0 + \hat{\gamma}_0) \\ IL &= \overline{s_i(t)s_{IL}(t)} \approx \frac{A}{2} R(\hat{\tau}_0 - \tau_0 - T_d)\cos(\gamma_0 + \hat{\gamma}_0) \end{aligned} \tag{4.3b-4.3c}$$

$$QP = \overline{s_i(t)s_{QP}(t)} \approx \frac{A}{2} R(\hat{\tau}_0 - \tau_0)\sin(\gamma_0 + \hat{\gamma}_0)$$

$$QE = \overline{s_i(t)s_{IE}(t)} \approx \frac{A}{2} R(\hat{\tau}_0 - \tau_0 + T_d)\sin(\gamma_0 + \hat{\gamma}_0) \qquad (4.3d\text{-}4.3f)$$

$$QL = \overline{s_i(t)s_{IL}(t)} \approx \frac{A}{2} R(\hat{\tau}_0 - \tau_0 - T_d)\sin(\gamma_0 + \hat{\gamma}_0)$$

where T_d is the spacing between the prompt and early, or the prompt and late correlators.

The correlation values expressed in equations 4.3a to 4.3f are used by the discriminator functions in the loop filters. The code and carrier loop filters generate corrections to the locally generated code and carrier respectively, to maintain the discriminator function output around zero (actually zero mean).

4.3.1 Code Tracking Loop

In a coherent type of discriminator for the code, the local carrier frequency and phase are assumed to be the same as the incoming carrier frequency and phase. In that case, the correlation values of the quadrature-arm correlators are zero, and they are not implemented. Only the in-phase arm correlators are used for the coherent type of code tracking loops. In that case, the Costas Loop reduces to a simple Phase Lock Loop (PLL).

Various code discriminator functions for a GPS receiver coherent and non-coherent type of DLL discriminators are given in Table 4.2.

A GPS receiver generally uses one of the non-coherent types of discriminators shown in Table 4.2. The dot-product discriminator is a popular one, as it requires the least computational burden. However the dot-product discriminator needs all three of the correlation values, unlike other discriminators. A normalized or modified form of the discriminator is also commonly used in practice.

Table 4.2: Various types of Delay Lock Loop Discriminators (Ward, 1996)

Discriminator Type	Description	Remarks
Coherent	$D_C = IE - IL$	Simplest of all. Does not require correlation values in the quadrature arm correlators
Non-coherent	$D_n = (IE^2 + QE^2) - (IL^2 + QL^2)$	Early minus late power. Can be normalized by early plus late power.
	$D_n = \sqrt{IE^2 + QE^2} - \sqrt{IL^2 + QL^2}$	Early minus late envelope. Can be normalized by early plus late envelope to remove amplitude sensitivity.
	$D_n = IP(IE - IL) + QP(QE - QL)$	Dot-product type of discriminator. It uses prompt correlation values in addition to early and late correlation values. Can be normalized by the signal power.

Using Equations 4.3a to 4.3f for a coherent discriminator, and assuming that the local carrier frequency and phase are the same as the incoming carrier frequency and phase, the discriminator function can be expressed as:

$$\begin{aligned} D_C &= IE - IL \\ &= \{R(\hat{\tau}_0 - \tau_0 + T_d)\} - \{R(\hat{\tau}_0 - \tau_0 - T_d)\} = R_{EL}(\hat{\tau}_0 - \tau_0) \end{aligned} \tag{4.4}$$

A similar expression can be derived for each type of the non-coherent discriminator function.

Figure 4.3 shows discriminator function responses for various types of coherent and non-coherent DLL discriminators using a standard correlator. A standard correlator, also called a wide correlator, has the early and the late correlators spaced at one half the code chip away from the prompt correlator. The discriminator output responses are plotted

against the code tracking errors input. The code tracking error is given by $\tau_e = \hat{\tau}_0 - \tau_0$. In the figure, infinite bandwidth of the incoming signal is assumed, such that the correlation triangle has a sharp peak. In reality, however, the correlation triangle is rounded-off near the peak due to a finite bandwidth limitation.

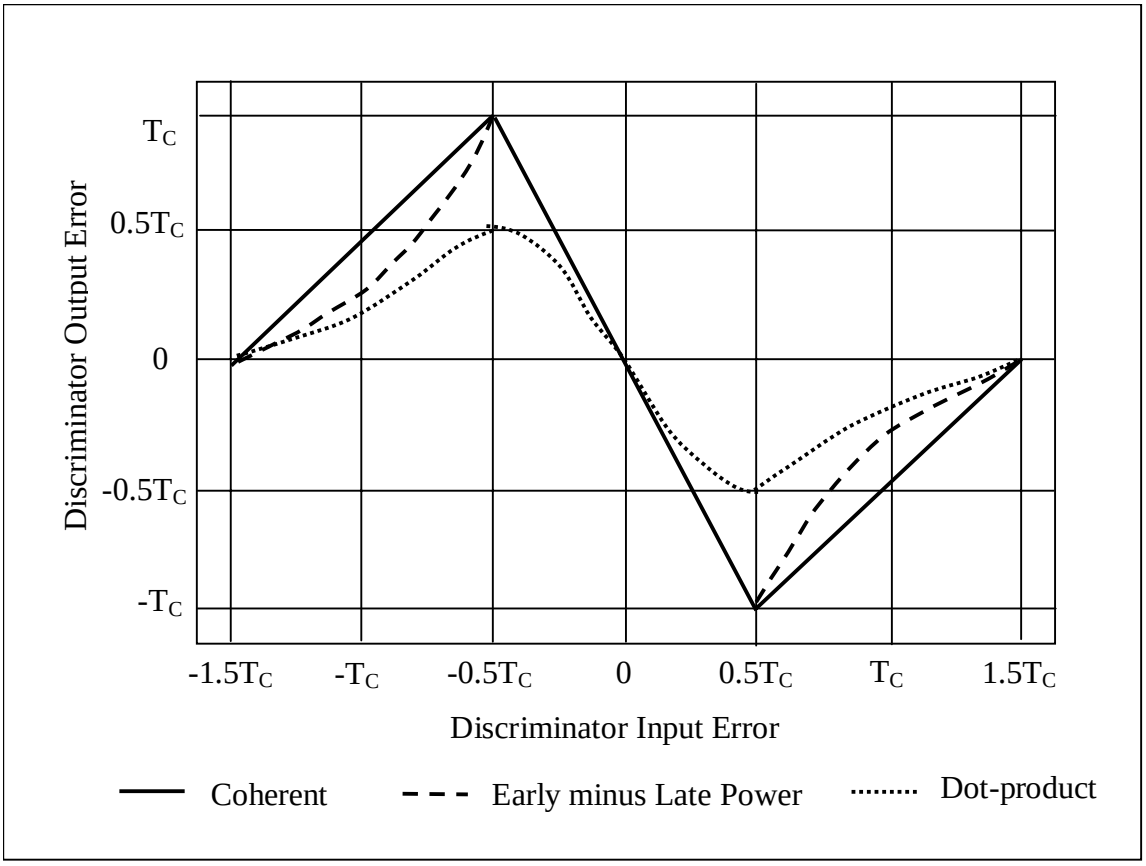

Figure 4.3: Various types of DLL discriminator functions responses

Figure 4.4 shows the discriminator function value ($R_{EL}(\tau_e)$) for a coherent discriminator in the case of an arbitrary early-late correlator spacing in the range of $0 \le 2T_d \le T_C$. This takes the shape of the familiar 'S' curve. Here, the discriminator function values saturate when the input code tracking error exceeds T_d. Hence, the discriminator is sensitive in the range of $-T_d$ and $+T_d$. As the correlator spacing increases, the horizontal segment of the 'S' curve decreases, and in a limiting case of a standard correlator, when $T_d = 0.5T_C$, the horizontal segment diminishes and the Figure 4.3 for coherent discriminator is obtained.

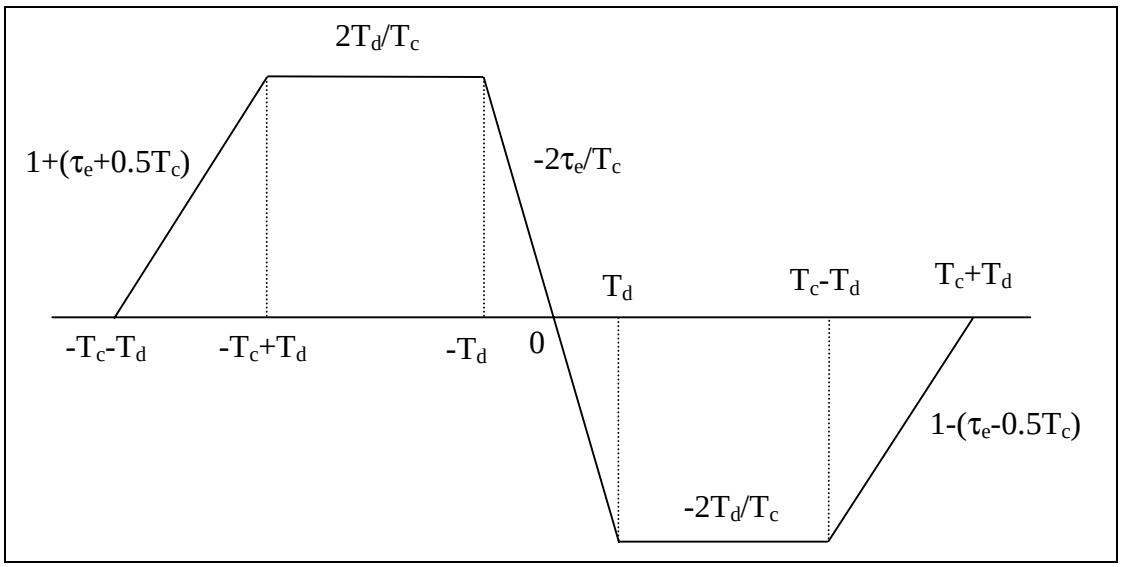

Figure 4.4: Response for a coherent discriminator with arbitrary early-late correlator spacing

Pre-correlation filtering is necessary to prevent aliasing and allow only the desired signal spectrum for signal processing (Van Dierendonck, 1996). In low cost receivers, a bandwidth of 2 MHz is usually used, which allows only the main lobe of the C/A code into the DSP section. Such receivers generally use a standard correlator with spacing of one chip between the early and the late correlators. High performance C/A code receivers, on the other hand, use 8-10 MHz bandwidth, allowing the main lobe and 4-5 side lobes into the DSP section. Such receivers generally use correlators with spacing of around 0.1 chip between the early and the late correlators. Figure 4.5 shows discriminator function responses for correlators using 1 chip and 0.1 chip spacing and 2 MHz and 10 MHz pre-correlation bandwidth respectively. It can be seen that, in the case of the lower bandwidth, the curve is rounded-off at the peak and has a larger trail compared to the ideal curve.

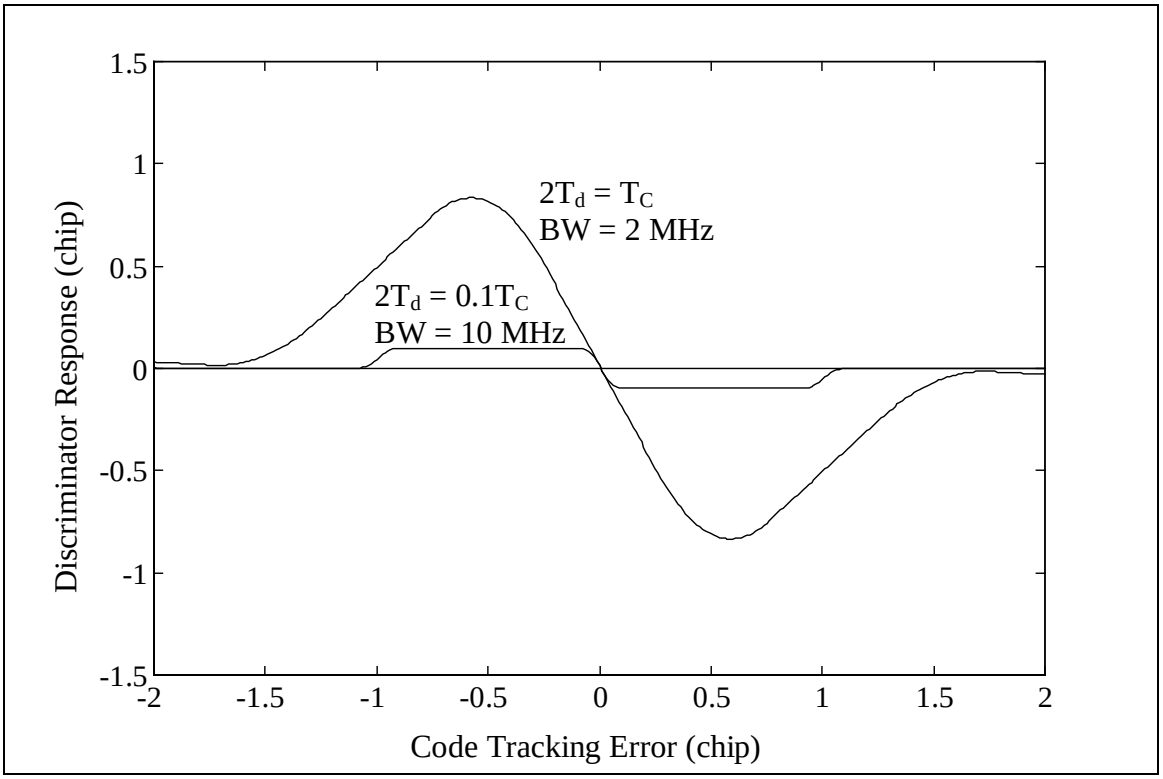

Figure 4.5: Coherent discriminator response for various correlator spacings and pre-correlation bandwidth limitation

The DLL in a GPS receiver always tries to track the zero crossing of the discriminator 'S' curve. In other words, it tries to minimize the input code tracking error. The output values of the discriminator function are fed to a loop filter, which generates corrections to the local code frequency and phase so as to minimize the code tracking error. The code lock loop filter is generally aided by the carrier lock loop filter and therefore has a low bandwidth.

4.3.2 Carrier Tracking Loop

In a Frequency Lock Loop (FLL), the local carrier frequency closely follows the incoming carrier frequency, but in a Phase Lock Loop (PLL), such as a Costas Loop, the local carrier phase closely follows the incoming carrier phase (Ward, 1996). The 50 Hz navigation data causes a 180° phase shift of the carrier. A simple PLL is sensitive to all

the phase changes of the carrier, and would apply correction to the local carrier even when the phase change is due to the navigation data bit transition. Conversely a Costas loop is insensitive to the 180° phase shift of the carrier. As a result, it does not apply correction to the local carrier when there is a phase shift due to a data bit transition. Therefore, a Costas Loop is generally used in all GPS receivers for carrier tracking.

Figure 4.2 shows various components of the carrier lock loop. The prompt correlation values in the in-phase and quadrature-phase arms are used in the discriminator function to compute the error between the incoming and the local carrier phase. The computed error is used in a third, second or first order loop filter, which generates correction to the local carrier NCO.

There are several types of carrier discriminator functions that can be used in a carrier lock loop discriminator. Some of the commonly used discriminator functions are shown in Table 4.3. A GPS receiver generally uses one of the discriminators shown in the table.

Table 4.3: Various types of Carrier Lock Loop Discriminators (Ward, 1996)

Discriminator Description	Remarks
$D_r = \text{sign}(IP) \bullet QP$	Least computational burden. Output proportional to sin(phase error)
$D_r = IP \bullet QP$	Moderate computational burden. Output proportional to sin (2*phase error)
$D_r = \arctan(QP/IP)$	High computational burden. Output proportional to the phase error

Using Equations 4.3a to 4.3f for an arctan type of discriminator, assuming that the local carrier frequency is the same as the incoming signal carrier frequency, the discriminator function may be expressed as:

$$D_r = \arctan\left\{\frac{R(\hat{\tau}_0 - \tau_0)\sin(\gamma_0 - \hat{\gamma}_0)}{R(\hat{\tau}_0 - \tau_0)\cos(\gamma_0 - \hat{\gamma}_0)}\right\} \qquad (4.5)$$
$$= \gamma_0 - \hat{\gamma}_0$$

Similar expressions can be derived for other types of discriminator functions.

Figure 4.6 shows discriminator function responses for various types of carrier lock loop discriminators. The discriminator output responses are plotted against the carrier tracking input errors. A carrier tracking loop attempts to track the zero crossing of the discriminator function response. In other words, it tries to minimize the input carrier phase error. The carrier phase error is zero, when the correlation value in the quadrature-phase arm is zero, and the correlation value in the in-phase arm is maximum.

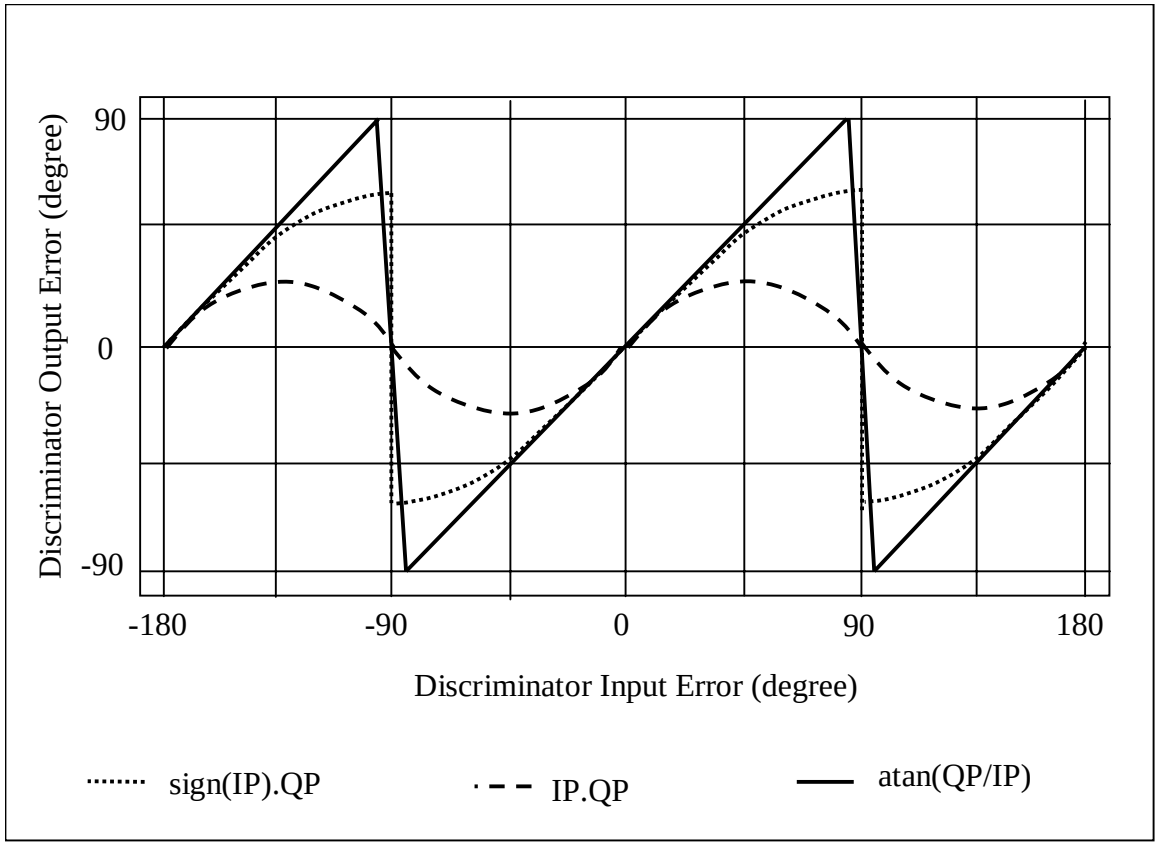

Figure 4.6: Various types of Costas Loop discriminator functions responses

The output values of the discriminator function are fed to a third, second or first order loop filter, which generates correction to the local carrier frequency and phase, so as to minimize the phase error. The bandwidth of the loop filter is fixed or changed adaptively, based upon the dynamic stress, SNR and the phase noise of the clock.

4.4 Correlation Properties of PRN Codes

The correlation between two signals is a measure of the similarity or relatedness between them (Taub and Schilling, 1986). If $c_1(t)$ and $c_2(t)$ are two real signals, then the correlation between them is defined as:

$$R_{1,2}(\tau) = \lim_{T\to\infty} \frac{1}{T} \int_{-T/2}^{T/2} c_1(t)c_2(t+\tau)dt \tag{4.6}$$

If $c_1(t)$ and $c_2(t)$ are periodic with the same fundamental period of T_0, then the correlation between them is:

$$R_{1,2}(\tau) = \frac{1}{T_0} \int_{-T_0/2}^{T_0/2} c_1(t)c_2(t+\tau)dt \tag{4.7}$$

The correlation of a signal with itself, i.e. if $c_1(t)$ and $c_2(t)$ are the same signal, then $R_{1,2}(\tau) = R(\tau)$ is called the autocorrelation. However, if $c_1(t)$ and $c_2(t)$ refer to two different signals, then $R_{1,2}(\tau)$ is called the cross-correlation.

Some of the important properties of an autocorrelation function are:

a) The autocorrelation for $\tau = 0$, i.e. R(0), gives the mean square value, or the average power of the signal. This is also the maximum correlation value between the two signals.
b) The autocorrelation is an even function of τ, i.e. $R(-\tau) = R(\tau)$.

c) The power spectral density and the autocorrelation function of a periodic signal are a Fourier Transform pair.

GPS satellite signals are transmitted in the same frequency band from all the satellites. However, to isolate signals from different satellites, it modulates the carrier by different P and C/A codes. This enables the Code Division Multiple Access (CDMA) capability of the GPS to the user.

As mentioned in Chapter 2, P and C/A codes are PRN sequences. However, the former is a Maximal Length code and the latter is a Gold-code. The sequences have unique correlation properties.

The autocorrelation function of a Maximal Length code has only two states (Holmes, 1982; Spilker, 1996):

$R(\tau) = N$, when $\tau = 0$, N = number of bits

$= -1$, when $\tau \neq 0$

Within +/-1 code chip misalignment between the two code sequences, the correlation value decreases along a triangle. The normalized autocorrelation values (i.e. autocorrelation values divided by the number of bits) of a Maximal Length code are shown in Figure 4.7.

The cross-correlation properties between two Maximal Length code sequences is such that it has only one state:

$R_{1,2}(\tau) = -1$, for all τ

This property is important to have multiple access capability.

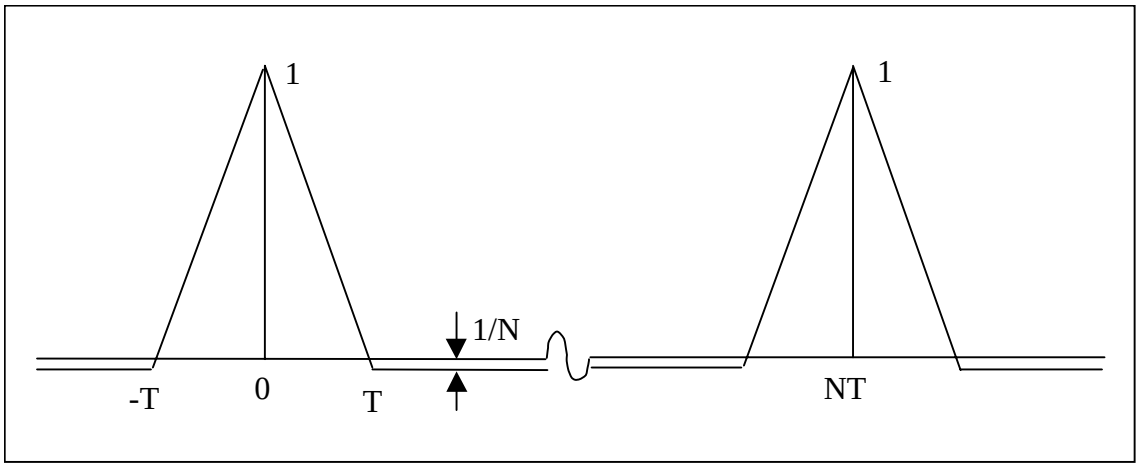

Figure 4.7: Autocorrelation properties of a Maximal Length code, such as P-code

The Gold code selected as the GPS C/A code, is a family of codes formed as the product (modulo-2 sum) of two different properly paired maximal length linear feedback shift registers. Both the shift registers are of the same period $N = 2^n-1$, where n is the number of shift registers (Spilker, 1996).

Table 4.4: Cross-correlation properties of Gold codes

Register Length	Code Length	Cross-correlation value	Cross-correlation value for GPS C/A code	Probability
n odd	$N = 2^n-1$	1/N		~0.50
		$-(2^{(n+1)/2}+1)/N$		~0.25
		$(2^{(n+1)/2}-1)/N$		~0.25
n even and not divisible by 4	$N = 2^n-1$	1/N	-1/1023	~0.75
		$-(2^{(n+1)/2}+1)/N$	-65/1023	~0.125
		$(2^{(n+1)/2}-1)/N$	63/1023	~0.125

However, the cross-correlation function of a Gold code is somewhat different than that of a Maximal Length code. The chosen Gold code for GPS has cross-correlation properties such that it can take three values as shown in Table 4.4 (Holmes, 1982; Spilker, 1996).

The C/A code autocorrelation properties are similar to that of the P code, except that in the C/A code there are smaller peaks of -65 and +63, while the highest peak value is 1023. The normalized autocorrelation values for satellite 3 for various code shifts are shown in Figure 4.8. It can be seen that there is a major peak (1023/1023 = 1) when the misalignment is zero, and several minor peaks (-65/1023 and 63/1023) at other misalignments.

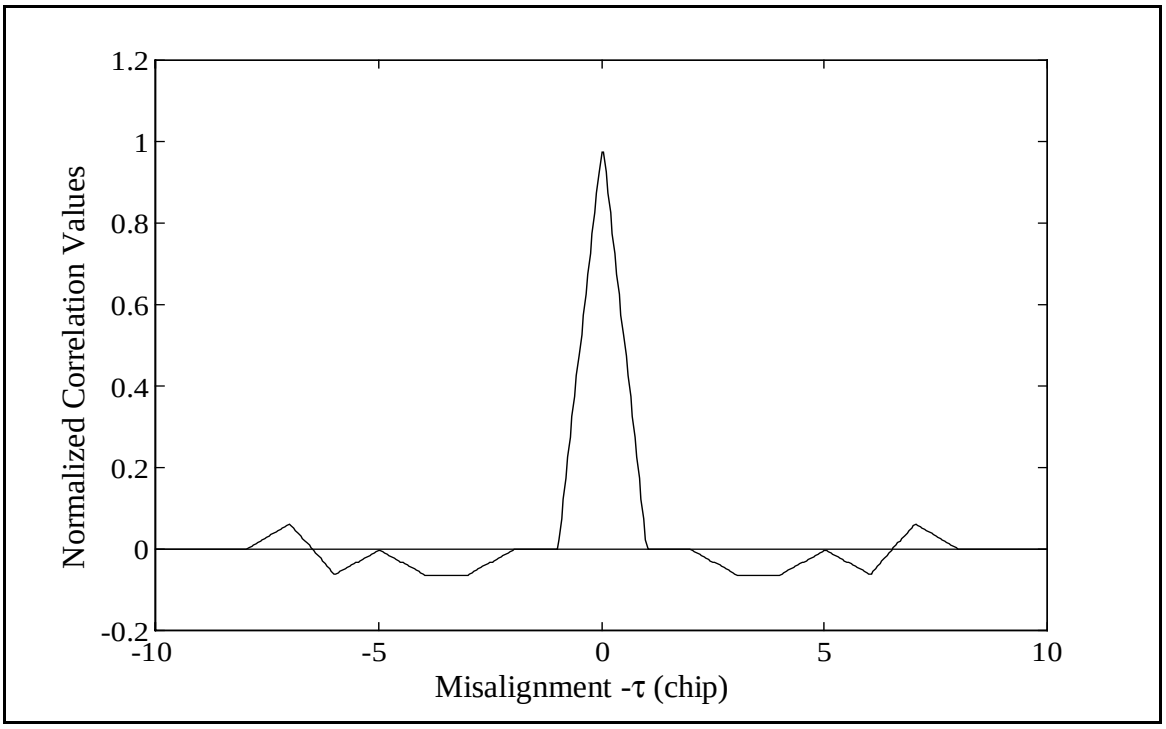

Figure 4.8: Autocorrelation properties of GPS C/A code for Satellite 3

In the frequency domain, both the P and C/A codes have one main lobe and several side lobes. In practice, the signal is band limited, so as to make the signal processing possible using the currently available technology. Through band limiting, only the main lobe and one or more side lobes are used for signal processing. As a result, sharp correlation peaks are rounded and the ends are trailed-off. Figure 4.9 shows a correlation triangle for code bandwidths of 2 MHz and 10 MHz.

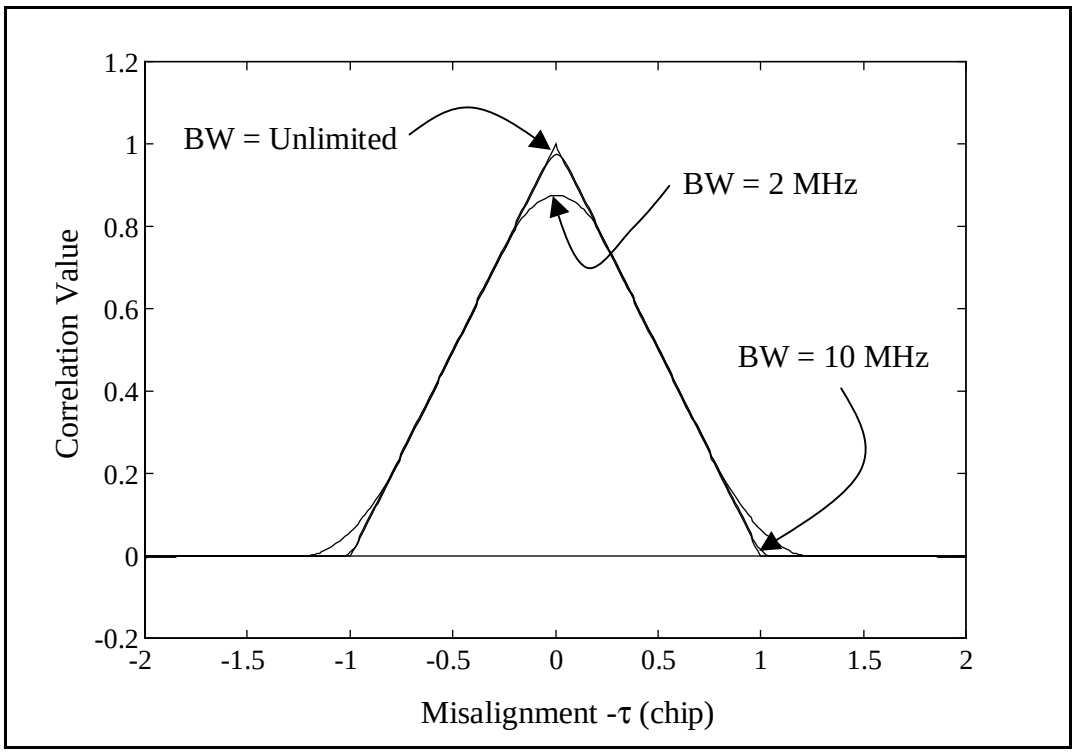

Figure 4.9: Effect of bandwidth limitation on correlation triangle

The correlation properties of GPS C/A and P codes are important considerations while designing and analyzing the receiver tracking loops. The cross-correlation values between the incoming code and the locally generated code are used in the code and carrier discriminator functions and loop filters, to generate corrections, as described in various sections in this chapter. The correlation properties in the presence of multipath signals and their effects on receiver tracking loops are described in Chapter 5.

CHAPTER 5

CHARACTERIZATION OF GPS CODE RANGE AND CARRIER PHASE MULTIPATH EFFECTS

5.1 Introduction

GPS receivers generate code range and carrier phase measurements from the receiver tracking loops, which are used for position computation in static and kinematic applications. These measurements are generally corrupted by multipath signals, and deteriorate the quality of data significantly. The effects of multipath on receiver tracking loops need to be analyzed for characterization of multipath errors in the measurements. It is generally difficult to characterize this multipath using field data, because the exact sources of the errors cannot be easily isolated.

In this chapter, the responses of receiver code and carrier tracking loops in the presence of multipath are analyzed through theoretical models. Code and carrier multipath errors are characterized in terms of their error envelopes, mean values and standard deviation values. Relationships between code, carrier and SNR multipath errors are described. In the second part of the chapter, multipath effects are analyzed from a geometrical perspective. A multipath simulation model is developed and described wherein various multipath and geometric parameters are varied and their influences observed. These parameters include; i) the reflection coefficient, ii) antenna to reflector distance, iii) reflector location, iv) existence of multiple reflectors, and v) the satellite dynamics. Only the specular component of multipath is discussed here, as the diffused component is random in nature and difficult to model in a deterministic form. This chapter is based on Ray and Cannon (1999).

5.2 Receiver Tracking Loops in the Presence of Multipath

5.2.1 Effects of Multipath on the Code Tracking Loop

The incoming GPS satellite signal in a receiver consists of a direct signal and, often, more than one reflected signal. Each of these direct and reflected signals consists of a carrier modulated by the code as well as the navigation data bits. Data bits are extracted in the receiver at a later stage, and the data bit is of no concern as long as the pre-detection integration times in the receiver tracking loops are from data bit boundary to boundary. The composite input signal, neglecting the navigation data bit and assuming that the multipath signal frequency is the same as the direct signal frequency, can be expressed from Equation 4.1 as:

$$s_I(t) = A \sum_{i=0}^{n} \alpha_i c(t - \tau_i) \cos(\omega_0 t + \gamma_i) \tag{5.1}$$

where,

- n is the number of reflected signals and n = 0 corresponds to the direct signal
- α_i are the direct and reflected signal coefficient, where α_0 corresponds to the direct signal and equal to 1, and
- γ_i is the satellite signal carrier phase, where γ_0 corresponds to the direct signal phase (rad).

The in-phase prompt correlation value (IP) can be obtained from Equation 4.3a. Assuming that the incoming and the locally generated carrier frequencies are the same, it is given by:

$$IP = \sum_{0}^{n} \alpha_i \frac{A}{2} R(\hat{\tau}_c - \tau_i) \cos(\gamma_i - \hat{\gamma}_c) \tag{5.2a}$$

where,

- $\hat{\tau}_c$ is the receiver estimate of the incoming signal code delay (m), and
- $\hat{\gamma}_c$ is the receiver estimate of the incoming signal carrier phase (rad).

Similarly, the in-phase early (IE), in-phase late (IL), quadrature-phase prompt (QP), quadrature-phase early (QE), and quadrature-phase late (QL) correlation values, as shown in Figure 4. 2 in the presence of multipath are, respectively,

$$\begin{aligned}
IE &= \sum_{0}^{n} \alpha_i \frac{A}{2} R(\hat{\tau}_c - \tau_i + T_d)\cos(\gamma_i - \hat{\gamma}_c) \\
IL &= \sum_{0}^{n} \alpha_i \frac{A}{2} R(\hat{\tau}_c - \tau_i - T_d)\cos(\gamma_i - \hat{\gamma}_c) \\
QP &= \sum_{0}^{n} \alpha_i \frac{A}{2} R(\hat{\tau}_c - \tau_i)\sin(\gamma_i - \hat{\gamma}_c) \\
QE &= \sum_{0}^{n} \alpha_i \frac{A}{2} R(\hat{\tau}_c - \tau_i + T_d)\sin(\gamma_i - \hat{\gamma}_c) \\
QL &= \sum_{0}^{n} \alpha_i \frac{A}{2} R(\hat{\tau}_c - \tau_i - T_d)\sin(\gamma_i - \hat{\gamma}_c)
\end{aligned} \qquad (5.2b\text{-}5.2f)$$

Using Equations 5.2a-5.2f for a coherent discriminator, and assuming that there is a single dominant reflector and the local carrier frequency is the same as the incoming carrier frequency, the discriminator function can be obtained from Equation 4.4 and expressed as,

$$\begin{aligned}
D_{cm} = &\{(R(\hat{\tau}_c - \tau_0 + T_d) - R(\hat{\tau}_c - \tau_0 - T_d)\}\cos(\gamma_0 - \hat{\gamma}_c) + \\
&\alpha_1\{(R(\hat{\tau}_c - \tau_1 + T_d) - R(\hat{\tau}_c - \tau_1 - T_d)\}\cos(\gamma_1 - \hat{\gamma}_c)
\end{aligned} \qquad (5.3)$$

Assuming τ_0 to be zero and replacing $\hat{\tau}_c - \tau_0$ by τ_e the following expression is obtained:

$$\begin{aligned}
D_{cm} = &\{(R(\tau_e + T_d) - R(\tau_e - T_d)\}\cos(\gamma_0 - \hat{\gamma}_c) + \\
&\alpha_1\{(R(\tau_e - \tau_1 + T_d) - R(\tau_e - \tau_1 - T_d)\}\cos(\gamma_1 - \hat{\gamma}_c)
\end{aligned} \qquad (5.4)$$

This can be rewritten as

$$D_{cm} = R_{EL}(\tau_e)\cos(\gamma_0 - \hat{\gamma}_c) + \alpha_1 R_{EL}(\tau_e - \tau_1)\cos(\gamma_1 - \hat{\gamma}_c) \qquad (5.5)$$

In Equation 5.5, the first term corresponds to an 'S' curve, due to the direct signal, and the second term corresponds to a delayed 'S' curve, due to the reflected signal. It is evident from the equation that the discriminator function value depends upon the multipath amplitude and phase.

Figures 5.1a and 5.1b show the discriminator function values due to a single reflected signal for a coherent discriminator using a standard correlator with early-late correlator spacing of one chip, and a narrow correlator with early-late spacing of one tenth of a code chip, respectively. The reflected signal is in-phase with the direct signal, and arrives half a chip delayed with respect to the direct signal. The discriminator values are plotted against the code tracking errors.

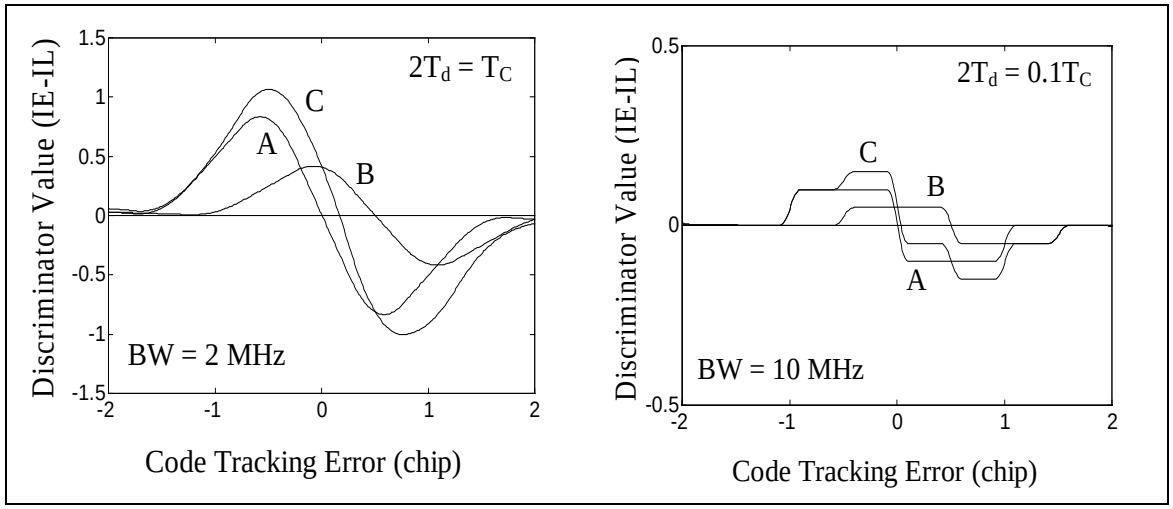

Figure 5.1a-5.1b: DLL discriminator response using correlator spacing of 1 chip and 0.1 chip respectively, in the presence of multipath signal of SMR equal to 6 dB, delayed by half code chip and has the same phase with respect to the direct signal

In Figures 5.1a and 5.1b, curve A corresponds to the 'S' curve due to direct signal and curve B corresponds to the 'S' curve due to reflected signal. The amplitude of the reflected signal is 6 dB below the amplitude of the direct signal (Signal to Multipath Ratio, $SMR = 20\log\frac{1}{\alpha_1}$). The curve C is the resultant of the other two curves. Pre-

correlation bandwidths of 2 MHz and 10 MHz are used for the standard and the narrow correlator respectively, to generate these plots.

If the received signal contains only the direct signal, then the code tracking loop tracks the zero crossing of the curve A, which corresponds to zero tracking error. However, in the presence of the multipath, the code tracking loop tracks the zero crossing of the curve C. Then, the delay between the zero crossings of the curves A and C is the multipath error. It is evident from the figure that the code tracking error is much higher in the case of a 1 chip correlator spacing, when compared with that of a 0.1 chip correlator spacing.

Figures 5.2a and 5.2b show the discriminator function value due to a single reflected signal for the same discriminators due to the same reflector as described for Figure 5.1a and 5.1b. However, now the reflected signal has a 180° phase offset with respect to the direct signal.

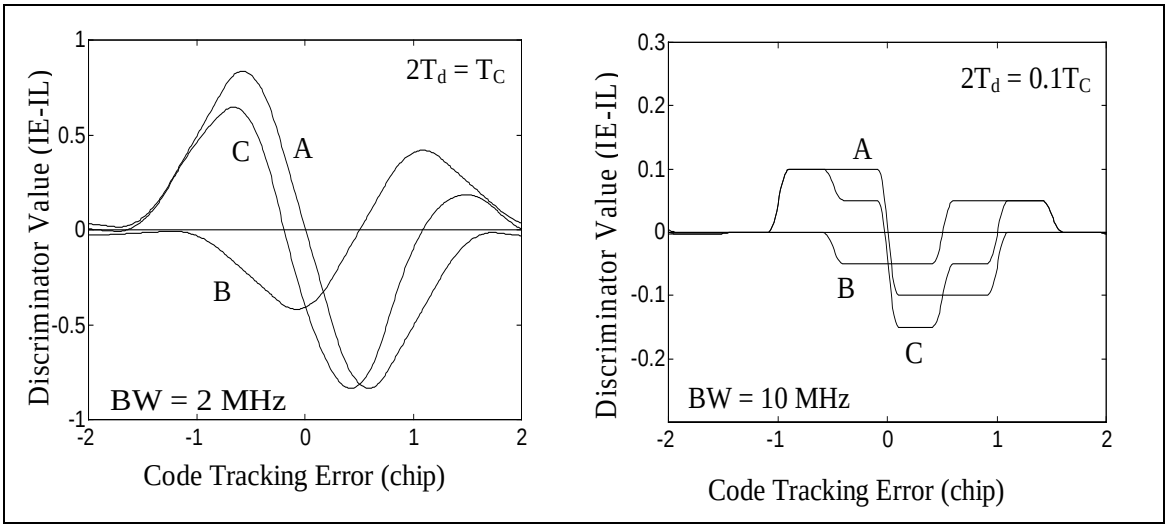

Figure 5.2a-5.2b: DLL discriminator response using correlator spacing of 1 chip and 0.1 chip, respectively, in the presence of a multipath signal of SMR equal to 6 dB, delayed by half code chip and has a 180 degrees phase offset with respect to the direct signal

Similar to the in-phase multipath signal case, the delay between the zero crossings of the curves A and C is the multipath error in this case. The sign of this error is opposite when compared with that of the in-phase reflected signal. Again, this error is much higher in the case of a 1 chip correlator spacing when compared with that of a 0.1 chip correlator spacing.

The relationship of multipath error envelope with respect to the multipath delay has been shown by Van Nee (1995) and Braasch (1996b). This has also been extensively verified for standard correlator (Braasch, 1996b) and high performance correlators (Cox et al., 1999). The error envelope with respect to multipath delay can be obtained by extending the above analysis for various multipath delays. An easy way to visualize this is to invert the 'S' curve due to the reflected signal and superimpose on the 'S' curve due to the direct signal (private communication with Dr. Braasch). The code error of $|\tau_e| \le T_d$ is the range in which the tracking loop operates under normal condition. The projection of the intersecting point of the 'S' curves on the X-axis within this sensitivity region is the zero crossing point of the resultant curve. Then, the delay between the zero crossing of the 'S' curve due to the direct signal and the projection of the intersecting point on the X-axis is the multipath error. This is illustrated in Figures 5.3a-5.3c.

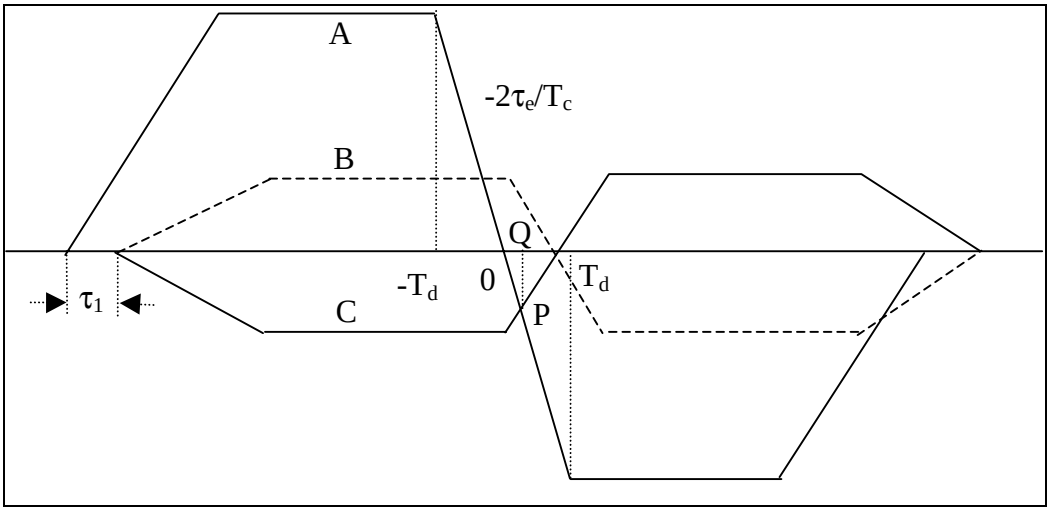

a) Multipath delay $0 \le \tau_1 < (1+\alpha_1)T_d$

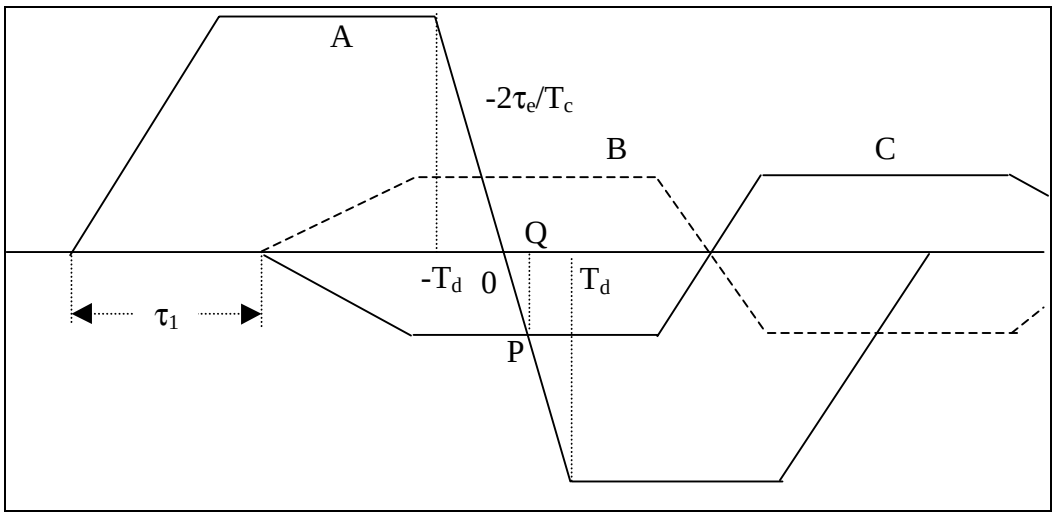

b) Multipath delay $(1+\alpha_1)T_d \le \tau_1 < T_C - (1-\alpha_1)T_d$

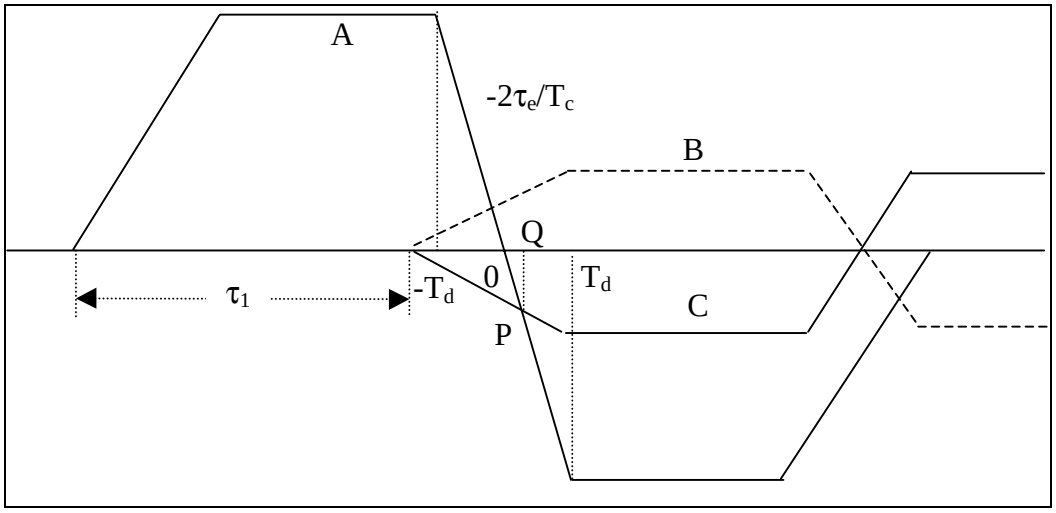

c) Multipath delay $T_C - (1-\alpha_1)T_d \le \tau_1 < T_C + T_d$

Figure 5.3a-5.3c: Multipath errors as a result of code tracking loop responses due to different multipath delays

In Figures 5.3a to 5.3c, A is the 'S' curve due to the direct signal and B is the 'S' curve due to the reflected signal, which is in-phase with the direct signal and delayed by τ_1. Curve B is inverted and named as C. The intersection point between curves A and C is the point P.

The projection of P on the X-axis is Q, which is actually the zero crossing of the resultant curve. The delay between points O and Q is then the multipath error.

It is easy to visualize from Figure 5.3a that as the multipath delay τ_1 increases, the multipath error initially increases. Beyond certain delay, the multipath error remains constant, as shown in Figure 5.3b. As the delay is further increased, the multipath error gradually decreases, until it becomes zero, which is shown in Figure 5.3c.

The upper part of the multipath error envelope (positive values) can be traced by assuming that the reflected signal is in-phase with respect to the direct signal. The lower part of the multipath error envelope (negative values) can similarly be traced, by assuming that the reflected signal is out-of-phase (180° offset) with respect to the direct signal. By employing a technique similar to the one shown in Figures 5.3a to 5.3c, the lower part of the error envelope can also be obtained. Also, it is clear that if the discriminator function characteristics of a particular DLL is known, the multipath error envelope can easily be found, using the technique demonstrated in Figures 5.3a to 5.3c.

To derive closed loop equations for the multipath error at various multipath delays, in the Equation 5.5, $R_{EL}(\tau_e)$ and $R_{EL}(\tau_e-\tau_1)$ are replaced by their values within the sensitivity range of $|\tau_e| \leq T_d$ as shown in Figure 4.4. While doing so, the expression for the former remains the same, but the expression for the later depends upon the multipath path delay (τ_1). After suitable replacements, Equation 5.5 is equated to zero and the multipath error is formulated in a closed form, as shown in Equations 5.6a to 5.6c, where, Equations 5.6a, 5.6b and 5.6c correspond to Figures 5.3a, 5.3b and 5.3c, respectively. Furthermore, in Equations 5.6a to 5.6c the upper sign of the composite sign (i.e. '+' in '±', or '–' in '∓') is for the in-phase multipath corresponding to the upper part of the error envelope, and the lower sign of the composite sign is for the out-of-phase multipath corresponding to the lower part of the error envelope.

In the range of $0 \le \tau_1 < (1 \pm \alpha_1)T_d$

$$D_{cm} = \frac{-2\tau_e}{T_C} \quad \frac{2\alpha_1(\tau_e - \tau_1)}{T_C} = 0$$
$$\tau_e = \pm \frac{\alpha_1 \tau_1}{1 + \alpha_1} \tag{5.6a}$$

In the range of $(1 \pm \alpha_1)T_d \le \tau_1 < T_C - (1 \quad \alpha_1)T_d$

$$D_{cm} = \frac{-2\tau_e}{T_C} \pm \frac{2\alpha_1 T_d}{T_C} = 0$$
$$\tau_e = \pm \alpha_1 T_d \tag{5.6b}$$

In the range of $(T_C - (1 \quad \alpha_1)T_d \le \tau_1 < T_C + T_d$

$$D_{cm} = \frac{-2\tau_e}{T_C} \quad \frac{\alpha_1(T_C + T_d + \tau_e - \tau_1)}{T_C} = 0$$
$$\tau_e = \pm \frac{\alpha_1(T_C + T_d - \tau_1)}{2 \quad \alpha_1} \tag{5.6c}$$

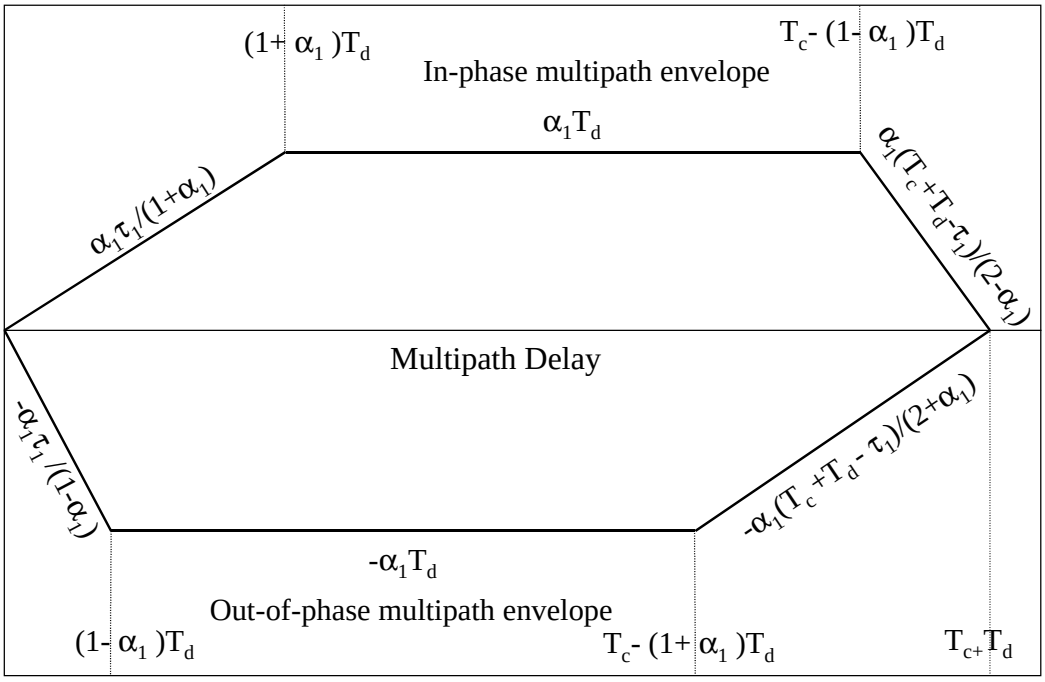

Figure 5.4: Multipath error envelope with respect to multipath delay

Figure 5.4 shows the error envelope with respect to the multipath delay. This shows that the multipath error envelope is non-symmetric about the time delay axis. The magnitude of the error initially increases with the multipath delay, and becomes constant after a particular multipath delay. Beyond another particular multipath delay, the multipath error envelope magnitude decreases before it diminishes.

Multipath error envelopes for some of the special cases are shown in Figure 5.5. They are for a standard correlator of one chip early-late spacing for C/A and P code tracking, and assuming zero correlation side lobes. The envelope is also shown for a narrow correlator of one tenth of a chip early-late spacing for the C/A code tracking. It is clear from the figure that narrowing the correlator spacing decreases the maximum and the minimum values of multipath error. Furthermore, the maximum path delay, beyond which reflected signals do not cause multipath error, is 1.05 chip for the narrow correlator and 1.5 chip for the standard correlator.

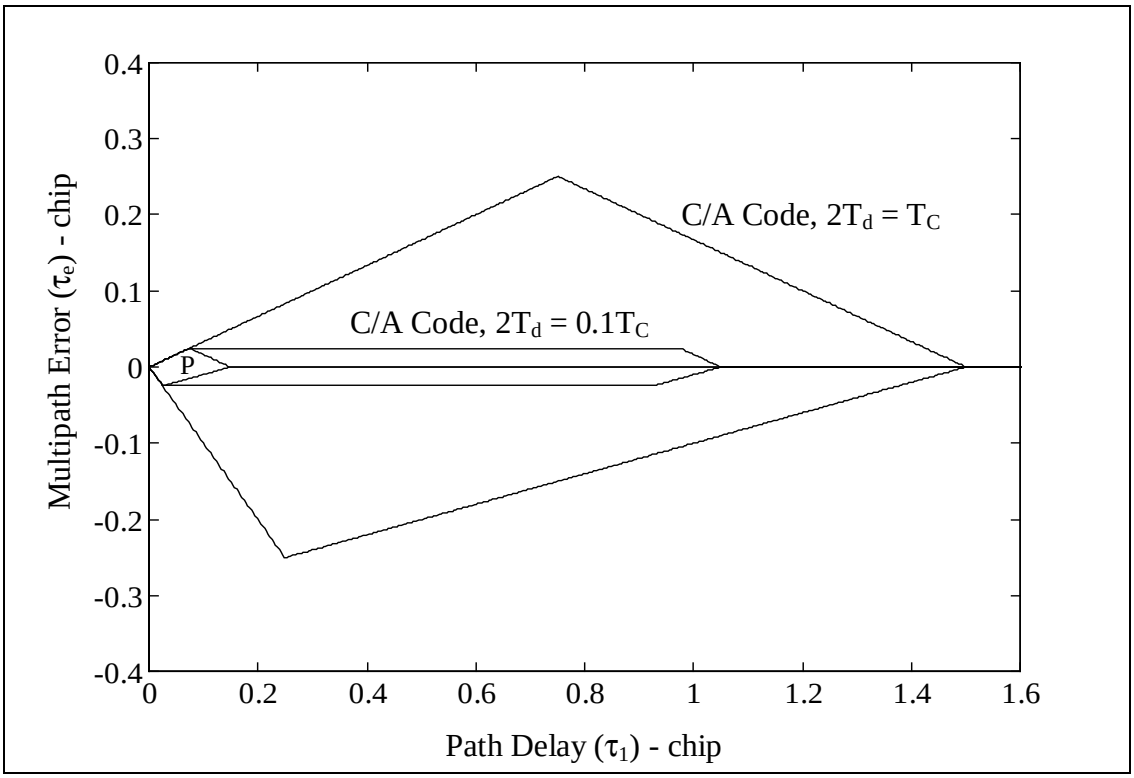

Figure 5.5: Multipath error envelope with respect to multipath delay for some special cases

In practice, however, the incoming signal is band limited. As a result, the correlation triangle is rounded-off near the peak and trailed-off near the end, as was shown in Figures 4.5 and 4.9. This affects the multipath error envelopes. Figure 5.6 shows the multipath error envelope for a standard correlator of one chip early-late spacing, and a narrow correlator of one tenth of a chip early-late spacing for the C/A code tracking with band limitation. A pre-correlation bandwidth of 2 MHz was used for the standard correlator, and 2 MHz and 10 MHz were used for the narrow correlator.

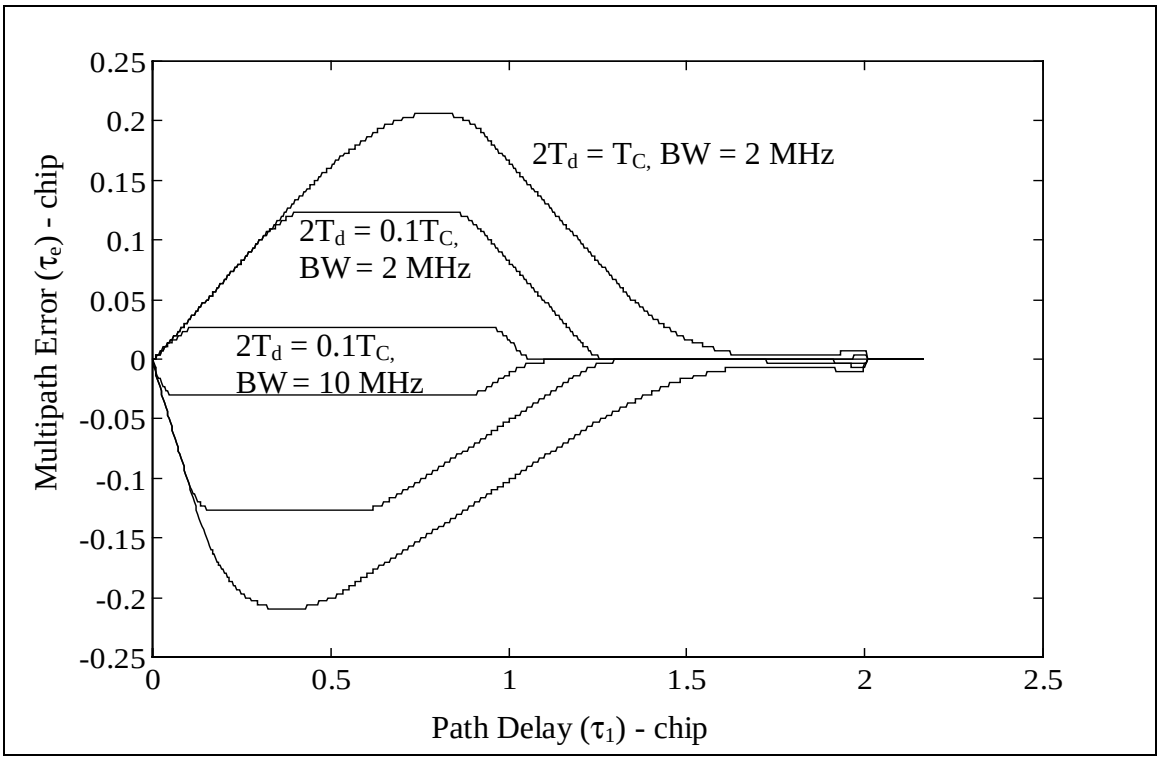

Figure 5.6: Multipath error envelope with respect to multipath delay for some special cases with band limitation

Several observations can be made from Figure 5.6. They are:

a) The maximum and minimum errors using a standard correlator are much higher when compared with that of the narrow correlator.

b) The pre-correlation bandwidth affects the maximum error value. In the illustrated example, a narrow correlator with a 10 MHz bandwidth shows superior performance compared to a narrow correlator with a 2 MHz bandwidth.

c) As the pre-correlation bandwidth is reduced, the sharp edges of the envelope are rounded off. This also causes multipath errors, due to multipath delays further than the theoretical limit of (T_C+T_d).

d) In the case of a standard correlator, the multipath error beyond a multipath delay of 1.5 chip does not become zero. This is because the C/A code autocorrelation characteristic is such that it has one major peak of a correlation value of 1023, and many minor peaks of correlation values 63 and -65. If a reflected signal arrives more than 1.5 chip delayed, it may cause a minor peak or a non-zero correlation value. This will influence the 'S' curve due to the direct signal, and introduce multipath errors as evident at around a two chip delay in the figure. The effect of autocorrelation side lobes on multipath errors was first shown by Braasch (1997).

The multipath error envelope, however, shows only the contours of the maximum and minimum values of the error for various multipath delays. In reality, the multipath error oscillates between the upper and lower boundary, depending upon the multipath phase, i.e. the relative phase of the reflected signal with respect to the direct signal at the antenna phase centre. The contours were obtained when the multipath phases were 0° and 180°.

Figures 5.7 and 5.8 show the multipath error in the short multipath delay. The multipath phase is obtained directly from the path delay. An SMR of 3 dB and 20 dB are used for the simulation. The plots also show the mean values of the errors.

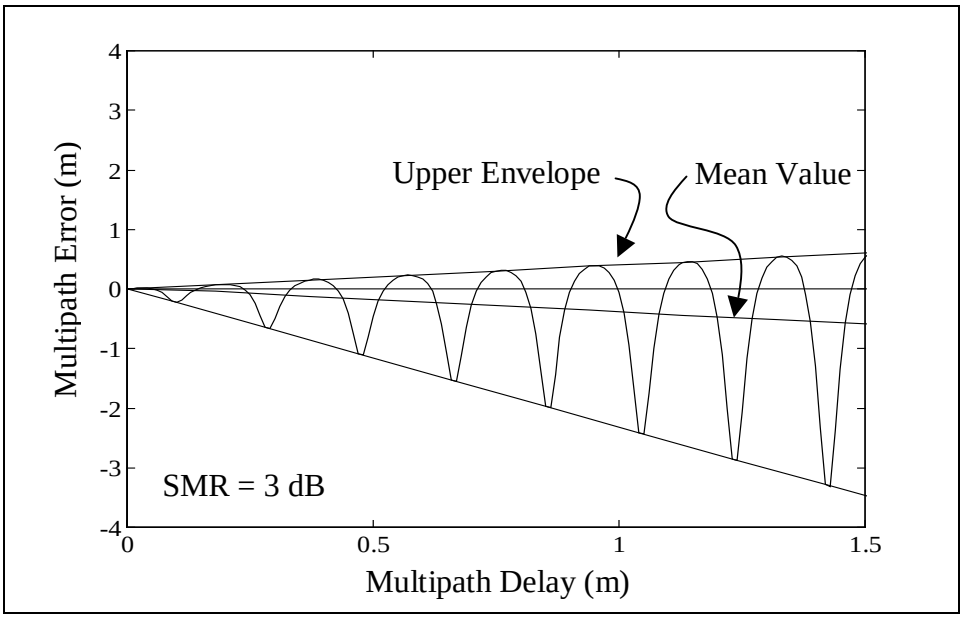

Figure 5.7: Multipath error pattern for short multipath delays due to a reflected signal of SMR = 3 dB

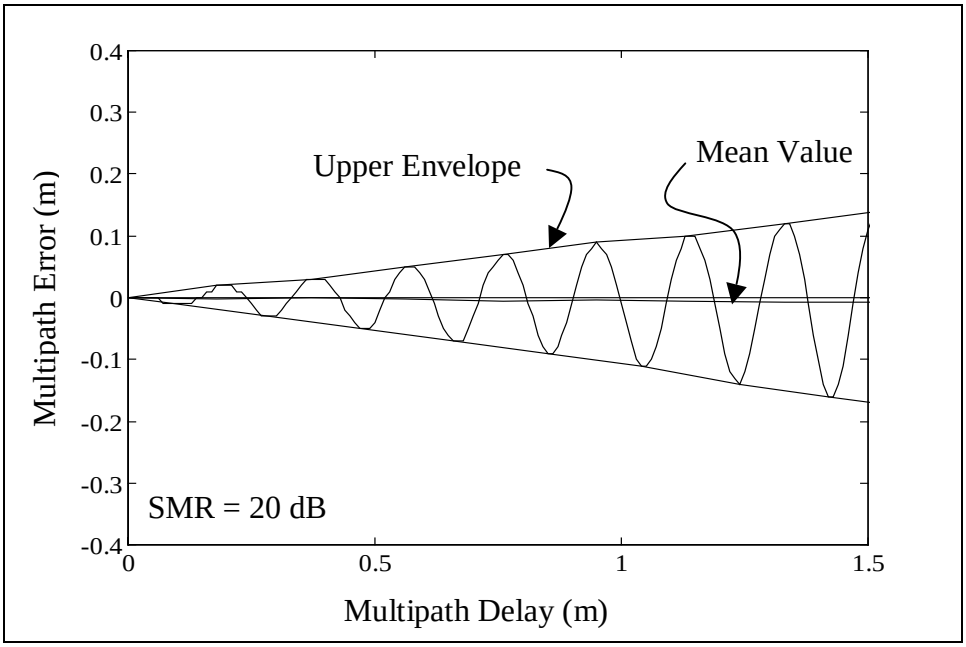

Figure 5.8: Multipath error pattern for short multipath delays due to a reflected signal of SMR = 20 dB

Several observations can be made from Figures 5.7 and 5.8:

a) Multipath errors due to a weak multipath signal have sinusoidal patterns, but for a strong multipath signal, the patterns are quite different. That is because a strong multipath signal causes non-sinusoidal carrier multipath errors, which in turn affect the code multipath errors, as evident from Equation 5.5.
b) The magnitude of the error is proportional to the strength of the multipath signal. In this example, the strong reflection caused multipath, which was of one order magnitude higher compared to its weaker counterpart.
c) The mean value of the multipath error is non-zero. For a short multipath delay, the mean multipath error is negative while using correlator spacing of 1 chip. Also, this mean value is higher for stronger multipath.

Figures 5.9a to 5.9b show the mean and standard deviation of multipath errors with respect to multipath delays for different multipath strengths using a standard correlator. These were computed by varying the reflected signal relative phase in discrete steps of $1/19^{th}$ of a cycle and then computing the multipath error at each step, and then taking their statistics. There was no bandwidth limitation in these simulations. This mean error is not only non-zero, but reaches several tens of metres for the C/A code due to strong multipath. Initially the mean error is negative, but reaches a positive maximum value prior to becoming zero, at a 1.5 chip delay. The standard deviation is also quite high.

Figures 5.10a and 5.10b are the mean and standard deviation of the multipath errors with respect to multipath delays using a correlator spacing of 0.1 chip. The mean value of the multipath error for the C/A code easily becomes several metres for strong reflections, even in this case.

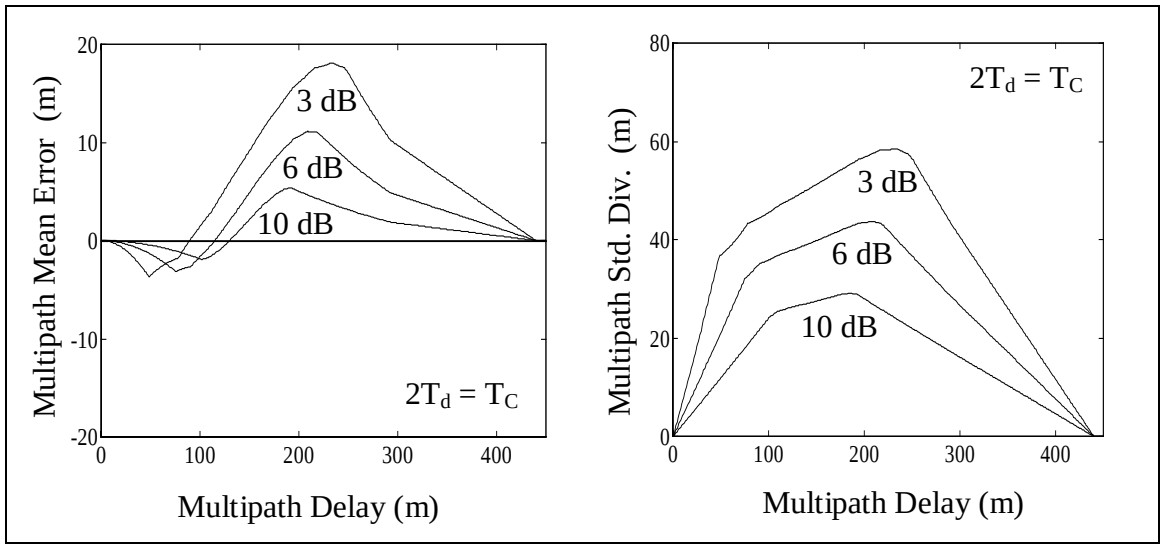

Figure 5.9a-5.9b: Mean and standard deviation of multipath errors for different multipath signal strengths while using a correlator spacing of 1 chip for C/A code in a coherent discriminator

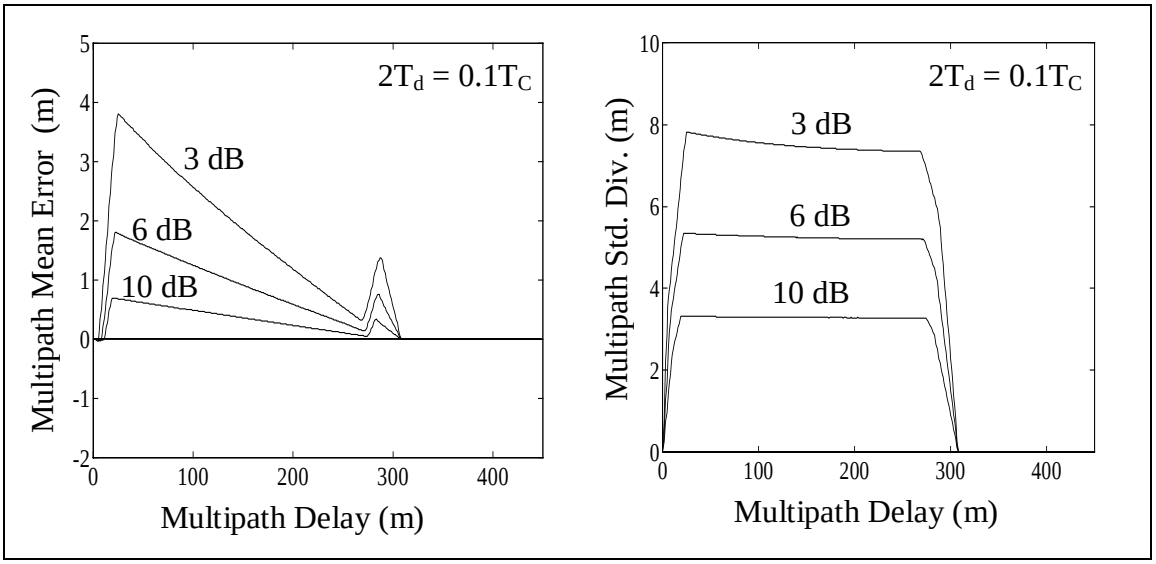

Figure 5.10a-5.10b: Mean and standard deviation of multipath errors for different multipath signal strengths while using a correlator spacing of 0.1 chip for C/A code in a coherent discriminator

In practice, however, a non-coherent type of discriminator is used for code tracking, and a dot-product type of discriminator is one such example. The following analysis is carried out for a non-coherent dot-product type of discriminator, as subsequent analysis with field data was done with a receiver employing this type of discriminator.

For a non-coherent dot-product discriminator, the discriminator function is given by (From Table 4.2),

$$D_n = IP(IE - IL) + QP(QE - QL) \tag{5.7a}$$

In the presence of a single dominant reflector, Equation 5.7a can be expressed by replacing correlators expressions from Equations 5.2a to 5.2f and is given by,

$$\begin{aligned} D_{nm} = & \sum_{i=0}^{1} \alpha_i R(\hat{\tau}_c - \tau_i)\cos(\gamma_i - \hat{\gamma}_c)\left\{\begin{array}{l} \sum_{i=0}^{1} \alpha_i R(\hat{\tau}_c - \tau_i + T_d)\cos(\gamma_i - \hat{\gamma}_c) \\ -\sum_{i=0}^{1} \alpha_i R(\hat{\tau}_c - \tau_i - T_d)\cos(\gamma_i - \hat{\gamma}_c) \end{array}\right\} \\ & + \sum_{i=0}^{1} \alpha_i R(\hat{\tau}_c - \tau_i)\sin(\gamma_i - \hat{\gamma}_c)\left\{\begin{array}{l} \sum_{i=0}^{1} \alpha_i R(\hat{\tau}_c - \tau_i + T_d)\sin(\gamma_i - \hat{\gamma}_c) \\ -\sum_{i=0}^{1} \alpha_i R(\hat{\tau}_c - \tau_i - T_d)\sin(\gamma_i - \hat{\gamma}_c) \end{array}\right\} \end{aligned} \tag{5.7b}$$

Equation 5.7b can be expanded and simplified to obtain the following expression (see Appendix A for details),

$$\begin{aligned} D_{nm} = & R(\hat{\tau}_c - \tau_0)\{R(\hat{\tau}_c - \tau_0 + T_d) - R(\hat{\tau}_c - \tau_0 - T_d)\} + \\ & \alpha_1^2 R(\hat{\tau}_c - \tau_1)\{R(\hat{\tau}_c - \tau_1 + T_d) - R(\hat{\tau}_c - \tau_1 - T_d)\} + \\ & \left\{\begin{array}{l} \alpha_1 R(\hat{\tau}_c - \tau_0)[R(\hat{\tau}_c - \tau_1 + T_d) - R(\hat{\tau}_c - \tau_1 - T_d)] + \\ \alpha_1 R(\hat{\tau}_c - \tau_1)[R(\hat{\tau}_c - \tau_0 + T_d) - R(\hat{\tau}_c - \tau_0 - T_d)] \end{array}\right\}\cos(\gamma_0 - \gamma_1) \end{aligned} \tag{5.7c}$$

This can be rewritten as

$$D_{nm} = R(\hat{\tau}_c - \tau_0)\{R_{EL}(\hat{\tau}_c - \tau_0)\} + \alpha_1^2 R(\hat{\tau}_c - \tau_1)\{R_{EL}(\hat{\tau}_c - \tau_1)\} \\ \alpha_1\{R(\hat{\tau}_c - \tau_0)[R_{EL}(\hat{\tau}_c - \tau_1)] + R(\hat{\tau}_c - \tau_1)[R_{EL}(\hat{\tau}_c - \tau_0)]\}\cos(\gamma_0 - \gamma_1) \quad (5.7d)$$

For continuous tracking, D_{nm} is equated to zero and the resultant delay error is computed. Equation 5.7d does not have the term $\hat{\gamma}_c$, which appeared in Equation 5.5. That means that in this case, (or for that matter, in any non-coherent discriminator), code tracking does not depend upon the carrier phase tracking, as long as the carrier frequency is locked. The multipath error can be computed by assuming that $\tau_0 = 0$; in that case $\hat{\tau}_c$ is the multipath error. More details on this are given in Chapter 6.

Multipath error envelopes for some of the special cases are shown in Figures 5.11a and 5.11b. They are for an early-late correlator spacing of 1 chip and 0.1 chip respectively for the C/A code tracking. It is clear from the figures that, similar to a coherent type of discriminator, narrowing the correlator spacing decreases the maximum and minimum values of the multipath error. The multipath error envelopes are nearly the same for both coherent and dot-product type of non-coherent discriminators.

Figures 5.12a and 5.12b show the mean and standard deviation of the multipath errors with respect to multipath delays for different multipath strengths using an early-late correlator spacing of 1 chip. Similarly, Figures 5.13a and 5.13b show corresponding values using an early-late correlator spacing of 0.1 chip. There was no bandwidth limitation for these simulations. Similar to a coherent discriminator case, the mean error is non-zero and becomes quite high for standard correlator spacing. For a narrow correlator spacing, the discriminator function responses of coherent and dot-product type non-coherent discriminators are nearly the same, and therefore, the error statistics are also nearly the same. For a wide correlator spacing, however, the statistics are slightly different.

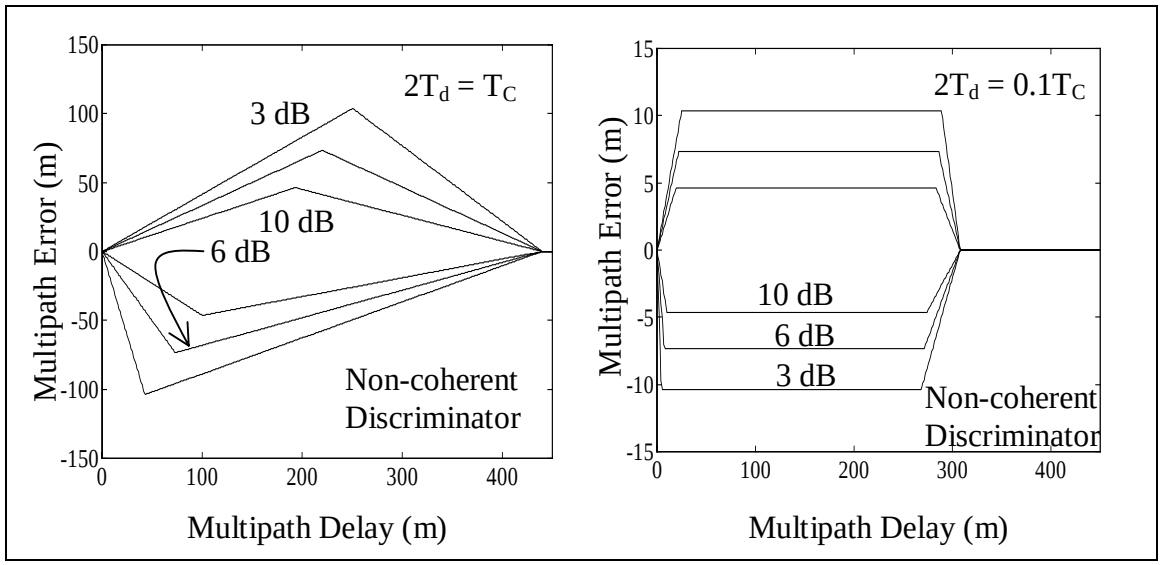

Figure 5.11a-5.11b: Multipath error envelopes with respect to multipath delays using a dot-product discriminator with early late correlator spacings of a) 1 chip and b) 0.1 chip for various signal strengths

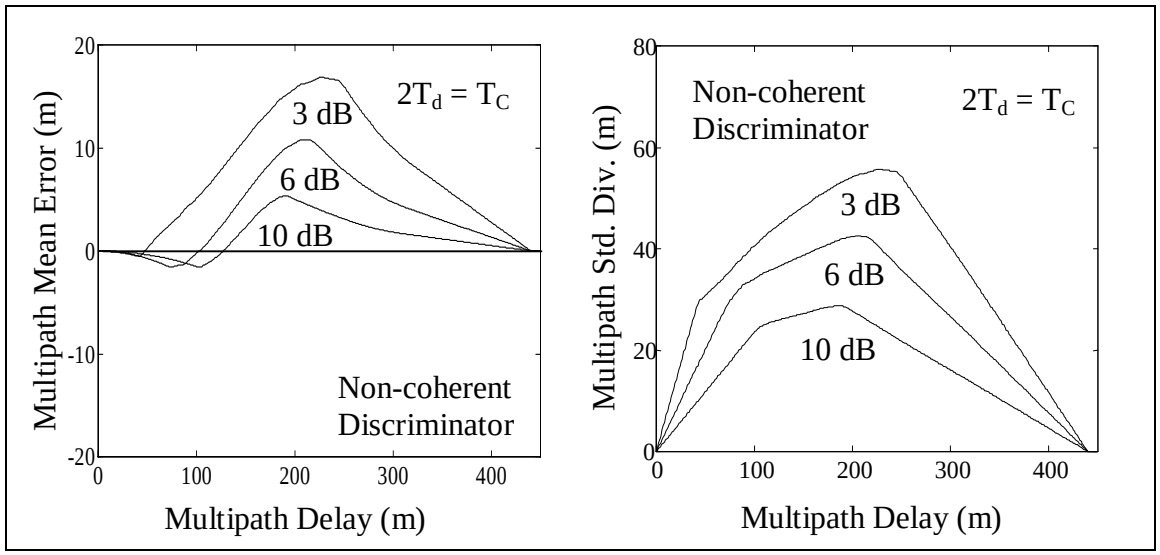

Figure 5.12a-5.12b: Mean and standard deviation of multipath errors for different multipath signal strengths while using a correlator spacing of 1 chip for C/A code in a dot-product discriminator

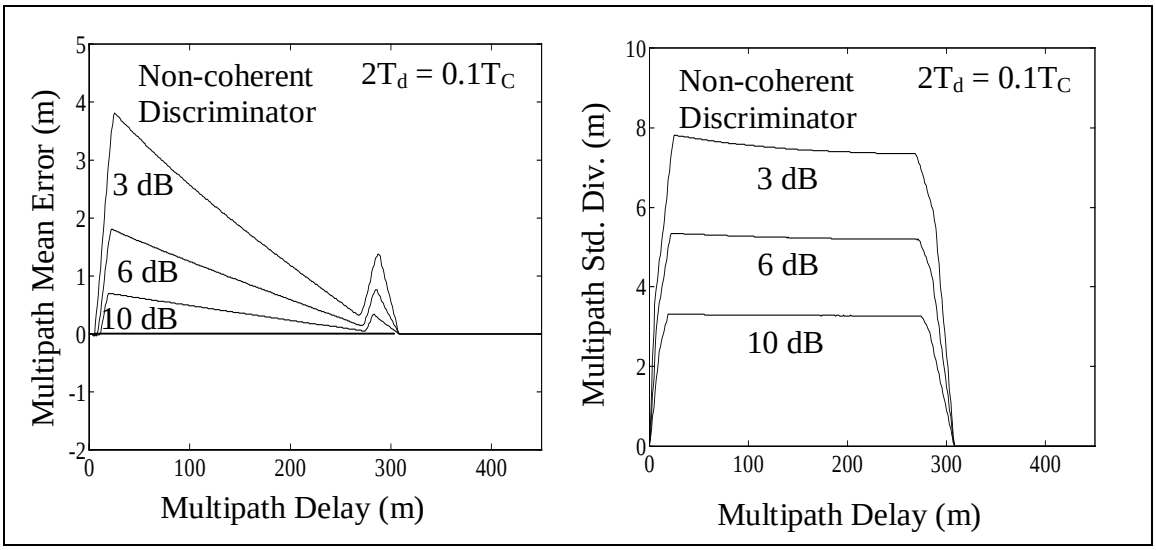

Figure 5.13a-5.13b: Mean and standard deviation of multipath errors for different multipath signal strengths while using a correlator spacing of 0.1 chip for C/A code in a dot-product discriminator

The above analysis on coherent and non-coherent discriminator functions assumes that the multipath frequency is low and comparable to the loop bandwidth of the code tracking filter. This is generally the case for stationary receivers, where the multipath frequency is due to satellite dynamics only. In cases where the multipath frequency is high compared to the loop bandwidth of the code tracking filter, the filter can not track the fast varying multipath. Under such situations, the filter tracks the time-average of the 'S' curve zero crossing (Van Nee, 1995). More recent results on this is available in Kelly and Braasch (2000).

5.2.2 Effects of Multipath on the Carrier Tracking Loop

In a GPS receiver, the carrier phase is measured by accumulating the phase of the NCO output as shown in Figure 4.2. In a benign environment, where there are no reflected signals, the incoming signal carrier is the same as the direct signal carrier. The NCO-generated local carrier locks onto the direct carrier very accurately, and, as a result, the true phase difference between the incoming signal carrier and the locally generated

carrier is nearly zero, (actually zero mean), at steady state. The resulting phase measurements are very accurate. In the presence of multipath, however, the composite signal phase shifts from the direct signal phase, and the NCO-generated local carrier locks onto the composite carrier phase, resulting in an error in the phase measurement. This error is equal to the difference between the composite signal carrier phase and the direct signal carrier phase.

Using Equations 5.2a to 5.2f and assuming that there is a single dominant reflector and the local carrier frequency is the same as the incoming carrier frequency, the arctan discriminator function (from Table 4.3) can be expressed as,

$$\begin{aligned} D_{rm} &= \arctan\left(\frac{QP}{IP}\right) \\ &= \arctan\left(\frac{R(\hat{\tau}_c - \tau_0)\sin(\gamma_0 - \hat{\gamma}_c) + \alpha_1 R(\hat{\tau}_c - \tau_1)\sin(\gamma_1 - \hat{\gamma}_c)}{R(\hat{\tau}_c - \tau_0)\cos(\gamma_0 - \hat{\gamma}_c) + \alpha_1 R(\hat{\tau}_c - \tau_1)\cos(\gamma_1 - \hat{\gamma}_c)}\right) \end{aligned} \tag{5.8}$$

The carrier tracking loop tries to minimize D_{rm} during signal tracking, and generally its value will be close to zero (actually zero mean). Assuming τ_0 and γ_0 to be zero, replacing $\Delta\Psi = \hat{\gamma}_c - \gamma_0$, equating Equation 5.8 to zero, and by performing the proper manipulation, the following expression is obtained (see Appendix B for details):

$$\Delta\Psi = \arctan\left(\frac{\alpha_1 R(\hat{\tau}_c - \tau_1)\sin\gamma_1}{R(\hat{\tau}_c) + \alpha_1 R(\hat{\tau}_c - \tau_1)\cos\gamma_1}\right) \tag{5.9}$$

Here, $\Delta\Psi$ is the difference between the composite signal phase, (which is tracked by the receiver), and the direct signal phase; it is therefore the carrier phase multipath error. From Equation 5.9, it is clear that the reflection coefficient, multipath delay and the multipath phase are the multipath parameters. These multipath parameters are always defined with respect to the direct signal.

Furthermore, from Equation 5.9, it can be observed that the multipath error amplitude (in radians) is independent of the carrier wavelength. This means that the L1 and L2 carriers will have the same amplitude of multipath error (in radians). The amplitude is also a function of the multipath phase, or the antenna-reflector distance through the correlation function. If the multipath delay is large (which generally happens when the reflector is far away from the antenna), the correlation value decreases and so does the multipath error amplitude. As the delay approaches the PRN code chip, the correlation value, as well as the multipath error, diminish.

The carrier phase multipath error is better illustrated using a phasor diagram as shown in Figure 5.14. In Figure 5.14, the multipath phase (i.e. the reflected signal relative phase with respect to the direct signal phase), determines the instantaneous value of the multipath error for a particular reflected signal. It is evident from the phasor diagram that for the relative phases of 0° and 180°, the phase multipath error is zero.

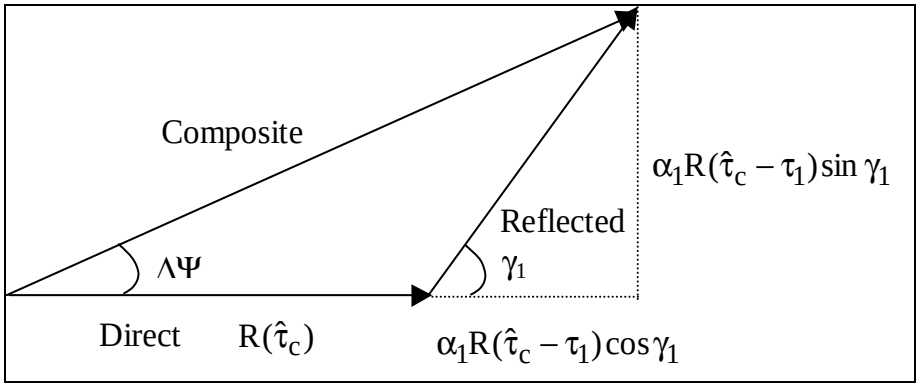

Figure 5.14: Phasor diagram of direct, reflected and composite signals and carrier phase multipath error

Figures 5.15a and 5.15b show multipath errors for short multipath delays due to reflectors with SMR equal to 20 dB and 3 dB respectively. In the former case, the error has small magnitude and a sinusoidal pattern, whereas in the latter case the error magnitude is quite high and has a saw-tooth pattern. In both the cases however, the mean values are zero.

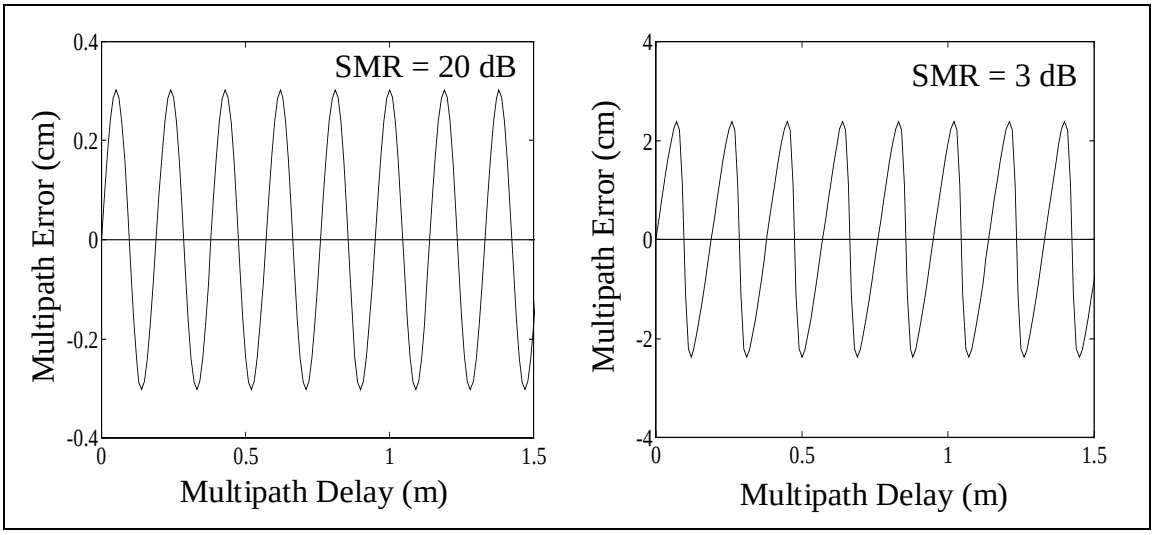

Figure 5.15: Carrier phase multipath error pattern for short multipath delays due to a reflected signal of SMR equal to a) 20 dB and b) 3 dB

The multipath error reaches an absolute maximum when the reflected signal phasor is perpendicular to the composite signal phasor (in Figure 5.14). The maximum value is then given by

$$\Delta\Psi = \arcsin\left(\frac{\alpha_1 R(\hat{\tau}_c - \tau_1)}{R(\hat{\tau}_c)}\right) \tag{5.10}$$

The multipath phases corresponding to the maxima and minima of the error can be computed by differentiating Equation 5.9 with respect to γ_1, equating it to zero, and solving for γ_1. By performing the steps described above (see Appendix C for details) it can be determined that the multipath errors reach the maxima and minima at $\gamma_1(\max) = \cos^{-1}\left(-\frac{\alpha_1 R(\hat{\tau}_c - \tau_1)}{R(\hat{\tau}_c)}\right)$ and $\gamma_1(\min) = 2\pi - \cos^{-1}\left(-\frac{\alpha_1 R(\hat{\tau}_c - \tau_1)}{R(\hat{\tau}_c)}\right)$.

Figure 5.16 shows error envelopes of the L1 carrier phase multipath with respect to the multipath delay for different multipath signal strengths using a coherent discriminator for the code DLL and employing a correlator spacing of 0.1 code chip. The error envelopes are quite similar when a dot-product type of discriminator is used for the code DLL and a

similar correlator spacing is employed. From the figure it is clear that multipath signals with path delays of more than one chip generally do not affect the phase measurements when a narrow correlator is used for the code DLL.

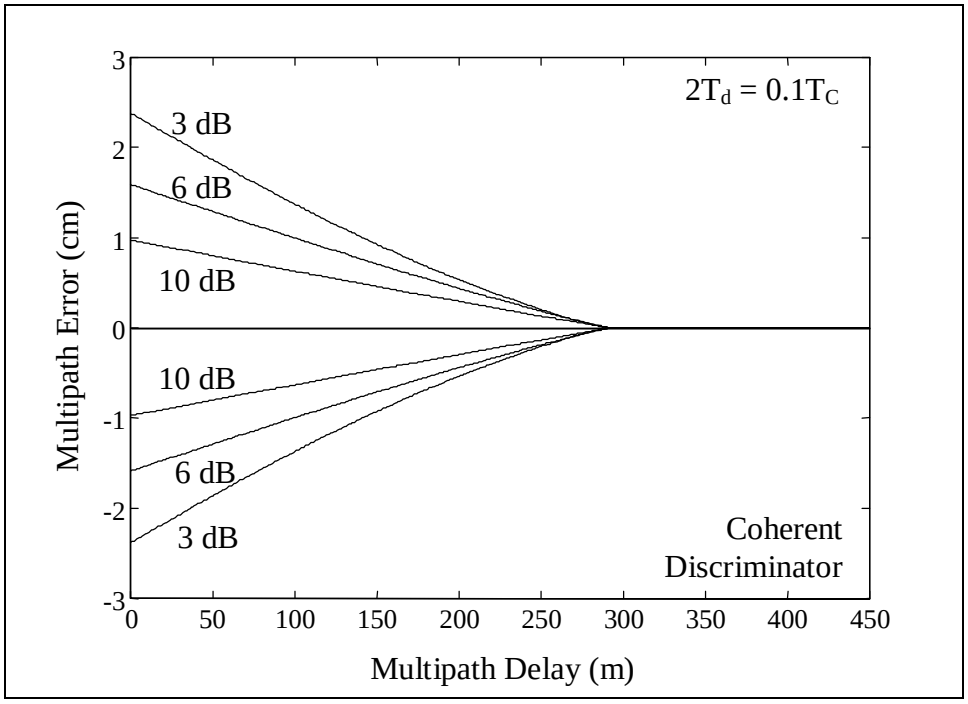

Figure 5.16: L1 Carrier phase multipath error envelope for different multipath signal strength using correlator spacing of 0.1 chip for code DLL

Figure 5.17 shows similar error envelopes using a dot-product discriminator for a code DLL, and employing a correlator spacing of 1 code chip. The envelopes are similar for a coherent discriminator as well employing the same correlator spacing. It can be seen that, in this case, the envelopes are extended beyond one code chip delay of the multipath signal. Figures 5.16 and 5.17 do not assume any band limitation.

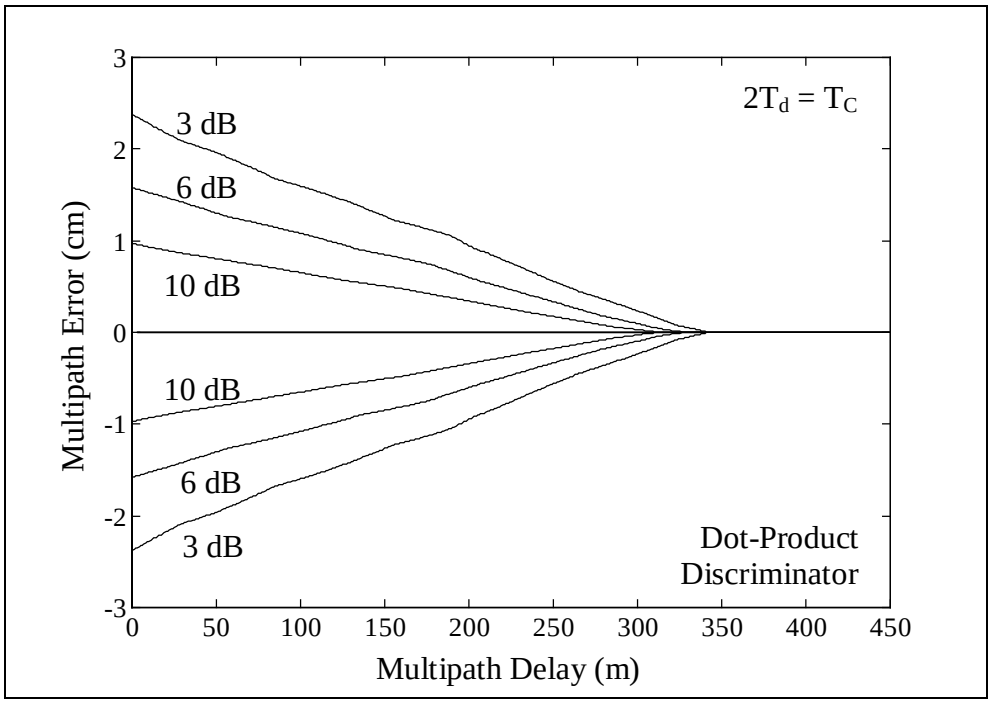

Figure 5.17: L1 Carrier phase multipath error envelope for different multipath signal strength using correlator spacing of 1 chip in the code DLL

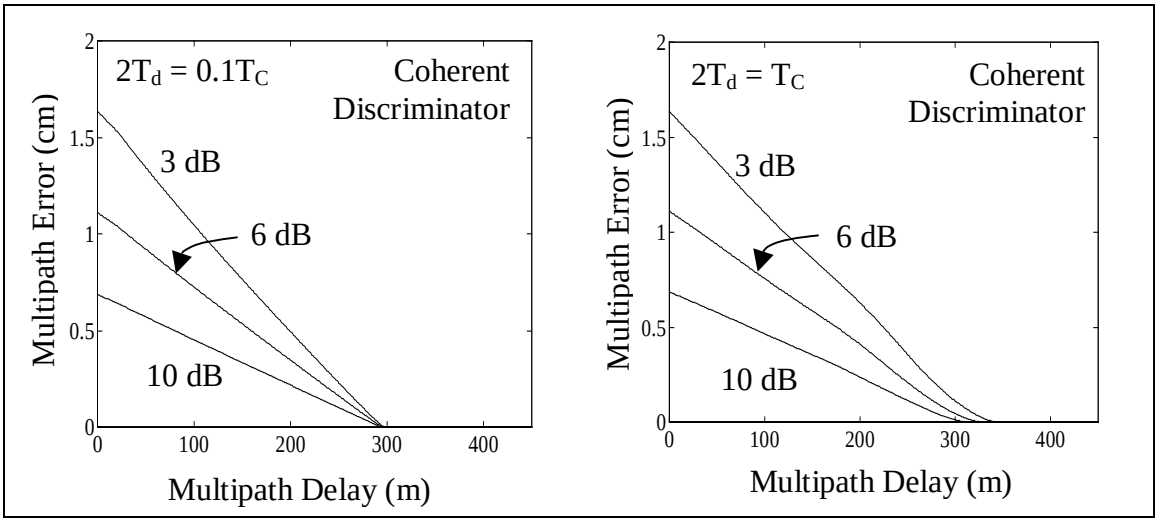

Figure 5.18a-5.18b: Standard deviations of L1 carrier phase multipath errors using coherent discriminator for code DLL with correlator spacings of a) 0.1 chip and b) 1 chip

Figures 5.18a and 5.18b show the standard deviations of the carrier phase multipath errors with respect to multipath delays for different multipath strengths using a correlator spacing of 0.1 chip and 1 chip respectively, and using a coherent discriminator for code tracking. The mean values of the multipath errors were found to be zero. This was computed by varying the reflected signal relative phase in discrete steps of $1/19^{th}$ of a cycle, computing the multipath error at each step, and then taking their statistics. The code multipath errors were taken into consideration while determining the carrier multipath errors using Equation 5.9.

Figures 5.19a and 5.19b show the standard deviations of the carrier phase multipath errors with respect to multipath delays for different multipath strengths using a correlator spacing of 0.1 chip and 1 chip, respectively, and using a dot-product type of discriminator for code tracking. Here, too, the mean values were found to be zero. The standard deviation plots are quite similar to those of a coherent discriminator. The subtle differences, if any, are due to the differences in the code multipath errors in different types of discriminator functions for code tracking.

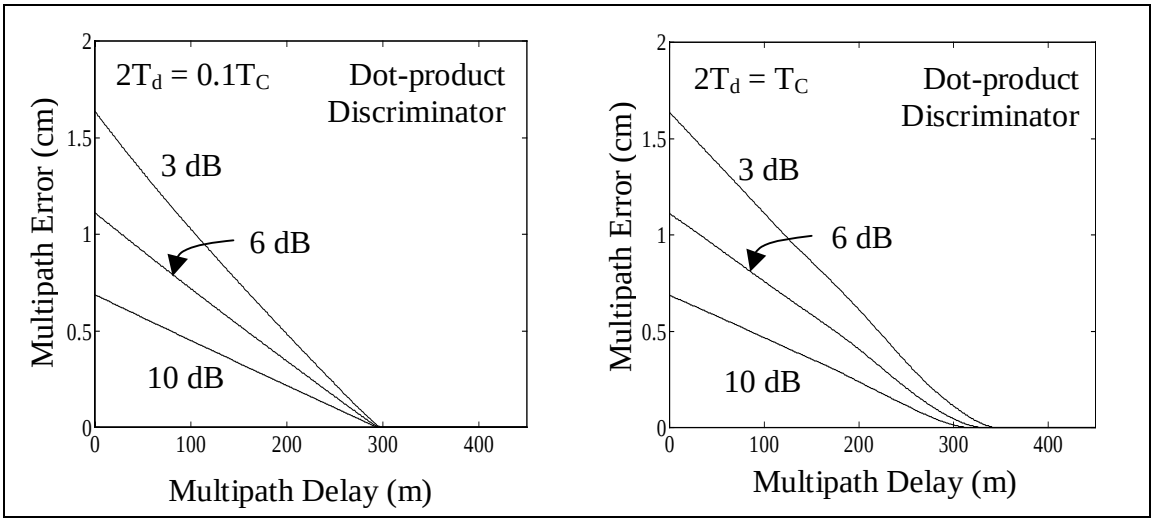

Figure 5.19a-5.19b: Standard deviations of L1 carrier phase multipath errors using dot-product discriminator for code DLL with correlator spacings of a) 0.1 chip and b) 1 chip

Unlike code multipath errors, which are largely affected by the pre-detection bandwidth, carrier multipath errors are not greatly affected by the bandwidth limitation. Lowering the bandwidth has two affects: a) the code multipath errors depend on the bandwidth and, in turn, affect the carrier multipath errors, and b) the change in shape of the prompt correlation triangle (in Figure 4.9) affects the carrier multipath errors.

5.2.3 Effects of Multipath on the SNR

A GPS signal is transmitted from the satellite through a shaped pattern antenna array to compensate for the increased path loss to the users at low elevation angles (Spilker, 1996). Another element that affects the signal power at the receiver is the antenna gain pattern. The antenna gain pattern, in reality, may be quite different from its ideal shape, due to the effects of the ground plane, nearby large metal structures, or proximity to other antennas.

Multipath affects not only the code range and carrier phase measurements, but also the measured signal power, which is an average of the composite signal power due to the direct and reflected signal carrier. As the reflected signal adds constructively and destructively with the direct signal (as the relative phase varies with time), the power of the composite signal also varies with time, and so does the measured power.

It should be emphasized that the code and data bits in the GPS signal do not contribute to the signal power, as they merely change the phase of the carrier depending upon the modulation technique employed. The signal power with or without the data and code bits remains the same. Therefore, the receiver determines the power of the carrier, not code and data, and generally expresses it as the ratio of average signal power to noise power spectral density or C/N_0 (Spilker, 1996).

In a receiver, the average signal power is generally measured using the prompt correlators and is given by,

$$P = IP^2 + IQ^2 \tag{5.11}$$

By assuming a uniform antenna gain pattern and a single dominant reflector, and by replacing the values of IP and IQ from Equations 5.2a to 5.2f, the signal power can be found and is given by,

$$\begin{aligned} P &= R^2(\hat{\tau}_c) + \alpha_1^2 R^2(\hat{\tau}_c - \tau_1) + 2\alpha_1 R(\hat{\tau}_c) R(\hat{\tau}_c - \tau_1)\cos\gamma_1 \\ &= R^2(\hat{\tau}_c)\left(1 + \alpha_1^2 \alpha'^2 + 2\alpha_1 \alpha' \cos\gamma_1\right) \end{aligned} \tag{5.12}$$

where the correlation ratio is, $\alpha' = \dfrac{R(\hat{\tau}_c - \tau_1)}{R(\hat{\tau}_c)}$. (5.13)

From Equation 5.12, the average signal power in the receiver is a function of the reflection coefficient, multipath delay and multipath phase.

Using Equation 5.12 it is easy to relate the reflection coefficient and correlation ratio with the C/N_0 using Equation 5.14 (see Appendix D for details).

$$\alpha_1 \alpha' = \frac{\sqrt{R} - 1}{\sqrt{R} + 1} \tag{5.14}$$

where, $R = \dfrac{10^{\left(\frac{(C/N_0)_{max}}{20}\right)}}{10^{\left(\frac{(C/N_0)_{min}}{20}\right)}}$. (5.15)

These relationships may be used to estimate the reflection parameters from the SNR.

Figures 5.20a and 5.20b show the SNR plots in terms of C/N_0 due to a weak (SMR = 20 dB) and a strong reflector (SMR = 3 dB), respectively. It is evident that in the case of strong multipath, the error is one order in magnitude higher compared to that of weak multipath. Also, for the strong multipath, the error has sharp changes, unlike the weak multipath case. That is because, from Equation 5.12, the signal power is a function of the code multipath error and multipath phase. As the code multipath error has sharp changes due to a strong reflector (Figure 5.7), so does the SNR pattern.

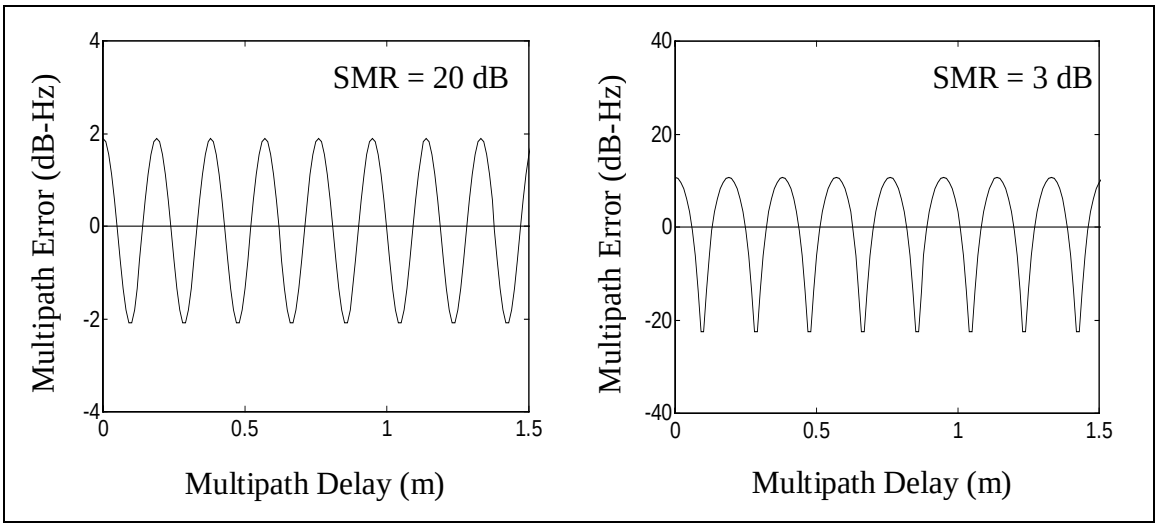

Figure 5.20a-5.20b: SNR errors due to short delay multipath with signal strengths of a) SMR = 20 dB, and b) SMR = 3 dB

5.3 Synergy among Code, Carrier and SNR Multipath Errors

The code, carrier and SNR are affected by multipath in different ways, which are explained in earlier sections. The following section discusses the relationships among these three types of errors.

Figures 5.21 and 5.22 show the code, carrier and SNR error patterns in the presence of a multipath signal of SMR = 20 dB and 3 dB respectively. It can be seen that the code and SNR error patterns are in-phase with respect to each other, whereas the carrier phase error pattern is quadrature-phase with respect to the code and SNR errors. At low multipath signal strengths the errors have nearly sinusoidal patterns with respect to the multipath delays, and therefore have a narrow band of frequency components. However at high multipath signal strengths the error patterns are far from sinusoidal. They have sharp discontinuities and therefore have a wide band of frequency components. The uniform pattern of these errors and their inter-relationships is such that if any of these three errors is known, it might be possible to estimate the other two, if a suitable relationship can be established among the three.

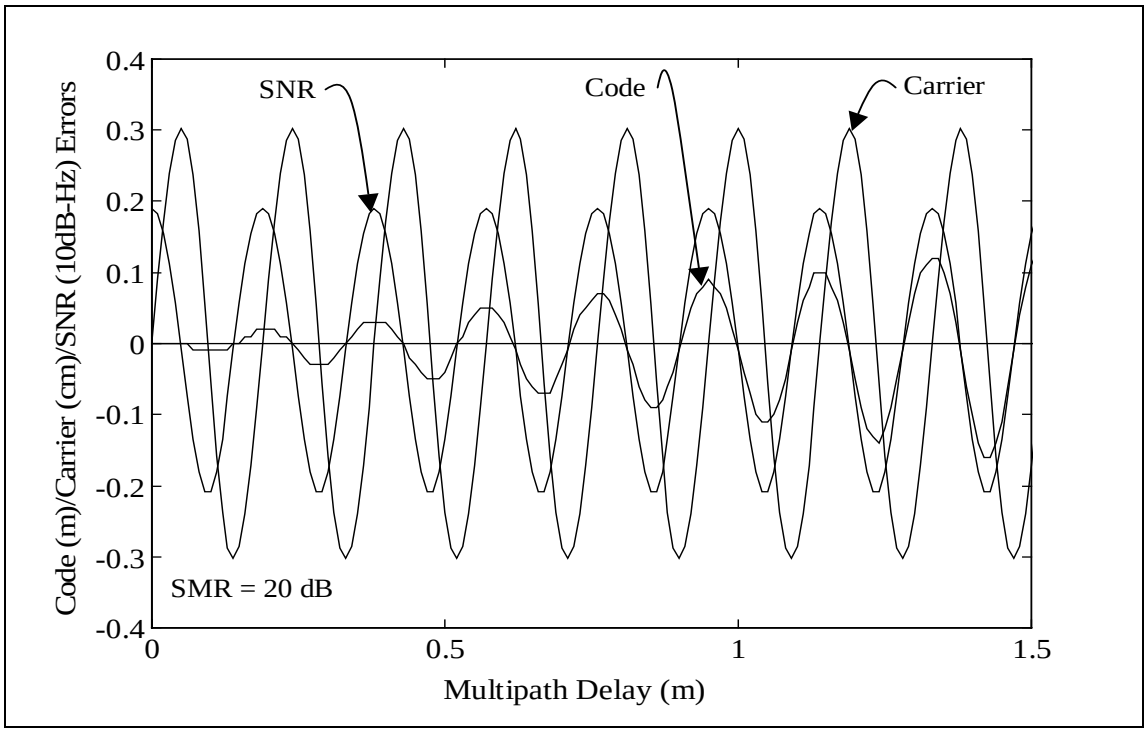

Figure 5.21: Code, carrier and SNR multipath due to a reflector with SMR = 20 dB

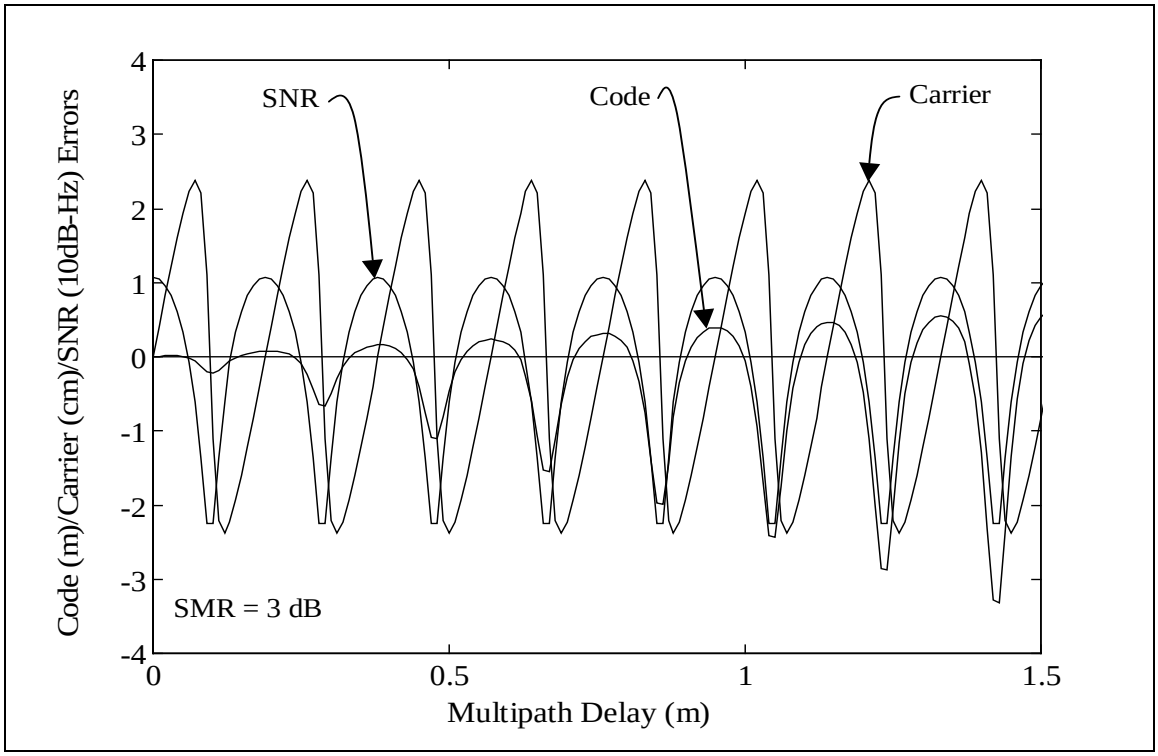

Figure 5.22: Code, carrier and SNR multipath due to a reflector with SMR = 3 dB

Table 5.1 lists out some of the important differences between the code and carrier multipath errors.

Table 5.1: Comparison between code and carrier multipath errors

C/A code multipath error	L1 carrier multipath error
• Maximum error +/- 150 m in code range using a wide correlator • Non-zero mean, especially in high multipath environments • Asymmetric error envelope • Affected by multipath signal delayed up to 450 metres (using a wide correlator) • High multipath environment does not necessarily mean high multipath error • Can be mitigated by reducing the early-late correlator spacing • Highly dependent on the pre-correlation bandwidth • Possible to isolate by code - carrier technique	• Maximum error +/- 4.75 cm in carrier phase for wide or narrow correlator • Zero mean in all multipath environments • Symmetric error envelope • Affected by multipath signal delayed up to 300 metres • High multipath environment means high multipath error • Can be mitigated by reducing the correlation function width • Nearly independent of pre-correlation bandwidth • Generally not possible to isolate

5.4 Multipath Errors from a Geometrical Perspective

In Figure 5.23, a typical multipath scenario is shown, whereby A0 to A4 are several antennas placed close together in a multi-antenna system, and the reflections from two sources to A0 are shown. The other four antennas will also be affected by the reflected signals in a similar way.

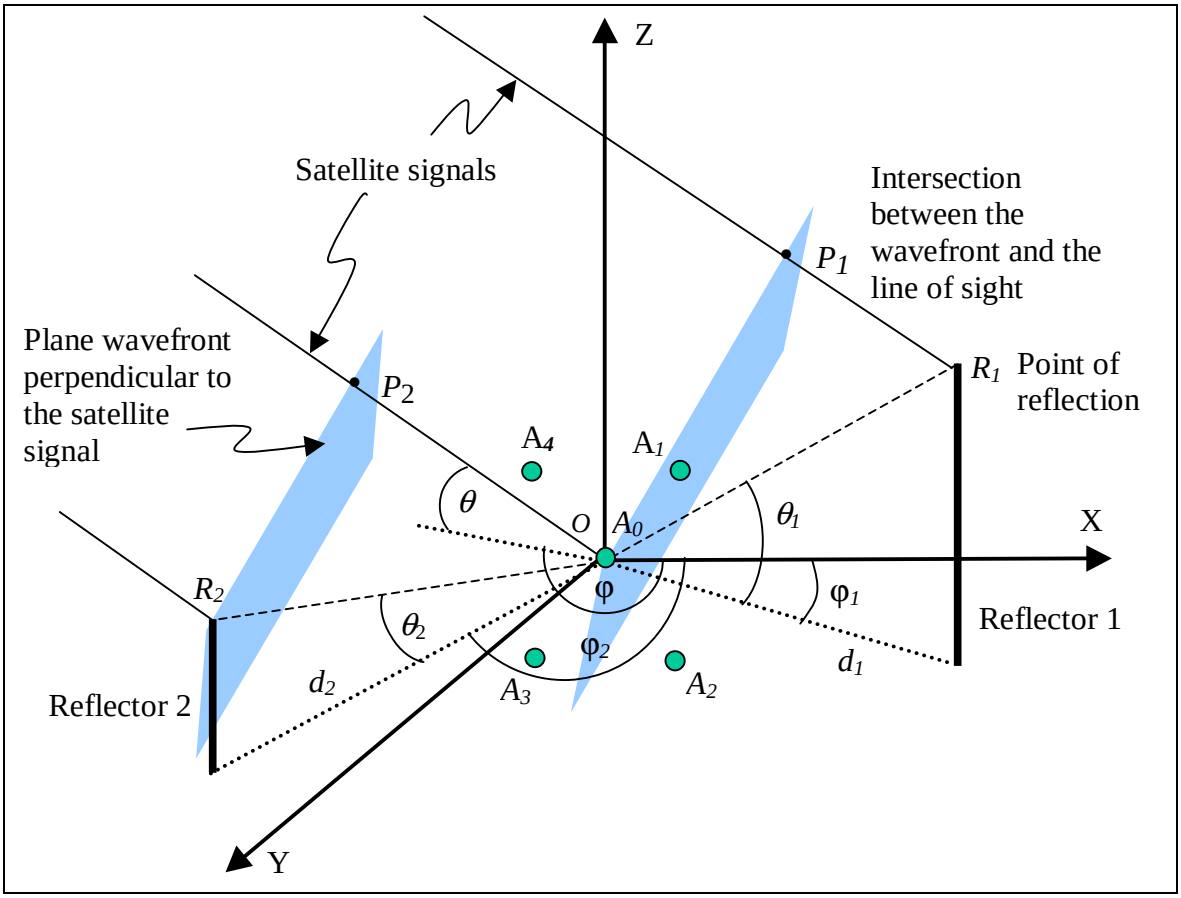

Figure 5.23: Direct and reflected signals to an antenna in a multi-antenna system

In the diagram, θ and φ are the elevation and azimuth of the direct signal to the antenna, while θ_k and φ_k are the elevation and azimuth of the *k*th reflected signal to the antenna. The distance between the antenna and the reflector in the horizontal plane is denoted by d_k, where, k represents a particular reflector.

Two distinct scenarios are shown in the figure. In the first case, (Reflector 1), the antenna (A0) is closer to the satellite compared to the reflector, whereas in the second case, (Reflector 2), the reflector is closer to the satellite compared to the antenna (A0). These two cases are generalized situations and representative of all the possible scenarios of the antenna-reflector geometry.

Since the satellite is 20,000 km above the earth, the GPS signal can be assumed to travel as parallel rays on the earth's surface. A plane wavefront perpendicular to the line of sight can be assumed to have the same carrier phase. When this plane intersects the phase centre of Antenna 0, the carrier phase at all points on the plane is the same, including point P_1 (which is the intersection of the plane and the line of sight from Reflector 1 to the satellite). Therefore, the differential path delay of this reflected signal with respect to the direct signal is $P_1R_1 + R_1O$. The corresponding differential phase delay is computed by dividing the differential path delay by the signal wavelength. This assumes no phase change due to reflection of the signal. This assumption is acceptable to characterize multipath errors and their dependency on geometry in a relative sense. To determine the absolute multipath errors, however, the phase change due to reflection of the signal should be accounted for.

Similarly, for case 2, a plane perpendicular to the line of sight from Reflector 2 to the satellite intersects the line of sight from the antenna under consideration at point P_2. In this case, the differential path delay is given by $R_2O - P_2O$.

Therefore, if the direct signal phase at the antenna is available, the reflected signal phase can be computed by adding the differential phase delay due to the differential path delay (under the above mentioned assumption), to the direct signal phase.

In order to compute the effects of multipath, the above mentioned differential path delays need to be formulated by a mathematical expression. Using solid geometry, it can be

shown that the differential path delay in either situation is given by (see Appendix E for details),

$$a_k = d_k\left(\frac{1}{\cos\theta_k} - \tan\theta_k \sin\theta - \cos\theta\cos(\varphi - \varphi_k)\right) \tag{5.16}$$

where,

- a_k is the differential path delay of the *k*th reflected signal (m)
- d_k is the horizontal distance between the antenna and the *k*th reflector (m)
- θ is the elevation of the direct satellite signal (rad)
- φ is the azimuth of the direct satellite signal (rad)
- θ_k is the elevation of the *k*th reflected signal (rad), and
- φ_k is the azimuth of the *k*th reflected signal (rad)

The differential path delay expression is a function of the satellite elevation and azimuth, the reflected signal elevation and azimuth, and the antenna-reflector distance in the local level horizontal plane. This expression is further exploited to analyze the behaviour of the code and carrier phase multipath error.

With the assumption that the multipath phase is only due to the differential path delay, it can be expressed as,

$$\gamma_{0k} = \gamma_k - \gamma_0 = \frac{2\pi a_k}{\lambda_L} \tag{5.17}$$

where

- γ_0 is the direct signal phase at the antenna phase centre (rad)
- γ_k is the *k*th reflected signal phase at the antenna phase centre (rad), and
- λ_L is the wavelength of the carrier (m).

The multipath error phase is directly related to the multipath phase. The multipath error variation is due to the variation in the multipath phase or the differential path delay. The

multipath frequency depends upon the rate of change of multipath phase, or the differential path delay. The multipath frequency due to a single dominant reflector may be computed by taking the time derivative of the multipath phase expression from Equations 5.16 and 5.17, and is given by,

$$\frac{\delta\gamma_{01}}{\delta t} = \frac{2\pi d_1}{\lambda_L}\left(\{\sin\theta\cos(\varphi-\varphi_1) - \cos\theta\tan\theta_1\}\frac{\delta\theta}{\delta t} + \{\cos\theta\sin(\varphi-\varphi_1)\}\frac{\delta\varphi}{\delta t}\right) \qquad (5.18)$$

Equation 5.18 relates multipath error frequency with the satellite dynamics. The expression is obtained under the assumption that the antenna-reflector geometry (defined by d_1, θ_1 and φ_1) does not change significantly over the period under consideration. This assumption does not generally hold for kinematic receivers, where the antenna-reflector geometry may change rapidly. Furthermore, in stationary situations, the antenna-reflector geometry changes can be taken care of by taking the partial derivatives with respect to the reflected signal elevation and azimuth in Equation 5.18.

It is evident from Equation 5.18 that the multipath error frequency is,

- directly proportional to the distance between the antenna and the reflector
- inversely proportional to the wavelength of the carrier signal
- directly proportional to the rate of change of elevation of the satellite
- directly proportional to the rate of change of azimuth of the satellite, and
- dependent upon the antenna-reflector and the line-of-sight vectors.

The above statements allow an analysis of the multipath characteristics as follows:

a) reflectors which are far away from an antenna cause high frequency or fast-changing multipath, and close-by reflectors cause low frequency or slowly changing multipath

b) for the same differential path delay, GPS L1 and L2 carriers will have different multipath phases. As a result, they will have the same multipath amplitude but

different instantaneous phases. The L1 carrier will have higher frequency multipath compared to the L2 carrier

c) a low elevation satellite is more likely to cause multipath error, (due to more potential reflectors), but requires a larger surface (due to the large Fresnel zone) for strong multipath. On the other hand, a high elevation satellite is less likely to cause multipath errors, but requires a smaller surface for strong multipath (Braasch, 1998).

5.5 Multipath Simulation Description

A Multipath Simulation and Mitigation software (MultiSiM) for the GPS was developed on a PC platform. The software consists of two main parts: Simulation and Mitigation. The first part allows the user to define the multipath environment and the antenna setup through the input parameters. The second part, on the other hand, uses various multipath mitigation schemes to reduce the simulated multipath errors.

The major inputs to the simulator are,

- reflector parameters, and
- antenna parameters

while the major outputs from the simulator are,

- true range and phase
- measured range and phase contaminated with multipath and receiver noise, and
- estimated range and phase.

The user can input the number of reflectors per satellite and their locations with respect to the antenna position in order to simulate a controlled multipath environment. The user can also configure the antenna setup, (i.e. the number of antennas in the antenna array), absolute position of one of the antennas (named as reference antenna) and relative

positions of all other antennas (named as secondary antenna) with respect to the reference antenna.

The range and phase of the direct and reflected signals at each antenna may be determined by computing the distance traveled by the signal up to the antenna. For the direct signal, it is the distance between the satellite and the antenna while for the reflected signals, it is the total distance from the satellite to the reflector, plus the reflector to the antenna. The phases of the direct and reflected signals are assumed to be only a function of the ranges, and are computed directly from the ranges. The possible change in phase due to reflection of the signal is not considered for this simulation. The satellite position is determined from stored ephemeris data.

The noiseless measured code range is the sum of the direct range between the antenna and the satellite, and the code multipath error. The code multipath error is computed by using Equation 5.3 (for a coherent discriminator), or Equation 5.7d (for a dot-product discriminator), and finding the difference between the zero crossings of the multipath corrupted discriminator function and the multipath-free discriminator function. A single observation from the direct and the numerous reflected signals is generated per satellite-antenna combination.

The measured carrier phase without noise contains two parts: the integer and fractional cycle components. Assuming that the direct signal is stronger than the indirect signal, the integer cycles in the measured carrier phase are the same as the direct signal's integer cycles. The phase of the fractional cycle of the reflected signal is what actually corrupts the phase of the fractional cycle of the direct signal, depending upon its relative strength and phase. Equation 5.9 is used to compute the multipath error on the fractional part of the carrier phase.

5.6 Multipath Simulation Results

Figures 5.24a to 5.24e show the effect of a reflected signal on a direct signal for three different situations. In Figure 5.24a, the direct signal modulated by the code and data is shown. There are many L1 carrier cycles within a code bit, and only a small fraction of it is illustrated to demonstrate the behaviour. Figure 5.24b is the reflected signal delayed by two integer cycles. It is also 90 degrees out of phase with respect to the direct signal, and one half its amplitude.

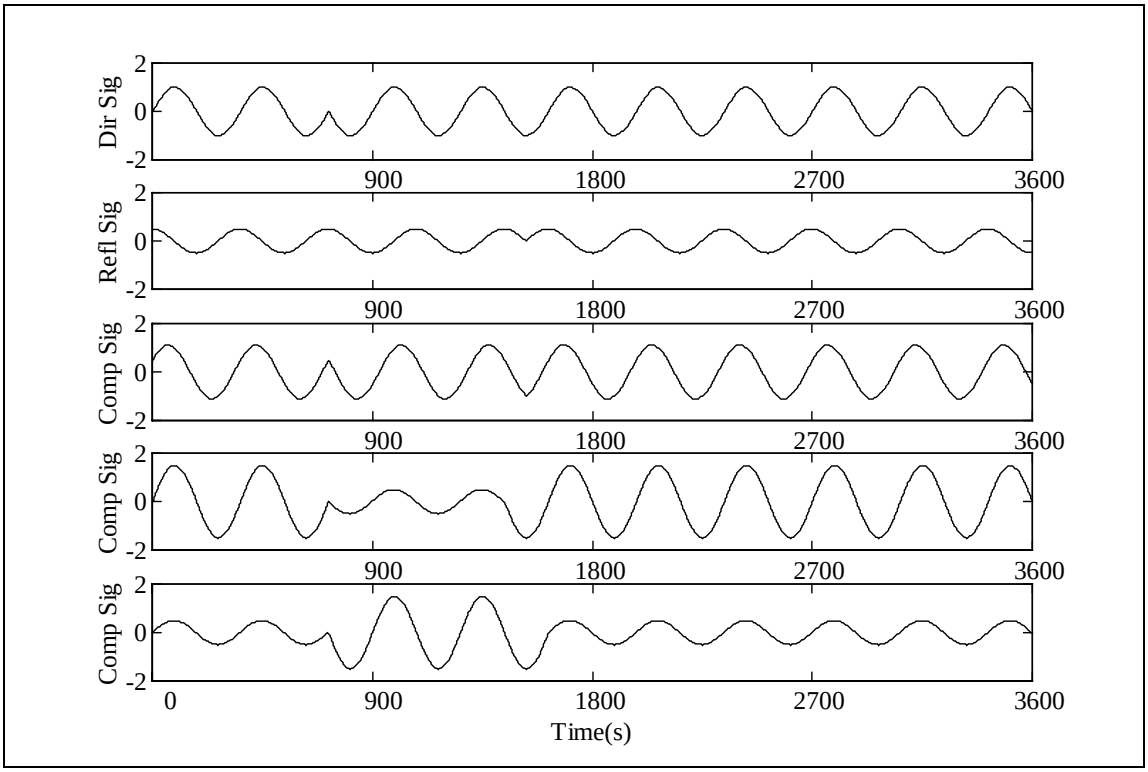

Figure 5.24a-5.24e: Waveforms of the direct, reflected and composite signals for 90, 0 and 180 degrees relative phases of the reflected signals, due to a reflector with SMR = 6 dB

Figures 5.24c, 5.24d and 5.24e show the composite signals consisting of a direct and reflected signal for a multipath phase of 90, 0, and 180 degrees, respectively. It can be observed that in the first case, the composite signal has a phase error but no change in amplitude. To observe the phase error, the direct and composite signal phases can be compared at the 3600^{th} epoch. In contrast, in the second and third cases the composite

signals do not exhibit phase error, but the signal amplitude is increased and decreased respectively. This will introduce code multipath error, and affect the SNR, (or the more widely used C/N_0), of the carrier. For a large out-of-phase reflected signal, the receiver may lose lock of the incoming signal.

Figures 2.25a to 2.25d demonstrate the variation of the multipath error as a function of the satellite elevation and azimuth for satellite 4. Figures 2.25c and 2.25d show carrier phase multipath errors which are due to a reflector with SMR of 6 dB, at a distance of 20 m and 5 m from the antenna respectively. A nominal phase noise of 3 mm (1σ) was added. In practice, it is unlikely to have reflection from the same point for a long period. In this case, however, it serves the purpose of understanding the general behaviour of the multipath error over time. In the figure, the multipath frequency changes with time, depending upon the rate of change of the satellite elevation and azimuth.

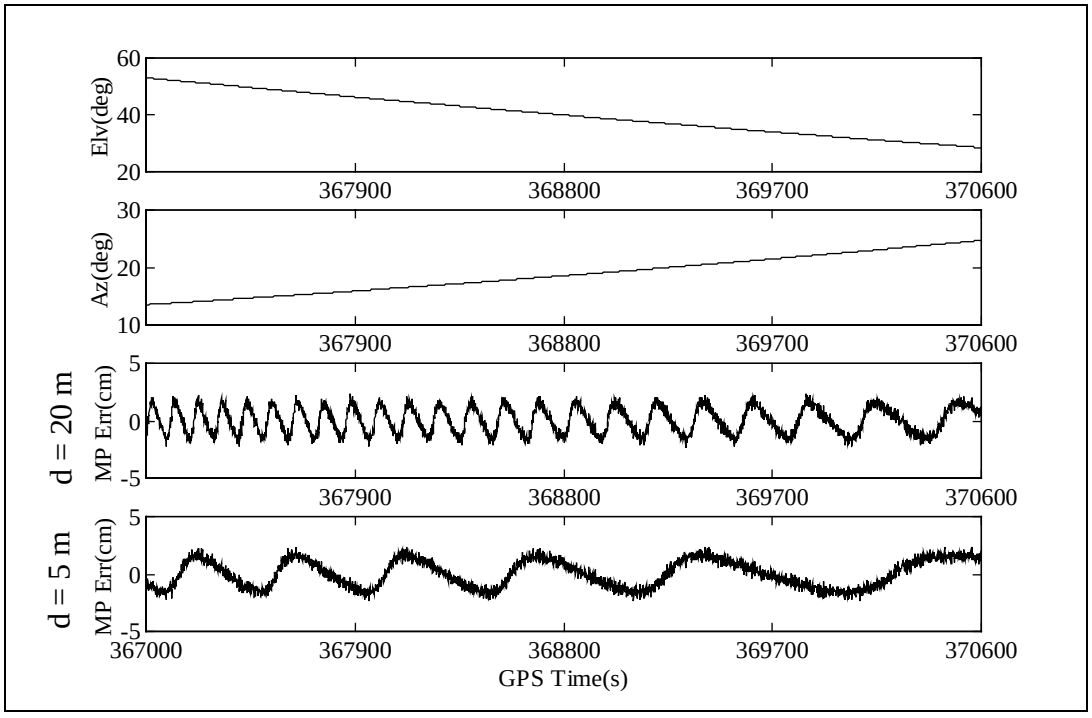

Figure 5.25: L1 carrier phase multipath error variations as a function of elevation and azimuth for satellite 4 due to a reflector with SMR of 6 dB at distances of 20 m and 5 m from the antenna

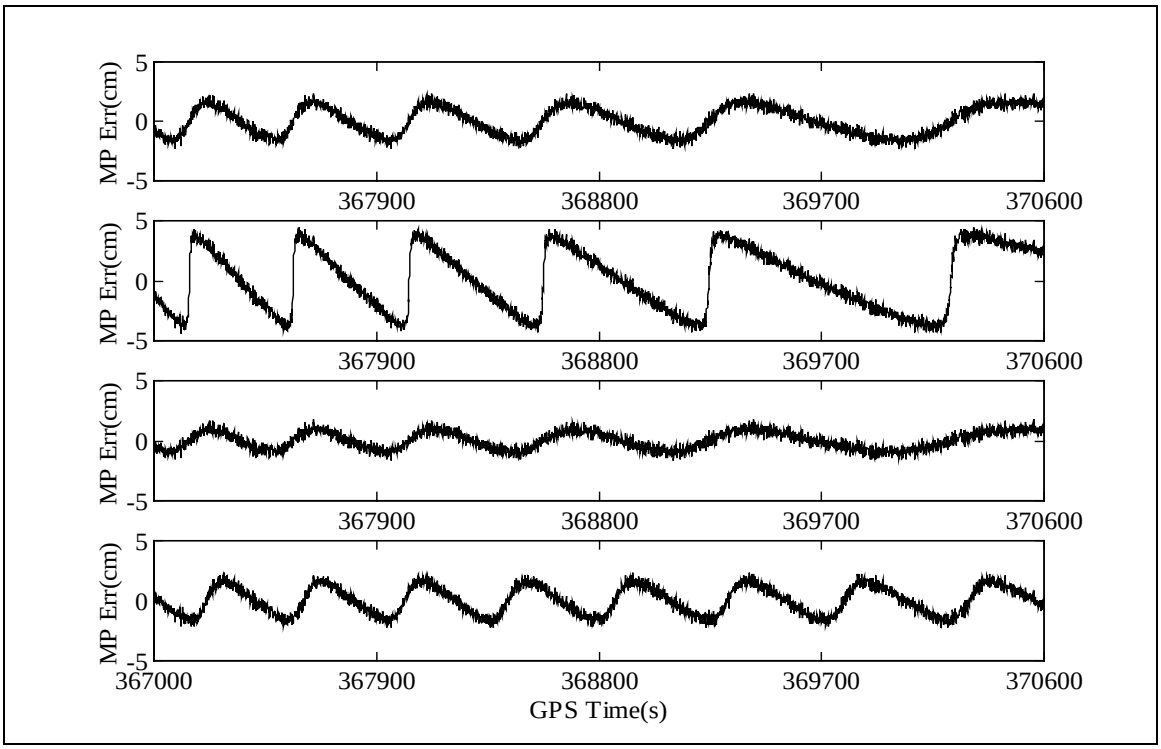

Figure 5.26a-5.26d: Carrier multipath errors for satellite 4 due to a single reflector with reflection coefficients of 0.5, 0.95, 0.3 and 0.5 respectively at a distance of 5 m from the antenna. In 5.26d, the reflector is at a different location.

Figures 5.26a to 5.26d are generated under similar circumstances as in Figure 5.25d, except that in Figures 5.26b and 5.26c the reflection coefficient is changed to 0.95 (SMR ≈ 0.5 dB) and 0.3 (SMR ≈ 10 dB), respectively. Furthermore, in Figure 5.26d, the reflector is placed in a different location, but at the same distance with respect to the antenna. These figures show several important characteristics of multipath. It is clear from the figures that in a weak multipath situation, the error tends to be sinusoidal, whereby the maxima and the minima are uniformly spaced at 90 and 270 degrees relative to the phase of the reflected signal. In a strong multipath situation, however, the error tends to be a saw-tooth shape, with sharp transitions in the vicinity of the 180 degree relative phase of the reflected signal. Furthermore, the multipath phase and frequency are highly dependent on the location of the reflector with respect to the antenna. In fact, a small change in location, on the order of several cm, may change the differential path

delay, thereby causing a change in the reflected signal relative phase and multipath error. This makes the day-to-day prediction of carrier phase multipath highly vulnerable, unless the environment remains exactly the same.

Figures 5.27a to 5.27d are generated under similar circumstances as in Figures 5.26a to 5.26d. It is clear from the figures that in a weak multipath situation, the errors tend to be sinusoidal, while in a strong multipath situation, the errors have spikes and are discontinuous. That is because, the carrier multipath error is sinusoidal with weak multipath, but has large swings at the vicinity of 180 degrees of multipath phase. Therefore, phase multipath error in turn affect the code multipath error as shown in Equation 5.5. Furthermore, the periodicity of the code multipath error is the same as that of the carrier multipath error due to a single reflector. The multipath phase and frequency are highly dependent upon the location of the reflector.

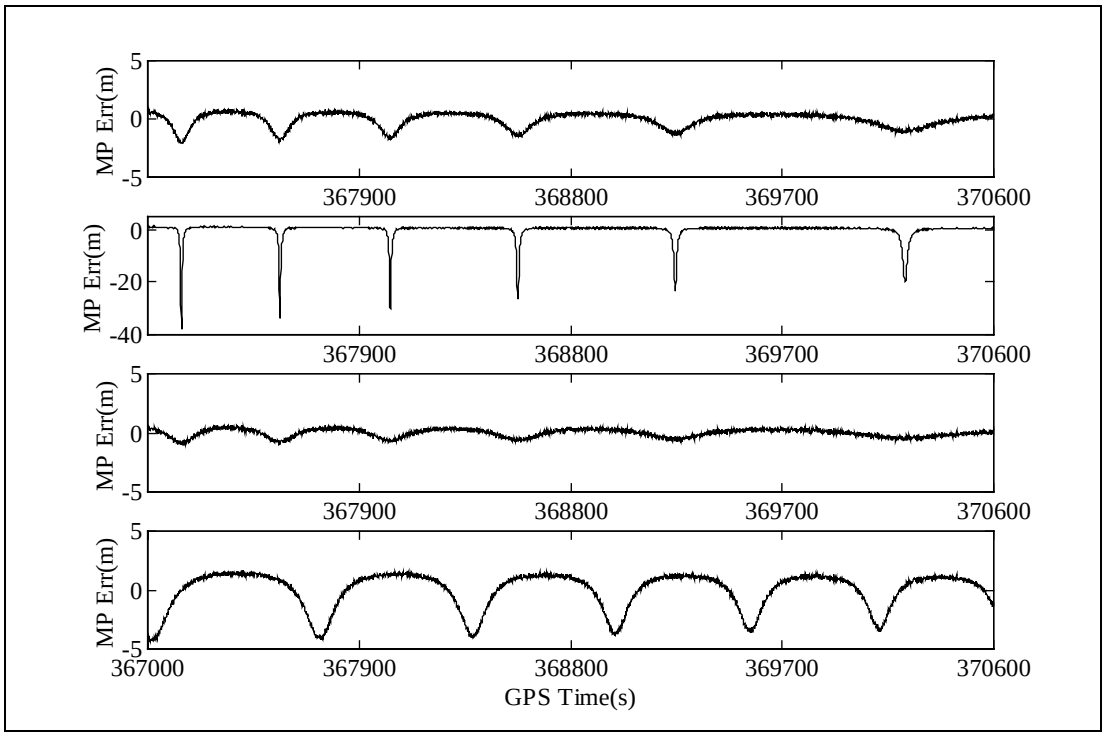

Figure 5.27a-5.27d: Code multipath errors for satellite 4 due to a single reflector with reflection coefficients of 0.5, 0.95, 0.3 and 0.5 respectively at a distance of 5 m from the antenna. In 5.27d, the reflector is at a different location.

Figures 5.28a to 5.28d show carrier multipath errors from a large reflector at various closely-spaced antennas, and Figures 5.29a to 5.29d show their code counterparts. It is clear from the figure that the multipath errors are highly correlated between antennas, and have very similar patterns within a small area. They have different phases due to different differential path delays of the reflected signal. Due to these phase differences, multipath errors do not get cancelled by taking a single difference of the errors in two closely-spaced antennas, contrary to popular belief. However, their relationships can be exploited to estimate the multipath error at individual antennas as described in Chapters 6 and 7.

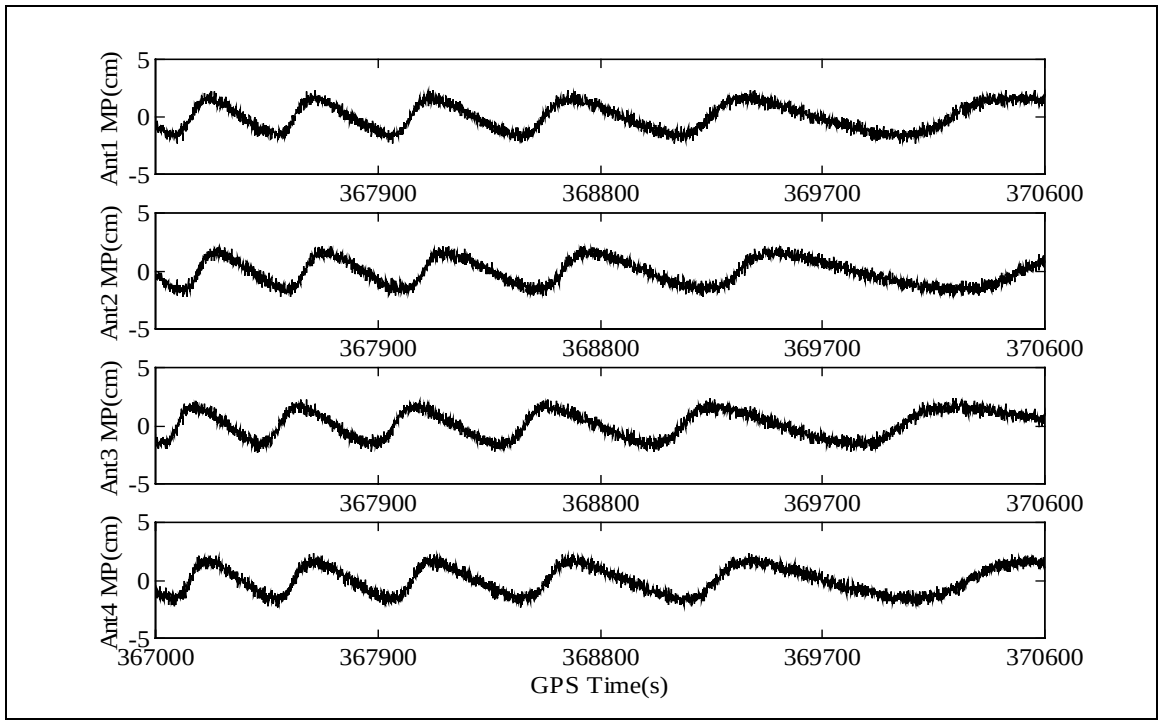

Figure 5.28a-5.28d: Carrier multipath at multiple antennas separated by 5 to 10 cm

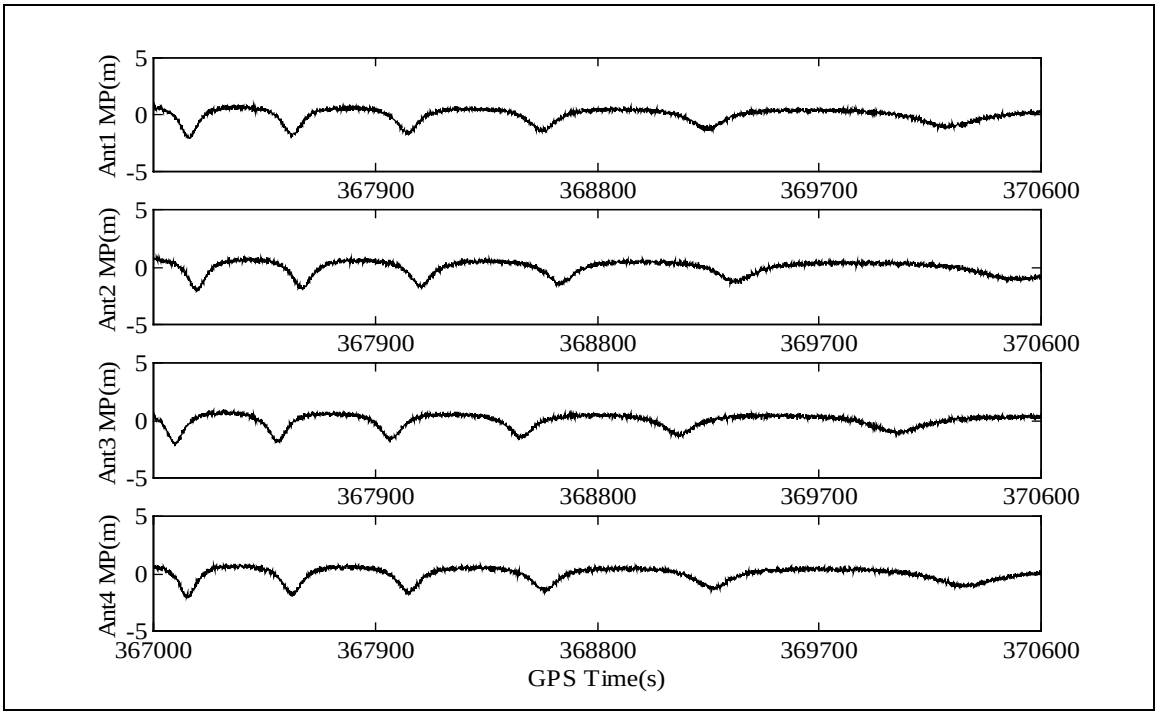

Figure 5.29a-5.29d: Code multipath at multiple antennas separated by 5 to 10 cm

Figure 5.30a displays the multipath error due to an additional reflector, compared to the set-up used to generate data for Figure 5.28a. It demonstrates the error behaviour for both L1 and L2 carriers for satellite 4. Figure 5.30b shows the error behaviour for satellite 16, due to the same reflectors. In these figures, the dark shaded errors correspond to the L1 carrier and the light shaded errors to the L2 carrier. Several important observations can be made from the figures: i) the multipath error may change substantially due to the addition or subtraction of another reflector, ii) the same set of reflectors may have a different effect on a different satellite signal depending upon the line-of-sight vector, antenna-reflector vector, elevation and azimuth of the satellite, iii) the multipath error has the same amplitude (in radians) for the L1 and L2 carrier (though, when multiplied by the wavelength to convert the error into the unit of distance, the L2 multipath error has a larger amplitude than that of L1), iv) the multipath error has a different phase for the L1 and L2 carrier. At a particular instant, the multipath error for the L1 and L2 carriers look arbitrary, but over a time-span, it becomes evident that the error signals have similar

patterns. The multipath error dependency on frequency is also explained in Georgiadou and Kleusberg (1988).

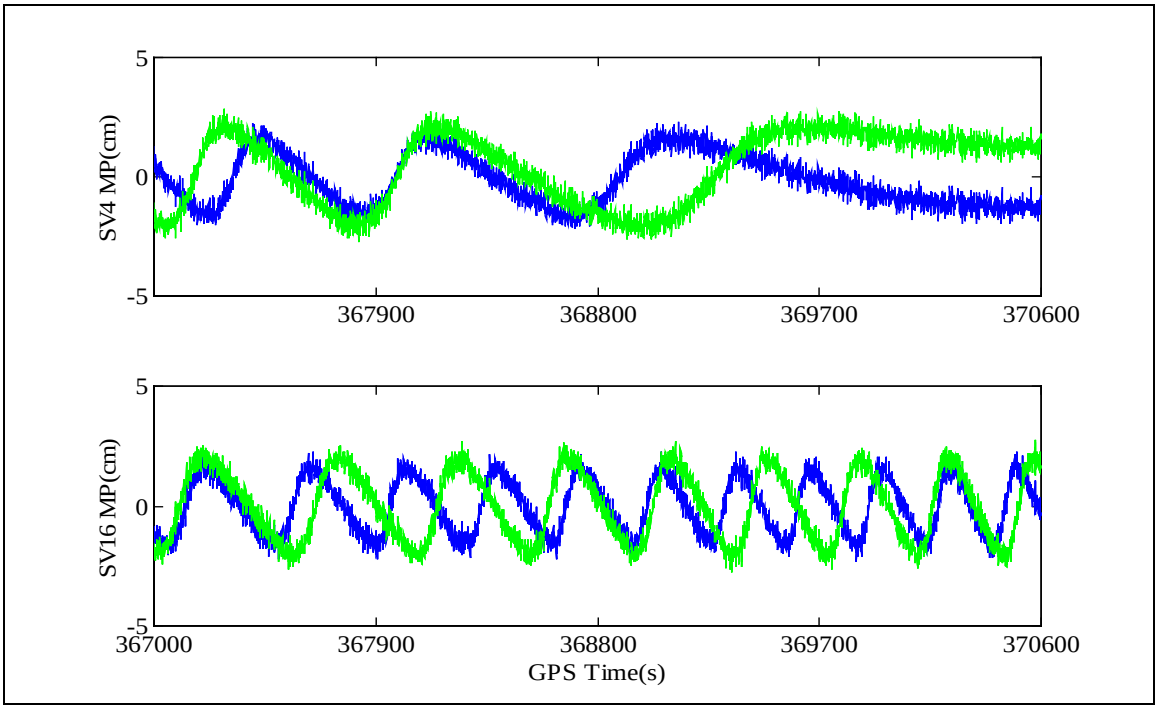

Figure 5.30a-5.30b: L1 and L2 multipath errors due to two reflectors for a) satellite 4 and b) satellite 16

Figures 5.31a and 5.31c show the multipath error for satellites 4 and 16, respectively, while Figures 5.31b and 5.31d are their estimated periods. Periods are estimated, not from the errors themselves, but from the antenna-reflector geometry using Equation 5.18. Comparing the errors with their estimated periods, it can be observed that the estimation is approximately correct for the entire duration. In these figures, the estimation is based on the known position of the reflector, which is not available in practical applications. However, this relationship (Equation 5.18) may be used in addition to other measurements to estimate the multipath errors. For example, one can assume the reflector position and reflection coefficient to be the unknown state variables and then estimate them using measurements from the closely-spaced antennas.

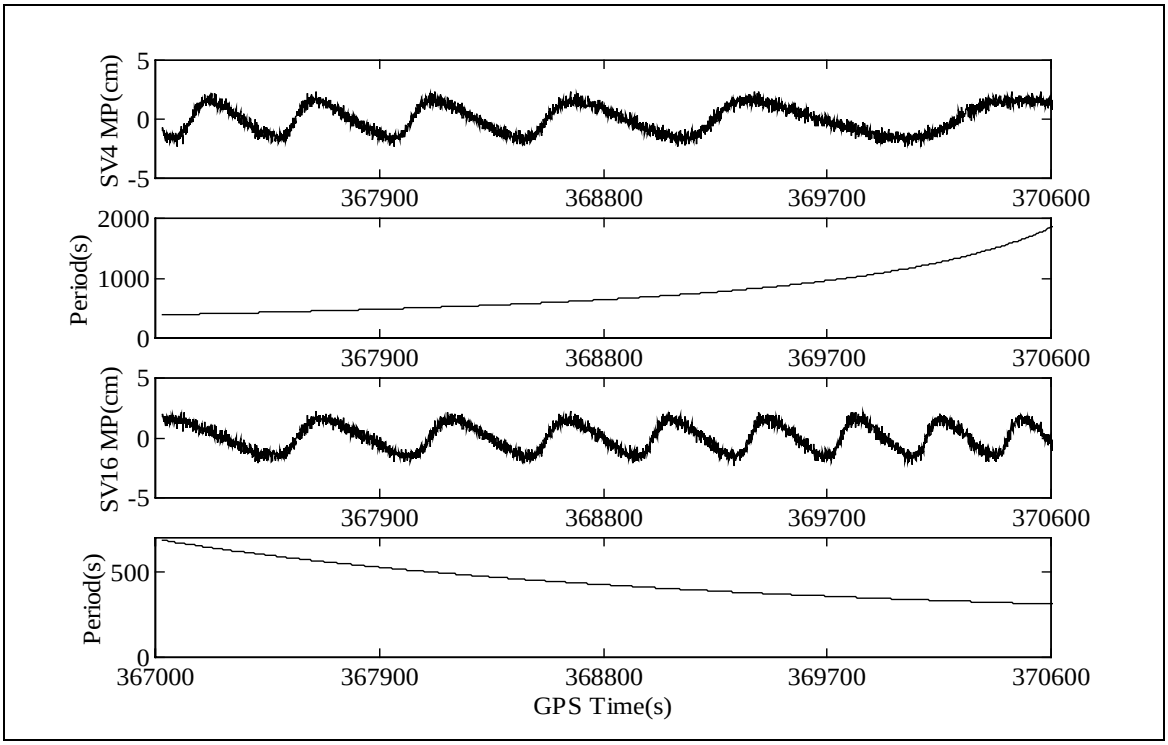

Figure 5.31a-5.31d: Multipath errors and their estimated periods for satellites 4 and 16

In this chapter, effects of multipath on code and carrier tracking loops were investigated, and code, carrier and SNR multipath error characteristics were analyzed from theoretical and simulation models. The problem was also approached from a geometrical perspective, and exploits the antenna-reflector geometry to characterize multipath. The analysis was also extended for multiple reflectors and multiple closely-spaced antennas.

CHAPTER 6

MULTILTIPATH MITIGATION ALGORITHM AND SIMULATION RESULTS

6.1 Introduction

Chapter 4 and 5 derive various relationships of code and carrier phase multipath with some multipath and geometric parameters. These parameters may be estimated from some observations available from a GPS receiver. Once the parameters are estimated, the multipath errors may also be computed.

In this chapter, a technique is described that can be used to estimate the multipath and geometric parameters using a multi-antenna array consisting of multiple antennas placed in a close proximity. The mathematical model of the proposed algorithm and the estimation filter is given in this chapter.

A Multipath Simulation and Mitigation software program (MultiSiM) was developed to prove the concept of estimating multipath errors using simulations. Numerous simulations with different conditions are carried out and described in this chapter, to underline the strengths and drawbacks of the proposed algorithm.

6.2 Multipath Effects in Closely-Spaced Antennas

6.2.1 Code Multipath Error

Various types of coherent and non-coherent discriminator functions are employed for code tracking in a receiver. Here, the analysis is carried out for a non-coherent dot-product type of discriminator, as subsequent analysis with field data was done with a receiver employing this type of discriminator. For this discriminator, the multipath error due to a single dominant reflector, or a virtual reflector, which is the mathematical equivalent of a combination of physical reflectors (Ray et al., 1999a), can be determined from Equation 5.7d,

$$\begin{aligned} D_{nm} = {} & R(\hat{\tau}_c - \tau_0)\{R_{EL}(\hat{\tau}_c - \tau_0)\} + \alpha_1^2 R(\hat{\tau}_c - \tau_1)\{R_{EL}(\hat{\tau}_c - \tau_1)\} \\ & \alpha_1\{R(\hat{\tau}_c - \tau_0)[R_{EL}(\hat{\tau}_c - \tau_1)] + R(\hat{\tau}_c - \tau_1)[R_{EL}(\hat{\tau}_c - \tau_0)]\}\cos(\gamma_0 - \gamma_1) \end{aligned} \quad (5.7d)$$

Each term in Equation 5.7d is described in Chapter 5. In Equation 5.7d, if $\tau_0 = 0$, then $\hat{\tau}_c$ is the code multipath error.

Some of the currently available high performance correlator-based techniques, such as MET™ (Townsend and Fenton, 1994), MEDLL™ (Van Nee, 1995), Enhanced Strobe Correlator™ (Garin and Rousseau, 1997), ClearTrak™ (Stansell and Maenpa, 1999), effectively mitigate multipath errors caused by far away reflectors. But, multipath errors caused by nearby reflectors (example: τ_1 < 30 m for C/A code receivers, using 0.1 chip correlator spacing) still remained a major problem. The following formulation is for code multipath errors caused by nearby reflectors.

For a nearby dominant reflector ($0<\tau_1<T_d$), substituting the correlation symbol 'R_{EL}' by its values in Figure 4.4 (in the code tracking error range of $-T_d$ and T_d) and then equating it to zero, the following is obtained,

$$D_{nm} = R(\hat{\tau}_c)\left\{-2\frac{\hat{\tau}_c}{T}\right\} + \alpha_1^2 R(\hat{\tau}_c - \tau_1)\left[-2\frac{\hat{\tau}_c - \tau_1}{T}\right]$$
$$\alpha_1\left\{R(\hat{\tau}_c)\left[-2\frac{\hat{\tau}_c - \tau_1}{T}\right] + R(\hat{\tau}_c - \tau_1)\left[-2\frac{\hat{\tau}_c}{T}\right]\right\}\cos(\gamma_0 - \gamma_1) = 0 \quad (6.1)$$

In Equation 6.1, both sides may be divided by $R(\hat{\tau}_c)$; and $\frac{R(\hat{\tau}_c - \tau_1)}{R(\hat{\tau}_c)}$ may be replaced by α', the correlation ratio. Then,

$$D_{nm} = \left\{-2\frac{\hat{\tau}_c}{T}\right\} + \alpha_1^2\alpha'\left[-2\frac{\hat{\tau}_c - \tau_1}{T}\right] +$$
$$\alpha_1\left\{\left[-2\frac{\hat{\tau}_c - \tau_1}{T}\right] + \alpha'\left[-2\frac{\hat{\tau}_c}{T}\right]\right\}\cos(\gamma_0 - \gamma_1) = 0 \quad (6.2)$$

In Equation 6.2, τ_1 is the multipath delay, which may be expressed in terms of α' as follows:

$$\alpha' = \frac{R(\hat{\tau}_c - \tau_1)}{R(\hat{\tau}_c)}$$
$$= \frac{1 - \frac{|\hat{\tau}_c - \tau_1|}{T}}{1 - \frac{|\hat{\tau}_c|}{T}} = \frac{T - |\hat{\tau}_c - \tau_1|}{T - |\hat{\tau}_c|} \quad (6.3a)$$

$$= \frac{T - \tau_1 + \hat{\tau}_c}{T - \hat{\tau}_c} \text{ if } \hat{\tau}_c > 0 \text{ and } \frac{T - \tau_1 + \hat{\tau}_c}{T + \hat{\tau}_c} \text{ if } \hat{\tau}_c < 0 \quad (6.3b)$$

Figure 6.1 plots the code multipath error ($\hat{\tau}_c$) and correlation ratio (α') with respect to the multipath delay (τ_1). It can be seen that the correlation ratio has a gradual downward trend and small oscillations. The downward trend is due to the reduction in correlation values along the slant side of a correlation triangle as the code misalignment increases. The small oscillations are caused by the code multipath error term in Equation 6.3b. As an approximation, the oscillations in correlation ratio can be neglected and only the downward trend is used for further analysis. This approximation leads to the following expression for the correlation ratio:

$$\alpha' = \frac{T - \tau_1}{T} \tag{6.3c}$$

and

$$\tau_1 = T - \alpha' T \tag{6.4}$$

From Equations 6.2 and 6.4, replacing γ_{01} = multipath phase = (γ_1-γ_0), and rearranging,

$$\hat{\tau}_c = \frac{\alpha_1 T(1-\alpha')(\alpha_1\alpha' + \cos\gamma_{01})}{1 + \alpha_1^2\alpha' + \alpha_1\cos\gamma_{01} + \alpha_1\alpha'\cos\gamma_{01}} \tag{6.5}$$

Equation 6.5 is a closed form expression for code multipath error in a dot-product discriminator due to a short delay multipath.

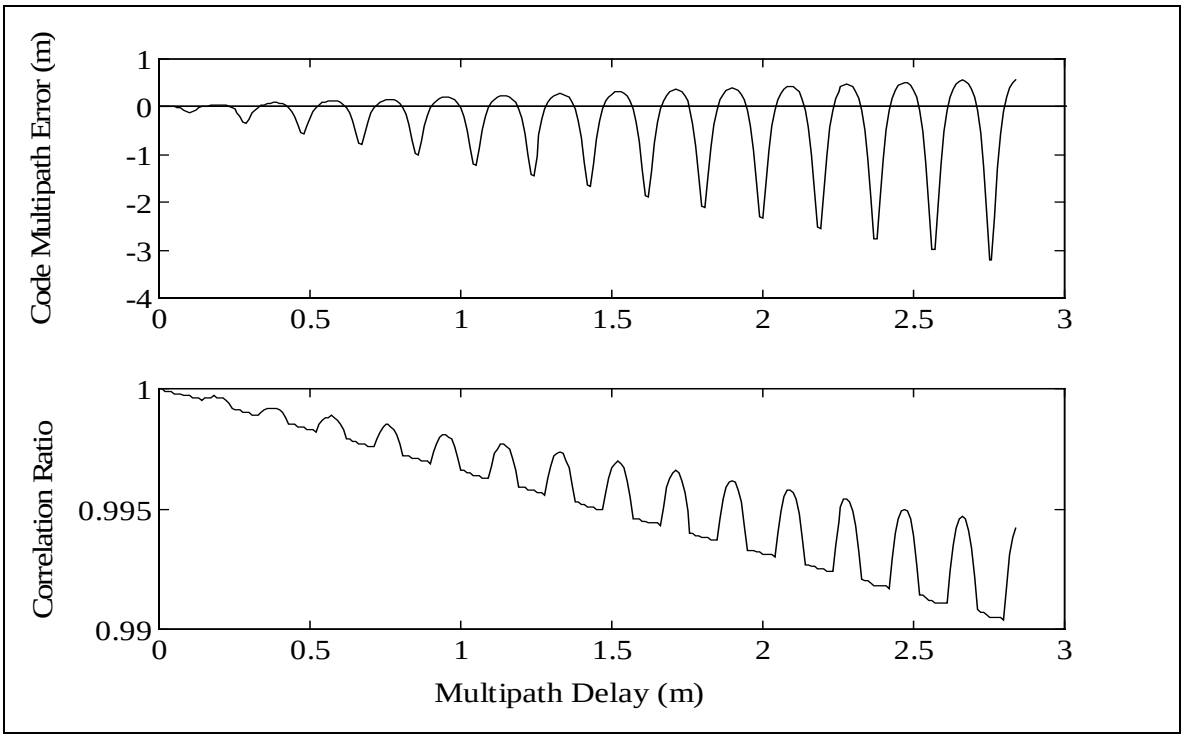

Figure 6.1: a) Code multipath error and b) correlation ratio with respect to multipath delay for a non-coherent dot-product discriminator

Multipath errors within a small area are strongly related, as described in Chapter 5. If several antennas are placed close-by in a multi-antenna assembly, then the multipath experienced by each antenna will be strongly related, provided the reflector is large enough, compared to the largest spacing between the antennas. If all the antennas in the antenna array have similar gain patterns, then the satellite signal will be equally amplified or attenuated by each antenna during the signal reception. By neglecting the effect of the antenna gain pattern, and assuming that the reflected signal strength is the same at each antenna, the difference in code multipath error at two closely-spaced antennas in the antenna array is then given by,

$$\begin{aligned}\Delta\tau_{0,i} &= \hat{\tau}_{c0} - \hat{\tau}_{ci} \\ &= \frac{T\left(\alpha_1 - \alpha_1\alpha' - \alpha_1^3\alpha'^2 + \alpha_1^3\alpha'^3\right)\left(\cos\gamma_{01} - \cos\gamma_{i1}\right)}{\begin{aligned}&1 + 2\alpha_1^2\alpha' + \alpha_1^4\alpha'^2 + \alpha_1\cos\gamma_{01} + \alpha_1\cos\gamma_{i1} + \alpha_1\alpha'\cos\gamma_{01} + \alpha_1\alpha'\cos\gamma_{i1} \\ &+ \alpha_1^2\cos\gamma_{01}\cos\gamma_{i1} + 2\alpha_1^2\alpha'\cos\gamma_{01}\cos\gamma_{i1} + \alpha_1^2\alpha'^2\cos\gamma_{01}\cos\gamma_{i1} \\ &+ \alpha_1^3\alpha'\cos\gamma_{01} + \alpha_1^3\alpha'\cos\gamma_{i1} + \alpha_1^3\alpha'^2\cos\gamma_{01} + \alpha_1^3\alpha'^2\cos\gamma_{i1}\end{aligned}}\end{aligned} \quad (6.6)$$

where,

γ_{01} is the multipath phase at antenna 0 due to reflector 1 (rad), and

γ_{i1} is the multipath phase at antenna *i* due to reflector 1 (rad).

Equation 6.6 relates the single difference code range multipath error at two closely-spaced antennas in terms of the reflection coefficient, correlation ratio and reflected signal relative phases. This relationship is exploited in the subsequent sections to estimate multipath errors at each antenna.

The notation for multipath phase in Equation 6.6 must be clarified. The multipath phase at *i*th antenna, due to *j*th reflector is given by

$$\gamma_{ij} = \gamma_j^i - \gamma_0^i \quad (6.7)$$

where

γ_j^i is the *j*th reflected signal phase at *i*th antenna (rad), and

γ_0^i is the direct signal phase at the *i*th antenna (rad).

6.2.2 Carrier Phase Multipath Error

Carrier phase multipath error due to a single dominant reflector is given by Equation 5.9 and is reproduced here,

$$\Delta\Psi = \arctan\left(\frac{\alpha_1 R(\hat{\tau}_c - \tau_1)\sin\gamma_{01}}{R(\hat{\tau}_c) + \alpha_1 R(\hat{\tau}_c - \tau_1)\cos\gamma_{01}}\right) \tag{5.9}$$

Here, it can be noted that, γ_1 in Equation 5.9 is replaced by γ_{01}. That is because, while deriving Equation 5.9, the direct signal phase γ_0 was assumed to be zero. In that case, the multipath phase $\gamma_{01} = \gamma_1 - \gamma_0 = \gamma_1$ = reflected signal phase.

By replacing $\frac{R(\hat{\tau}_c - \tau_1)}{R(\hat{\tau}_c)} = \alpha'$, the following is achieved:

$$\Delta\Psi = \arctan\left(\frac{\alpha_1 \alpha' \sin\gamma_{01}}{1 + \alpha_1 \alpha' \cos\gamma_{01}}\right) \tag{6.8}$$

Equations 6.5 and 6.8 represent multipath errors in the code and carrier respectively. It is evident from the equations that the code and the carrier multipath errors have the same set of multipath parameters; namely, the reflection coefficient, multipath delay and multipath phase. This also means that the code and the carrier multipath errors are closely related to each other. This evokes a synergistic relationship between the two types of multipath.

Furthermore, it is interesting to note that when the multipath error is due to a close-by ($\alpha' \approx 1$) and weak ($\alpha_1 << 1$) reflector, then from Equations 6.5 and 6.8, the code and carrier multipath errors have the following expressions:

$$\hat{\tau}_c \approx K\left(\frac{\alpha_1 \cos\gamma_{01}}{1+2\alpha_1 \cos\gamma_{01}}\right) \tag{6.9}$$

$$\Delta\Psi \approx \left(\frac{\alpha_1 \sin\gamma_{01}}{1+\alpha_1 \cos\gamma_{01}}\right) \tag{6.10}$$

where K is a function of α'.

The multipath error within a small area is strongly related. The difference in the carrier phase multipath error between two antennas in an antenna array consisting of multiple closely-spaced antennas, assuming that a) the antenna gain pattern is the same for both antennas, and b) the reflected signal strength is the same at both the antennas, is then given by,

$$\begin{aligned}\Delta\Psi_{0,i} &= \Delta\Psi_0 - \Delta\Psi_i \\ &= \arctan\left(\frac{\alpha_1\alpha'\sin\gamma_0 - \alpha_1\alpha'\sin\gamma_i + \alpha_1^2\alpha'^2\sin(\gamma_{01}-\gamma_{i1})}{1+\alpha_1\alpha'\cos\gamma_0 + \alpha_1\alpha'\cos\gamma_i + \alpha_1^2\alpha'^2\cos(\gamma_{01}-\gamma_{i1})}\right)\end{aligned} \tag{6.11}$$

Equation 6.11 relates the single difference carrier phase multipath errors at two closely-spaced antennas in terms of the reflection coefficient, correlation ratio and reflected signal phases. This relationship is exploited in the subsequent sections to estimate multipath errors at each antenna.

6.2.3 Multipath Effects on the SNR

Multipath affects not only the code range and carrier phase measurements, but also the SNR, which is commonly expressed as C/N_0. Assuming a uniform gain pattern of the receiver antenna, the average signal power is given by Equation 5.12 and is reproduced here for further analysis:

$$P = R^2(\hat{\tau}_c)\left(1+\alpha_1^2\alpha'^2 + 2\alpha_1\alpha'\cos\gamma_{01}\right) \tag{5.12}$$

The SNR errors due to multipath in multiple closely-spaced antennas are also strongly related, though the relationship is not the same as the relationship for the code and the carrier. This is because the code, carrier and the SNR errors are related to the multipath parameters through different relationships, as given by Equation 6.5, 6.8 and 5.12 respectively. The relationship of the SNR errors among the antennas may be exploited to estimate multipath parameters. By carefully arranging the antennas in the antenna array, it is possible to reduce the antenna phase centre variations with elevation changes, and to have similar gain patterns for all the antennas in the array.

Assuming that the noise power spectral density is the same in each antenna (i.e. $N_0 = N_i$) in an antenna array consisting of multiple closely-spaced antennas, the ratio of the SNR (or the difference of the C/N_0) between two antennas is given by,

$$R_{0,i} = \frac{P_i / N_i}{P_0 / N_0} = \frac{1 + \alpha_1^2 \alpha'^2 + 2\alpha_1 \alpha' \cos \gamma_{i1}}{1 + \alpha_1^2 \alpha'^2 + 2\alpha_1 \alpha' \cos \gamma_{01}} \tag{6.12}$$

Equation 6.12 relates the ratio of the SNR at two closely-spaced antennas in terms of the reflection coefficient, correlation ratio and reflected signal phases. Here it is assumed that the correlation peak values are the same in both the antennas for small code multipath error, such that, $R(\hat{\tau}_{c0}) \approx R(\hat{\tau}_{ci})$. This relationship is exploited in the subsequent sections to estimate multipath parameters, and thereby determine multipath errors at each antenna.

6.3 Multipath Mitigation Model

If the reflector is large enough compared to the largest spacing between the antennas in a multi-antenna assembly, the multipath errors in these antennas are strongly related and the multipath signal strength, or the reflection coefficient at all antennas, can be assumed to be the same. Similarly, if the reflector is far away compared to the largest spacing

between the antennas in the antenna assembly, then the correlation ratio can be assumed to be the same for all antennas.

Assuming that the reflection coefficient and correlation ratio are the same for all antennas, and that the gain patterns of the antennas in the assembly are identical and uniform, then the multipath errors at each antenna vary only due to the reflected signal relative phase or multipath phase.

The multipath phase, however, cannot be assumed to be the same for all antennas, as it is highly sensitive to the reflected signal path delay. For a path delay of 10 cm, the multipath phase will have a 180 degree phase shift for an L1 signal carrier.

The reflection of a satellite signal can be viewed from a geometrical perspective. For example, as the satellite is far away, the GPS signal can be assumed to arrive as parallel rays and remain so after reflection from a plane surface. Then, the phase of the reflected signal at each antenna phase centre in a group of closely-spaced antennas, is a function of the reflected signal direction (i.e. azimuth and elevation) as well as the relative geometry of the antennas with respect to each other.

In Figure 6.2, Antennas A_0 and A_i are closely-spaced antennas, and their distance is significantly smaller than the distance and dimension of the plane reflector. Each antenna receives a direct signal from the satellite, and a reflected signal from a nearby plane object. The antennas are placed on a horizontal plane with relative spacing of a_{0i}, and A_i makes an angle ϕ_{0i} with respect to the local X-axis. θ_1 and φ_1 are the elevation and azimuth of the reflected signal at both A_0 and A_i. A wavefront perpendicular to the reflected signal at Antenna 0, will have the same phase for all the other parallel reflected signals from the same plane object. In the figure, OQ is a plane perpendicular to the reflected signals.

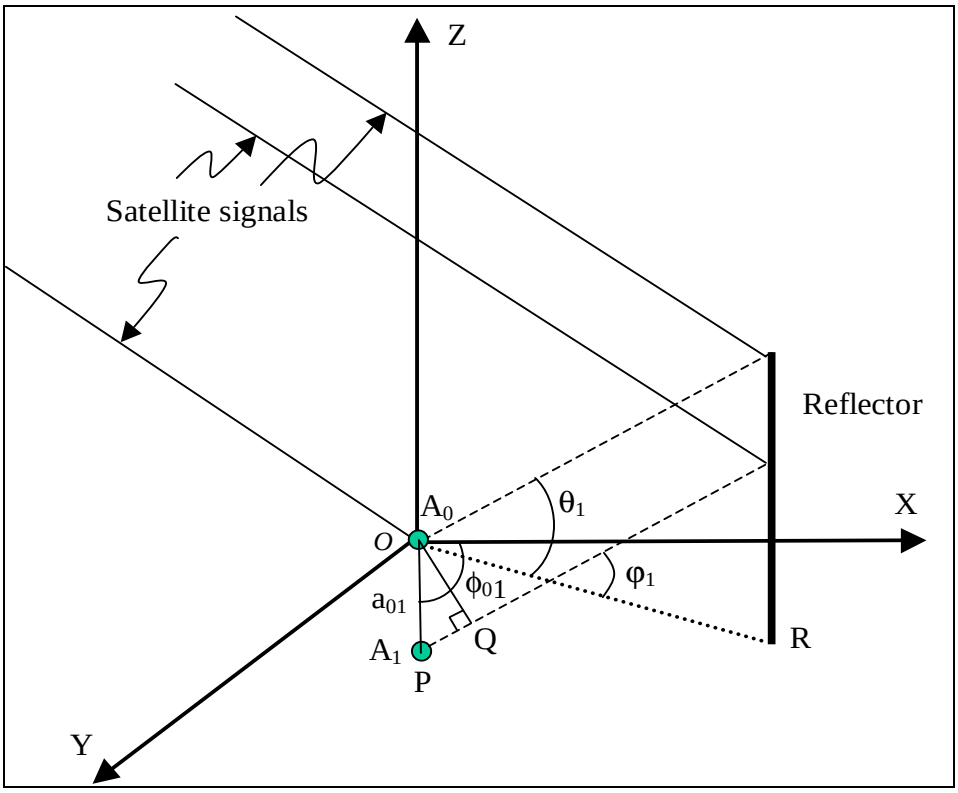

Figure 6.2: Correlated multipath errors can be related to each other through signal direction and known geometry between the antennas

The phase of the reflected signal at Ai is equal to the phase of the reflected signal at A0 plus the phase corresponding to the differential path delay corresponding to PQ in the figure. Therefore,

$$\gamma_1^i = \gamma_1^0 - \frac{2\pi}{\lambda_L} a_{0i} \cos(\varphi_1 - \phi_{0i}) \cos\theta_1 \tag{6.13}$$

where,

γ_1^i is the phase of the reflected signal at A_i (rad)

γ_1^0 is the phase of the reflected signal at A_0 (rad)

a_{0i} is the distance between A_0 and A_i (m)

ϕ_{0i} is the azimuth of the vector OP, and (rad)

φ_1 is the azimuth of the reflected signal (rad), and

θ_1 is the elevation of the reflected signal (rad).

From Equation 6.13 it can be observed that if there is a phase change due to reflection and change in polarization, then that will affect both γ_1^0 and γ_1^i by the same amount. As a result, if γ_1^0 is estimated accurately, then γ_1^i can also be computed accurately using this equation, even when there is a phase change during reflection. Therefore, this equation does not depend upon the probable phase change due to reflection.

Now, the multipath phases at Antennas A0 and Ai are

$$\gamma_{01} = \gamma_1^0 - \gamma_0^0 \tag{6.14a}$$

$$\gamma_{i1} = \gamma_1^i - \gamma_0^i = \gamma_1^i - \gamma_0^0 - \Delta\gamma_{0i} \tag{6.14b}$$

where

γ_0^i is the direct signal phase at Ai (rad)

γ_0^0 is the direct signal phase at A0 (rad), and

$\Delta\gamma_{0i}$ is the differential phase of the direct signal at Ai with respect to the direct signal phase at A0 (rad), such that, $\Delta\gamma 0i = \gamma_0^i - \gamma_0^0$.

Using Equations 6.13, 6.14a and 6.14b, multipath phase at Ai is given by

$$\begin{aligned}\gamma_{i1} &= \gamma_1^i - \gamma_1^0 + \gamma_{01} - \Delta\gamma_{0i} = \gamma_{01} + (\gamma_1^i - \gamma_1^0) - \Delta\gamma_{0i} \\ &= \gamma_{01} - \frac{2\pi}{\lambda_L} a_{0i} \cos(\varphi_1 - \phi_{0i}) \cos\theta_1 - \Delta\gamma_{0i}\end{aligned} \tag{6.15}$$

In Equations 6.6, 6.11 and 6.12, the multipath errors on the code, carrier and SNR in two closely-spaced antennas due to a single dominant reflector are expressed in terms of various multipath parameters. Therefore, for a cluster of m closely-spaced antennas, there

will be 3*(m-1)* such equations. Assuming that the reflection coefficient and correlation ratio are the same for all antennas, there will be *(m+2)* unknown parameters (one reflection coefficient, one correlation ratio and m multipath phases). By using Equation 6.15, it is possible to relate the m multipath phases (γ_{01}, γ_{11} ….. $\gamma_{m\text{-}11}$) in terms of three unknown parameters; namely, the multipath phase at one antenna, known as the reference antenna (γ_{01}), the elevation (θ_1) and the azimuth (φ_1) of the reflected signal.

Replacing the value of γ_{i1} in Equation 6.6, the single difference code multipath error is given by,

$$\Delta\tau_{0,i} = \left(\begin{array}{l} \dfrac{\begin{array}{l} T\left(\alpha_1 - \alpha_1\alpha' - \alpha_1^3\alpha'^2 + \alpha_1^3\alpha'^3\right) \\ \left(\cos\gamma_{01} - \cos\left(\gamma_{01} - \dfrac{2\pi}{\lambda_L} a_{0i} \cos(\varphi_1 - \phi_{0i}) \cos\theta_1 - \Delta\gamma_{0i} \right) \right) \end{array}}{\left(\begin{array}{l} 1 + 2\alpha_1^2\alpha' + \alpha_1^4\alpha'^2 + \alpha_1 \cos\gamma_{01} \\ + \alpha_1\alpha' \cos\gamma_{01} + \alpha_1^3\alpha' \cos\gamma_{01} \\ + \alpha_1^3\alpha'^2 \cos\gamma_{01} \end{array} \right) + \left(\begin{array}{l} \alpha_1 + \alpha_1\alpha' + \alpha_1^3\alpha' + \alpha_1^3\alpha'^2 \\ + \alpha_1^2 \cos\gamma_{01} + 2\alpha_1^2\alpha' \cos\gamma_{01} \\ + \alpha_1^2\alpha'^2 \cos\gamma_{01} \end{array} \right)} \\ \cos\left(\gamma_{01} - \dfrac{2\pi}{\lambda_L} a_{0i} \cos(\varphi_1 - \phi_{0i}) \cos\theta_1 - \Delta\gamma_{0i} \right) \end{array} \right) \tag{6.16}$$

Similar to Equation 6.16, the single difference carrier phase multipath error can be expressed in the following form, using Equations 6.11 and 6.15:

$$\Delta\Psi_{0,i} = \arctan\left(\frac{\begin{array}{l} \alpha_1\alpha' \sin\gamma_{01} - \alpha_1\alpha' \sin\left(\gamma_{01} - \frac{2\pi}{\lambda_L} a_{0i} \cos(\varphi_1 - \phi_{0i}) \cos\theta_1 - \Delta\gamma_{0i} \right) \\ + \alpha_1^2\alpha'^2 \sin\left(\frac{2\pi}{\lambda_L} a_{0i} \cos(\varphi_1 - \phi_{0i}) \cos\theta_1 + \Delta\gamma_{0i} \right) \end{array}}{\begin{array}{l} 1 + \alpha_1\alpha' \cos\gamma_{01} - \alpha_1\alpha' \cos\left(\gamma_{01} - \frac{2\pi}{\lambda_L} a_{0i} \cos(\varphi_1 - \phi_{0i}) \cos\theta_1 - \Delta\gamma_{0i} \right) \\ + \alpha_1^2\alpha'^2 \cos\left(\frac{2\pi}{\lambda_L} a_{0i} \cos(\varphi_1 - \phi_{0i}) \cos\theta_1 + \Delta\gamma_{0i} \right) \end{array} \right) \tag{6.17}$$

Similarly, the ratio of the SNRs between two closely-spaced antennas can be expressed by using Equations 6.12 and 6.15:

$$R_{0,i} = \frac{\left(1 + \alpha_1^2\alpha'^2 + 2\alpha_1\alpha'^2 \cos\left(\gamma_{01} - \frac{2\pi}{\lambda_L} a_{0i} \cos(\varphi_1 - \phi_{0i}) \cos\theta_1 - \Delta\gamma_{0i} \right) \right)}{\left(1 + \alpha_1^2\alpha'^2 + 2\alpha_1\alpha' \cos\gamma_{01} \right)} \tag{6.18}$$

In Equations 6.16, 6.17 and 6.18, the single difference code, carrier and SNR multipath errors are expressed in terms of various known and unknown parameters, such as, α_1, α', γ_{01}, θ_1, φ_1, a_{0i}, ϕ_{0i}, $\Delta\gamma_{0i}$. Among these, the last three parameters are either known, or can be computed. The first five parameters, however, are unknown, and common in all the expressions. If multiple antennas are used, then several measurements can be made from which these common multipath and geometric parameters may be estimated.

After the common parameters are estimated, the code multipath error at each antenna can then be computed by replacing the estimated parameters in Equation 6.19, which is formulated from Equations 6.5 and 6.15:

$$\hat{\tau}_{ci} = \frac{\alpha_1 T(1-\alpha')\left(\alpha_1\alpha' + \cos\left(\gamma_{01} - \frac{2\pi}{\lambda_L} a_{0i}\cos(\varphi_1 - \phi_{0i})\cos\theta_1 - \Delta\gamma_{0i}\right)\right)}{1 + \alpha_1^2\alpha' + (\alpha_1 + \alpha_1\alpha')\cos\left(\gamma_{01} - \frac{2\pi}{\lambda_L} a_{0i}\cos(\varphi_1 - \phi_{0i})\cos\theta_1 - \Delta\gamma_{0i}\right)} \tag{6.19}$$

Similarly, the carrier phase multipath error at each antenna can be computed from the estimated parameters using Equation 6.20, which is formulated from Equations 6.8 and 6.15,

$$\Delta\Psi_i = \arctan\left(\frac{\alpha_1\alpha'\sin\left(\gamma_{01} - \frac{2\pi}{\lambda_L} a_{0i}\cos(\varphi_1 - \phi_{0i})\cos\theta_1 - \Delta\gamma_{0i}\right)}{1 + \alpha_1\alpha'\cos\left(\gamma_{01} - \frac{2\pi}{\lambda_L} a_{0i}\cos(\varphi_1 - \phi_{0i})\cos\theta_1 - \Delta\gamma_{0i}\right)}\right) \tag{6.20}$$

6.4 Multipath Estimation Technique

The multipath and geometric parameters may be estimated using different estimation techniques, such as a Least Squares Estimator (Krakiwsky, 1990; Mikhail, 1976), a Modified Wave Estimator (Salychev, 1998; Ray et al., 1999c) or an Extended Kalman Filter (Gelb, 1979; Brown and Hwang, 1992; Maybeck, 1994). Multiple antennas are placed close together on a horizontal plane to ensure strongly related multipath signals. Generally at least six antennas are to be used, and a typical layout (for a six-antenna case) is shown in Figure 6.3.

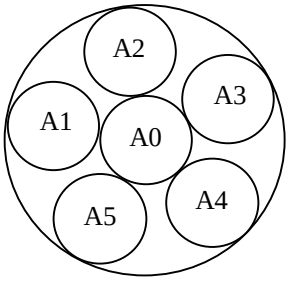

Figure 6.3: Typical antenna assembly for six antennas

One of the antennas in the antenna assembly is defined as the reference antenna. All the parameters of the reflected signal and the placement of other antennas are defined with respect to the reference antenna.

If an Extended Kalman Filter (EKF) is used as the estimator, the state vector for the EKF is

$$x = \begin{bmatrix} \alpha_1 \\ \alpha' \\ \gamma_{01} \\ \theta_1 \\ \varphi_1 \end{bmatrix} = \begin{bmatrix} \text{Re flection coefficient} \\ \text{Correlation ratio} \\ \text{Multipath phase at the reference antenna} \\ \text{Multipath signal elevation} \\ \text{Multipath signal azimuth} \end{bmatrix} \tag{6.21}$$

Single differenced (between antennas) code multipath errors, carrier phase multipath errors and SNR ratios are used to update the state variables. Later in Chapter 7, it will be shown that adjusted single differenced code measurements (between antennas) are effectively the single differenced code multipath errors, assuming that the bias due to other sources is negligible. Similarly, adjusted single differenced carrier phase measurements (between antennas) are effectively the single differenced carrier phase multipath errors. Therefore, in an antenna array consisting of *m* closely-spaced antennas, if one of the antennas in the (*m*-1) antenna pairs is common, then there would be (*m*-1) single differenced code multipath measurements, (*m*-1) single differenced carrier phase multipath measurements and (*m*-1) SNR ratios. Therefore,

$$z = \left[\Delta\tau_{0,1} \,..\, \Delta\tau_{0,m-1} \quad \Delta\Psi_{0,1} \,..\, \Delta\Psi_{0,m-1} \quad R_{0,1} \,..\, R_{0,m-1}\right]^T \tag{6.22}$$

The relationships between the state variables and the measurements are described in the design matrix (H). As the relationships are non-linear in nature, they are obtained by computing the partial derivatives of Equations 6.6 (or 6.16), 6.11 (or 6.17) and 6.12 (or 6.18) with respect to the unknown parameters. The resulting design matrix is,

$$H = \begin{bmatrix} \frac{\delta(\Delta\tau_{0,1})}{\delta\alpha_1} & \frac{\delta(\Delta\tau_{0,1})}{\delta\alpha'} & \frac{\delta(\Delta\tau_{0,1})}{\delta\gamma_{01}} & \frac{\delta(\Delta\tau_{0,1})}{\delta\theta_1} & \frac{\delta(\Delta\tau_{0,1})}{\delta\varphi_1} \\ --- & --- & --- & --- & --- \\ \frac{\delta(\Delta\tau_{0,m-1})}{\delta\alpha 1} & \frac{\delta(\Delta\tau_{0,m-1})}{\delta\alpha'} & \frac{\delta(\Delta\tau_{0,m-1})}{\delta\gamma_0} & \frac{\delta(\Delta\tau_{0,m-1})}{\delta\theta_1} & \frac{\delta(\Delta\tau_{0,m-1})}{\delta\varphi_1} \\ \frac{\delta(\Delta\Psi_{0,1})}{\delta\alpha_1} & \frac{\delta(\Delta\Psi_{0,1})}{\delta\alpha'} & \frac{\delta(\Delta\Psi_{0,1})}{\delta\gamma_{01}} & \frac{\delta(\Delta\Psi_{0,1})}{\delta\theta_1} & \frac{\delta(\Delta\Psi_{0,1})}{\delta\varphi_1} \\ --- & --- & --- & --- & --- \\ \frac{\delta(\Delta\Psi_{0,m-1})}{\delta\alpha_1} & \frac{\delta(\Delta\Psi_{0,m-1})}{\delta\alpha'} & \frac{\delta(\Delta\Psi_{0,m-1})}{\delta\gamma_{01}} & \frac{\delta(\Delta\Psi_{0,m-1})}{\delta\theta_1} & \frac{\delta(\Delta\Psi_{0,m-1})}{\delta\varphi_1} \\ \frac{\delta(R_{0,1})}{\delta\alpha_1} & \frac{\delta(R_{0,1})}{\delta\alpha'} & \frac{\delta(R_{0,1})}{\delta\gamma_{01}} & \frac{\delta(R_{0,1})}{\delta\theta_1} & \frac{\delta(R_{0,1})}{\delta\varphi_1} \\ --- & --- & --- & --- & --- \\ \frac{\delta(R_{0,m-1})}{\delta\alpha_1} & \frac{\delta(R_{0,m-1})}{\delta\alpha'} & \frac{\delta(R_{0,m-1})}{\delta\gamma_{01}} & \frac{\delta(R_{0,m-1})}{\delta\theta_1} & \frac{\delta(R_{0,m-1})}{\delta\varphi_1} \end{bmatrix} \quad (6.23)$$

where

$$\frac{\delta\Delta\tau_{0,i}}{\delta\alpha_1} = \frac{1}{b_i^2}\left(b_i \frac{\delta a_i}{\delta\alpha_1} - a_i \frac{\delta b_i}{\delta\alpha_1} \right) \quad (6.24a)$$

$$\frac{\delta\Delta\tau_{0,i}}{\delta\alpha'} = \frac{1}{b_i^2}\left(b_i \frac{\delta a_i}{\delta\alpha'} - a_i \frac{\delta b_i}{\delta\alpha'} \right) \quad (6.24b)$$

$$\frac{\delta\Delta\tau_{0,i}}{\delta\gamma_{01}} = \frac{1}{b_i^2}\left(b_i \frac{\delta a_i}{\delta\gamma_{01}} - a_i \frac{\delta b_i}{\delta\gamma_{01}} \right) \quad (6.24c)$$

$$\frac{\delta\Delta\tau_{0,i}}{\delta\theta_1} = \frac{1}{b_i^2}\left(b_i \frac{\delta a_i}{\delta\theta_1} - a_i \frac{\delta b_i}{\delta\theta_1} \right) \quad (6.24d)$$

$$\frac{\delta\Delta\tau_{0,i}}{\delta\varphi_1} = \frac{1}{b_i^2}\left(b_i \frac{\delta a_i}{\delta\varphi_1} - a_i \frac{\delta b_i}{\delta\varphi_1} \right) \quad (6.24e)$$

where,

a_i is the numerator of Equation 6.6

b_i is the denominator of Equation 6.6

$$\frac{\delta a_i}{\delta \alpha_1} = T(1 - \alpha' - 3\alpha_1^2\alpha'^2 + 3\alpha_1^2\alpha'^3)(\cos\gamma_{01} - \cos\gamma_{i1}) \tag{6.25a}$$

$$\begin{aligned}\frac{\delta b_i}{\delta \alpha_1} = {} & 4\alpha_1\alpha' + 4\alpha_1^3\alpha'^2 + \cos\gamma_{01} + \cos\gamma_{i1} + \alpha'\cos\gamma_{01} + \alpha'\cos\gamma_{i1} + \\ & 2\alpha_1\cos\gamma_{01}\cos\gamma_{i1} + 4\alpha_1\alpha'\cos\gamma_{01}\cos\gamma_{i1} + \\ & 2\alpha_1\alpha'^2\cos\gamma_{01}\cos\gamma_{i1} + 3\alpha_1^2\alpha'\cos\gamma_{01} + 3\alpha_1^2\alpha'\cos\gamma_{i1} + \\ & 3\alpha_1^2\alpha'^2\cos\gamma_{01} + 3\alpha_1^2\alpha'^2\cos\gamma_{i1}\end{aligned} \tag{6.25b}$$

$$\frac{\delta a_i}{\delta \alpha'} = T(-\alpha_1 + 2\alpha_1^3\alpha' + 3\alpha_1^3\alpha'^2)(\cos\gamma_{01} - \cos\gamma_{i1}) \tag{6.25c}$$

$$\begin{aligned}\frac{\delta b_i}{\delta \alpha'} = {} & 2\alpha_1^2 + 2\alpha_1^4\alpha' + \alpha_1\cos\gamma_{01} + \alpha_1\cos\gamma_{i1} + 2\alpha_1^2\cos\gamma_{01}\cos\gamma_{i1} + \\ & 2\alpha_1^2\alpha'\cos\gamma_{01}\cos\gamma_{i1} + \alpha_1^3\cos\gamma_{01} + \alpha_1^3\cos\gamma_{i1} + \\ & 2\alpha_1^3\alpha'\cos\gamma_{01} + 2\alpha_1^3\alpha'\cos\gamma_{i1}\end{aligned} \tag{6.25d}$$

$$\frac{\delta a_i}{\delta \gamma_{01}} = T(\alpha_1 - \alpha_1\alpha' - \alpha_1^3\alpha'^2 + \alpha_1^3\alpha'^3)(-\sin\gamma_{01} + \sin\gamma_{i1}) \tag{6.25e}$$

$$\begin{aligned}\frac{\delta b_i}{\delta \gamma_0} = {} & -\alpha_1\sin\gamma_{01} - \alpha_1\sin\gamma_{i1} - \alpha_1\alpha'\sin\gamma_{01} - \alpha_1\alpha'\sin\gamma_{i1} - \\ & \alpha_1^2\cos\gamma_{01}\sin\gamma_{i1} - \alpha_1^2\sin\gamma_{01}\cos\gamma_{i1} - 2\alpha_1^2\alpha'\cos\gamma_{01}\sin\gamma_{i1} - \\ & 2\alpha_1^2\alpha'\sin\gamma_{01}\cos\gamma_{i1} - \alpha_1^2\alpha'^2\cos\gamma_{01}\sin\gamma_{i1} - \\ & \alpha_1^2\alpha'^2\sin\gamma_{01}\cos\gamma_{i1} - \alpha_1^3\alpha'\sin\gamma_{01} - \alpha_1^3\alpha'\sin\gamma_{i1} - \\ & \alpha_1^3\alpha'^2\sin\gamma_{01} - \alpha_1^3\alpha'^2\sin\gamma_{i1}\end{aligned} \tag{6.25f}$$

$$\frac{\delta a_i}{\delta \theta_1} = T(\alpha_1 - \alpha_1\alpha' - \alpha_1^3\alpha'^2 + \alpha_1^3\alpha'^3)\sin\gamma_{i1}\frac{\delta\gamma_{i1}}{\delta\theta_1} \tag{6.25g}$$

$$\begin{aligned}\frac{\delta b_i}{\delta \theta_1} = {} & (-\alpha_1\sin\gamma_{i1} - \alpha_1\alpha'\sin\gamma_{i1} - \alpha_1^2\cos\gamma_{01}\sin\gamma_{i1} - \\ & 2\alpha_1^2\alpha'\cos\gamma_{01}\sin\gamma_{i1} - \alpha_1^2\alpha'^2\cos\gamma_{01}\sin\gamma_{i1} - \alpha_1^3\alpha'\sin\gamma_{i1} - \\ & - \alpha_1^3\alpha'^2\sin\gamma_{i1})\frac{\delta\gamma_{i1}}{\delta\theta_1}\end{aligned} \tag{6.25h}$$

$$\frac{\delta a_i}{\delta \varphi_1} = T(\alpha_1 - \alpha_1\alpha' - \alpha_1^3\alpha'^2 + \alpha_1^3\alpha'^3)\sin\gamma_{i1}\frac{\delta\gamma_{i1}}{\delta\varphi_1} \tag{6.25i}$$

$$\frac{\delta b_i}{\delta \varphi_1} = (-\alpha_1\sin\gamma_{i1} - \alpha_1\alpha'\sin\gamma_{i1} - \alpha_1^2\cos\gamma_{01}\sin\gamma_{i1} - 2\alpha_1^2\alpha'\cos\gamma_{01}\sin\gamma_{i1} - \alpha_1^2\alpha'^2\cos\gamma_{01}\sin\gamma_{i1} - \alpha_1^3\alpha'\sin\gamma_{i1} - \alpha_1^3\alpha'^2\sin\gamma_{i1})\frac{\delta\gamma_{i1}}{\delta\varphi_1} \tag{6.25j}$$

where

$$\frac{\delta\gamma_{i1}}{\delta\theta_1} = \frac{2\pi}{\lambda_L}a_{0i}\cos(\varphi_1 - \phi_{0i})\sin\theta_1 \tag{6.26a}$$

$$\frac{\delta\gamma_{i1}}{\delta\varphi_1} = \frac{2\pi}{\lambda_L}a_{0i}\sin(\varphi_1 - \phi_{0i})\cos\theta_1 \tag{6.26b}$$

Similarly,

$$\frac{\delta\Delta\Psi_{0,i}}{\delta\alpha_1} = \frac{1}{c_i^2 + d_i^2}\left(d_i\frac{\delta c_i}{\delta\alpha} - c_i\frac{\delta d_i}{\delta\alpha}\right) \tag{6.27a}$$

$$\frac{\delta\Delta\Psi_{0,i}}{\delta\alpha'} = \frac{1}{c_i^2 + d_i^2}\left(d_i\frac{\delta c_i}{\delta\alpha'} - c_i\frac{\delta d_i}{\delta\alpha'}\right) \tag{6.27b}$$

$$\frac{\delta\Delta\Psi_{0,i}}{\delta\gamma_{01}} = \frac{1}{c_i^2 + d_i^2}\left(d_i\frac{\delta c_i}{\delta\gamma_{01}} - c_i\frac{\delta d_i}{\delta\gamma_{01}}\right) \tag{6.27c}$$

$$\frac{\delta\Delta\Psi_{0,i}}{\delta\theta_1} = \frac{1}{c_i^2 + d_i^2}\left(d_i\frac{\delta c_i}{\delta\theta_1} - c_i\frac{\delta d_i}{\delta\theta_1}\right) \tag{6.27d}$$

$$\frac{\delta\Delta\Psi_{0,i}}{\delta\varphi_1} = \frac{1}{c_i^2 + d_i^2}\left(d_i\frac{\delta c_i}{\delta\varphi_1} - c_i\frac{\delta d_i}{\delta\varphi_1}\right) \tag{6.27e}$$

where,

c_i is the numerator of Equation 6.11

d_i is the denominator of Equation 6.11

$$\frac{\delta c_i}{\delta\alpha_1} = \alpha'(\sin\gamma_{01} - \sin\gamma_{i1} + 2\alpha_1\alpha'\sin(\gamma_{01} - \gamma_{i1})) \tag{6.28a}$$

$$\frac{\delta d_i}{\delta \alpha_1} = \alpha'(\cos\gamma_{01} + \cos\gamma_{i1} + 2\alpha_1\alpha'\cos(\gamma_{01} - \gamma_{i1})) \quad (6.28b)$$

$$\frac{\delta c_i}{\delta \alpha'} = \alpha_1(\sin\gamma_{01} - \sin\gamma_{i1} + 2\alpha_1\alpha'\sin(\gamma_{01} - \gamma_{i1})) \quad (6.28c)$$

$$\frac{\delta d_i}{\delta \alpha'} = \alpha_1(\cos\gamma_{01} + \cos\gamma_{i1} + 2\alpha_1\alpha'\cos(\gamma_{01} - \gamma_{i1})) \quad (6.28d)$$

$$\frac{\delta c_i}{\delta \gamma_{01}} = \alpha_1\alpha'(\cos\gamma_{01} - \cos\gamma_{i1}) \quad (6.28e)$$

$$\frac{\delta d_i}{\delta \gamma_{01}} = \alpha_1\alpha'(-\sin\gamma_{01} - \sin\gamma_{i1}) \quad (6.28f)$$

$$\frac{\delta c_i}{\delta \theta_1} = \alpha_1\alpha'(-\cos\gamma_{i1} - \alpha_1\alpha'\cos(\gamma_{01} - \gamma_{i1}))\frac{\delta\gamma_{i1}}{\delta\theta_1} \quad (6.28g)$$

$$\frac{\delta d_i}{\delta \theta_1} = \alpha_1\alpha'(-\sin\gamma_{i1} + \alpha_1\alpha'\sin(\gamma_{01} - \gamma_{i1}))\frac{\delta\gamma_{i1}}{\delta\theta_1} \quad (6.28h)$$

$$\frac{\delta c_i}{\delta \varphi_1} = \alpha_1\alpha'(-\cos\gamma_{i1} - \alpha_1\alpha'\cos(\gamma_{01} - \gamma_{i1}))\frac{\delta\gamma_{i1}}{\delta\varphi_1} \quad (6.28i)$$

$$\frac{\delta d_i}{\delta \varphi_1} = \alpha_1\alpha'(-\sin\gamma_{i1} + \alpha_1\alpha'\sin(\gamma_{01} - \gamma_{i1}))\frac{\delta\gamma_{i1}}{\delta\varphi_1} \quad (6.28j)$$

Similarly,

e_i is the numerator of Equation 6.12

f_i is the denominator of Equation 6.12

$$\frac{\delta R_{0,i}}{\delta \alpha_1} = \frac{1}{f_i^2}\left(f_i\frac{\delta e_i}{\delta\alpha} - e_i\frac{\delta f_i}{\delta\alpha}\right) \quad (6.29a)$$

$$\frac{\delta R_{0,i}}{\delta \alpha'} = \frac{1}{f_i^2}\left(f_i\frac{\delta e_i}{\delta\alpha'} - e_i\frac{\delta f_i}{\delta\alpha'}\right) \quad (6.29b)$$

$$\frac{\delta R_{0,i}}{\delta \gamma_{01}} = \frac{1}{f_i^2}\left(f_i\frac{\delta e_i}{\delta\gamma_{01}} - e_i\frac{\delta f_i}{\delta\gamma_{01}}\right) \quad (6.29c)$$

$$\frac{\delta R_{0,i}}{\delta \theta_1} = \frac{1}{f_i^2}\left(f_i\frac{\delta e_i}{\delta\theta_1} - e_i\frac{\delta f_i}{\delta\theta_1}\right) \quad (6.29d)$$

$$\frac{\delta R_{0,i}}{\delta \varphi_1} = \frac{1}{f_i^2}\left(f_i \frac{\delta e_i}{\delta \varphi_1} - e_i \frac{\delta f_i}{\delta \varphi_1} \right) \tag{6.29e}$$

where

$$\frac{\delta e_i}{\delta \alpha_1} = 2\alpha'(\alpha_1\alpha' + \cos\gamma_{i1}) \tag{6.30a}$$

$$\frac{\delta f_i}{\delta \alpha_1} = 2\alpha'(\alpha_1\alpha' + \cos\gamma_{01}) \tag{6.30b}$$

$$\frac{\delta e_i}{\delta \alpha'} = 2\alpha_1(\alpha_1\alpha' + \cos\gamma_{i1}) \tag{6.30c}$$

$$\frac{\delta f_i}{\delta \alpha'} = 2\alpha_1(\alpha_1\alpha' + \cos\gamma_{01}) \tag{6.30d}$$

$$\frac{\delta e_i}{\delta \gamma_{01}} = -2\alpha_1\alpha'\sin\gamma_{i1} \tag{6.30e}$$

$$\frac{\delta f_i}{\delta \gamma_{01}} = -2\alpha_1\alpha'\sin\gamma_{01} \tag{6.30f}$$

$$\frac{\delta e_i}{\delta \theta_1} = -2\alpha_1\alpha'\sin\gamma_{i1}\frac{\delta \gamma_{i1}}{\delta \theta_1} \tag{6.30g}$$

$$\frac{\delta f_i}{\delta \theta_1} = 0 \tag{6.30h}$$

$$\frac{\delta e_i}{\delta \varphi_1} = -2\alpha_1\alpha'\sin\gamma_{i1}\frac{\delta \gamma_{i1}}{\delta \varphi_1} \tag{6.30i}$$

$$\frac{\delta f_i}{\delta \varphi_1} = 0 \tag{6.30j}$$

In the above formulation, the parameter α' is a function of the path delay. In the formulation of the carrier multipath and SNR errors, the parameters α_1 and α' appear together, as can be seen from Equations 6.17 and 6.18. This implies that the reflection coefficient and correlation ratio affect the multipath error in the same way, and therefore it is not possible to distinguish their effects or separate their influences. In other words, for a given multipath error, there is no unique solution for α_1 and α'. Instead there would

be many values of α' which satisfy the equation, and for each value of α', an α_1 can be found which satisfies the equation. This argument was substantiated through simulations and real data analysis. In fact, it is possible to combine the two parameters, to create a modified reflection coefficient $\alpha''=\alpha_1\alpha'$, in Equations 6.17 (or 6.11) and 6.18 (or 6.12), and the filter equations can be reformulated. This cannot be done for the code multipath error equations, as α_1 and α' do not appear simultaneously in Equation 6.16. Furthermore, it is possible to hold the value of the correlation ratio to a constant, and then estimate the other four parameters. In this case, however, the other parameters will have to absorb the influences of the time variation of the correlation ratio as shown in Figure 6.1.

Therefore, an alternative approach to the estimation problem is to assume a value of α' and then reformulate the filter equations. That way, only four unknown parameters are estimated using the filter, where the state vector is given by:

$$x = [\alpha_1 \quad \gamma_{01} \quad \theta_1 \quad \varphi_1]^T \tag{6.31}$$

Correspondingly, the design matrix reduces to,

$$H = \begin{bmatrix} \frac{\delta(\Delta\tau_{0,1})}{\delta\alpha_1} & \frac{\delta(\Delta\tau_{0,1})}{\delta\gamma_{01}} & \frac{\delta(\Delta\tau_{0,1})}{\delta\theta_1} & \frac{\delta(\Delta\tau_{0,1})}{\delta\varphi_1} \\ --- & --- & --- & --- \\ \frac{\delta(\Delta\tau_{0,m-1})}{\delta\alpha_1} & \frac{\delta(\Delta\tau_{0,m-1})}{\delta\gamma_{01}} & \frac{\delta(\Delta\tau_{0,m-1})}{\delta\theta_1} & \frac{\delta(\Delta\tau_{0,m-1})}{\delta\varphi_1} \\ \frac{\delta(\Delta\Psi_{0,1})}{\delta\alpha_1} & \frac{\delta(\Delta\Psi_{0,1})}{\delta\gamma_{01}} & \frac{\delta(\Delta\Psi_{0,1})}{\delta\theta_1} & \frac{\delta(\Delta\Psi_{0,1})}{\delta\varphi_1} \\ --- & --- & --- & --- \\ \frac{\delta(\Delta\Psi_{0,m-1})}{\delta\alpha_1} & \frac{\delta(\Delta\Psi_{0,m-1})}{\delta\gamma_{01}} & \frac{\delta(\Delta\Psi_{0,m-1})}{\delta\theta_1} & \frac{\delta(\Delta\Psi_{0,m-1})}{\delta\varphi_1} \\ \frac{\delta(R_{0,1})}{\delta\alpha_1} & \frac{\delta(R_{0,1})}{\delta\gamma_{01}} & \frac{\delta(R_{0,1})}{\delta\theta_1} & \frac{\delta(R_{0,1})}{\delta\varphi_1} \\ --- & --- & --- & --- \\ \frac{\delta(R_{0,m-1})}{\delta\alpha_1} & \frac{\delta(R_{0,m-1})}{\delta\gamma_{01}} & \frac{\delta(R_{0,m-1})}{\delta\theta_1} & \frac{\delta(R_{0,m-1})}{\delta\varphi_1} \end{bmatrix} \tag{6.32}$$

In the Kalman filter, the state variables are described as simple first order Gauss-Markov processes (Gelb, 1979; Maybeck, 1994). The correlation time is selected to be about 1-2 minute(s) and an appropriate process noise is chosen to drive the system dynamics model. The choice of various parameters to describe the dynamic and the measurement models is explained in Chapter 7.

The filter described herein is used to estimate the unknown multipath and geometric parameters for a particular satellite. As the filter estimates the parameters based on the measurements that are affected by multipath from all sources in the environment, the estimated parameters refer to the composite multipath. After the parameters are estimated, the code and carrier multipath errors can be readily computed by using Equations 6.19 and 6.20, respectively. This technique has to be repeated for each satellite, or, alternatively, a parallel independent filter is to be used for each satellite.

The above formulation is quite generic in nature, and includes code, carrier and SNR information. However, it is possible to estimate the multipath and geometric parameters from a subset of these measurements. For example, in principle it is possible to estimate multipath parameters from either code, carrier, or SNR information alone, or their combinations, as long as there is a sufficient number of measurements.

6.5 Multipath Mitigation using Simulations

The multipath mitigation algorithm was first tested on simulated code, carrier and SNR data. Different multipath mitigation models were used to mitigate the simulated multipath errors in the code and carrier, and their performances were evaluated in the simulated multipath environment. Later, the simulated measurements were replaced by the actual measurements from the field data. The core mitigation algorithms, however, remained the same. Figure 6.4 shows various steps of multipath mitigation using a simulated multipath environment.

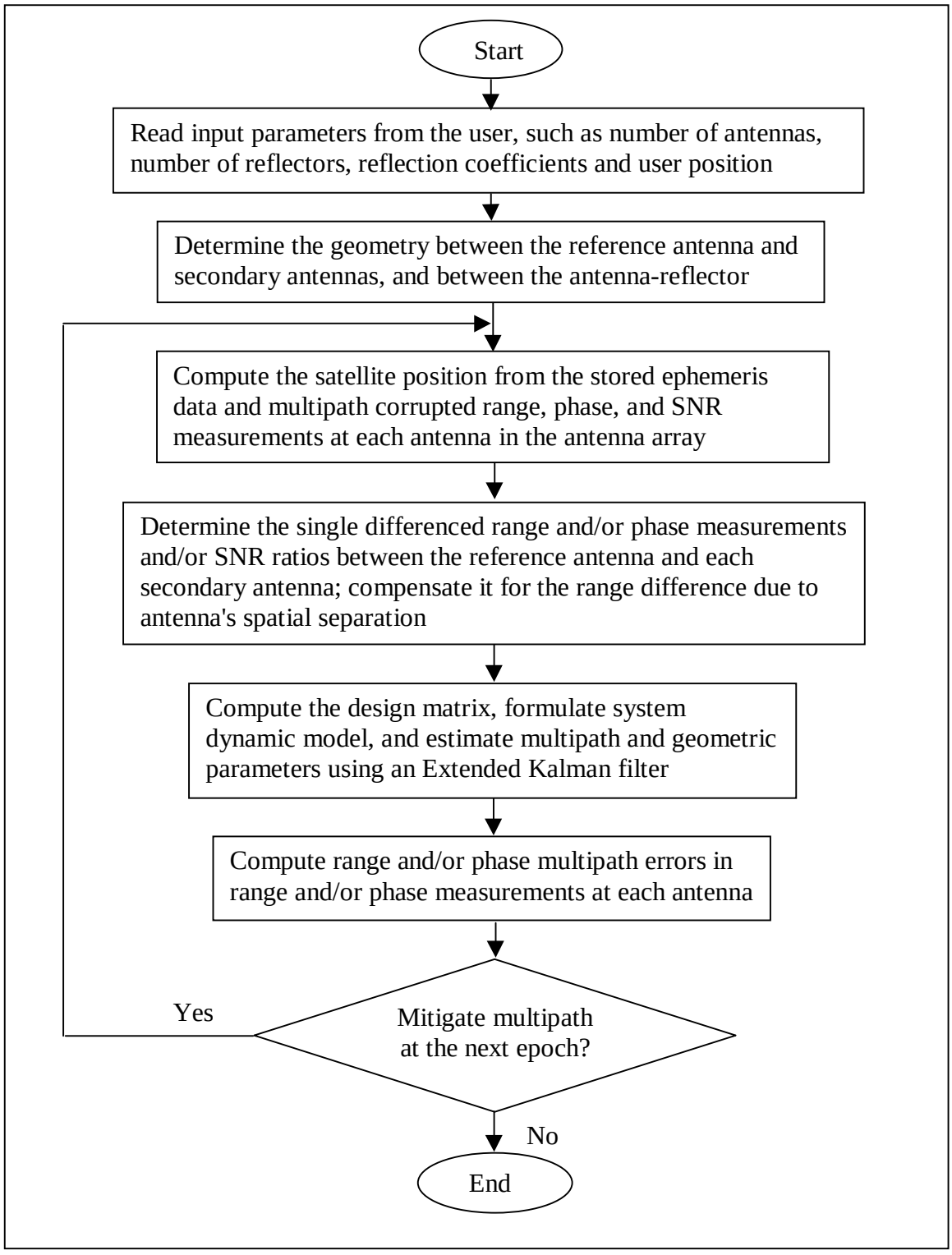

Figure 6.4: Flowchart of multipath mitigation technique

For multipath mitigation, code, carrier and SNR measurements are used either individually or collectively. Measurements are single differenced between the reference antenna and each secondary antenna in the antenna array. The range or phase difference between the reference antenna and each secondary antenna due to their spatial separation is computed and subtracted from the single differenced measurements. The adjusted single differenced measurements are fed to a Kalman Filter to estimate the state variables.

The Kalman Filter estimates the state variables at each epoch (which is at 1 Hz in this case). The estimated state variables are used to compute the code and carrier multipath errors using Equations 6.19 and 6.20 respectively. The estimated multipath error is removed from the raw code and carrier measurements to obtain multipath-reduced measurements.

The difference between the multipath-corrupted measurements and the true measurements (i.e. the measurements due to the direct signal only) gives the *truth value* of multipath error. Multipath errors computed from the estimated multipath parameters give the *estimated value* of the multipath error. The difference between the *truth value* and the *estimated value* gives the residual multipath error, and may be used as a measure to evaluate multipath mitigation performances using various multipath mitigation models.

The multipath mitigation algorithm was tested in several steps. First, the simulated code measurements alone were used to estimate code multipath errors. Then, the simulated carrier phase measurements alone were used to estimate carrier phase multipath errors. The SNR measurements were then used to estimate code and carrier phase multipath errors. Finally, code, carrier and SNR measurements were collectively used to estimate code and carrier multipath errors. Some of the problems of using all the measurements together are described and substantiated with simulations. Finally, multipath errors due to multiple reflectors are estimated, and the performance of this technique under such situations is evaluated.

6.5.1 Code Multipath Mitigation using Code Measurements

In this simulation, six antennas are used in a closely-spaced cluster at approximately 5-10 cm from each other (centre to centre). A reflector, which has a reflection coefficient of 0.3, is placed at a distance of 6 metres from the antenna cluster, and is assumed to be the only reflector in the environment. The multipath phase is computed from the path delay alone.

Figure 6.5 shows the single differenced multipath corrupted ranges between the reference antenna (A0) and some of the secondary antennas in the antenna array. The single differenced measurements are compensated for the differential ranges, due to spatial separation of the antennas. It can be seen that the errors are correlated between the single differenced measurements, when observed over a time span, though at a particular instant they may appear uncorrelated. This is due to the fact that, even though a common large reflector corrupts the measurements at each antenna, the multipath phases are different at different antennas.

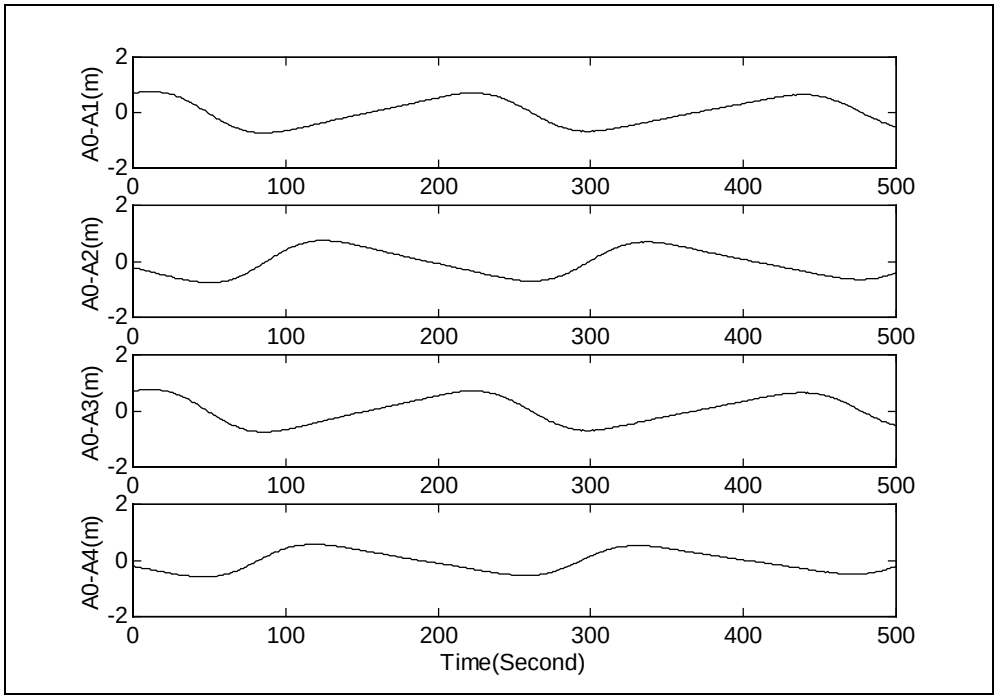

Figure 6.5: Single differenced range measurements between the reference and secondary antennas (reflection coefficient = 0.3 and reflector distance = 6 m)

The single differenced code measurements are used in the Kalman Filter, which estimates multipath and geometric parameters from the single differenced range measurements only. The design matrix of the Kalman Filter has only the first *m-1* rows in the H matrix in Equation 6.32. Figure 6.6 shows the state variables estimated by the filter. It is evident that the filter takes some time to converge to the right values. The steady state values of the parameters match their expected values.

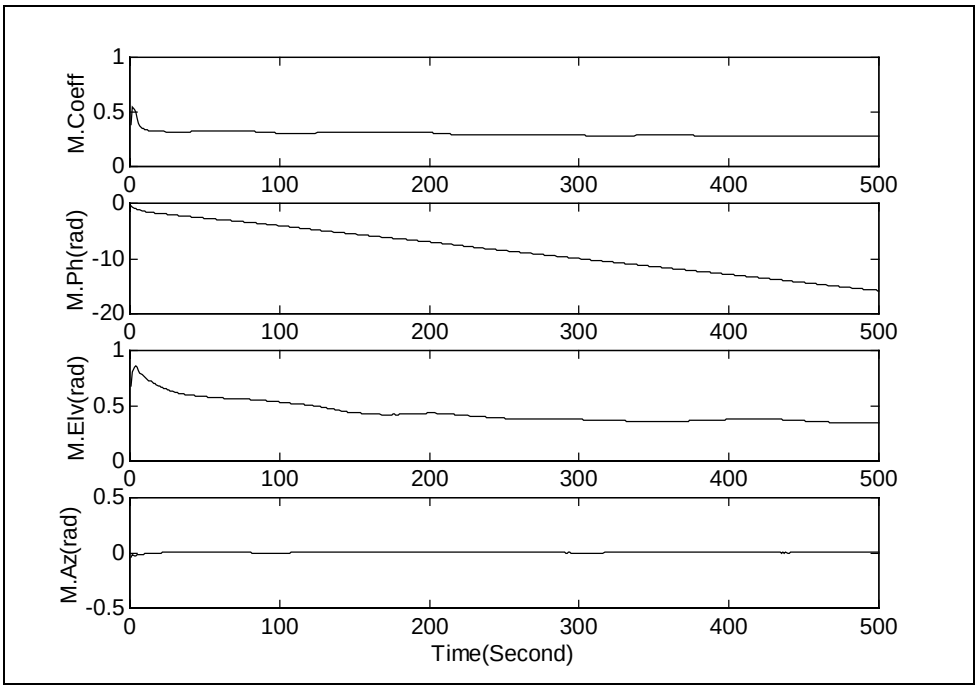

Figure 6.6: Estimated parameters by a Kalman Filter using only code measurements

Figure 6.7 shows the *truth values* of the code multipath errors at antennas 0 to 3, which are computed by subtracting the direct ranges from the multipath-corrupted ranges for each antenna in the antenna array. Figure 6.8 shows the *estimated values* of the code multipath errors computed from the estimated parameters at those antennas, and using Equation 6.19. The estimated values look similar to the *truth* values. Figure 6.9 shows the difference between the *truth* and the *estimated* code multipath errors. It is evident from the figure that small estimation errors only appear during convergence. At steady state,

the estimation error is close to zero. The results at other antennas were also the same and are not shown here. The performance of this mitigation technique was further evaluated by simulating different multipath scenarios and mitigating the multiapth error using this technique. In all cases, similar results were obtained, that confirmed the effectiveness of this technique. This proves that by using this technique, the code multipath error can be estimated and mitigated using only code measurements.

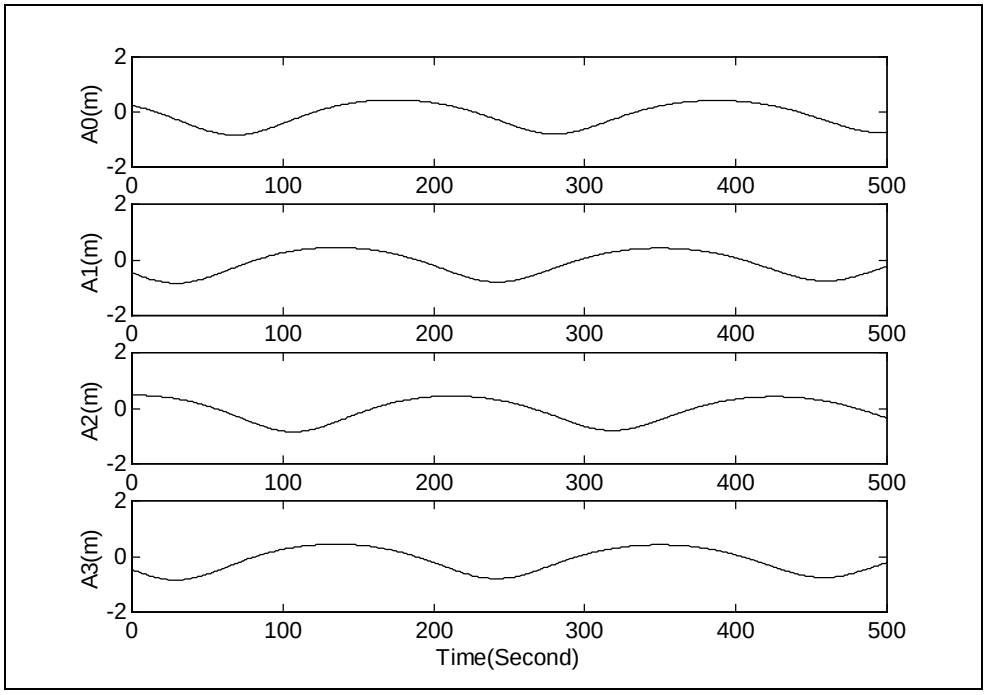

Figure 6.7: True code multipath errors at each antenna

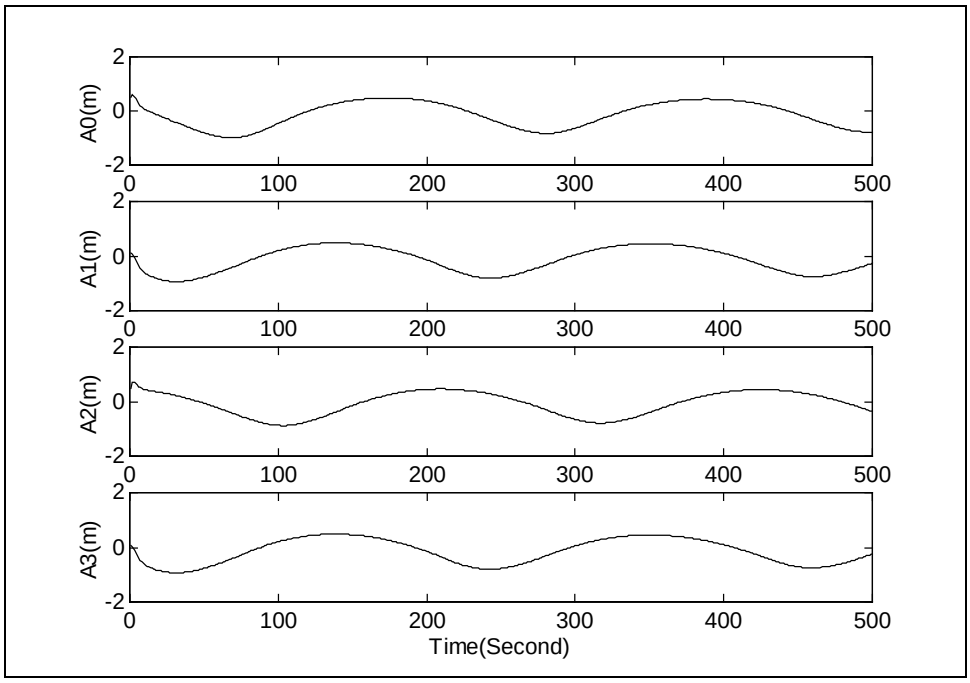

Figure 6.8: Estimated code multipath errors at each antenna

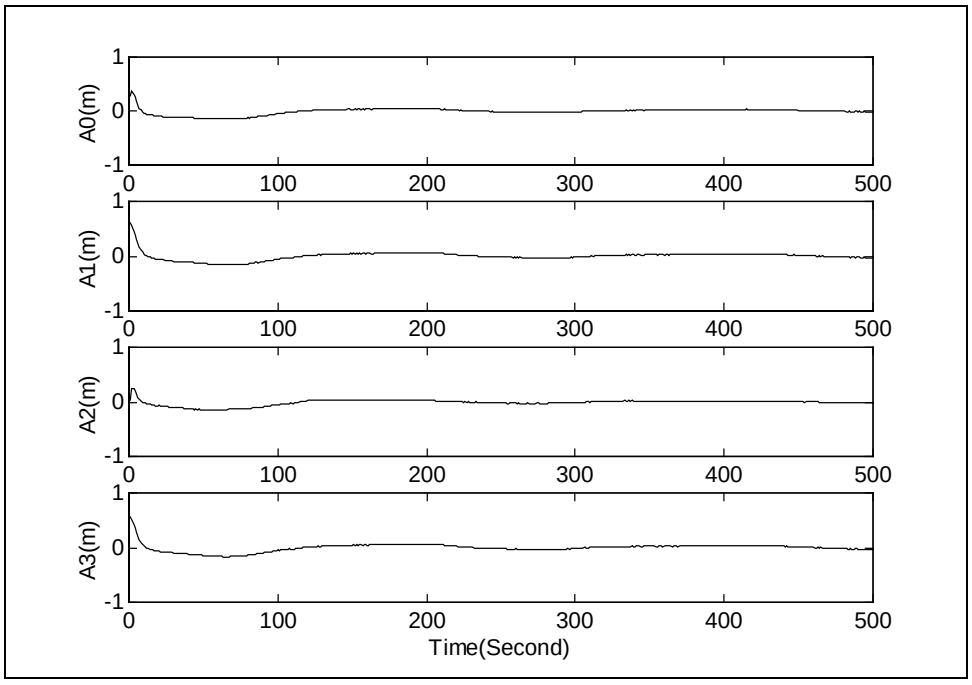

Figure 6.9: Code multipath estimation error using the proposed technique

6.5.2 Carrier Phase Multipath Mitigation Using Carrier Phase Measurements

In this simulation, a reflector with a reflection coefficient of 0.6 is placed at a distance of 9 metres from the antenna cluster. The location of the reflector is different when compared to the location in code multipath mitigation simulation. That was done to check whether the mitigation technique works for different multipath scenarios. The multipath phase is computed from the differential path delay only.

The phase measurement between a satellite and each antenna in the antenna array, in the presence of the reflector, is computed using Equation 5.9. Figure 6.10 shows the single differenced multipath corrupted phase measurements between the reference antenna (A0) and secondary antennas in the antenna array. The single differenced measurements are compensated for the range differences, due to spatial separation of the antennas. Though the single differenced errors at each antenna pair appear uncorrelated, they indeed are related by various multipath parameters. The multipath phase at each antenna is such that the errors add constructively or destructively in the single differenced measurements and result in such patterns, which may appear uncorrelated.

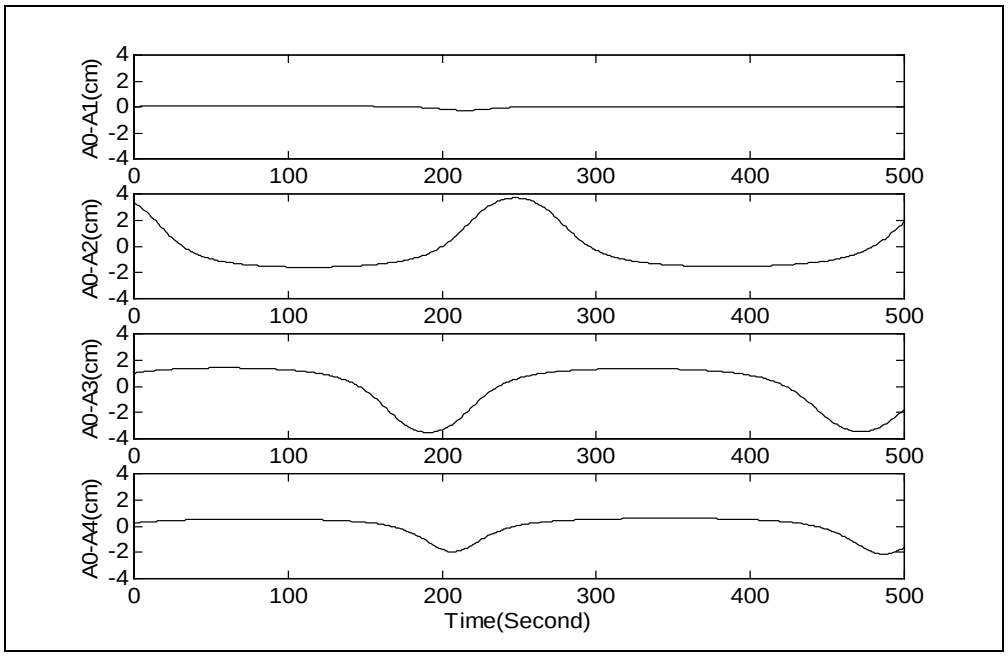

Figure 6.10: Single differenced phase measurements between the reference and secondary antennas (reflection coefficient = 0.6 and reflector distance = 9 m)

The single differenced carrier phase measurements are used in the Kalman Filter, which estimates multipath parameters from the single differenced carrier phase measurements only. The design matrix of the Kalman Filter has only the middle *m-1* rows of the H matrix in Equation 6.32. Figure 6.11 shows the multipath parameters estimated by the filter. It is evident that the filter takes some time to converge to the right values. The steady state values of the parameters match their expected values.

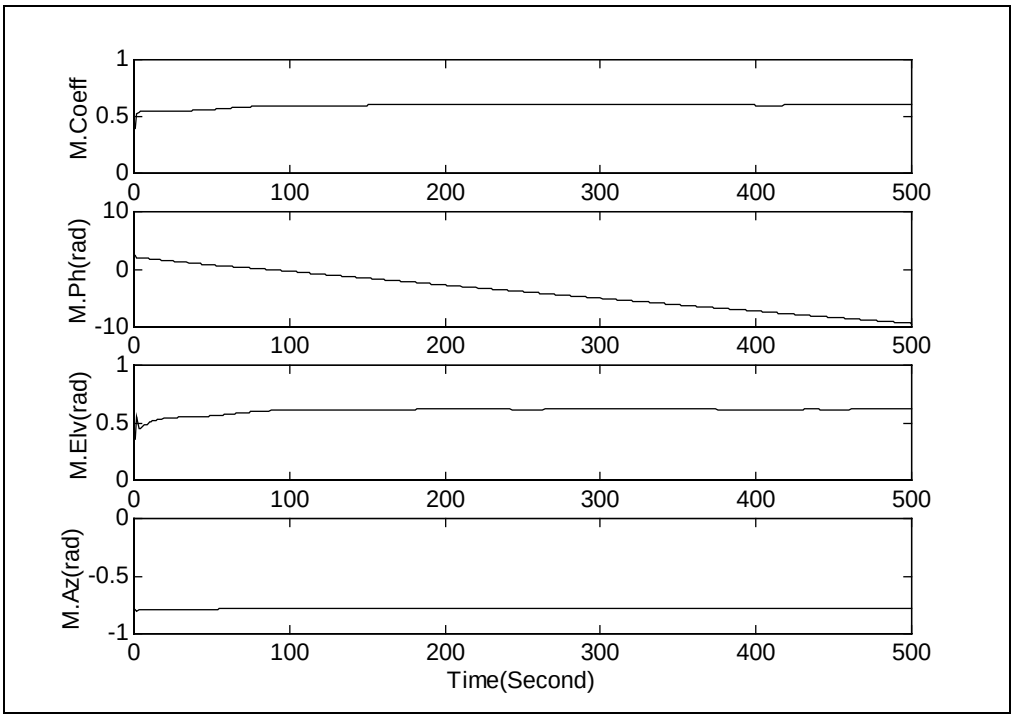

Figure 6.11: Estimated parameters by using phase measurements only

Figure 6.12 shows the *truth values* of the carrier phase multipath errors at antennas 0 to 3, which are computed by subtracting the phases due to the direct signals from the multipath-corrupted phases for each antenna in the antenna array. Figure 6.13 shows the *estimated values* of the phase multipath errors computed from the estimated parameters, and using Equation 6.20. The estimated values look similar to the *truth* values. Figure 6.14 shows the difference between the *truth* and the *estimated* phase multipath errors. It is evident from the figure that small estimation errors only occur during convergence. At

steady state, the estimation error is close to zero. The results at other antennas were also the same and are not shown here. The performance of this mitigation technique was further evaluated by simulating different multipath scenarios and mitigating the carrier phase multiapth error using this technique. In all cases, similar results were obtained, that confirmed the effectiveness of this technique. This proves that the carrier phase multipath error can be estimated and mitigated using only phase measurements using this technique.

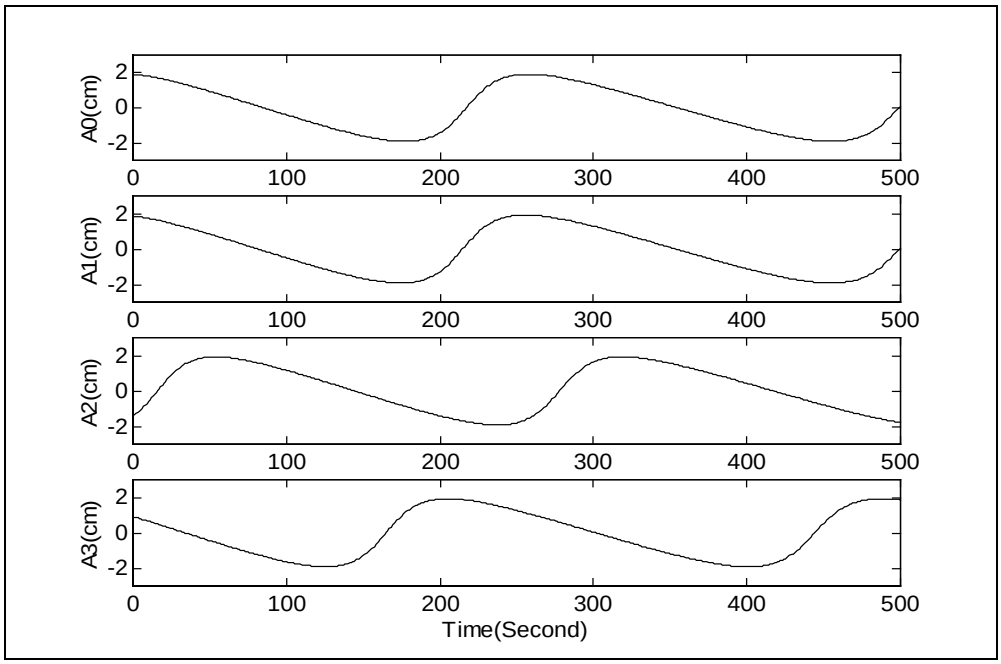

Figure 6.12: True carrier phase multipath errors at each antenna

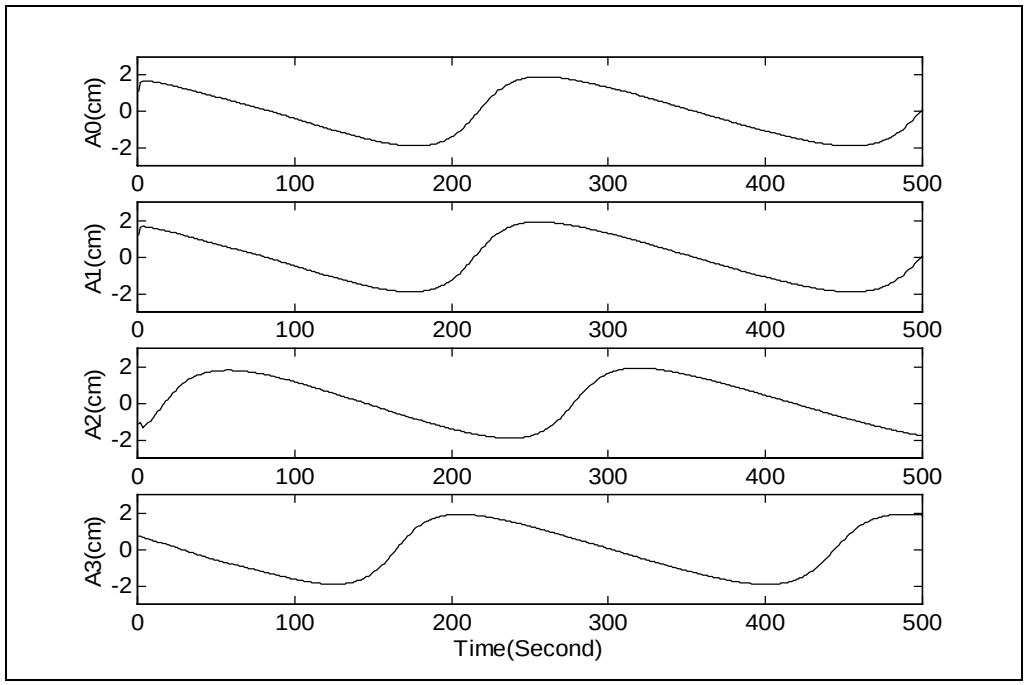

Figure 6.13: Estimated carrier phase multipath errors at each antenna

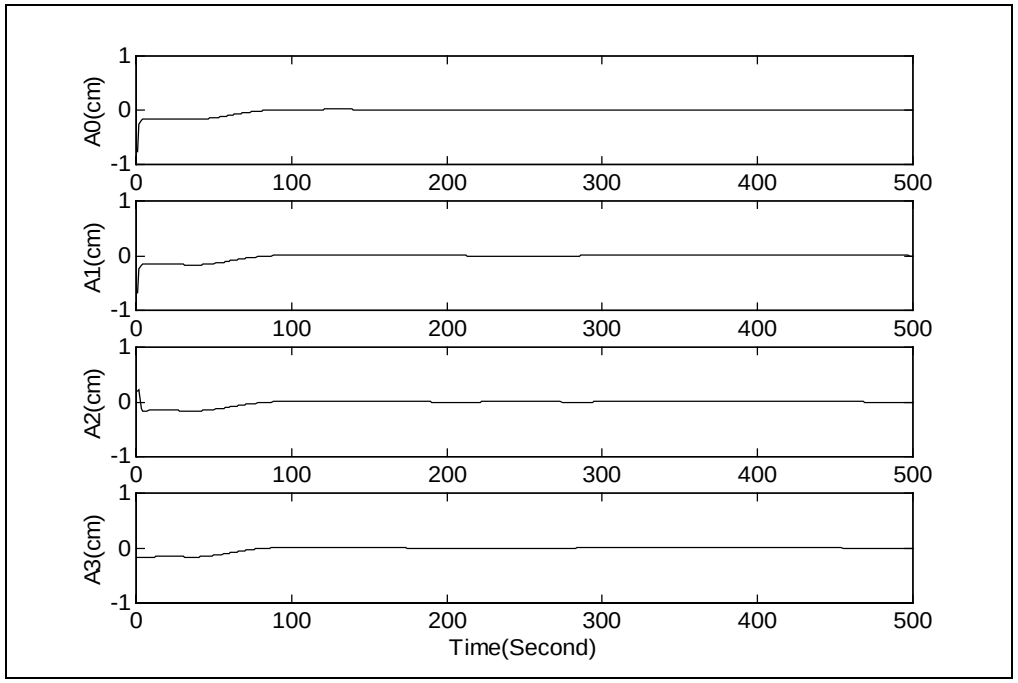

Figure 6.14: Carrier phase multipath estimation error using the proposed technique

6.5.3 Code and Carrier Phase Multipath Mitigation using SNR Measurements

As the multipath parameters are common for code, carrier and SNR measurements in a receiver, it is, in principle, possible to estimate the code and the carrier multipath errors from SNR measurements. Only multipath errors due to a close-by reflector are considered for this simulation. In the simulation, a reflector with a reflection coefficient of 0.8 is placed at a distance of 7 metres from the antenna cluster. The location of the reflector is different when compared to the locations used for code and carrier multipath mitigation simulations to evaluate the effectiveness of this technique at different multipath scenarios. The multipath phase is computed directly from the differential path delay.

The SNR of the incoming signal in the receiver is computed using Equation 5.12. Here, it is assumed that each antenna has a uniform gain pattern in all directions, and that the gain pattern is the same for all antennas in the antenna cluster. With this assumption, it is not necessary to include the antenna gain parameter in the multipath error estimation equations. The signal power, or SNR, in the receiver varies with time, due to satellite elevation changes. But, as the magnitude of variation is the same in all antennas in the cluster, it does not affect the ratio of SNRs (or the single difference of the C/N_0s). Figure 6.15 shows the single differenced multipath corrupted SNRs between the reference antenna (A0) and secondary antennas in the antenna cluster. The single differenced errors look correlated, but are of different amplitudes, due to the differences in the multipath phase.

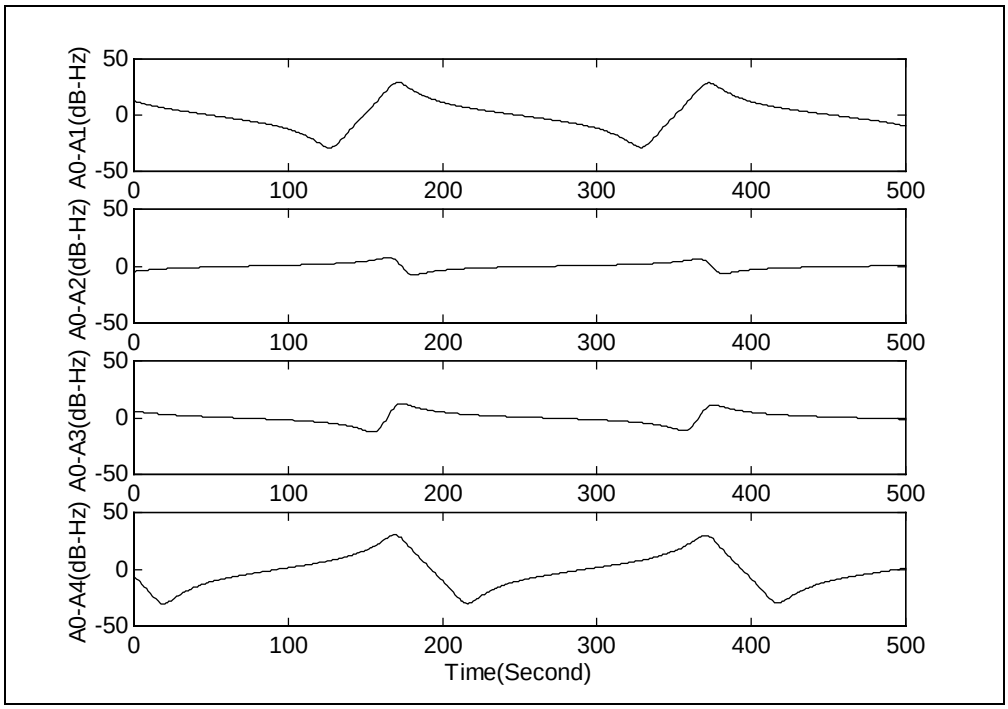

Figure 6.15: Single differenced SNR measurements between the reference and secondary antennas (reflection coefficient = 0.8 and reflector distance = 7 m)

The single difference SNR measurements are input to the Kalman Filter, which estimates multipath parameters from the ratio of SNR measurements only. The design matrix of the Kalman Filter has only the last *m-1* rows of the H matrix in Equation 6.32. The multipath parameters were estimated by the filter and the parameters were found to match their expected values at steady state.

The *estimated values* of the code multipath errors are computed from the estimated parameters. Figure 6.16 shows the estimation error, (i.e. the difference between the *truth* and the *estimated* code multipath errors). It can be seen that the estimation error or the residual error is nearly zero, except when the multipath error dips to a very low value. The reason for the residual error, is that when the multipath error decreases very rapidly, the correlation ratio (α') also decreases very quickly, as shown in Figure 6.1. However, the correlation ratio is fixed to a constant value during this estimation process, which results in the residual multipath error.

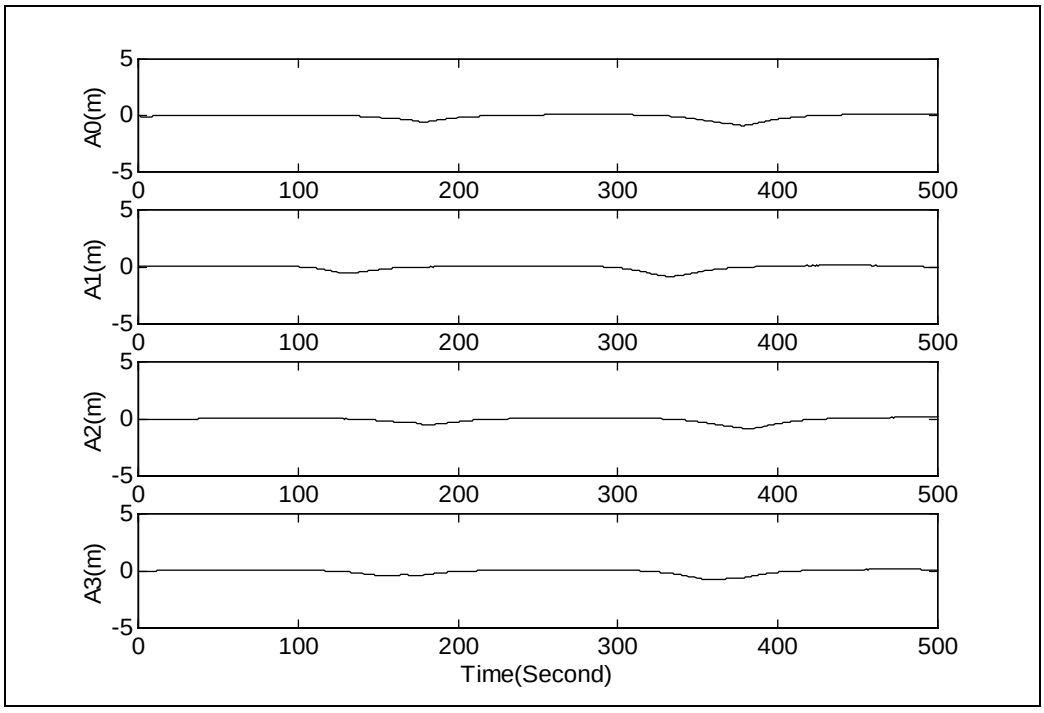

Figure 6.16: Code multipath estimation errors using the proposed technique

From the estimated parameters, the carrier phase multipath errors are also computed and compared with their truth values. Figure 6.17 shows the estimation error, i.e. the difference between the *truth* and the *estimated* values. It can be seen that the estimation error, or the residual error, is nearly zero. This proves that using this technique, code and carrier phase multipath errors can be estimated from SNR measurements alone.

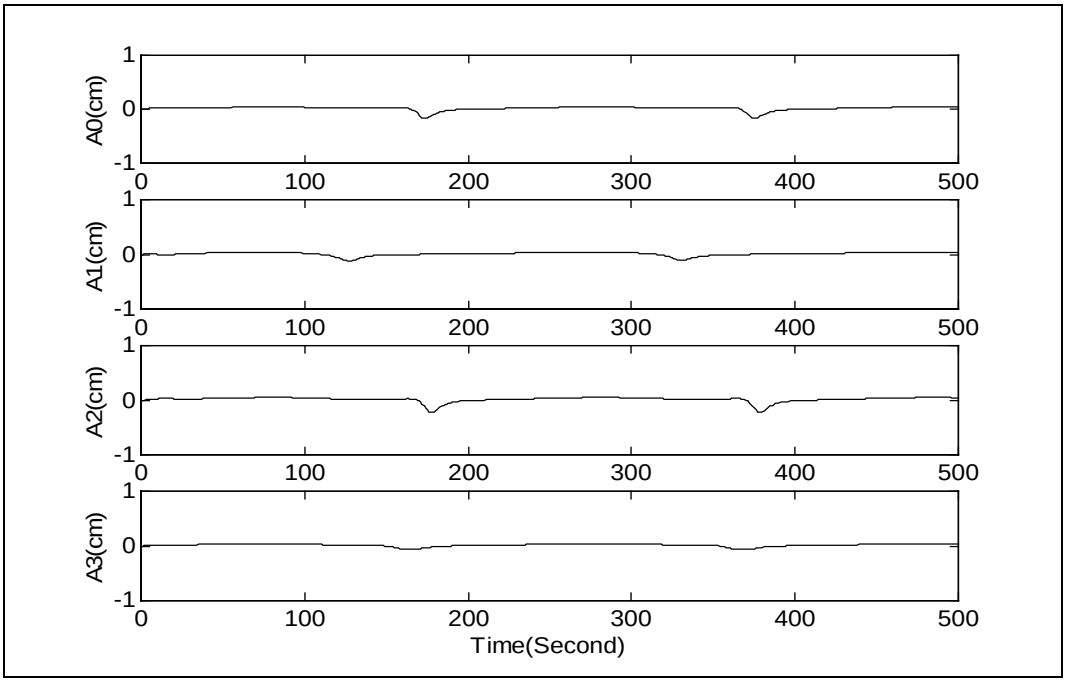

Figure 6.17: Carrier phase multipath estimation errors using the proposed technique

6.5.4 Code and Carrier Multipath Mitigation using Code, Carrier and SNR measurements

Close-by reflector

In this simulation a reflector with a reflection coefficient of 0.5 is placed at a distance of 6 metres from the cluster. The antenna gain pattern is assumed to be uniform in all directions, and the multipath phase is computed from the differential path delay only.

The single differenced code, carrier and SNR measurements between the reference antenna and secondary antennas, are input to the Kalman Filter, which estimates multipath parameters from all these measurements. The design matrix of the Kalman Filter has all the elements in the H matrix in Equation 6.32. Figure 6.18 shows the parameters estimated by the filter. The steady state values of the parameters match their expected values. Some small oscillations in some of the parameters, such as elevation, are evident. These oscillations absorb the variations in the correlation coefficient as the

coefficient is assumed to be a constant despite having small oscillations, as shown in Figure 6.1.

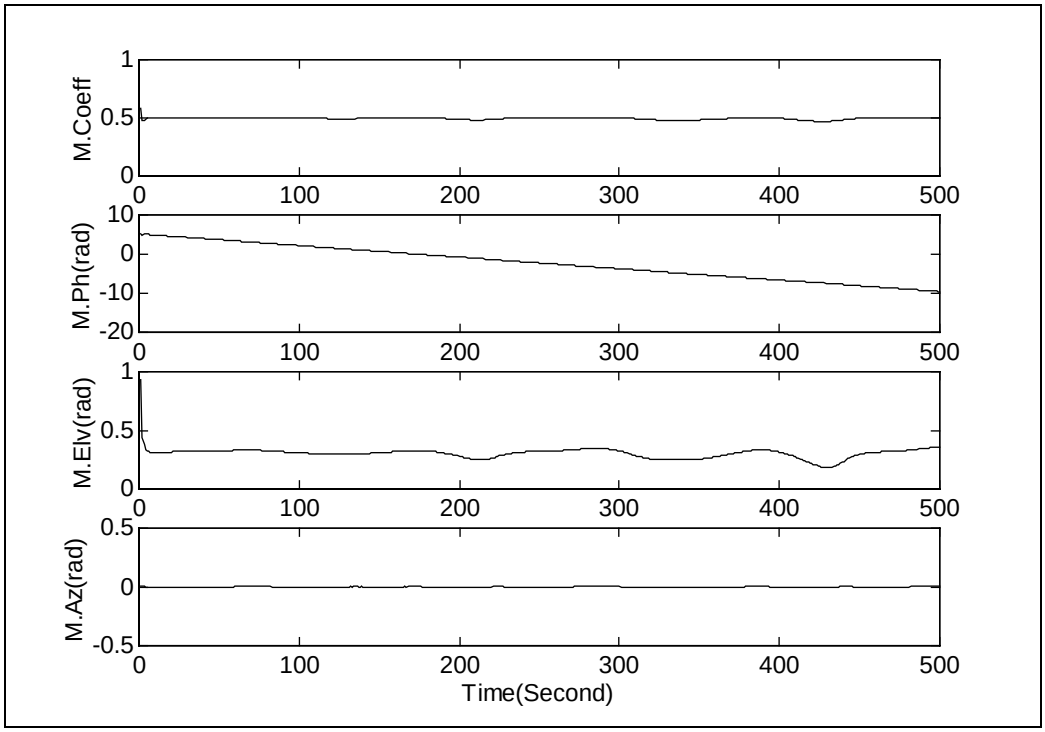

Figure 6.18: Estimated parameters by using code, carrier and SNR measurements

The *estimated values* of the code multipath errors are computed from the estimated parameters. Figure 6.19 shows the estimation error, i.e. the difference between the *truth* and the *estimated* code multipath errors. It can be seen that the estimation error, or the residual error, is nearly zero, except when the multipath error dips to a very low value. This is because the correlation coefficient is held to a constant value, as described earlier.

From the estimated parameters, the carrier phase multipath errors are also computed and compared with their truth values. Figure 6.20 shows the estimation error, (i.e. the difference between the *truth* and the *estimated* values). It can be seen that the estimation error, or the residual error, is nearly zero. This proves that using this technique, code and carrier phase multipath errors due to a close-by reflector can be estimated from combined code, carrier and SNR measurements.

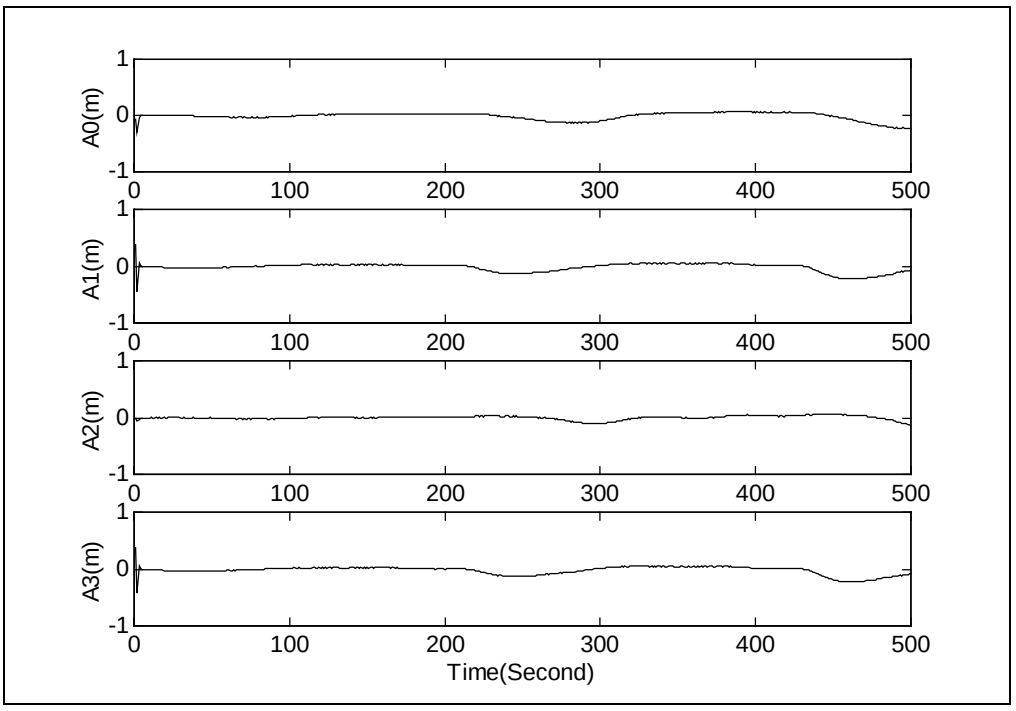

Figure 6.19: Code multipath estimation errors using the proposed technique

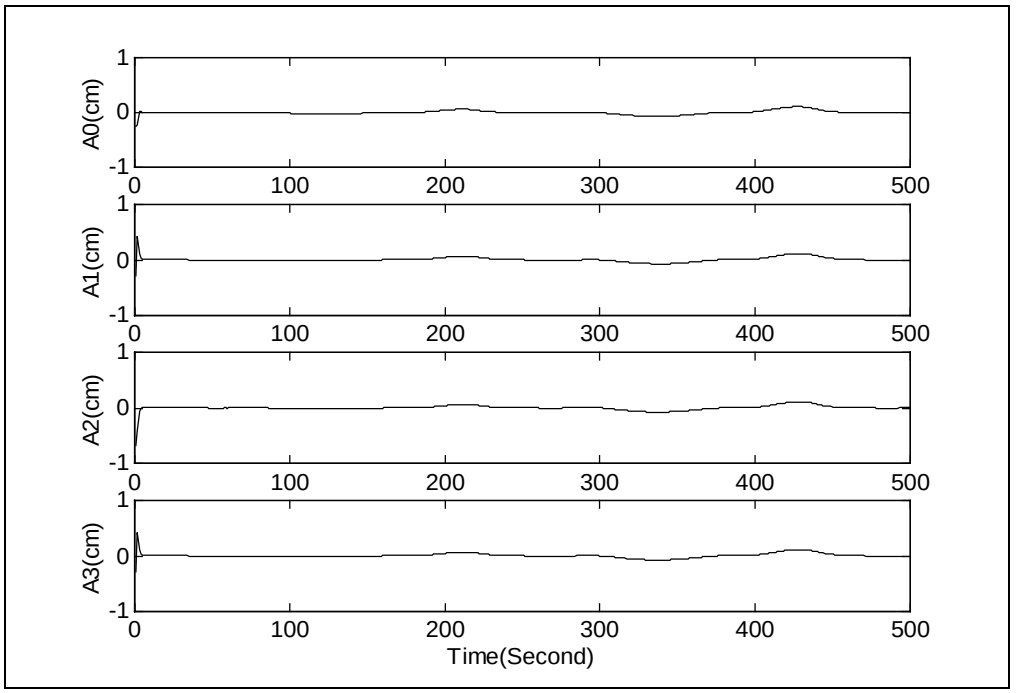

Figure 6.20: Carrier phase multipath estimation errors using the proposed technique

Far away reflector

If the multipath effects are due to reflectors from far away objects, the formulation described in the earlier sections does not apply anymore. That is because, though the formulations for carrier phase multipath and SNR errors hold for all multipath delays, the formulation of the code multipath error holds only for short multipath delays. This is explained with simulations.

In this simulation, a reflector is placed 60 m from the antenna array (which causes an actual multipath delay of about 54 m) and is the only source of multipath error in the environment. Figure 6.21 shows the *truth values* of the code multipath errors. The *estimated values* of the code multipath errors are computed from the estimated parameters and are shown in Figure 6.22. The estimated code multipath errors vary significantly from their true values.

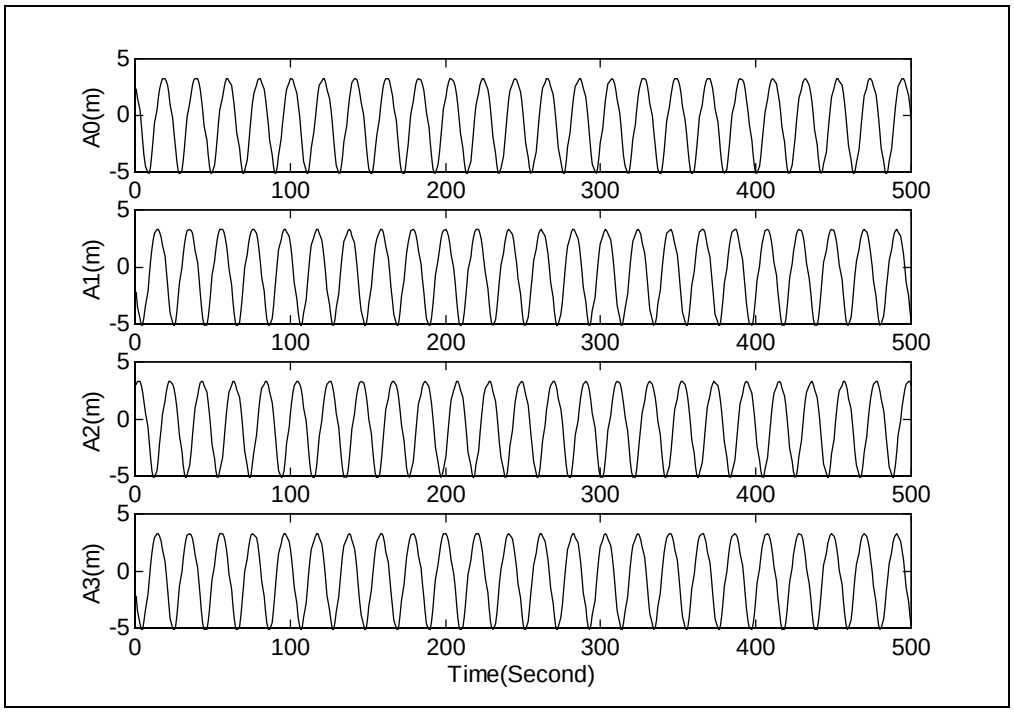

Figure 6.21: True code multipath errors at each antenna due to a far away reflector

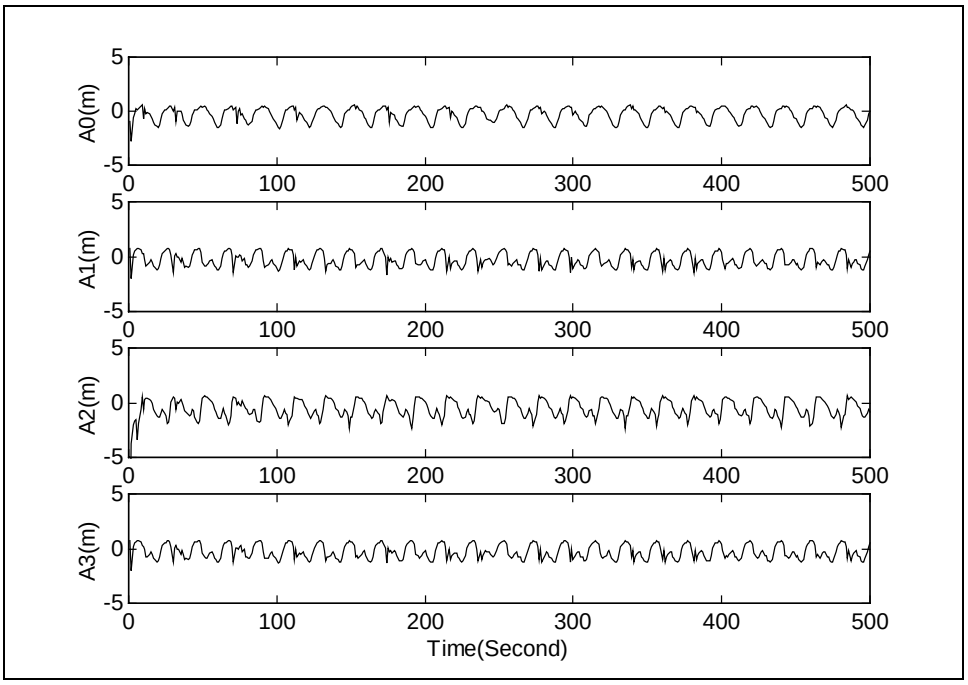

Figure 6.22: Estimated code multipath errors using code, carrier and SNR measurements

From the estimated parameters, the carrier phase multipath errors are also computed and compared with their truth values. Figure 6.23 shows the *truth values* of the carrier phase multipath errors and Figure 6.24 shows the *estimated values*. It can be seen that even in this case the estimated phase multipath errors are somewhat different from their *truth values*. However, the carrier estimation is better than the code estimation. That is because, the carrier measurements are deemed to be of higher accuracy compared to their code counterparts in the Kalman Filter.

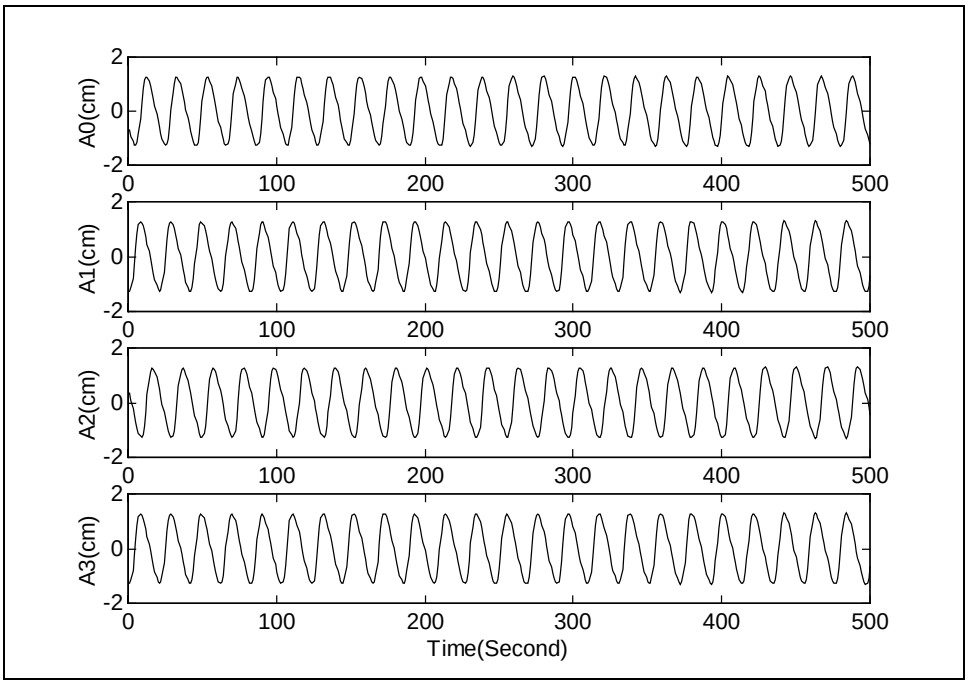

Figure 6.23: True carrier phase multipath errors at each antenna due to a far away reflector

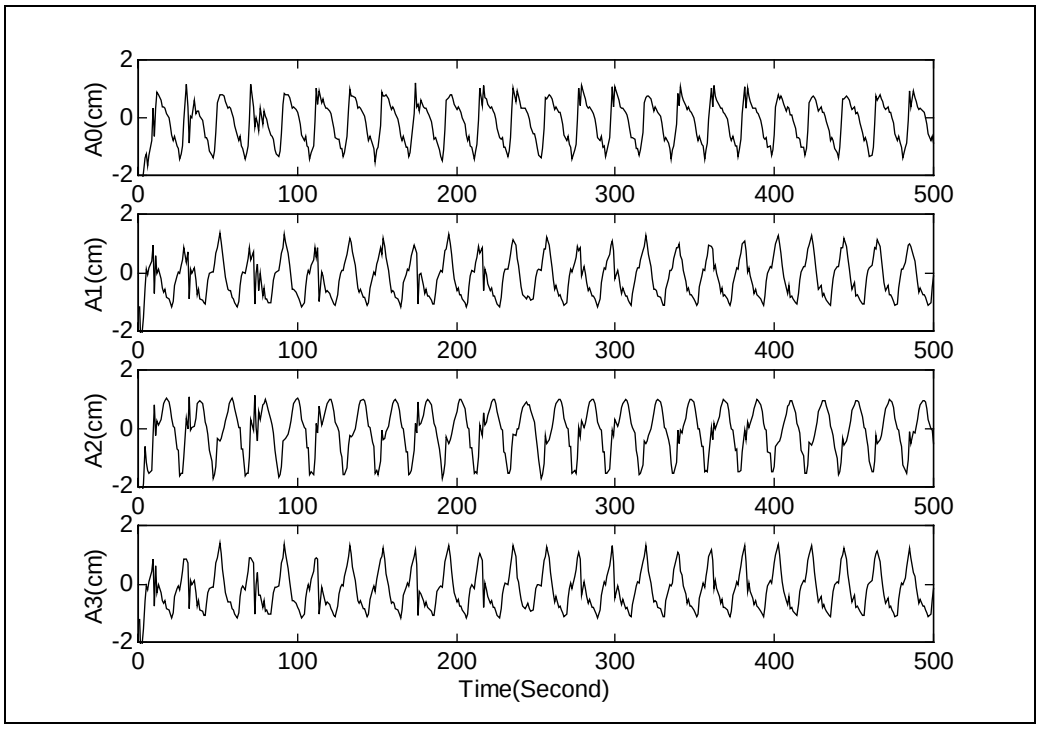

Figure 6.24: Estimated carrier phase multipath error using code, carrier and SNR measurements

Furthermore, for the same simulated multipath environment, the carrier and SNR measurements are given a normal weight (carrier phase measurement variance equal to 10^{-5} m^2 and SNR measurement variance equal to 10^{-1}), but the code measurements are given a very low weight (code measurement variance equal to 10^4 m^2), such that estimates are heavily dependent upon the phase measurements and the phase multipath model.

Figure 6.25 shows the code multipath estimation errors, while Figure 6.21 shows their truth values. As expected, the estimation is not good. Similarly, Figure 6.26 shows the estimation errors of the carrier phase multipath, while Figure 6.23 shows their truth values. In this case, however, the estimated values are very close to the truth values and the estimation error is very close to zero. This suggests that this technique is effective in mitigating long delay carrier phase multipath.

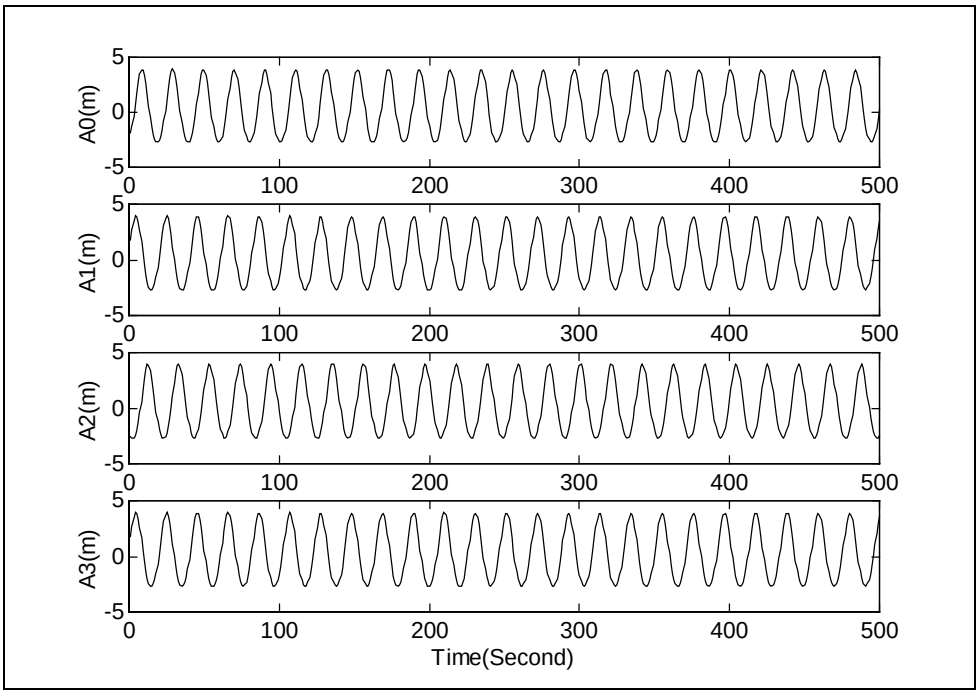

Figure 6.25: Code multipath estimation errors with very low weight to code measurements and normal weights to carrier and SNR measurements for a long delay multipath

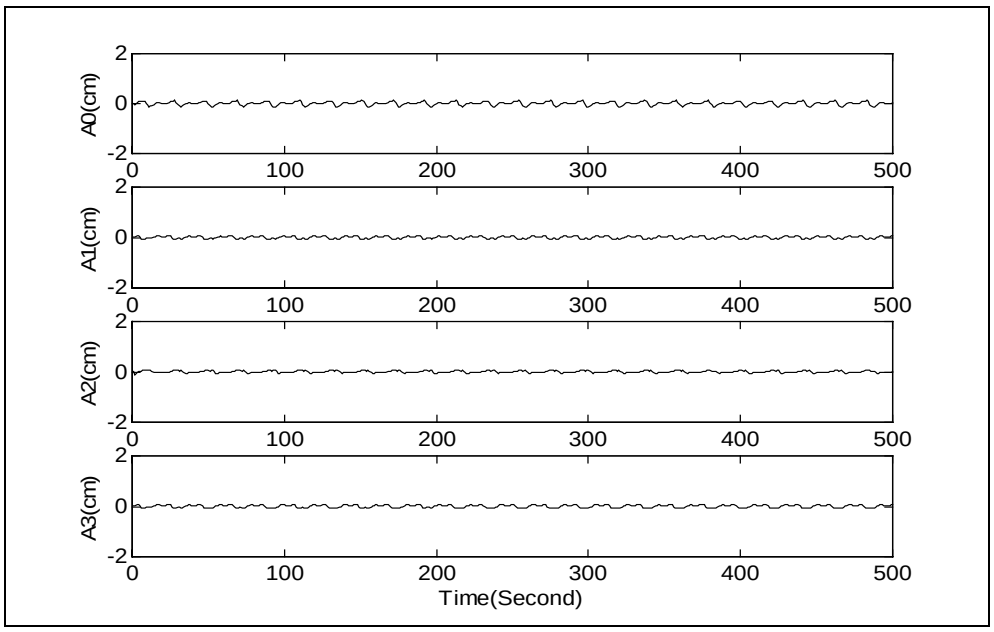

Figure 6.26: Carrier phase multipath estimation errors with very low weight to code measurements and normal weights to carrier and SNR measurements for a long delay multipath

Finally, for the same simulated multipath environment, code measurements are given a normal weight (code measurement variance equal to 10^{-2} m^2), while the carrier and SNR measurements are given very low weights (carrier phase measurement variance equal to 10^4 m^2 and SNR measurement variance equal to 10^4), such that estimates are heavily dependent upon the code measurements and the code multipath model.

Figure 6.27 shows the code multipath estimation errors, while Figure 6.21 shows their truth values. Similarly, Figure 6.28 shows the carrier phase multipath estimation errors, while Figure 6.23 shows their truth values. The estimates are heavily dependent upon the code multipath model, which is improper for long delay multipath. As one would expect, the estimated parameters are therefore incorrect, and both the code and carrier multipath estimates are erroneous. This suggests that this technique cannot mitigate long delay code multipath.

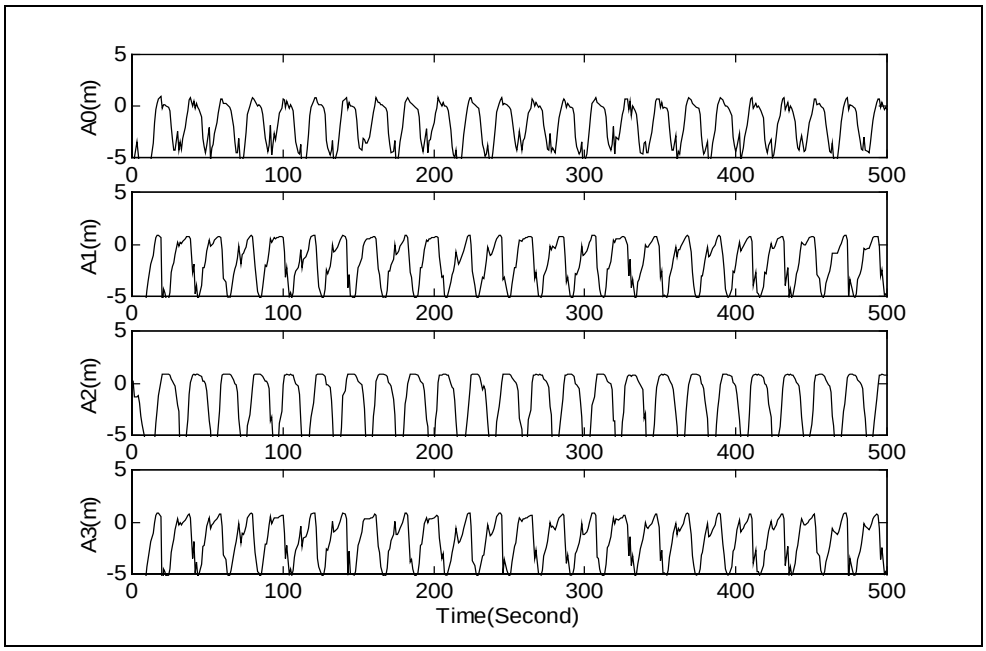

Figure 6.27: Code multipath estimation errors with normal weights to code measurements and very low weight to carrier and SNR measurements for a long delay multipath

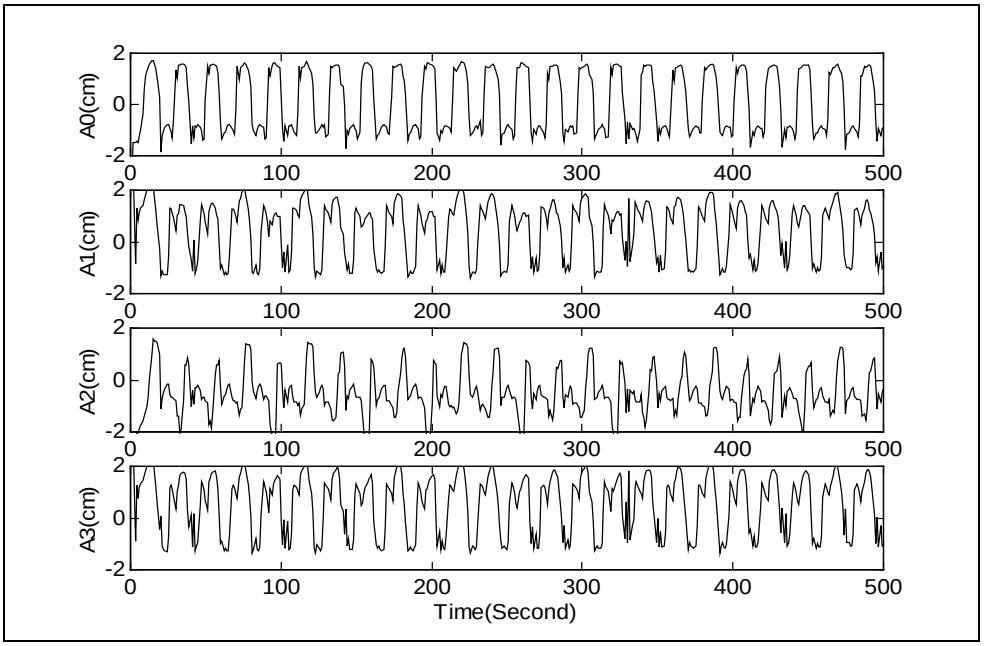

Figure 6.28: Carrier phase multipath estimation errors with normal weights to code measurements and very low weights to carrier and SNR measurements for a long delay multipath

In reality, however, measurements are corrupted by short delay as well as long delay multipath. The long delay code multipath can be mitigated using some of the currently available correlator based technology as described in Chapter 1. The short delay code multipath, however, is a major concern.

The code multipath model described in this chapter can be used to mitigate the short delay code multiapth, but the carrier multipath model described here can be used to mitigate both the short and long delay carrier phase multipath, as also suggested by the simulations. Therefore, in spite of a synergistic relationship between the code and carrier multipath errors, it is better to estimate code multipath errors from code measurements only and carrier multipath errors from carrier measurements only. Furthermore, the SNR measurements in a receiver are directly affected by the antenna gain pattern, in addition to multipath. Therefore, if the SNR measurements are to be used for multipath mitigation, they should first be compensated for the antenna gain pattern variation, as the satellite elevation and azimuth changes.

6.5.5 Multi-Reflector Environment

The multipath mitigation technique was further tested in a simulated *multi-reflector* environment. In this case, the multipath error was caused by more than one reflector in the vicinity of the antenna (see Appendix A for details). The mitigation algorithm, however, remained unchanged and the effectiveness of the technique to estimate the composite multipath error was evaluated.

Figure 6.29 shows the true code multipath error due to three reflectors with reflection coefficients 0.5, 0.1 and 0.1 and placed at 6m, 8m and 10m from the antenna respectively. They are placed at different locations with respect to the antenna and have different antenna-reflector geometry introducing composite multipath effects. As a result, the true multipath errors are somewhat irregular compared to the errors due to a single reflector.

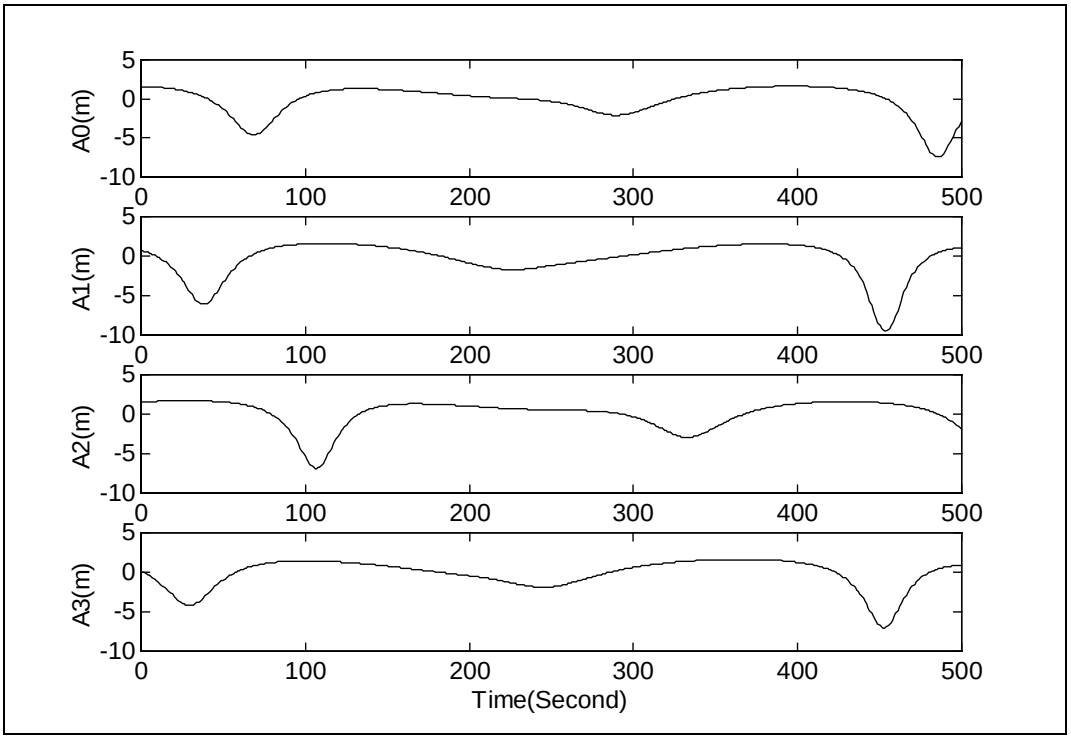

Figure 6.29: True code multipath errors at various antennas due to multiple reflectors

The multipath-corrupted single differenced code and carrier measurements are input to the Kalman filter, which estimates the multipath and geometric parameters. The estimated parameters oscillate, but they are generally close to the values corresponding to the dominant reflector (i.e. the one with reflection coefficient 0.5).

Figure 6.30 shows the code multipath estimation error, (i.e., the difference between the *true multipath* error and the *estimated multipath* error). The estimation errors are quite small as the estimated multipath errors closely follow the true multipath errors. Figure 6.31 shows the estimation error of the carrier phase multipath. In this case, the estimation errors are also quite small as the estimated multipath errors closely follow the true multipath errors.

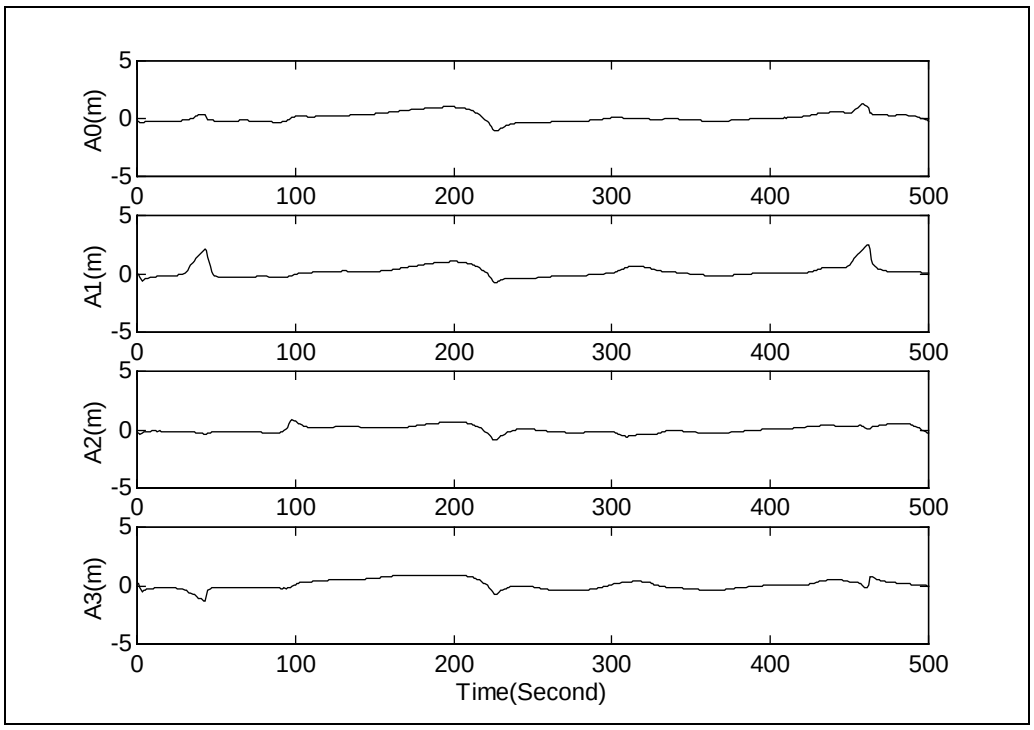

Figure 6.30: Code multipath estimation error in the case of a multi-reflector environment

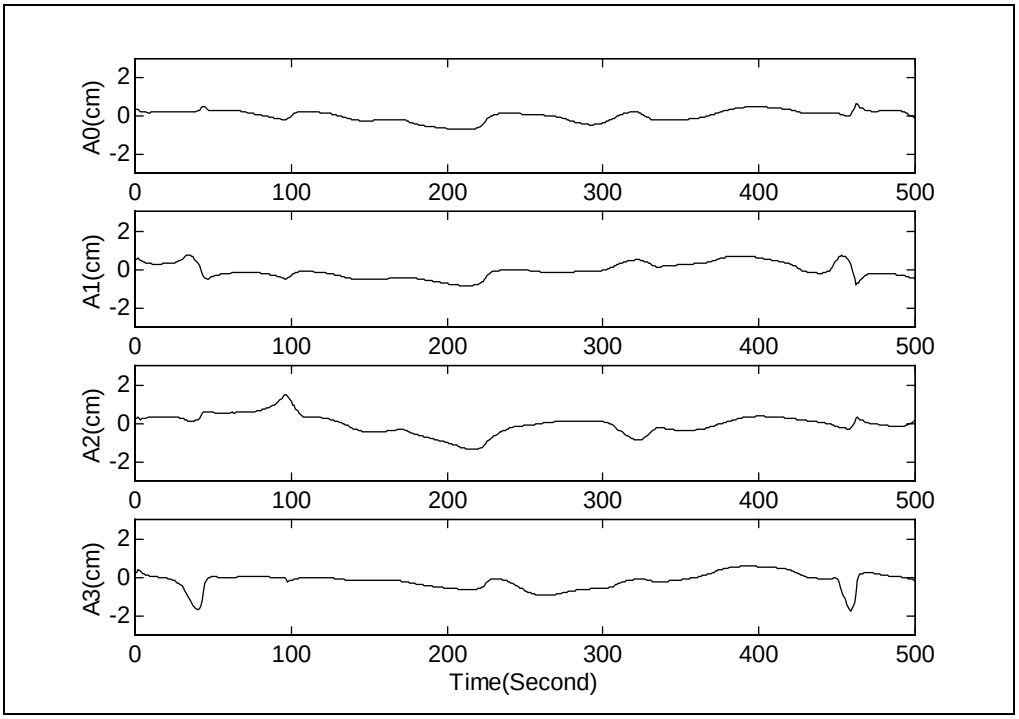

Figure 6.31: Carrier phase multipath estimation error in the case of a multi-reflector environment

Similar observations were made with reflectors having different coefficients placed at different locations with respect to the antenna. Furthermore, it was noticed that the estimation is quite sensitive to the choice of various initial parameters and process noise values.

From the above discussion it is evident that multipath errors in a multi-reflector environment can be mitigated to a good extent by using this technique. In real life situations, multipath occurs due to several reflectors in the vicinity of the antenna. One or two of these reflectors generally is the source of the dominant error, similar to the situation simulated here. The capability of the system to perform well in the simulated multi-reflector environment gives confidence of its usability in the real life situations.

CHAPTER 7

MULTIPATH MITIGATION USING FIELD DATA - ANALYSIS AND RESULTS

7.1 Introduction

The multipath mitigation technique described in Chapter 6 was first tested on simulated multipath data. After having successfully demonstrated the mitigation of multipath on simulated data, the same approach was applied to field data.

This chapter describes in detail the test setup used for field data collection, and the environment in which the data were collected. The day-to-day repeatability of multipath errors is confirmed with the aid of the correlation coefficient and correlation time. The step-by-step procedure of using these data in the proposed algorithm is described. A detailed analysis is done on the code and carrier multipath error estimation from the field data. The estimated multipath errors are removed from the raw measurements, and residuals are generated in the measurement and position domains. Error statistics of the residual errors are compared before and after applying the multipath mitigation technique, to evaluate the performance when using field data.

7.2 Test Setup

7.2.1 Test Setup Description

In order to test the multipath mitigation technique using field data, a special antenna array was assembled, whereby a thick aluminum plate was used to rigidly mount six antennas close together. Novatel Model 521 antennas were used, as they are small, with a diameter of approximately 5.6 cm. All the antennas in the antenna assembly were manually

mounted with the approximately the same orientation so as to nullify the effect of phase centre variation. As all the antennas are of the same type and from the same manufacturer, they are likely to have the same phase centre variations. As a result, the single differenced measurements between two antennas in the antenna assembly are likely to cancel the variation effects. Furthermore, orienting the antennas to the same direction helps to ensure an identical gain pattern for each antenna in a particular direction. This would introduce identical amplification or attenuation to the incoming signals from a particular direction. Various issues related to antenna coupling are addressed in section 7.4.2. The multi-antenna assembly is shown in Figure 7.1.

Figure 7.1: Multi-antenna array assembly

NovAtel BeeLine™ (Ford et al., 1997) receivers were used for data collection. The BeeLine™ is a high-performance GPS receiver with Narrow Correlator™ technology, capable of receiving and tuning to the L1 C/A code and L1 carrier phase of up to eight GPS satellites from two separate antennas. Its dual antenna capabilities allow: a) 20 cm real-time kinematic (RTK) accuracy with on-the-fly (OTF) initialization, b) real-time azimuth determination with 0.4 degrees accuracy for 1 metre antenna separation, and c) L1 C/A code and carrier tracking (BeeLine, 1998). The last of the above capabilities is used for the particular experiments discussed herein. A BeeLine™ receiver is shown in Figure 7.2.

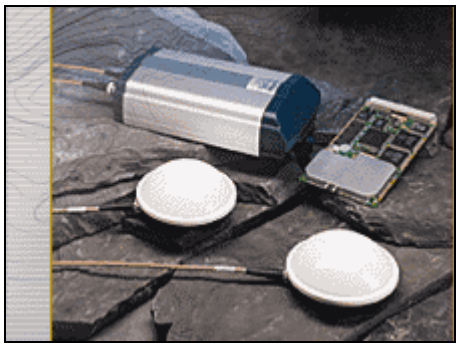

Figure 7.2: BeeLine™ Receiver

A rubidium oscillator - model FRK (L) LN, from the Efratom division of Ball Corporation (Efratom, 1989), was used as external clock, and is shown in Figure 7.3. This has a short and long term stability of around 10^{-11}. This model is a compact, atomic resonance-controlled oscillator, which provides an extremely pure and stable sinusoidal signal of 5 or 10 MHz, at 1 V (RMS) into a 50 ohm load. The unit is designed for use in high-performance communication systems, frequency standard equipment, advanced navigation equipment and similar applications. The clock signal was split by using a signal splitter, and fed to each receiver.

Figure 7.3: FRK (L) LN rubidium oscillator

Use of a rubidium clock, however, was not a necessity, as a TCXO capable of driving the receivers would have been sufficient. A common clock, although not a highly accurate one was needed for driving all the receivers. This is because the clock errors (the drift component) are cancelled by single differencing of range or phase measurements between the antennas in the antenna assembly, when driven by a common clock.

Figure 7.4 shows a block diagram of the multi-antenna system setup. Data were collected for several sessions spread over successive days, on the roof of the Engineering building at the University of Calgary.

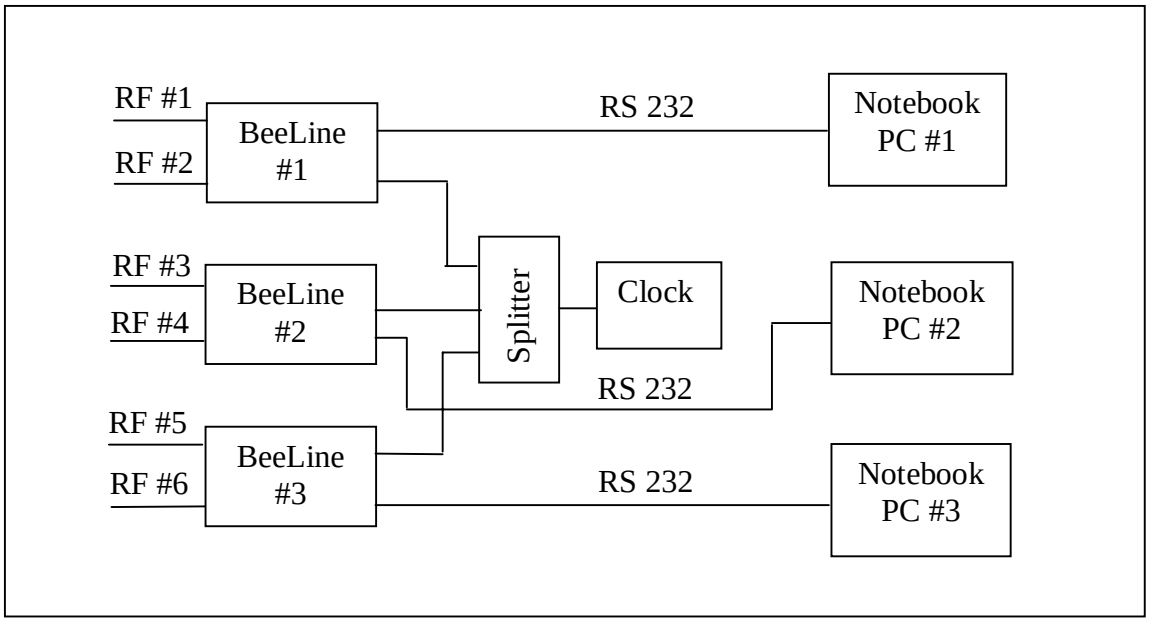

Figure 7.4: Multi-antenna system setup

The multi-antenna assembly was placed on a surveyed pillar of the roof of the Engineering building, where there are concrete sidewalls of approximately 3 m in height on the east side and 1 m in height on the south side, as can be seen in Figure 7.5. It was expected that these walls would cause the most significant multipath signals. The multi-antenna system was used as the reference station during the tests.

Figure 7.5: Reference station test environment

A NovAtel MiLLennium^{TM} receiver (MiLLennium, 1997) with a choke ring antenna, was placed in an open field where there were no major objects in the range of 80 to 100 m from the antenna, as shown in Figure 7.6. This was used as the user receiver during the tests.

Figure 7.6: User antenna test environment

The reason for keeping the user antenna in a relatively benign environment, was that in order to evaluate the performance of the reference antenna assembly as a multipath mitigator, the user antenna is assumed to have zero or very low multipath errors. As the carrier phase multipath errors can not be isolated between the reference (monitor) and the user (remote) antennas in the double difference carrier phase residuals (described in detail in subsequent sections), any multipath error in the user antenna would affect the performance evaluation process. The baseline separation between the reference station and the user receiver was approximately 500 m. Only L1 data from the MiLLennium™ was used for the tests. The experimental setup is shown in Figure 7.7.

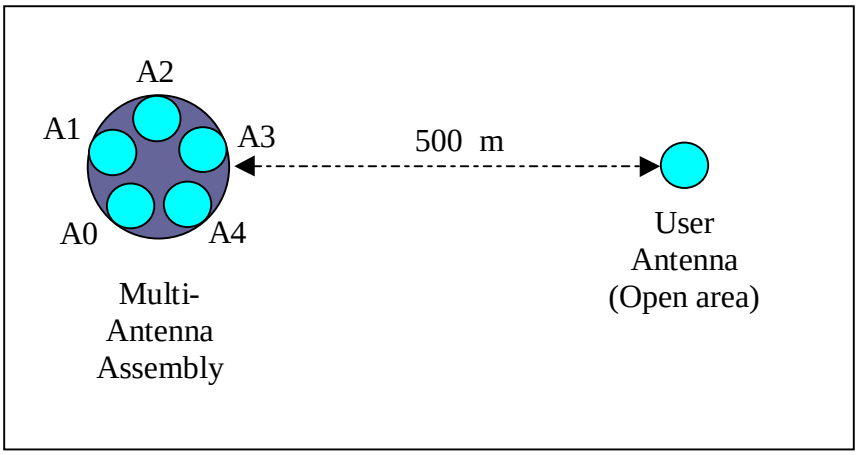

Figure 7.7: Experimental setup

7.2.2 Data Collection Scheme

Data were collected over several days in 1998. Table 7.1 summarises the data collection scenarios and how they have been used for the experiments.

7.3 Isolation of Multipath Errors

To evaluate the performance of the multipath mitigation technique, it is necessary to have a measure of the multipath error *truth values*. To generate *truth values*, multipath errors need to be isolated from the available measurements. The code multipath errors can be

isolated by using the well-known code-minus-carrier technique (Braasch, 1995), but the carrier multipath errors can not be easily isolated. The following describes the methods used to isolate multipath errors from code range and carrier phase measurements in a receiver.

Table 7.1: Data collection scheme

Date	Duration	Tests conducted
August 25 and 26, 1998	1.5 hours, one session	Carrier phase multipath mitigation Performance evaluation in the measurement domain
October 7 and 8, 1998	1.5 hours, one session	Day-to-day repeatability
October 7 and 8, 1998	12 hours, several sessions	Antenna gain pattern test
October 20, 1998	1.5 hours, one session	Code range multipath mitigation Carrier phase multipath mitigation Performance evaluation in measurement domain and position domain

7.3.1 Code Multipath Isolation

Equations 2.4 and 2.5 are the expressions for GPS code and carrier measurements. Many of the errors in the code measurement also appear in carrier measurements, as described in Chapter 2. By taking the difference between the code range and carrier phase measurements, and assuming the hardware delay to be the same for the code and the carrier, the following expression is obtained,

$$P - \Phi = 2d_{ion} - \lambda N + \varepsilon_{Mp} - \varepsilon_{M\varphi} + \varepsilon_{p} - \varepsilon_{\varphi} \quad \text{(m)} \tag{7.1}$$

In Equation 7.1, the term corresponding to the differential ionospheric error is slowly varying with correlation time of 15-30 minutes (Mannucci et al., 1997; Skone, 1998). The range due to the differential integer ambiguity is constant over time in the absence of cycle slips, and has a step function characteristic in the presence of a cycle slip. Carrier multipath and receiver noise is in the order of a few cm and a few mm at most, respectively, in most modern receivers. Therefore, they can be neglected when compared with the code multipath and receiver noise, which are in the order of a few metres and a few tens of cm, respectively.

Ideally, the ionospheric error component can be computed and then removed from the code and carrier measurements using the standard L1-L2 dual frequency measurement technique. However, the standard technique involves the use of noisy, multipath-contaminated pseudorange measurements; thus removing the ionospheric term actually increases the noise level, and makes the identification of the multipath error (Braasch, 1995) quite difficult.

One way to eliminate most of the ionospheric delay error, is to use a second order polynomial that best fits the slow variation primarily caused by the ionospheric delay error. The estimated ionospheric delay error is removed from the residual obtained by using Equation 7.1. In the absence of cycle slips, the mean of the adjusted residual is removed, which cancels the effect of the integer cycle ambiguity. Assuming that the carrier phase noise and multipath error are negligible, the adjusted residual then contains the code multipath error and receiver noise, and is given by:

$$(P - \Phi)_{adj} \approx \varepsilon_{Mp} + \varepsilon_{p} \tag{7.2}$$

This method, however, has some flaws, namely: a) by removing the mean of the differences (to remove the range due to the differential integer ambiguity), the mean multipath error is also removed. It should be noted that the mean multipath error is non-zero when the multipath error bandwidth is smaller than the tracking loop bandwidth,

which is generally the case for stationary receivers, and b) slow varying multipath errors due to close-by reflectors behave similar to the ionospheric delay error. While removing the ionospheric error using polynomial curve fitting, some of the low frequency multipath error is also removed.

7.3.2 Carrier Phase Multipath Isolation

The carrier phase accuracy is nearly two orders of magnitude higher than the code range accuracy. Similarly, the carrier multipath error is almost two orders of magnitude smaller compared to its code counterpart. It is very difficult to isolate such small errors, and generally possible only with certain assumptions.

If two receivers are separated by a short distance, then the double difference observation, (between antennas and between satellites), is given by Equation 2.11, which is repeated here for further analysis:

$$\Delta\nabla\Phi = \Delta\nabla\rho + \Delta\nabla d\rho + \lambda\Delta\nabla N - \Delta\nabla d_{ion} + \Delta\nabla d_{trop} + \Delta\nabla\varepsilon_{M\varphi} + \Delta\nabla\varepsilon_{\varphi} \qquad (2.11)$$

In Equation 2.11,

a) The differential orbital error (second term), ionospheric delay error (fifth term), and tropospheric delay error (sixth term), are spatially correlated. If the baseline length is very short, (less than one kilometre), then they are almost zero.
b) The differential phase due to the spatial separation between the two antennas (first term) can be removed from the known position of the two antennas. The difference in range between each antenna and the satellite can be computed and removed from the residual phase.
c) After step (a) and (b) are performed, the residual phase error is due to the differential integer ambiguity, multipath, and phase noise. As the latter two error components combined is much smaller than a carrier cycle, the phase due to the integer number of cycles can be removed.

After steps (a) through (c) are performed, the resultant residual contains the double difference multipath errors and phase noise. The phase noise is of high frequency, and in most high performance receivers it is very small on the order of 1 mm. If one of the two antennas, (say, Antenna 2), is placed in a benign environment with a very low carrier phase multipath, then the double difference phase residuals thus obtained are mostly due to the multipath in the other antenna (i.e. Antenna 1).

Therefore,

$$\Delta\nabla\Phi_{adj} \approx \varepsilon_{M\varphi 1} + \Delta\nabla\varepsilon_{\varphi} \tag{7.3}$$

7.4 Test Description

7.4.1 Day-to-Day Repeatability Test

The multipath error depends upon several factors, including the satellite, user and reflector geometry and their relative motions. If the user is stationary and the environment is unchanged, then the multipath error changes due to the satellite motion. The GPS satellite has an orbital period of half a sidereal day, where a sidereal day is equal to 23 h, 56 min, 4.009054 s (e.g. Spilker and Parkinson, 1996). Therefore the multipath error repeats after a sidereal day, or almost four minutes less than a solar day.

7.4.1.1 Code Multipath Day-to-Day Repeatability

Data collected on October 7 and 8, 1998, was used to test the day-to-day repeatability of multipath errors. The code multipath error was isolated using the technique described in the previous section. The adjusted code range minus carrier phase measurements without ionospheric correction for satellite 21 is shown in Figure 7.8.

In Figure 7.8, the upward trend of the error is due to the change in the ionospheric delay error (the plot actually contains twice the ionspheric value). The actual ionospheric delay error cannot be determined by using this technique, as the bias value of the ionospheric

delay error behaves in the same way as the carrier phase integer ambiguity, and thus cannot be separated from the latter.

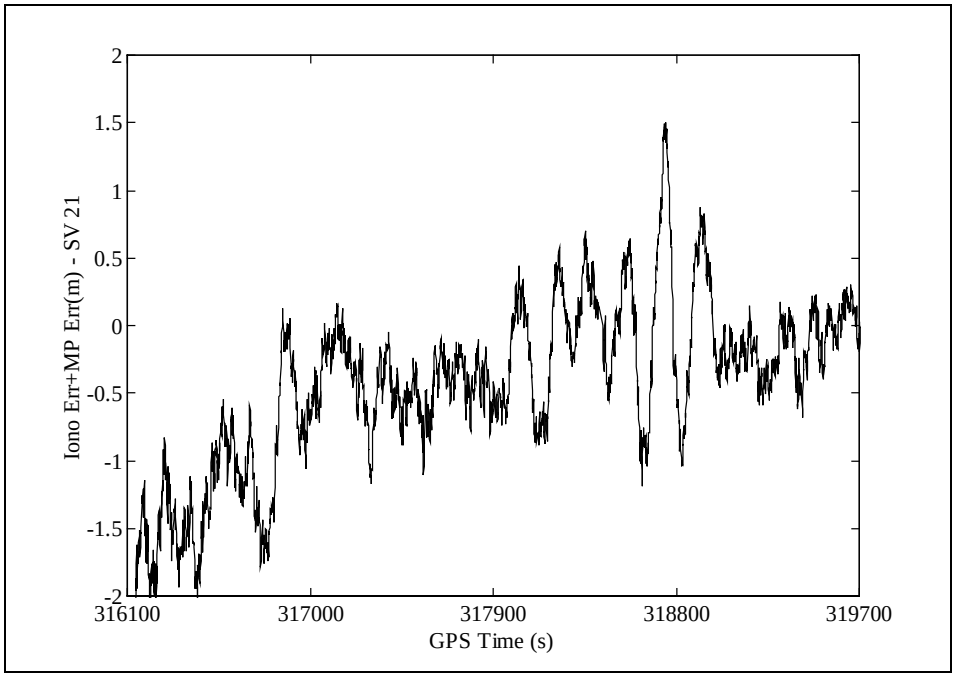

Figure 7.8: Code minus carrier residuals before removing ionospheric delay error for satellite 21 using data on October 7, 1998

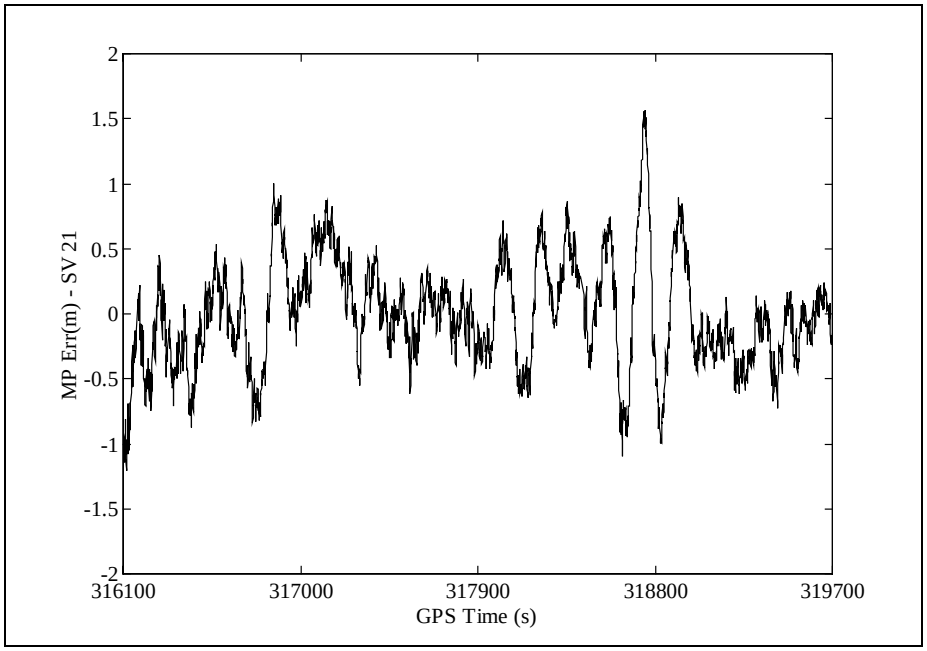

Figure 7.9: Code minus carrier residuals after removing ionospheric delay error for satellite 21 using data on October 7, 1998

The error due to ionospheric delay can be removed by using a second order polynomial which best fits the error trend. Figure 7.9 shows the modified residual after removing the trend using a second order polynomial.

The code multipath error was extracted for satellite 21 (elevation angle 50°- 75°) from the data collected on October 7 and 8, 1998, and is shown in Figure 7.10a using a shaded dark line and shaded light line for the two days. Similarly, Figure 7.10b shows the extracted code multipath error for satellite 31 (elevation angle 21°-34°) from the same data sets. Multipath errors extracted from the data on October 8 are plotted offset by four minutes with respect to the errors extracted from the data collected on October 7. From the figure, it is clear that multipath errors repeat after a sidereal day.

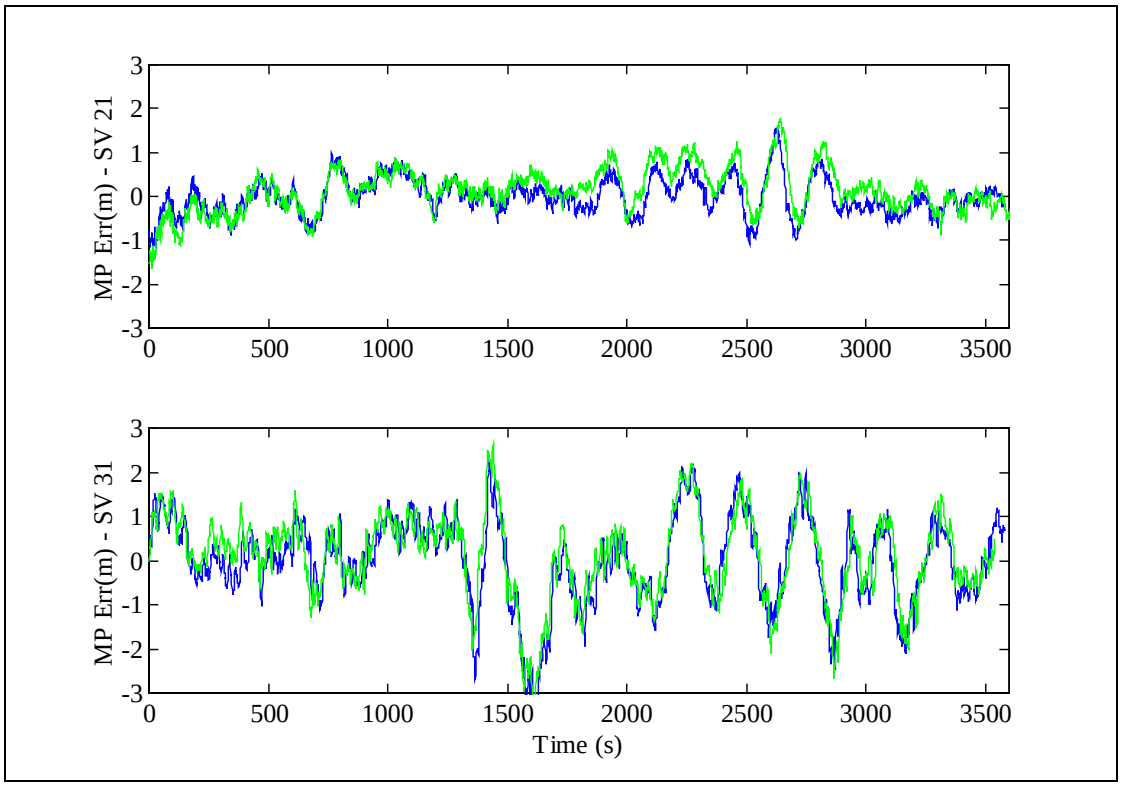

Figure 7.10a-7.10b: Code multipath errors for a) satellite 21 and b) satellite 31 in one of the reference antennas on October 7, 1998 shown in shaded dark line and on October 8, 1998 shown in a shaded light line

The degree of day-to-day repeatability of the code range multipath error was computed from the correlation coefficient between the errors on October 7 and October 8. The correlation coefficient was computed by using the following equation (Maybeck, 1994):

$$C_{XY} = \frac{E[(X - m_X)(Y - m_Y)]}{\sqrt{E[(X - m_X)^2]E[(Y - m_Y)^2]}} \tag{7.4}$$

where,

E [] is the expectation operator

X is a state variable (multipath errors on October 7)

Y is another state variable (multipath errors on October 8)

m_X is the mean of state variable X, and

m_Y is the mean of state variable Y.

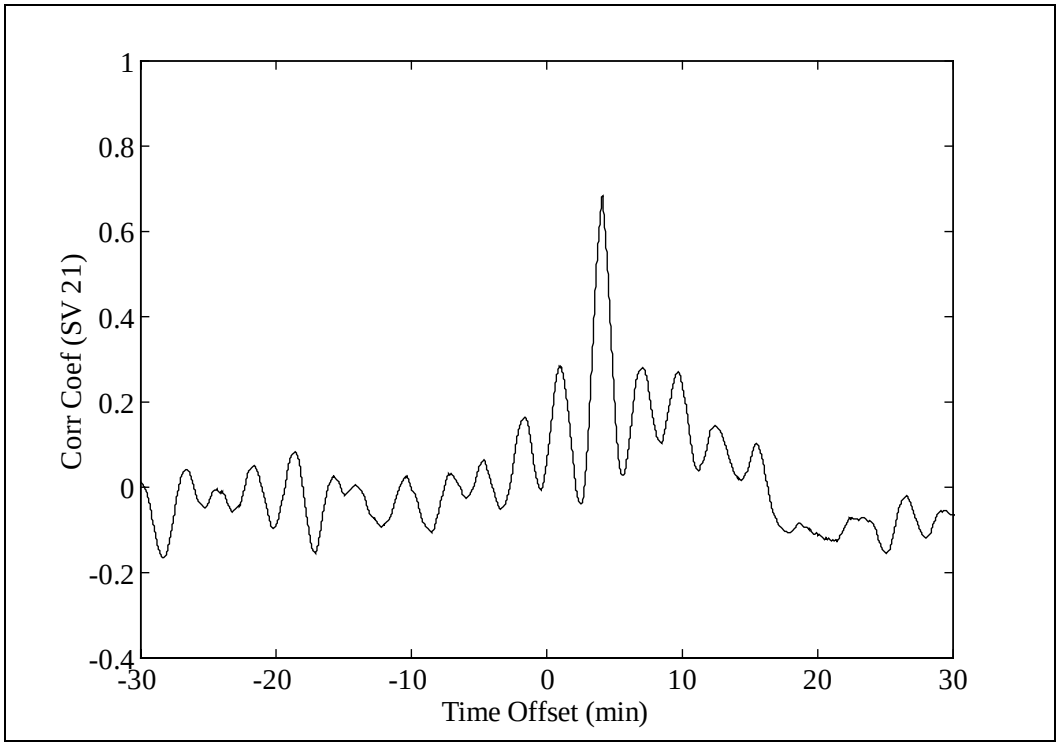

Figure 7.11: Correlation coefficients of code multipath errors for satellite 21 using the data collected on October 7 and 8, 1998

Figure 7.11 shows the correlation coefficients of the code multipath errors on October 7 and October 8 for satellite 21, while Figure 7.12 shows the corresponding values for satellite 31. From each figure it can be seen that the multipath errors have the maximum similarity after a sidereal day (as the correlation peak occurs at around 4 min shift, in the X axis). The extent of the repeatability is approximately 70% for satellite 21 and 90% for satellite 31. A correlation time of approximately 2-3 min was found in either case.

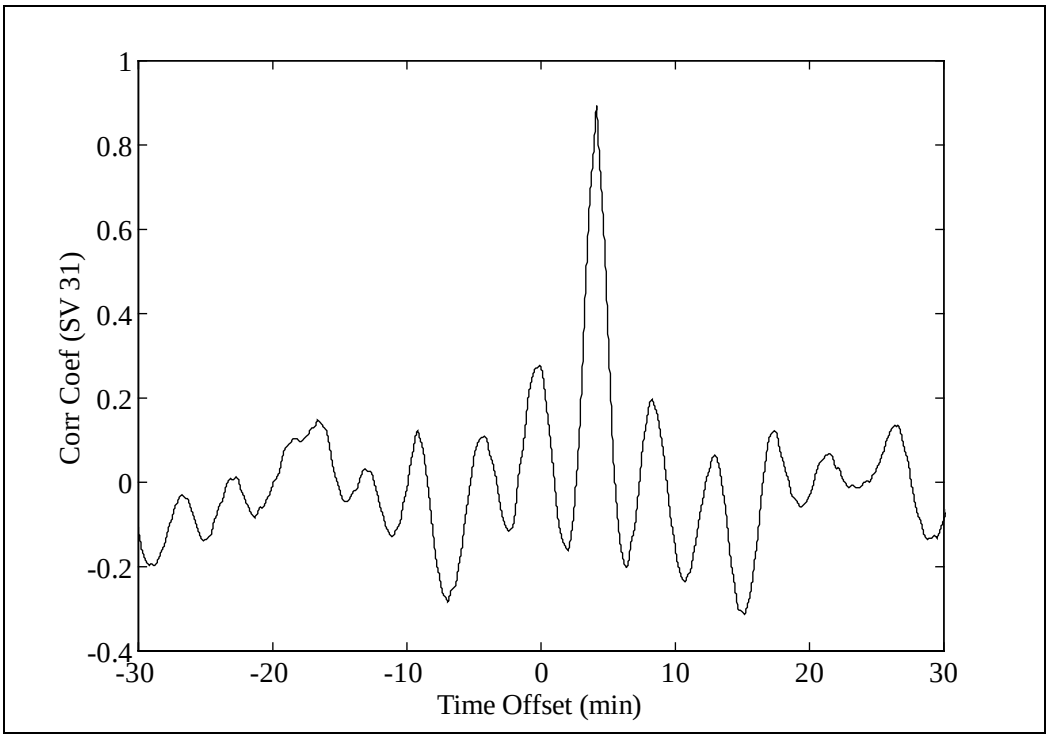

Figure 7. 12: Correlation coefficients of code multipath errors for satellite 31 using the data collected on October 7 and 8, 1998

7.4.1.2 Carrier Multipath Day-to-Day Repeatability

Similar to the code range multipath, the day-to-day repeatability of carrier phase multipath errors were also tested using data collected on October 7 and 8, 1998. Carrier phase multipath errors were isolated by using the technique described in Section 7.3.2. An antenna in the reference antenna assembly and the user antenna, were used for multipath error computation. Satellite 23 was at a high elevation (88° - 65°) and was used

as the base satellite for computing the adjusted double differenced phase residuals. The multipath errors for satellites 17 (elevation angle 51°- 24°) and 31 (elevation angle 21°-34°) were computed using data collected on October 7, 1998, and are shown in Figure 7.13 using a shaded dark line. Similarly, the multipath errors for the same satellites were computed using data collected on October 8, 1998, and superimposed on the same figure but shifted by four minutes in the time axis, and are shown using a shaded light line. From the figure, it is clear that the carrier phase multipath errors repeat after a sidereal day.

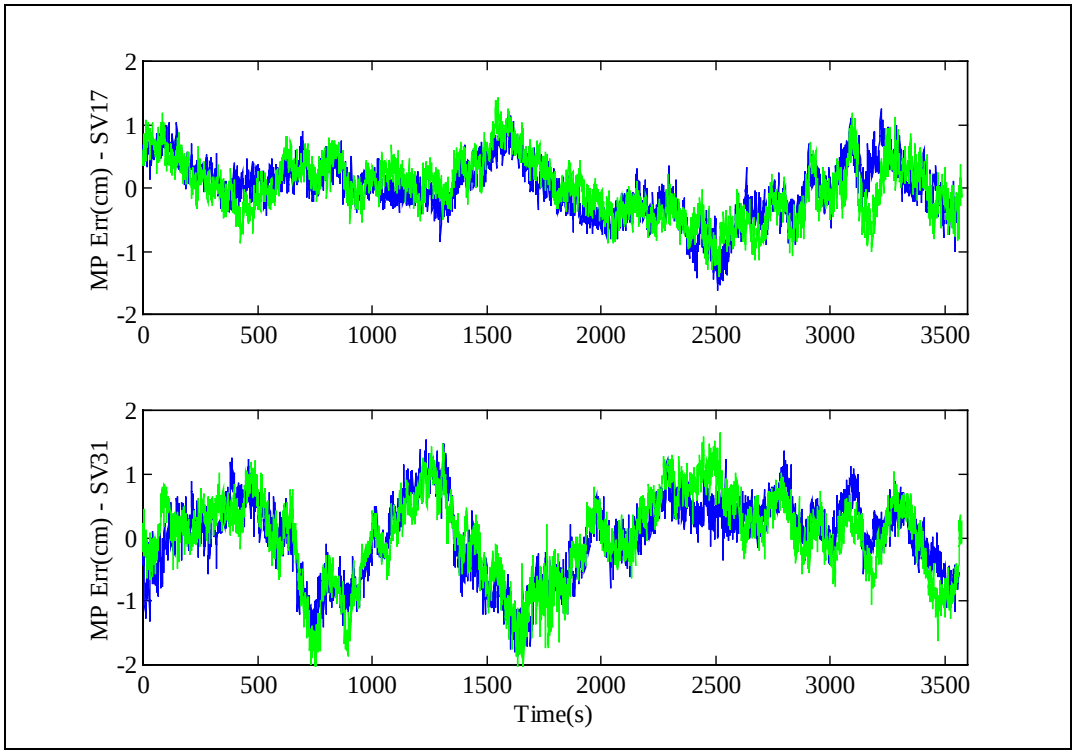

Figure 7.13: Carrier phase multipath errors for satellites 17 and 31 in one of the reference antennas on October 7, 1998 shown in shaded dark line and on October 8, 1998 shown in a shaded light line

The day-to-day repeatability of the carrier phase multipath error was computed from the correlation coefficients between the errors on October 7 and October 8. The correlation coefficients were computed using Equation 7.4.

Figure 7.14 shows the correlation coefficients of the carrier phase multipath errors on October 7 and October 8 for satellite 17, while Figure 7.15 shows the corresponding values for satellite 31. From each figure it can be seen that multipath errors have a maximum similarity after a sidereal day. The extent of repeatability is approximately 70% in either case. A correlation time of approximately 5-6 minutes was found in both cases, which indicates that the dominant phase multipath errors have low frequencies, which are caused by nearby reflectors.

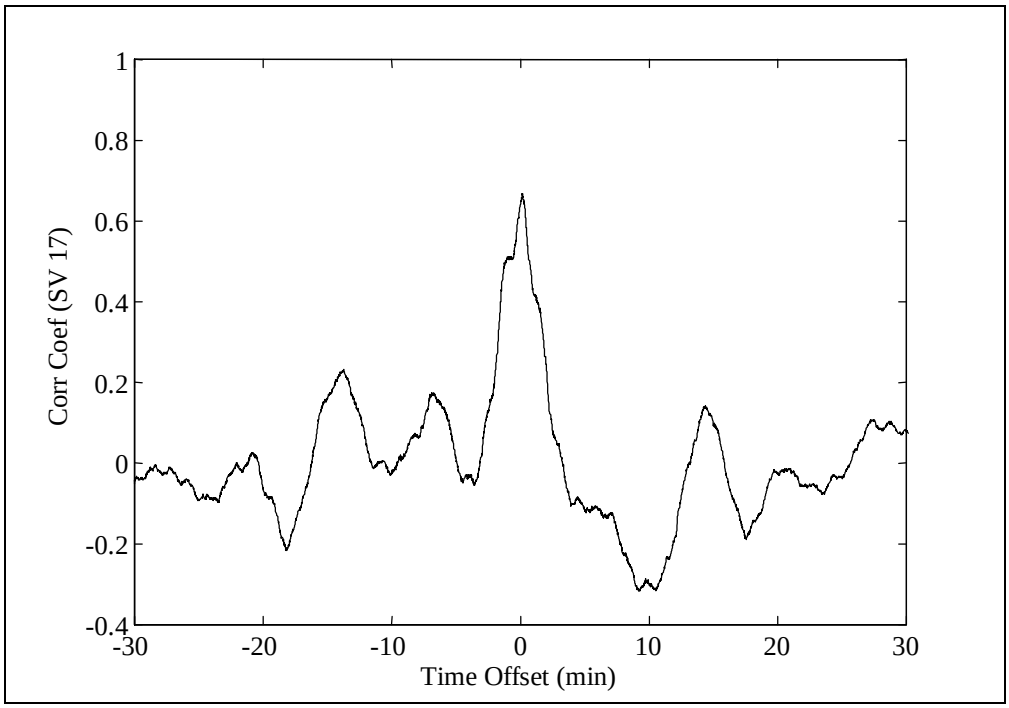

Figure 7.14: Correlation coefficients of carrier phase multipath errors for satellite 17 using the data collected on October 7 and 8, 1998

Comparing the correlation coefficients of the code and carrier multipath errors for satellite 31 in Figures 7.12 and 7.15, several comments can be made.

a) Code multipath errors have higher frequency components than that of the carrier phase. This is due to the fact that the code and the carrier discriminator functions in the receiver tracking loops respond differently in the presence of multipath signals. The code

discriminator produces multipath errors of high magnitude due to far away (or medium path delay) reflectors, which cause high frequency multipath (see Figure 5.6). Therefore, the code multipath error is dominated by high frequency components. On the other hand, the carrier discriminator produces multipath errors of high magnitude due to close-by reflectors (or short path delay), which cause low frequency multipath errors (see Figure 5.16). From Figures 7.10 and 7.13, it can be seen that the dominant reflectors in code and carrier multipath errors are not the same. For code multipath errors, it is the far away reflectors, whereas for carrier multipath errors, it is the close-by reflectors that dominate the composite multipath errors.

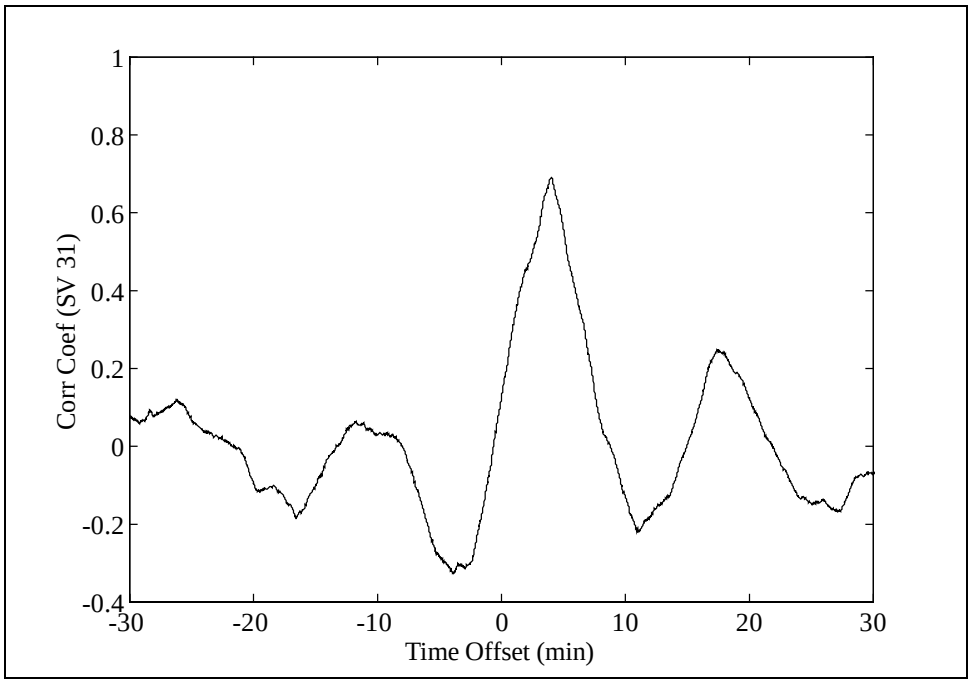

Figure 7.15: Correlation coefficients of carrier phase multipath errors for satellite 31 using the data collected on October 7 and 8, 1998

b) The correlation coefficients for code multipath errors are higher than those for the carrier phase errors. This is because the carrier phase residuals have high phase noise as they are double differenced residuals. Therefore, the effects of the carrier noise are higher compared to that of the code noise on the correlation coefficient. As the receiver noise on day one is uncorrelated with the noise on day two, code residuals, which are

comparatively less affected by the code noise, have higher correlation coefficients compared to their carrier phase counterparts.

7.4.2 Antenna Gain Pattern Test

The gain pattern of an antenna depends upon the environment in which it is used. The electromagnetic properties of the environment affect the antenna gain pattern. When multiple antennas are placed in proximity in an antenna assembly, then the gain pattern of each antenna is affected by the gain patterns of the neighbouring antennas. As a result, the gain pattern of an antenna in the antenna assembly is different from its pattern when placed in isolation. This may have an impact on the measurement characteristics and correlation of multipath errors. Therefore, it is important to determine the extent to which the gain pattern is affected by the proximity of neighbouring antennas and whether or not all the measurements from all the antennas are usable.

In order to evaluate the gain pattern of the antennas in the multi-antenna system, a series of tests were conducted in October, 1998. In these tests, raw L1 carrier phase data were collected at 0.1 Hz rate for about twelve hours per test, using the antenna array as described previously. The C/N_0 of each satellite in each receiver in the multi-antenna system was first analyzed for inter-antenna coupling using the data collected on October 7. This experiment was repeated using data collected on October 8.

The C/N_0 in a receiver depends upon several factors, including the nominal received power, elevation angle of the satellite, foliage attenuation, line loss, antenna gain pattern and multipath (Spilker, 1996). The specified received signal level peaks at 40° elevation by approximately 2 dB, with respect to the nominal signal level at a low elevation angle, due to the transmitting antenna gain pattern and the line loss (Spilker, 1996). In an ideal static environment, the C/N_0 values will have a parabolic signature due to the line of sight traversing the antenna gain pattern (Axelrad et al., 1996). If C/N_0 values for all visible satellites are plotted together, they should form a thin band.

Figure 7.16 shows the C/N_0 of the centre antenna in the antenna assembly, versus the elevation of all visible satellites during the October 7 test period. A wide spread in the signal power is observed even up to 60° elevation angles. In Figure 7.17, C/N_0 values are plotted for the same antenna with respect to the azimuth of all available satellites. Different shades are used to indicate various ranges of elevation angles. The signal power has a large dip, or non-uniformity, around the 180° azimuth angle mark. The spread and non-uniformity of the signal power is likely to be due to the heavy coupling of the centre antenna by the peripheral antennas.

Due to the large variations in the C/N_0 values, a second test was conducted with the centre antenna removed. Figures 7.18 and 7.19 show the C/N_0 values for all satellites for one of the peripheral antennas in the antenna assembly. In this case, the signal power spread is narrow compared to the previous case.

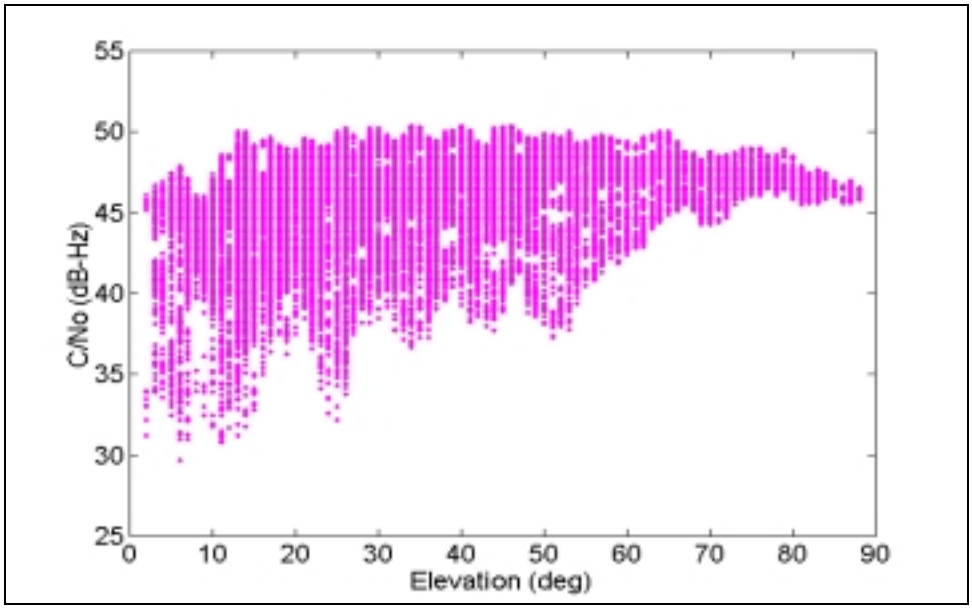

Figure 7.16 : Signal power to noise power spectral density of the centre antenna in the six-antenna assembly with respect to the elevation of the satellites

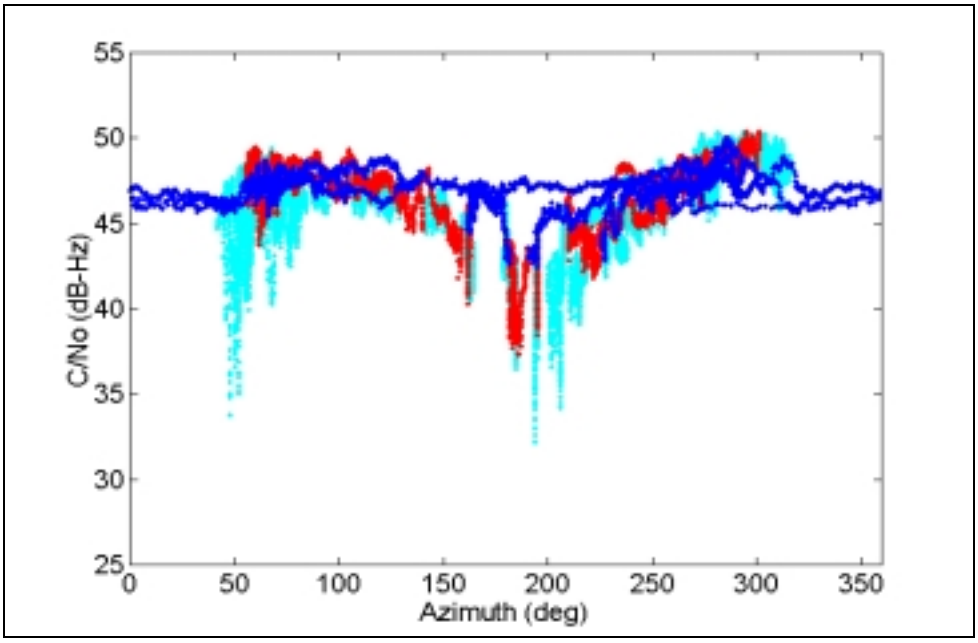

Figure 7.17: Signal power to noise power spectral density of the centre antenna in the six-antenna assembly with respect to the azimuth of the satellites. (Light shade: 20° ≤ Elv < 40°; Medium shade: 40° ≤ Elv < 60°; Dark shade: 60° ≤ Elv <90°)

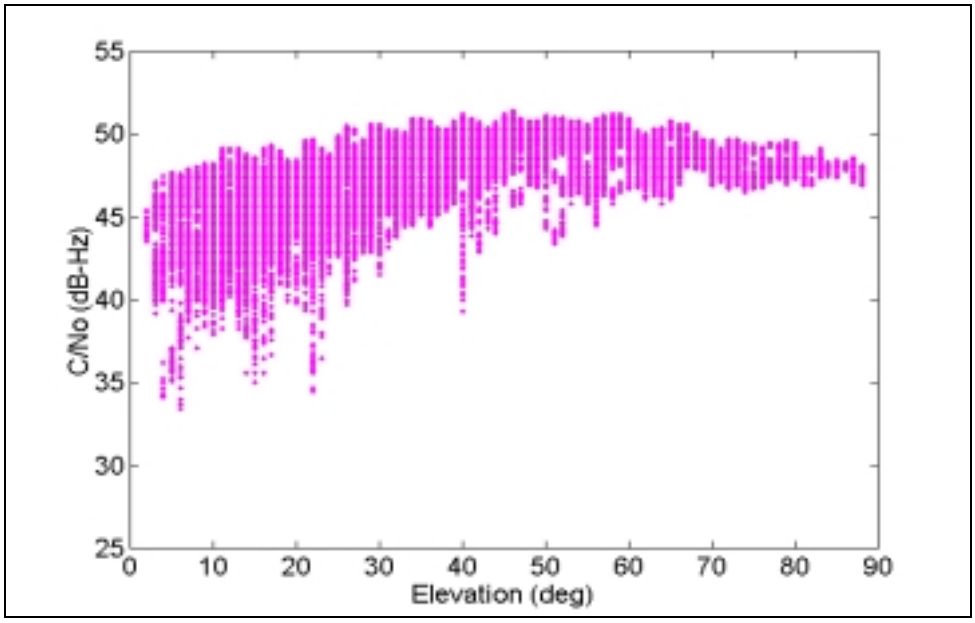

Figure 7.18: Signal power to noise power spectral density of a peripheral antenna in the five-antenna assembly with respect to the elevation of a satellite

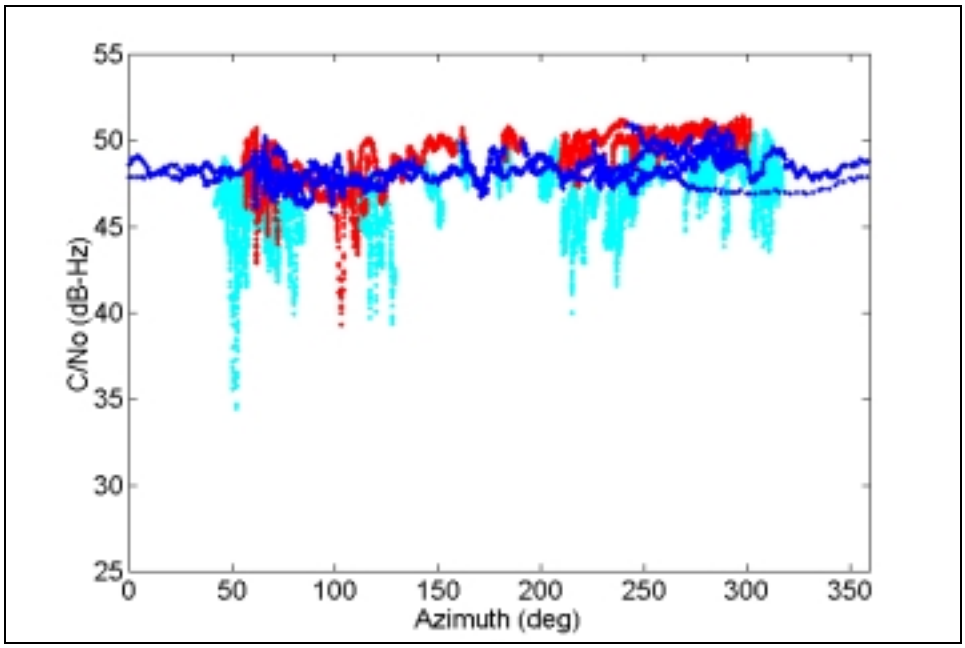

Figure 7.19: Signal power to noise power spectral density of a peripheral antenna in the five-antenna assembly with respect to the azimuth of a satellite. (Light shade: 20° ≤ Elv < 40°; Medium shade: 40° ≤ Elv < 60°; Dark shade: 60° ≤ Elv <90°)

This experiment was repeated again using different data sets, and for other peripheral antennas, and similar results were found. This suggests that the centre antenna in the six-antenna assembly was highly coupled, and its gain pattern was disturbed substantially. Therefore, the centre antenna was removed from the antenna assembly, and all the subsequent experiments were carried out with only five antennas.

7.4.3 Multipath Mitigation Test

An Extended Kalman Filter was developed to estimate the multipath error parameters as described in Chapter 6. Adjusted single differenced (between antenna) code range, carrier phase measurements (described below) and SNR ratios were used to update the state variables.

In a closely-spaced antenna array, the antennas are separated by a very short distance of the order of 6-10 cm. The single differenced code and carrier phase measurements are

then free from atmospheric delay errors, satellite orbital errors, and satellite clock errors in Equations 2.8 and 2.9. Assuming the differential hardware error is insignificant, the single differenced code and carrier phase measurements between two closely-spaced antennas are given by the following (Wells et al., 1987; Lachapelle, 1997):

$$\Delta P_{0i} = \Delta\rho_{0i} + c\Delta t_{0i} + \Delta\varepsilon_{Mp0i} + \Delta\varepsilon_{p0i} \tag{7.5}$$

$$\Delta\Phi_{0i} = \Delta\rho_{0i} + c\Delta t_{0i} + \Delta N_{0i}\lambda + \Delta\varepsilon_{M\varphi 0i} + \Delta\varepsilon_{\varphi 0i} \tag{7.6}$$

where the suffix '0' represents the reference antenna (A0) and the suffix 'i' represents a secondary antenna (A1-A4) in the multi-antenna assembly.

Each antenna in the multi-antenna system is connected to a different receiver (each BeeLine^{TM} receiver can take two RF feeds). If the receivers are driven by a common clock, and their code and carrier phase measurements are corrected by the range difference due to the spatial separation of the antennas, then the adjusted single differenced code range measurements contain only the single difference code multipath errors and receiver code noise. Similarly, the adjusted single differenced carrier phase measurements contain only the phase due to the differential integer ambiguity, single difference of carrier phase multipath errors, and phase noise. As the multipath errors and phase noise together are much smaller than the carrier wavelength, the phase due to differential integer cycles can be easily removed, and the resulting adjusted single differenced measurements contain only the difference of the carrier phase multipath errors and phase noise between the antennas. Neglecting receiver code noise and phase noise gives,

$$\Delta P_{0i}(\text{adj}) = \Delta\varepsilon_{Mp0i} = \Delta\tau_{0,i} \tag{7.7}$$

$$\Delta\Phi_{0i}(\text{adj}) = \Delta\varepsilon_{M\varphi 0i} = \Delta\Psi_{0,i} \tag{7.8}$$

The adjusted single differenced (between antennas) code range and carrier phase measurements described by Equations 7.7 and 7.8 are used as the input to the multipath mitigation filter.

Let C_0 and C_i be the C/N_0 values of a satellite signal at two closely-spaced antennas, and assume that the noise spectral densities of the two receivers are the same. The ratio of the average signal power is then given by,

$$R_{0i} = \frac{Pi}{P_0} = 10^{\frac{(C_i - C_0)}{10}} \tag{7.9}$$

Therefore, in *m* closely-spaced antennas, the useful measurements would be (*m*-1) single differenced code range measurements, (*m*-1) single differenced carrier phase measurements, and (*m*-1) ratios of SNRs, if one of the antennas in the (*m*-1) antenna pairs is common. Therefore,

$$z = [\Delta P_{01} \; .. \; \Delta P_{0m-1} \quad \Delta\Phi_{01} \; .. \; \Delta\Phi_{0m-1} \quad R_{01} \; .. \; R_{0m-1}]^T \tag{7.10}$$

The use of the SNR in the above formulation assumes that the noise level at each receiver in the reference station is the same, and the gain pattern of each antenna in the antenna assembly is identical. Under such circumstances, the C/N_0 from each receiver for a particular satellite would be the same in the absence of multipath and receiver noise. The validity of this assumption in the case of a multi-antenna assembly can be tested by comparing the C/N_0 values from each receiver for a high elevation satellite (which is generally less affected by multipath) in the reference antenna system.

Figure 7.20 shows the SNRs from all receivers connected to the multi-antennas for satellite 23, which has the highest elevation (71°-87°) during the test period. The SNR plots have an upward trend, medium frequency variations, and high frequency noise. The upward trend is due to the increase in signal strength with the increase in elevation angle. The medium frequency oscillations are primarily due to multipath errors and the high frequency components are due to the receiver noise.

The effects of multipath errors and receiver noise on C/N_0 can be corrected by removing the medium and high frequency components of the SNR. The SNR values can be smoothed using a moving window of 500 seconds to remove errors due to multipath and

receiver noise, and are shown in Figure 7.21. From this figure, it can be seen that each receiver has slightly different values of C/N_0, and that they vary with time.

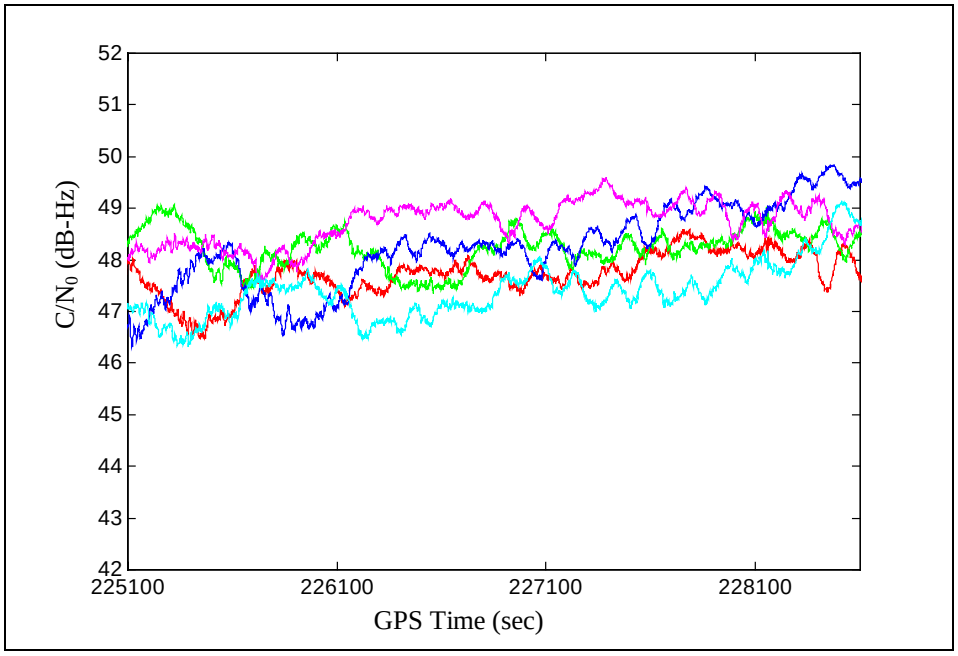

Figure 7.20: SNR at all the reference receivers for SV 23

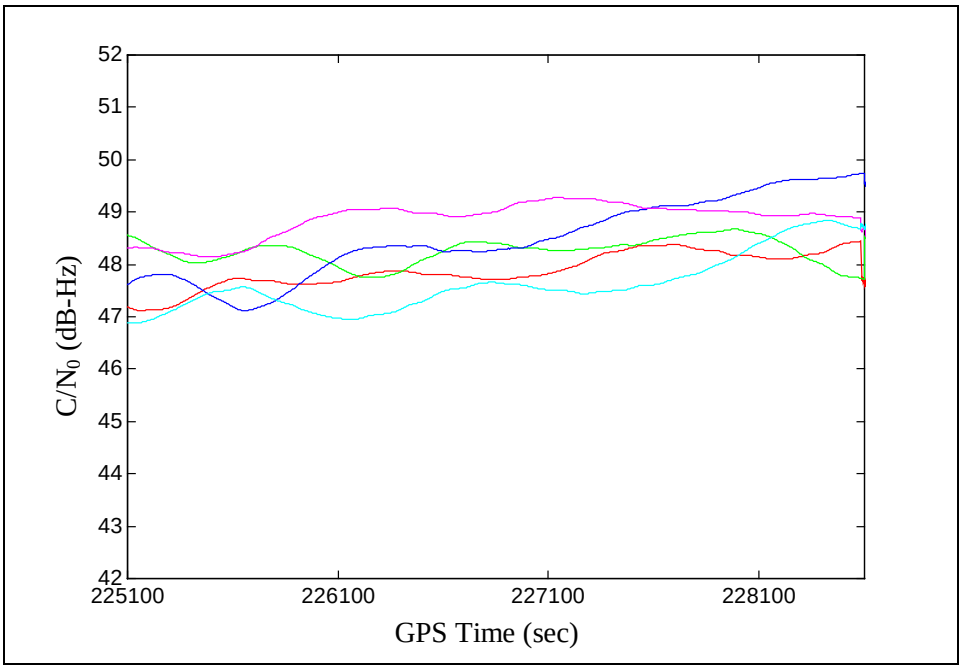

Figure 7.21: SNR at all the reference receivers for SV 23 averaged over a moving window of 500 seconds

A similar experiment was done with satellite 21, which was also at a high elevation (61°-83°) during the test period. Even in this case, similar variations of the C/N_0 were observed. This is probably due to the variations in the noise level (N_0), which could have been caused by variations in receiver hardware properties even within the same type of receiver from a manufacturer. The more likely cause is that the variations could be due to the fact that the gain patterns of each antenna in the antenna assembly are not identical. In spite of this problem, if the SNR measurements are used in the filter, the estimated parameters will be incorrect resulting in erroneous estimated multipath. Whatever the reason, the SNR measurements were not used for the multipath mitigation.

The code range and carrier phase measurements were used in the Kalman filter for the multipath mitigation. Appropriate weights ($R_{\Delta P_{0i}} = 0.02\,m^2$ and $R_{\Delta \Phi_{0i}} = 10^{-4}\,m^2$) were given to the code and carrier measurements, and the multipath parameters were estimated. The residuals were found to be quite high, and the computed code and carrier multipath errors were quite different from their measured values (more on measured values in the next section). Further investigations revealed that in the proposed model, code multipath was estimated for only close-by reflectors (i.e. multipath delay less than 15 metres for C/A code), whereas carrier phase multipath was estimated for all reflectors in the environment (detailed analysis and simulation in Chapter 6). Because of this discrepancy, the multipath parameters between the two measurements were not consistent. Furthermore, altering the Kalman filter to estimate the measurement and the process noise adaptively would not help in this case, as the problem is in the state dynamic model itself. To overcome this problem, only code measurements were used for code multipath error estimation and only carrier measurements were used for carrier multipath error estimation. Details of the code and carrier multipath mitigation with field data are given in the following sections.

7.5 Code Range Multipath Mitigation

After having successfully mitigated code multipath errors using simulated data, the technique was extended to mitigate multipath errors using field data. Field trials for code multipath mitigation were conducted on October 20, 1998 and test results were obtained from the collected data. The effectiveness of the technique to remove multipath errors was assessed in two ways; namely in the measurement domain and in the position domain. The measurement domain approach will be discussed first.

7.5.1 Analysis of results in the measurement domain

An important aspect of evaluating the performance of the proposed mitigation technique is to analyze the measurement residuals (code-minus-carrier residuals, compensated for the ionospheric delay as described by Equation 7.2) before and after multipath mitigation. Unlike carrier phase multipath, code multipath error can generally be isolated by the code-minus-carrier technique, as described in Section 7.3.1. The code multipath error as determined from this technique can be compared to the estimated multipath from the Kalman filter to assess the performance of the multipath mitigation technique.

Procedure

The position of each antenna in the multi-antenna assembly was accurately surveyed by using Semikin^{TM} (Cannon, 1990, Cannon, 1993), a software package developed at the University of Calgary for semi-kinematic position computation. The accuracy of the position was better than or equal to 1 cm (RMS) for all the antennas in the multi-antenna assembly. The inter-antenna vectors and the relative geometry of the antennas in the antenna assembly were then established.

The adjusted single difference residual code range measurements (described by Equation 7.7) for a particular satellite were input to the multipath mitigating filter to estimate the parameters of the composite multipath signal. Typical values of process and measurement noise selected for various parameters are as follows:

$$Q_{\alpha_1} = 10^{-4}\ s^{-1} \tag{7.11a}$$

$$Q_{\gamma_{01}} = 2.0x10^{-3}\ rad^2/s \tag{7.11b}$$

$$Q_{\theta_1} = 10^{-4}\ rad^2/s \tag{7.11c}$$

$$Q_{\varphi_1} = 10^{-4}\ rad^2/s \tag{7.11d}$$

$$R_{\Delta P_{0i}} = 0.02\,m^2 \tag{7.12}$$

The choice of process noise values was empirical. However, as the multipath and geometric parameters vary mainly due to the satellite dynamics (as it is a stationary case) and change in potential set of reflectors due to the changed antenna-reflector geometry, the process noise depends upon these factors. As the change in the set of reflectors is unpredictable, it is the satellite dynamics that mainly decides the choice of the process noise parameters. For example, change in the elevation and azimuth of the reflected signal is a function of the satellite dynamics. Furthermore, a correlation time of around 1-3 minutes were chosen for the Gauss-Markov process for various state variables. This is consistent with the correlation time of code multipath as described in section 7.4. The choice of measurement noise is from the receiver noise in range measurements.

After the parameters were estimated by the filter, the multipath errors in the range measurements at each antenna were estimated as described in Chapter 6.

Figure 7.22 shows a flowchart of this process used to compute the code residuals with and without the multipath errors removed. Code multipath errors were isolated by using the code-minus-carrier technique, whereby the ionospheric error was removed from the code range by a second order polynomial curve fit. The residual code range thus obtained, was deemed the *measured multipath* error. The multipath error computed from the estimated parameters was deemed as the *estimated multipath* error. The estimated multipath error was removed from the raw range measurement, and then again the code-minus-carrier technique was used to obtain multipath reduced residual code range.

Statistics were computed for the residual code range before and after multipath mitigation and compared, to evaluate the performance of this technique.

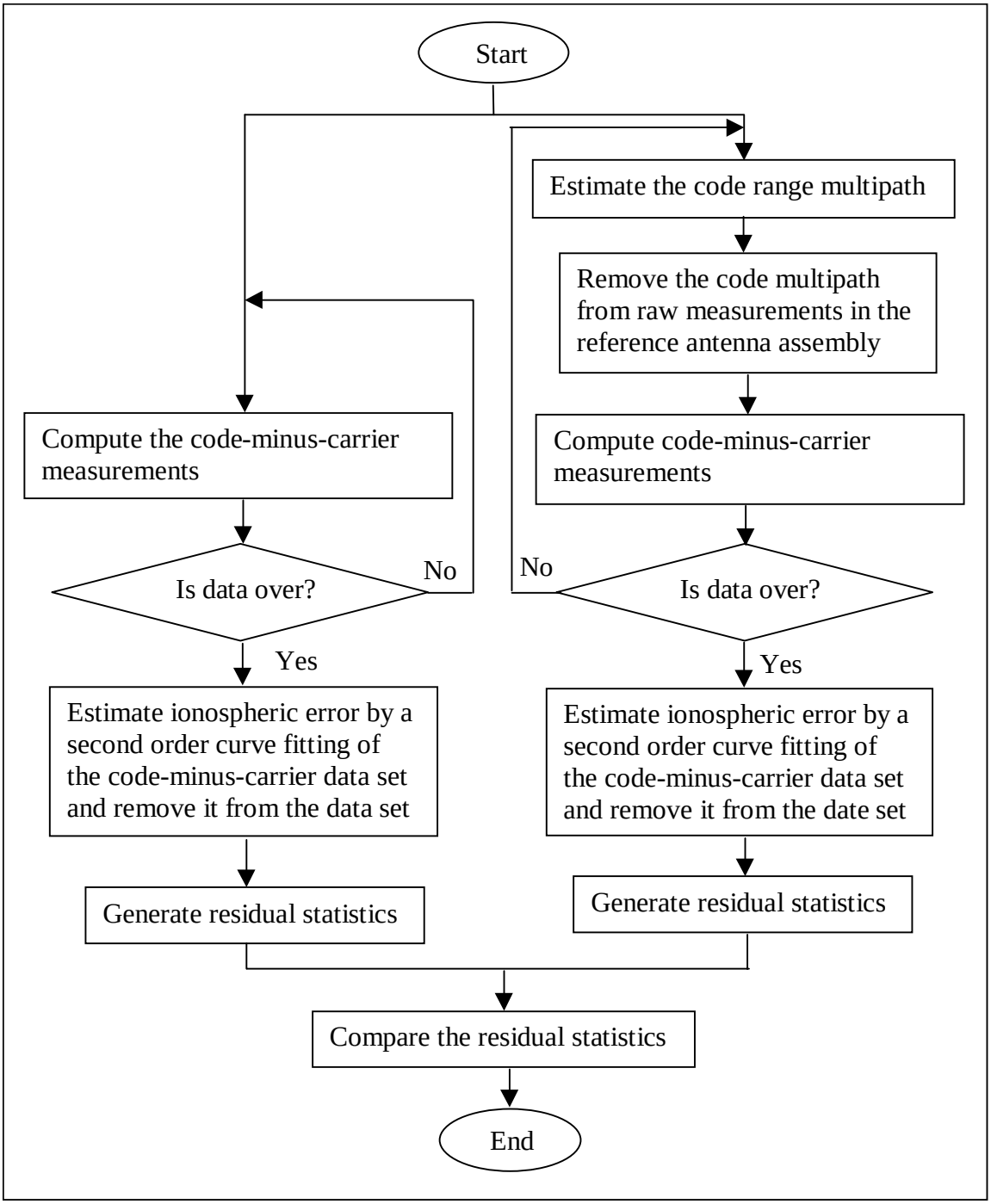

Figure 7.22: Flowchart of evaluating the performance of the code multipath mitigation algorithm in the measurement domain

Analysis of results

In order to demonstrate the effectiveness of this technique, the adjusted single differenced code measurements (described by Equation 7.7) for satellite 9 were computed from the data collected on October 20, 1998 and are shown in Figure 7.23. The plot contains the difference of code multipath errors only, in two close-by antennas, as other errors are either compensated or removed through differencing.

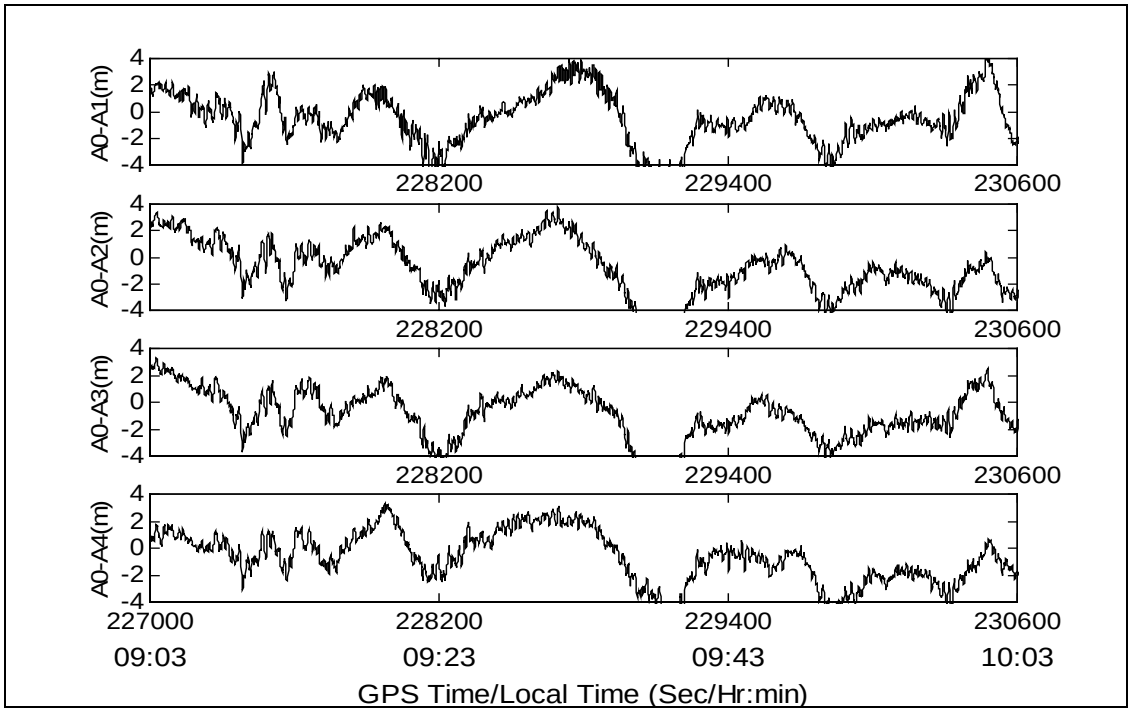

Figure 7.23: Adjusted single differenced code measurements for SV 9 on October 20, 1998 (A0-A*n* denotes single difference between antennas 0 and *n*)

Satellite 9 was a low elevation satellite during the test period, and therefore likely to be more affected by multipath. From the figure it can be seen that the multipath errors are correlated among the antennas in the multi-antenna array, and have many oscillations of various frequencies and amplitudes due to multiple reflectors in the environment. It also contains high frequency receiver noise. Furthermore, it is to be emphasised that code multipath does not cancel through differencing between two close-by antennas.

Figure 7.24 shows the estimated parameters of the composite reflected signal for satellite 9, as determined by the filter. As expected, the parameters vary with time to track many reflections from the environment. The reflected signal phase changes, which causes positive and negative multipath errors. The estimated standard deviations of the filter parameters were around 1.5×10^{-3}, 3.4×10^{-2} radian, 2.3×10^{-2} radian and 1.3×10^{-2} radian for the reflection coefficient, multipath phase, multipath signal elevation and multipath signal azimuth respectively. The reflected signal phase, and thereby the multipath errors at other antennas, were computed from the estimated parameters as described in Chapter 6. Estimated parameters for other satellites had similar characteristics.

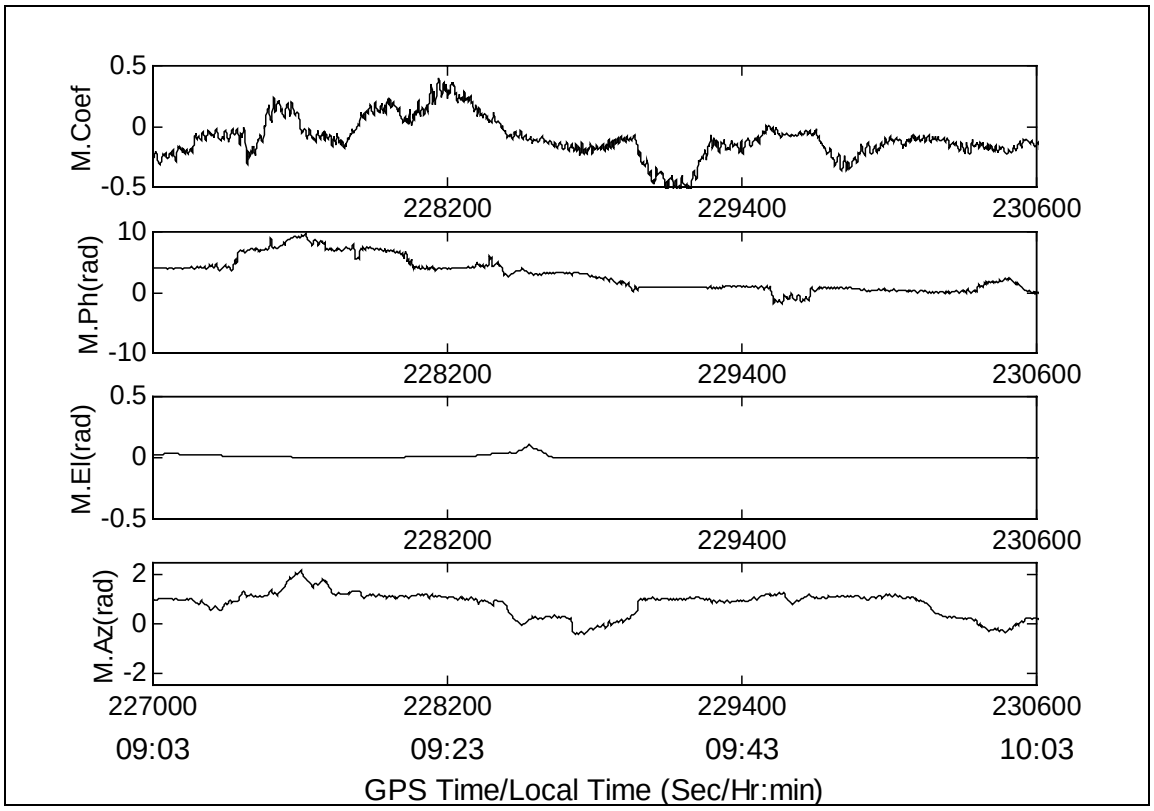

Figure 7.24: Estimated composite multipath signal parameters for SV 9

The residuals in this case, however, are not white and contain some oscillations. That is because the proposed technique modelled only the errors from nearby reflectors. Therefore, errors caused by far away reflectors were not removed by using this technique,

and they remained in the residuals, as previously described. The residuals for satellite 9 are shown in Figure 7.25. The dark lines correspond to the estimated two-sigma error bound. The residuals are generally within the error bounds.

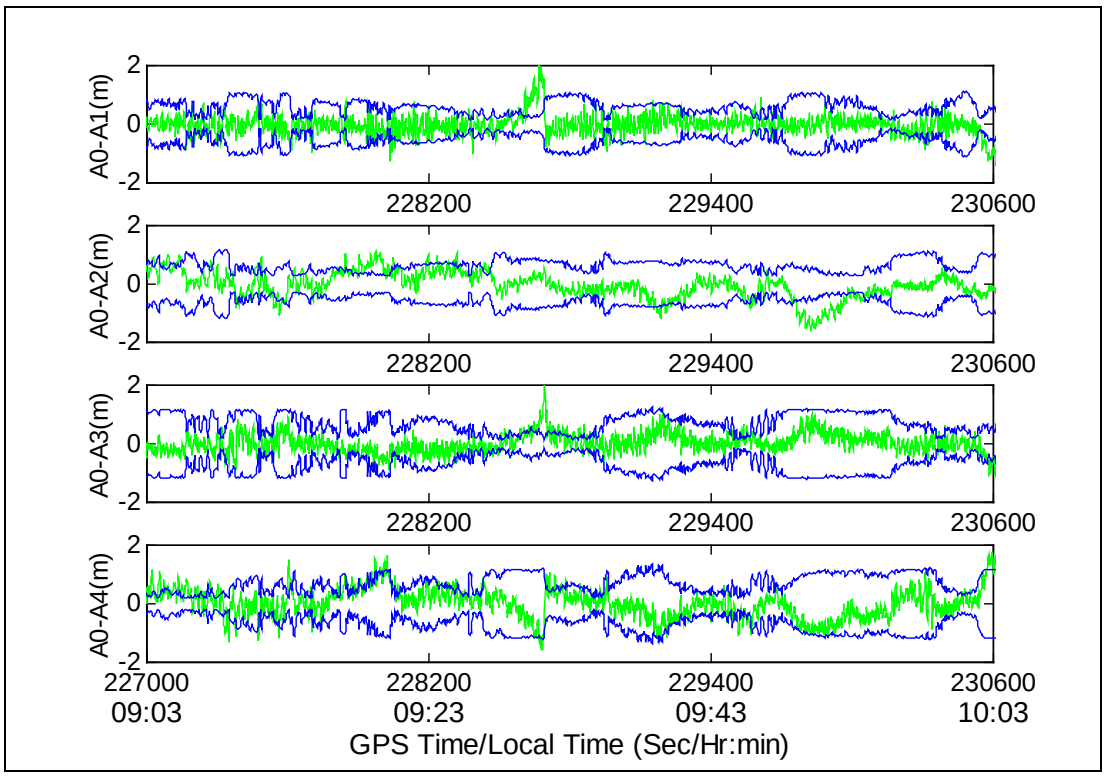

Figure 7. 25: Residuals of parameter estimation for SV 9

Figure 7.26 shows the computed multipath errors from the estimated parameters in a shaded dark line, and the measured multipath errors in a shaded light line. As can be seen, the estimated multipath closely follows the measured multipath errors. This confirms that the proposed technique does not estimate multipath errors due to a single reflector; rather, it estimates composite multipath errors due to major dominant reflectors in the environment.

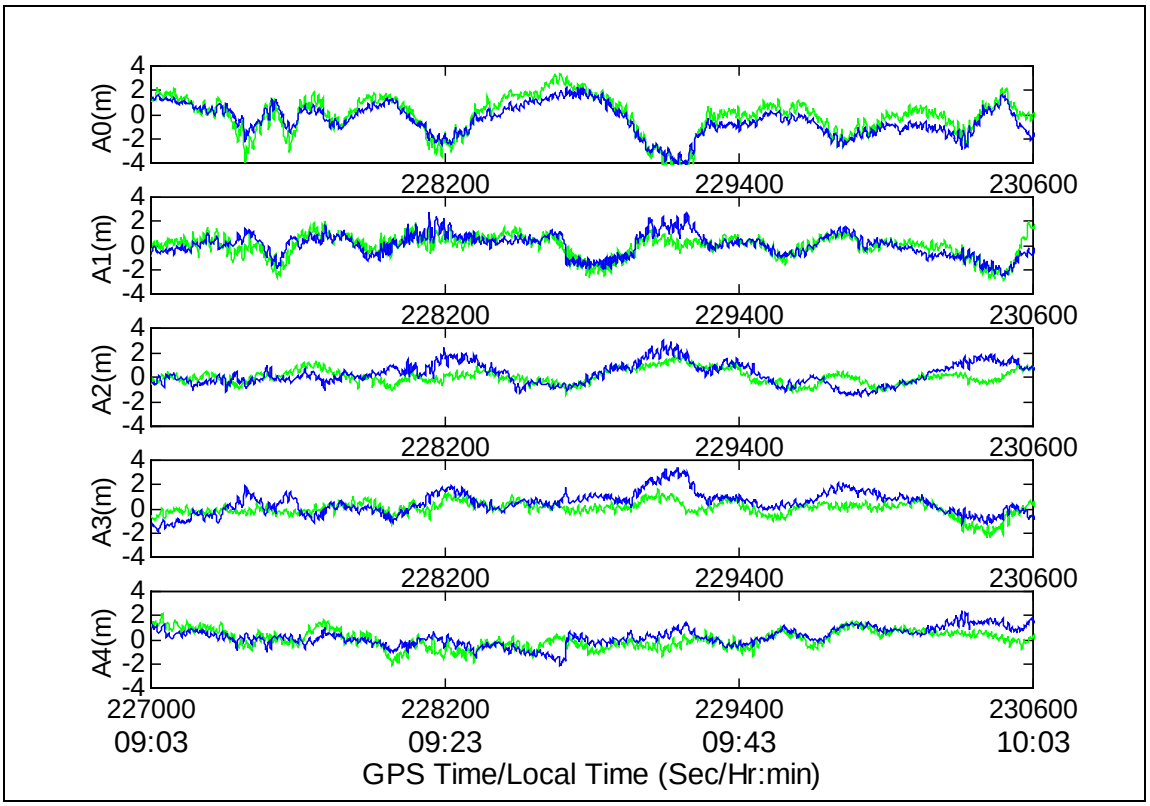

Figure 7.26: Measured multipath (light shade) and estimated multipath (dark shade) for SV 9. (A0…A*n* denote antennas 0…*n* in the antenna assembly)

Multipath errors were estimated in other satellites (SVs 1, 3, 17, 21, 23 and 31) as well, and compared with their measured values. Figures 7.27, 7.28 and 7.29 show the estimated and measured multipath errors for low elevation satellites 1, 17 and 31 respectively. In these cases too, the estimated values also closely follow the measured values.

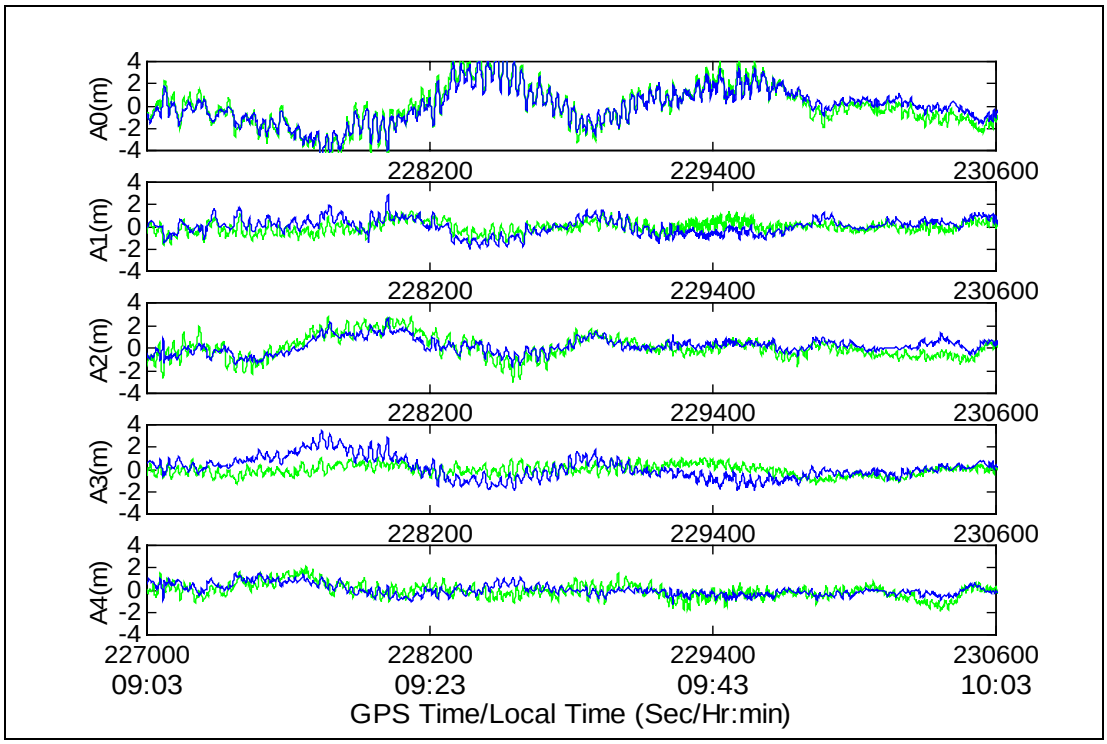

Figure 7.27: Measured multipath (light shade) and estimated multipath (dark shade) for SV 1. (A0…A*n* denote Antenna 0….*n*)

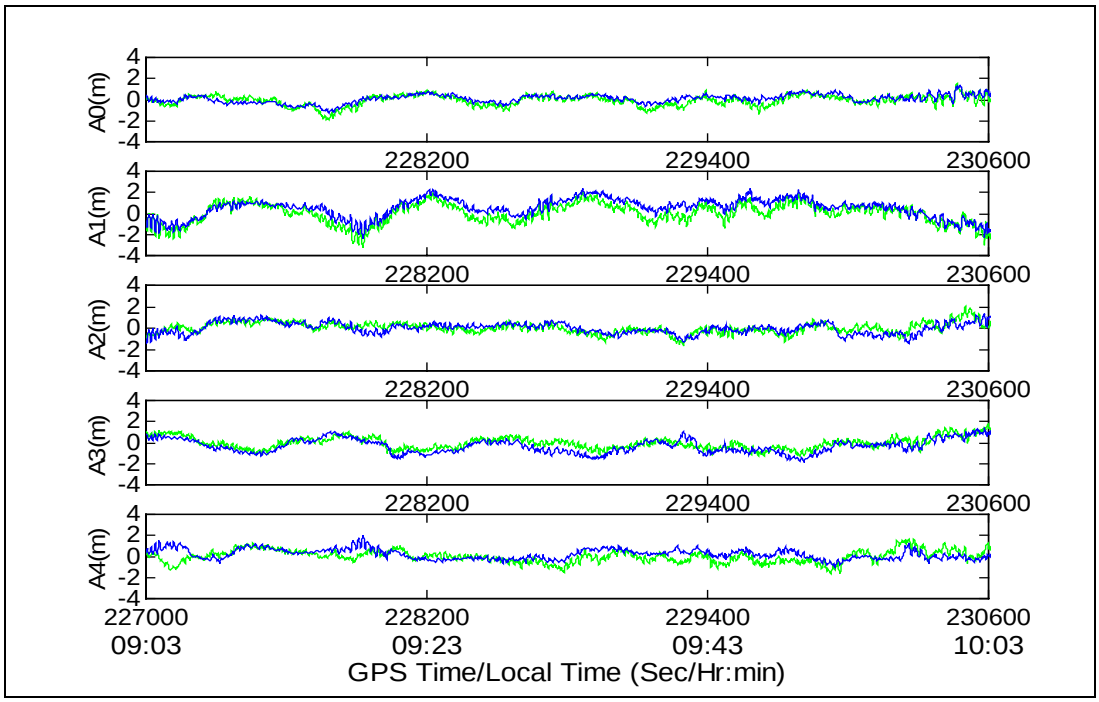

Figure 7.28: Measured multipath (light shade) and estimated multipath (dark shade) for SV 17. (A0…A*n* denote Antenna 0….*n*)

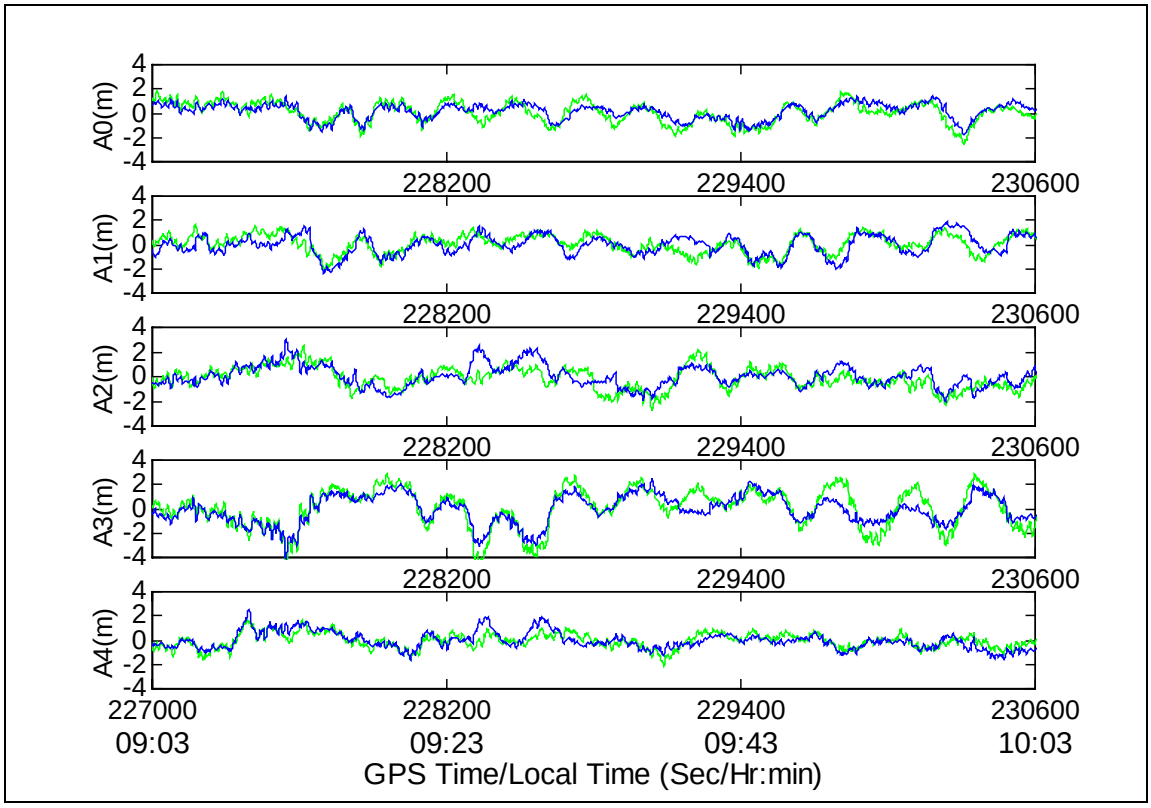

Figure 7.29: Measured multipath (light shade) and estimated multipath (dark shade) for SV 31. (A0…A*n* denote Antenna 0….*n*)

Figure 7.30 shows the adjusted code-minus-carrier and ionospheric delay compensated residuals for low elevation satellites in the reference Antenna 0 with and without multipath correction. It is clear that the multipath-corrected residuals have smaller magnitudes and oscillations compared to the uncorrected residuals.

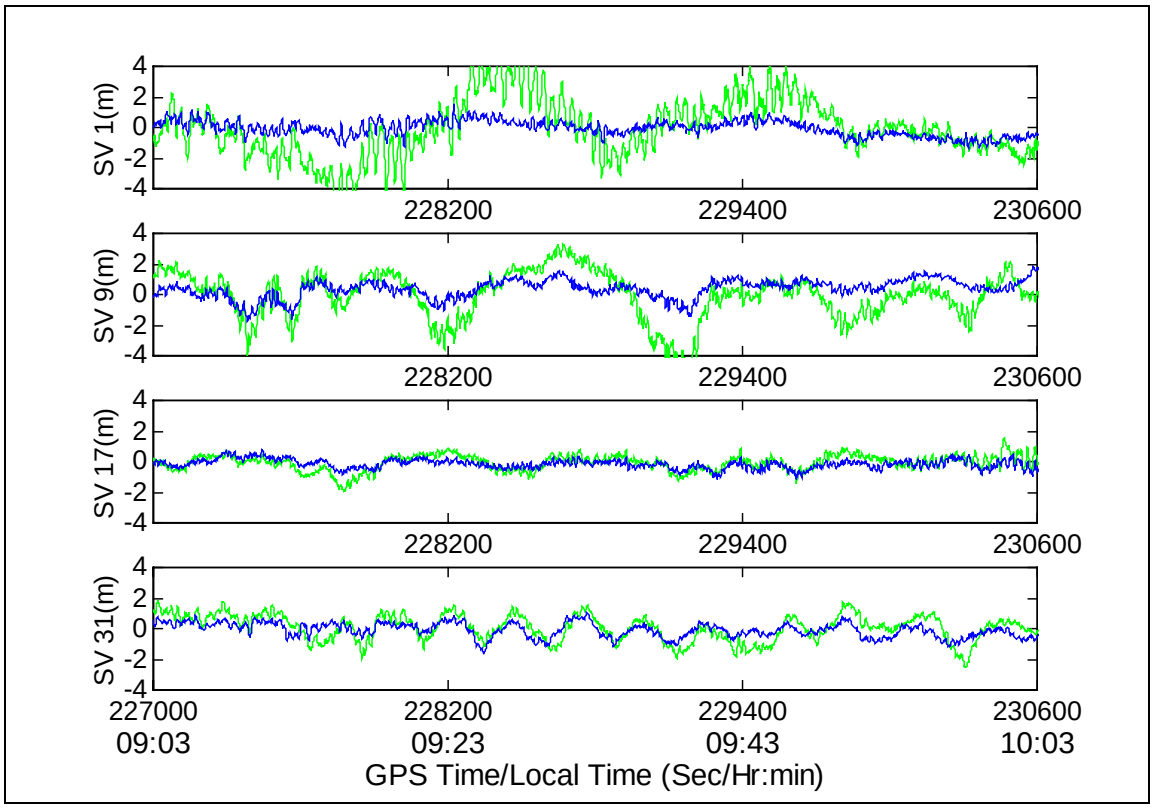

Figure 7.30: Code residuals before (light shade) and after (dark line) multipath correction for SVs 1, 9, 17 and 31 at the reference antenna A0

Table 7.2 gives the residual statistics before and after multipath correction for low elevation satellites during the observation period. The table shows the standard deviation of the code multipath error, as the mean value of the error is lost by the code-minus-carrier technique of multipath error isolation. The statistics were compiled from approximately one hour of data samples.

It can be observed that this method is very effective in a high multipath environment, decreasing the standard deviation of the residuals up to 73%. However, if the residuals are quite small before correction, the improvement is not significant (and can be negative). On average there was an approximately 22% improvement over all the low elevation satellites and all the antennas. This percentage would be somewhat higher, if

the effect of noise is removed from the residuals during calculation. This demonstrates the ability of the method to mitigate code multipath in this environment.

Table 7.2: Code minus carrier and ionospheric delay-compensated residuals before and after multipath correction (standard deviation)

SV No. (Elevation)	Ant. No.	Before Correction (m)	After Correction (m)	Improvement (%)
1 (14°-42°)	A0	1.89	0.51	73.1
	A1	0.54	0.61	-13.9
	A2	0.99	0.63	37.0
	A3	0.48	0.59	-21.2
	A4	0.66	0.55	16.6
9 (13°-27°)	A0	1.56	0.60	61.8
	A1	0.90	0.61	32.1
	A2	0.58	0.74	-26.4
	A3	0.58	0.75	-28.5
	A4	0.72	0.65	09.9
17 (48°-21°)	A0	0.52	0.30	41.6
	A1	0.95	0.37	60.9
	A2	0.50	0.44	12.8
	A3	0.55	0.37	31.6
	A4	0.56	0.61	-08.2
31 (23°-35°)	A0	0.85	0.47	44.6
	A1	0.76	0.64	15.3
	A2	0.88	0.71	19.4
	A3	1.57	0.75	52.1
	A4	0.61	0.46	23.9

7.5.2 Analysis of results in the position domain

The multipath reduced range measurements should also improve the differential position accuracy of the user receiver, which uses these multipath corrected measurements. Therefore, it is important to analyze the user position accuracy before and after multipath correction at the reference antenna assembly.

Procedure

A baseline test was carried out to analyze the impact in the user position accuracy when using corrected code range measurements from the multi-antenna system. The position of the user was first computed using carrier phase measurements from the reference station. This is deemed as the true position of the user antenna, against which the position derived from the differential code measurements was compared. The estimated multipath errors for each satellite in each antenna in the antenna array, were removed from the range measurements. The position of the user was then computed in differential mode (DGPS), first with the uncorrected range data from the reference station, and later using the multipath-corrected measurements. No multipath corrections were made at the user end. However the receiver was situated in an open field, and therefore it was assumed that the multipath effect would be minimal. The University of Calgary's C^3NAV^{TM} software (Cannon and Lachapelle, 1997) was used to compute DGPS positions.

A comparison between the position errors with and without corrections indicates the achievable improvement in user position using such a system. The user position was first computed using non-smooth code measurements and, later, by using carrier-smoothed code measurements. These were compared with respect to the true position, to generate appropriate statistics. Figure 7.31 shows a flowchart of this procedure.

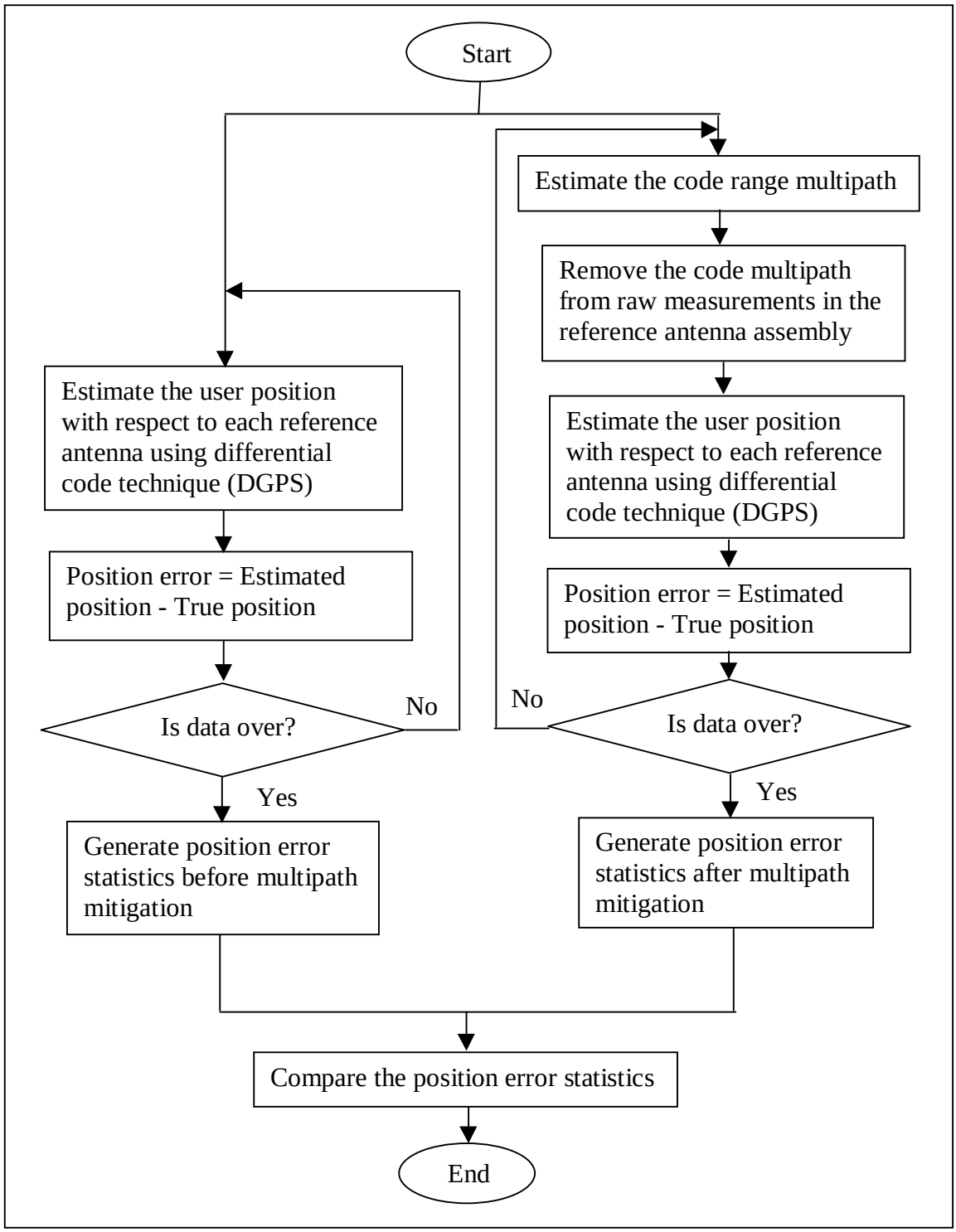

Figure 7.31: Flowchart of evaluating the performance of the code multipath mitigation algorithm in the position domain

Analysis of Results

The DGPS user position was first computed using the code measurements without multipath corrections. Antenna 0 of the multi-antenna assembly was used as the reference antenna for DGPS position computation. The position error, (i.e., the difference between the code DGPS position and the true position), is shown in Figure 7.32 using a shaded light line. The user position was recomputed using multipath-corrected code measurements, and the corresponding errors are shown in the same figure using a shaded dark line. It can be observed that the position errors with the corrected measurements have a smaller magnitude.

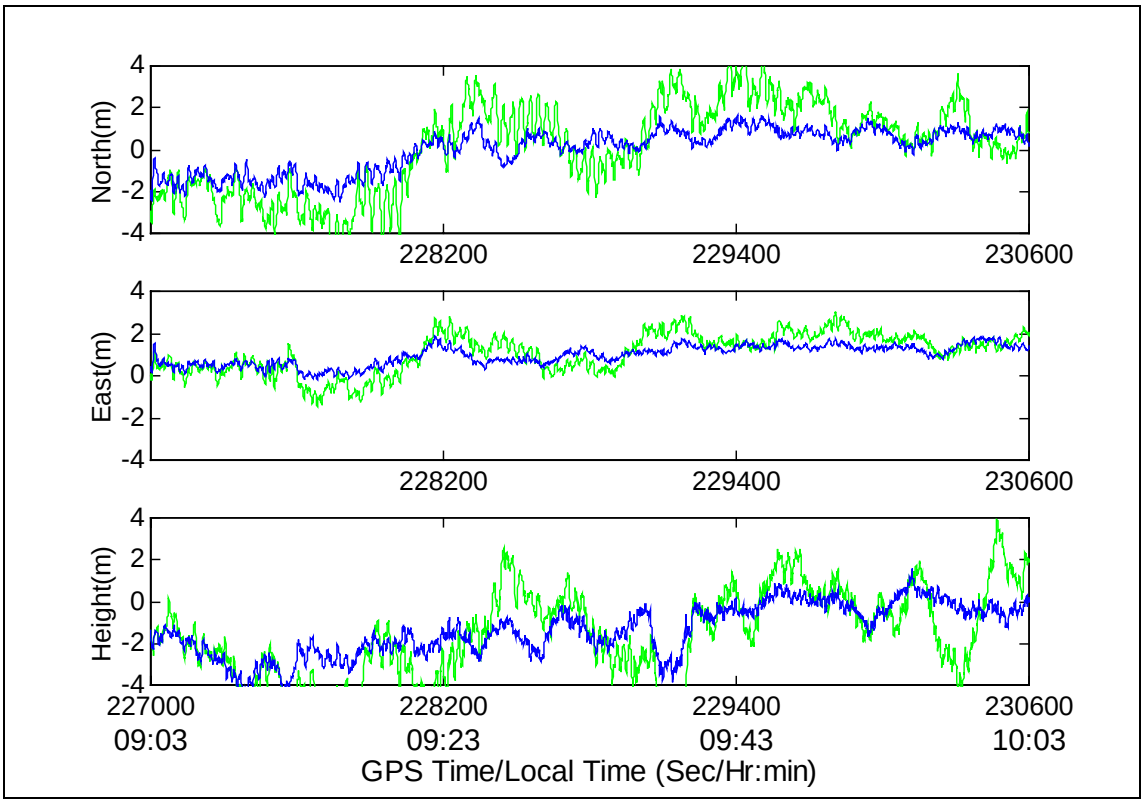

Figure 7.32: User position error using Antenna 0 as reference antenna before (light shade) and after (dark shade) code multipath correction using non-smooth code

The experiment was repeated with carrier-smoothed code data, using a smoothing period of 100 seconds, as shown in Figure 7.33. The smoothing process is likely to improve the quality of the code measurement by reducing the code multipath error and receiver noise,

at the expense of increased ionospheric error. A similar improvement in the position accuracy was observed after multipath correction.

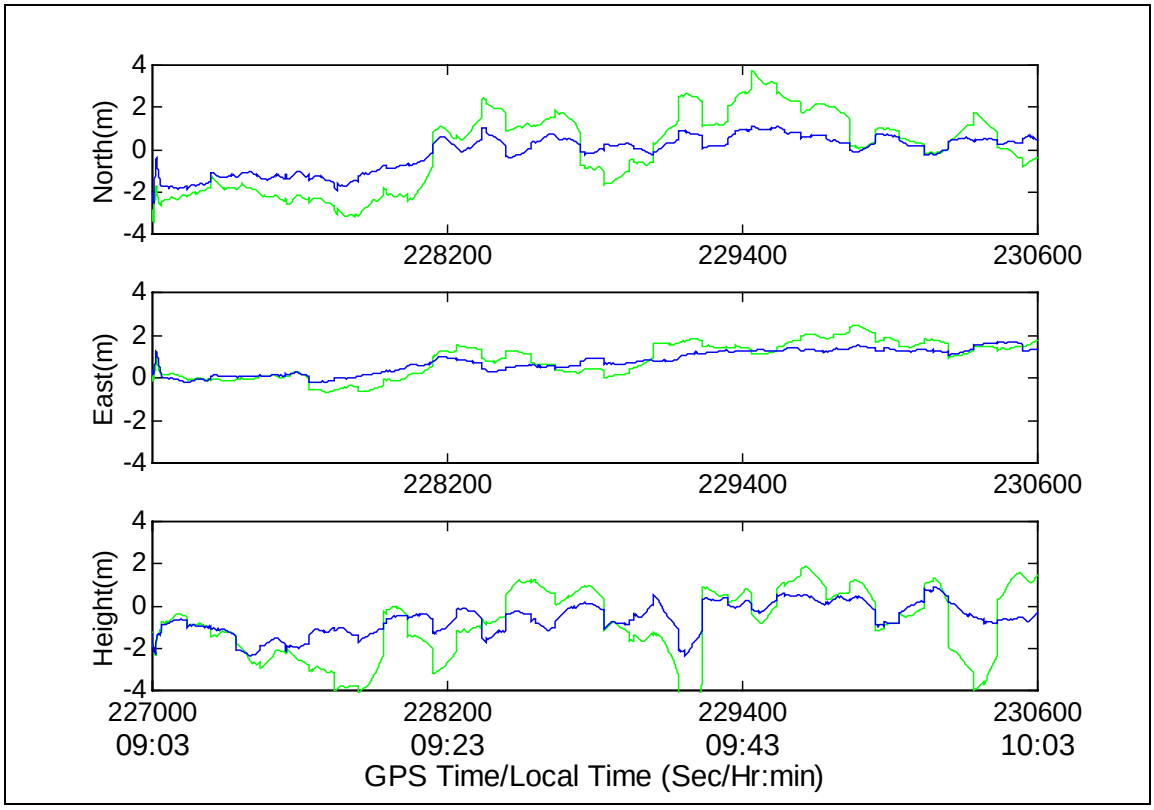

Figure 7.33: User position error using Antenna 0 as reference antenna before (light shade) and after (dark shade) code multipath correction using carrier-smoothed code

The analysis was repeated using each antenna in the multi-antenna assembly, and the statistics are shown in Tables 7.3 and 7.4 corresponding to the non-smoothed code and carrier-smoothed code cases. The 3D position error was computed using the following equation,

$$\sigma_{3D\,error} = \sqrt{\sigma^2_{lat\,error} + \sigma^2_{lon\,error} + \sigma^2_{hgt\,error}} \tag{7.13}$$

Improvements of up to 51% and 52% in the 3D position accuracies were achieved using this technique in the non-smoothed code, and the carrier-smoothed code cases respectively. The average improvement for all the five antennas were 21% and 23%

respectively for the non-smoothed code and the carrier-smoothed code cases. The improvement is significant when the position error is large (before correction) mainly due to high level of multipath error. Residuals were slightly deteriorated in some case (although the absolute error was quite small). The position error residuals after correction are generally quite similar even though the percentage of improvement is quite different in various antennas. Furthermore, comparing Tables 7.3 and 7.4, it can be noted that the position errors are smaller in the case of using the carrier-smoothed code, compared to the non-smoothed code in both before and after multipath correction.

Table 7.3: User position errors using non-smooth code before and after multipath correction

Antenna No.		Before Correction (m)	After Correction (m)	Improvement (%)	3D Improvement (%)
A0	Lat	2.11	1.01	52.2	50.8
	Lon	0.93	0.47	49.7	
	Hgt	2.22	1.11	49.9	
A1	Lat	1.04	0.94	09.1	20.6
	Lon	0.67	0.49	26.0	
	Hgt	1.46	1.08	26.0	
A2	Lat	1.01	0.68	32.8	06.6
	Lon	0.54	0.55	-01.4	
	Hgt	1.34	1.39	-04.1	
A3	Lat	1.01	1.14	-12.2	19.1
	Lon	0.67	0.54	18.9	
	Hgt	1.61	1.17	27.2	
A4	Lat	0.60	0.65	-08.3	06.8
	Lon	0.42	0.53	-26.0	
	Hgt	1.19	1.00	16.2	

Table 7.4: User position errors using carrier-smooth code before and after multipath correction

Antenna No.		Before Correction (m)	After Correction (m)	Improvement (%)	3D Improvement (%)
A0	Lat	1.79	0.84	53.1	52.3
	Lon	0.82	0.54	33.3	
	Hgt	1.71	0.74	56.9	
A1	Lat	0.85	0.84	01.2	21.1
	Lon	0.60	0.47	22.0	
	Hgt	1.21	0.81	32.8	
A2	Lat	0.89	0.53	40.3	08.3
	Lon	0.60	0.57	04.9	
	Hgt	1.20	1.25	-04.3	
A3	Lat	0.99	1.04	-05.9	20.4
	Lon	0.59	0.46	21.4	
	Hgt	1.44	1.03	28.4	
A4	Lat	0.47	0.50	-06.6	14.4
	Lon	0.47	0.53	-12.3	
	Hgt	0.98	0.71	28.0	

The percentage of improvement is smaller in the position domain compared to the measurement domain. This is because, a) the multipath errors in the user antenna were not mitigated, though used for position computation, and b) the position was computed from all the available measurements and the percentage of improvement in all the measurements were not of the same degree.

These results demonstrate that significant improvement in residuals and user position accuracy can be achieved by using such a multi-antenna system as a reference station,

using the proposed multipath mitigation technique. Though the percentage of improvement was not uniform for all the satellites or at all the antennas, the improvement was found to be more when the multipath were higher. This is a desirable attribute of the technique. Furthermore, there was no batch processing and inherent delay or storage requirement of the measurements, and therefore, this technique has potential to be used in real time multipath mitigation as demanded in various applications.

7. 6 Carrier Phase Multipath Mitigation

Similar to the case of code multipath, the mitigation technique was further extended to mitigate carrier phase multipath using field data. Data collected on August 25-26 and October 20 were used for analysis. The effectiveness of the mitigation technique in the case of the carrier phase is analyzed both in measurement and position domains for a more comprehensive evaluation.

7.6.1 Analysis of results in the measurement domain

As the multipath error corrupts the carrier phase measurements, it will, in turn, affect the residuals as described by Equation 7.3 or 7.8. However, the multipath error for a particular satellite in a single antenna can not be isolated. Therefore, the residuals are to be formed by using measurements from more than one antenna, as described previously. Two types of residual tests are performed for the carrier:

a) single differenced residuals between antennas in the multi-antenna assembly (described by Equation 7.8)
b) double differenced residuals between each antenna in the multi-antenna assembly and the user antenna (described by Equation 7.3)

However, in either case, parameters of the composite multipath signals are to be first estimated from the carrier phase measurements.

7.6.1.1 Single Difference Residual Test

Procedure

The position of the antennas in the multi-antenna assembly was determined first. This was done by fixing the position of one of the antenna's in the multi-antenna assembly (as the antenna assembly was mounted on a surveyed pillar, its position was known quite accurately) and then determining the differential position of the user antenna using carrier phase measurements with the Semikin^{TM} software. The position of the user antenna was then fixed and the differential position of each antenna in the multi-antenna assembly was computed using the carrier phase measurements. As the user antenna was placed in an open area, the accuracy of the differential position of the antennas in the multi-antenna assembly was affected by the multipath at the antenna assembly.

The adjusted single differenced carrier phase measurements for a particular satellite were formed as described in Equation 7.8, and input to the multipath mitigating filter. The Kalman filter estimates the parameters of the composite multipath signal due to all reflectors affecting the carrier phase that best fits the model. After the parameters were estimated, the multipath errors in the carrier phase measurements at each antenna in the antenna assembly were computed, as described in Chapter 6.

The estimated multipath errors at each secondary antenna can be subtracted from the corresponding errors in the reference antenna for a particular satellite. The resultant errors are then, once again, subtracted from the adjusted single difference phase residuals (which were input to the filter), to obtain adjusted singled differenced multipath-reduced phase residuals. The multipath-reduced phase measurements (which should ideally be white, due to receiver phase noise only) can then be analyzed to assess the performance of the technique. Figure 7.34 shows a flowchart of this procedure.

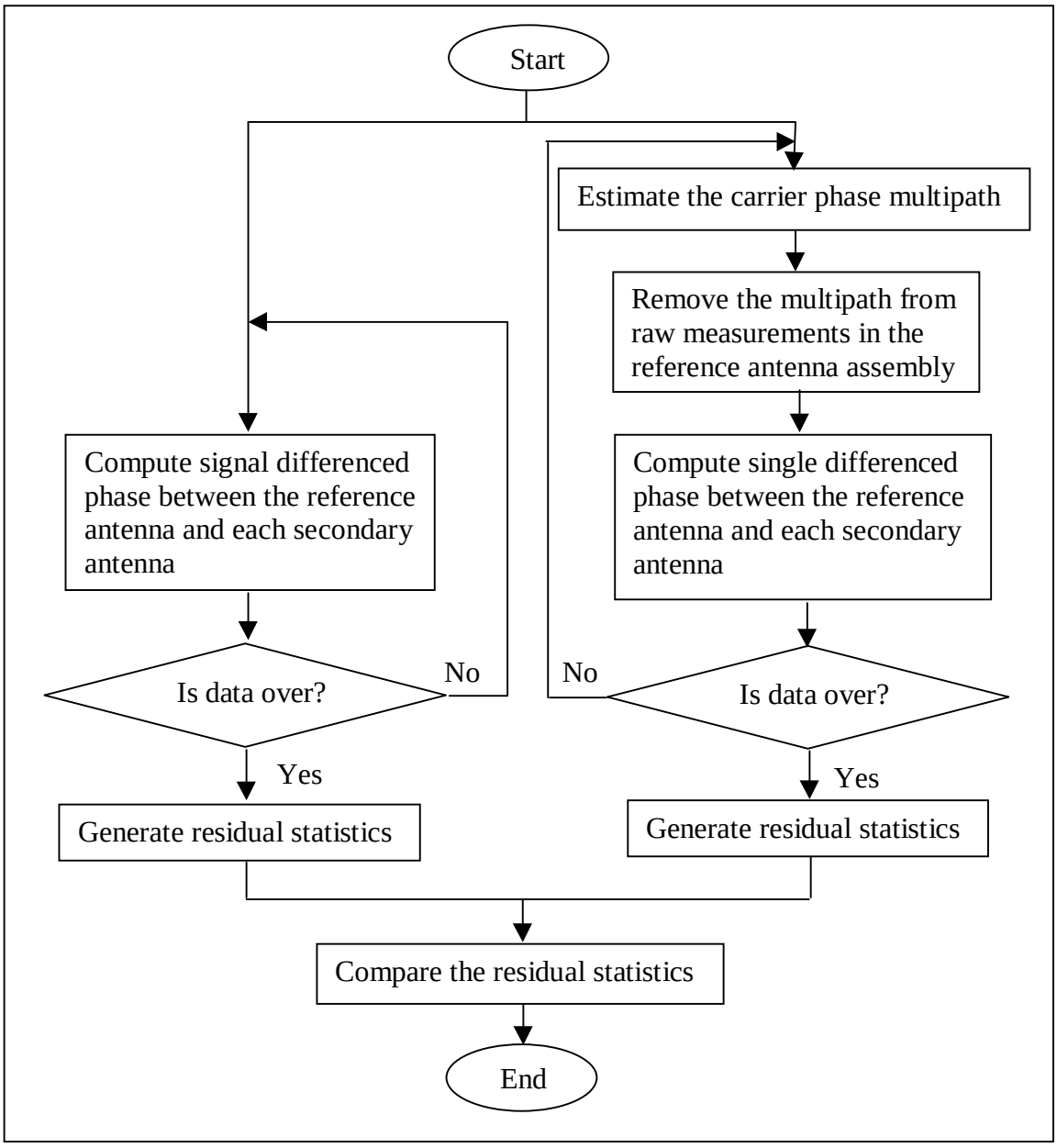

Figure 7.34: Flowchart of evaluating the performance of the multipath mitigation algorithm from the single differenced carrier phase residuals

Analysis of results

The adjusted single differenced residuals (described by Equation 7.8) contain carrier phase multipath errors and phase noise. In order to demonstrate the effectiveness of this

technique, the adjusted single differenced residual phase was computed for satellite 21 from the data collected on August 25, 1998, and is shown in Figure 7.35.

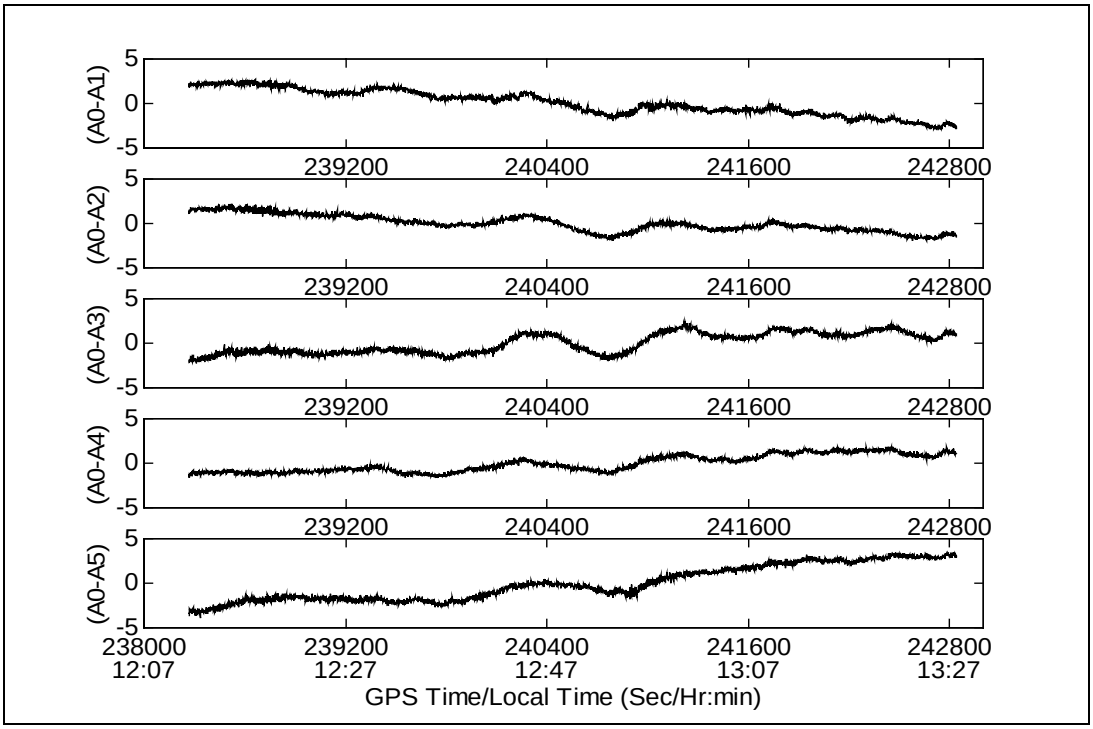

Figure 7.35: Single differenced residual carrier phase error before applying multipath correction for SV 21 on August 25, 1998 (Y-axis units in cm; A0-A*n* denotes single difference between antennas 0 and *n*)

Each plot has a distinct trend, which is different for each antenna. Some oscillatory errors of varying amplitude are also evident. Data collected on the subsequent two days, (at 4 minutes earlier than the previous day), also show a similar trend and oscillation pattern. The residual phase for the same satellite from the data collected on August 26 is shown in Figure 7.36.

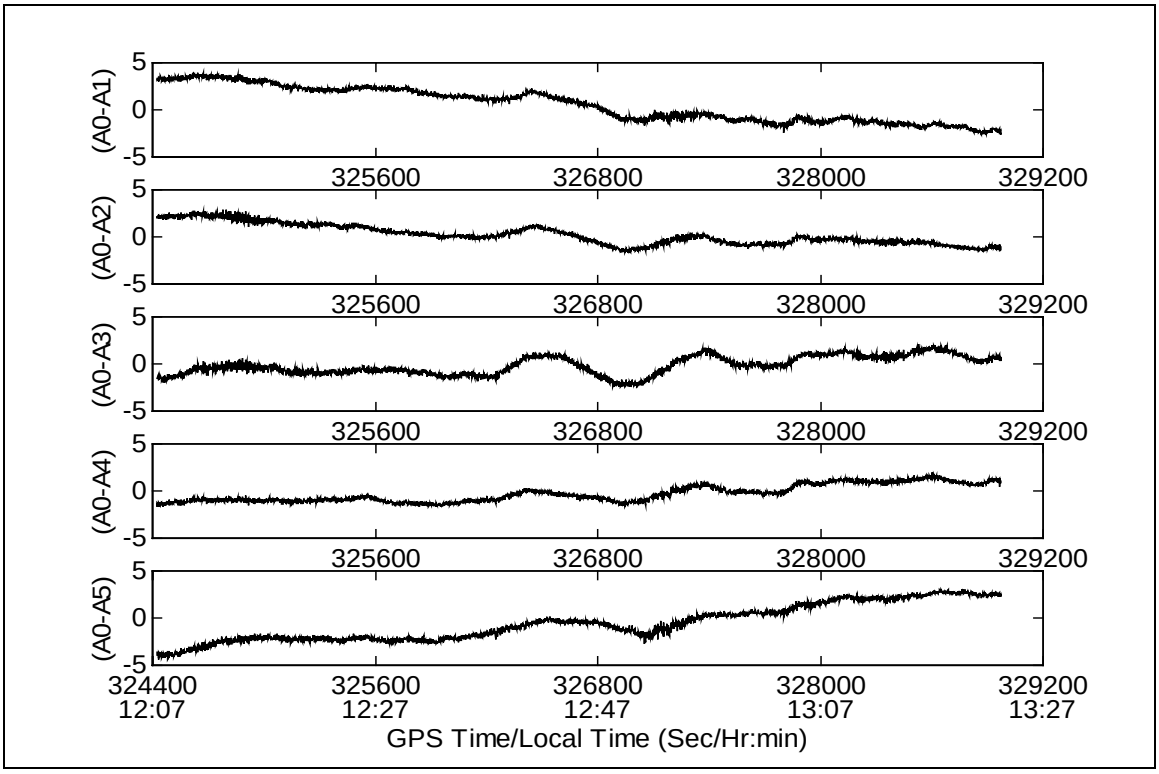

Figure 7.36: Single differenced residual carrier phase error before applying multipath correction for SV 21 on August 26 for the same time of day (shifted by 4 minutes) as in Figure 7.35 (Y-axis in cm; A0-A*n* denotes single difference between antennas 0 and *n*)

Neglecting the high frequency phase noise, the residuals consist of two distinct components; the slow trend and medium frequency oscillatory errors. The slow trend was initially attributed to multipath from a nearby strong reflector due to its day-to-day repeatability and presence of a similar trend in residuals for other satellites. However, later it was found that the trend is due to the insufficient accuracy of the antenna phase centre's position in the antenna assembly. The medium frequency errors, however, are due to multipath caused by various reflectors in the environment. The non-uniformity of the oscillatory patterns suggests multiple reflectors in the vicinity of the antenna assembly. All other satellites show similar oscillatory patterns, which repeat day-to-day.

In Figures 7.35 and 7.36 it can also be observed that multipath errors are correlated among the antennas. Such a high correlation of multipath across antennas is due to the close antenna spacing in the assembly, and is critical to the estimation of composite reflected signal parameters using the proposed algorithms.

The multipath-corrupted carrier phase measurement residuals are used as input to the mitigating filter. Figure 7.37 shows the parameters of the composite reflected signal estimated by the filter for SV 21 on August 25. The parameters of the composite reflector vary with time, to track the effect of the composite multipath error.

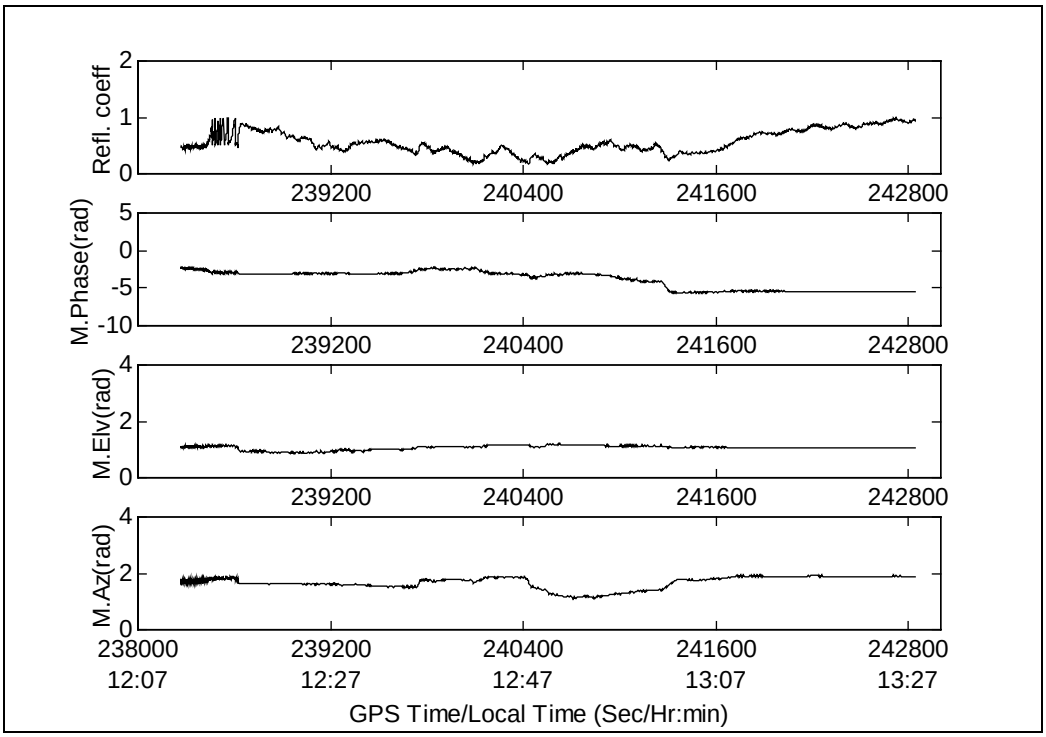

Figure 7.37: Estimated composite reflected signal parameters for SV 21 on August 25

Figure 7.38 shows the estimated multipath errors at each antenna computed from the estimated parameters of the composite reflected signal. The estimated multipath errors show non-uniform oscillations. This demonstrates the capability of the system to estimate composite reflection effects, rather than a single reflection effect. The slow trends, which

are also estimated by the filter, show the capability of the filter to correct residual errors due to insufficient accuracy in the reference antenna position.

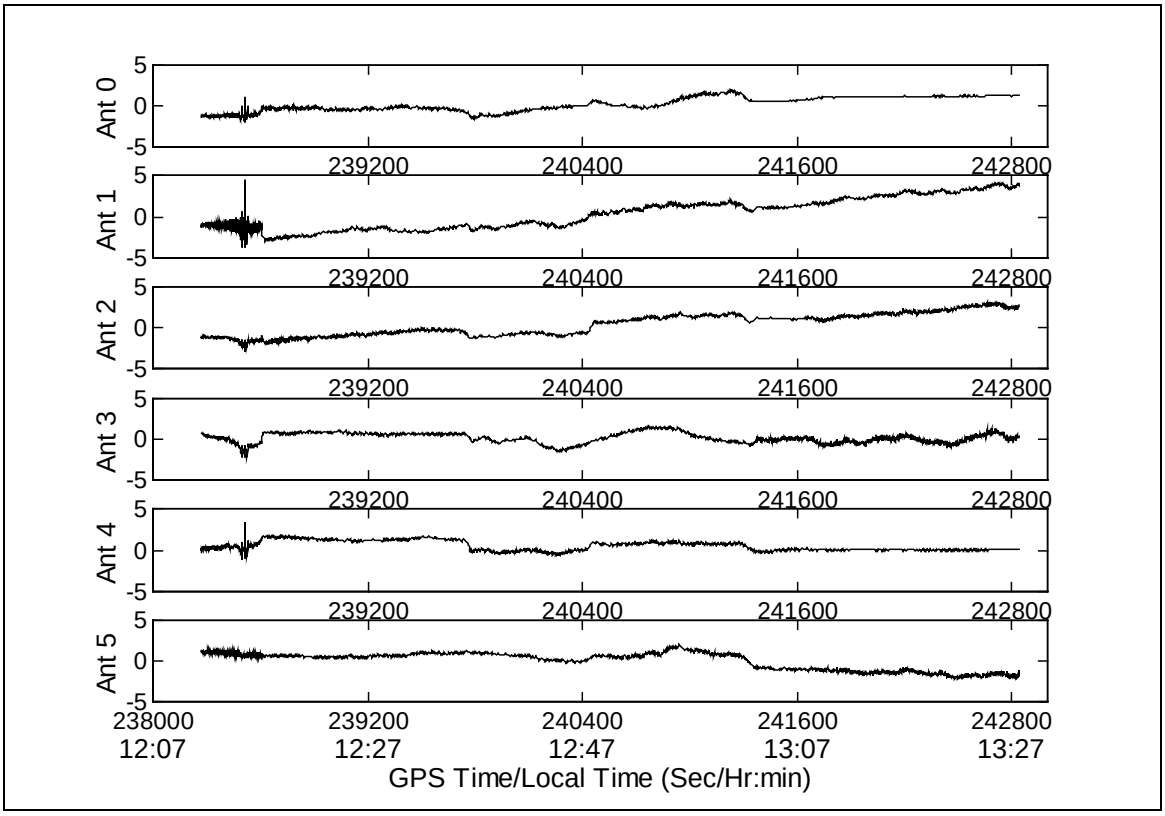

Figure 7.38: Estimated carrier phase multipath errors for SV 21 on August 25 for each antenna (Y-axis in cm)

Carrier phase measurements from each antenna can be corrected by the estimated multipath errors at that antenna. Figure 7.39 shows the adjusted single differenced residuals with the corrected measurements. It is clear from the figure that the residuals are more random in nature, and that phase errors due to multipath are nearly eliminated.

Figure 7.40 shows the multipath corrected measurement data for the same satellite on August 26. As in the previous case, the multipath errors are nearly eliminated, except during the filter convergence period. The high amplitude spikes at the beginning is due to the large residual errors in some of the input measurements as evident in Figure 7.36.

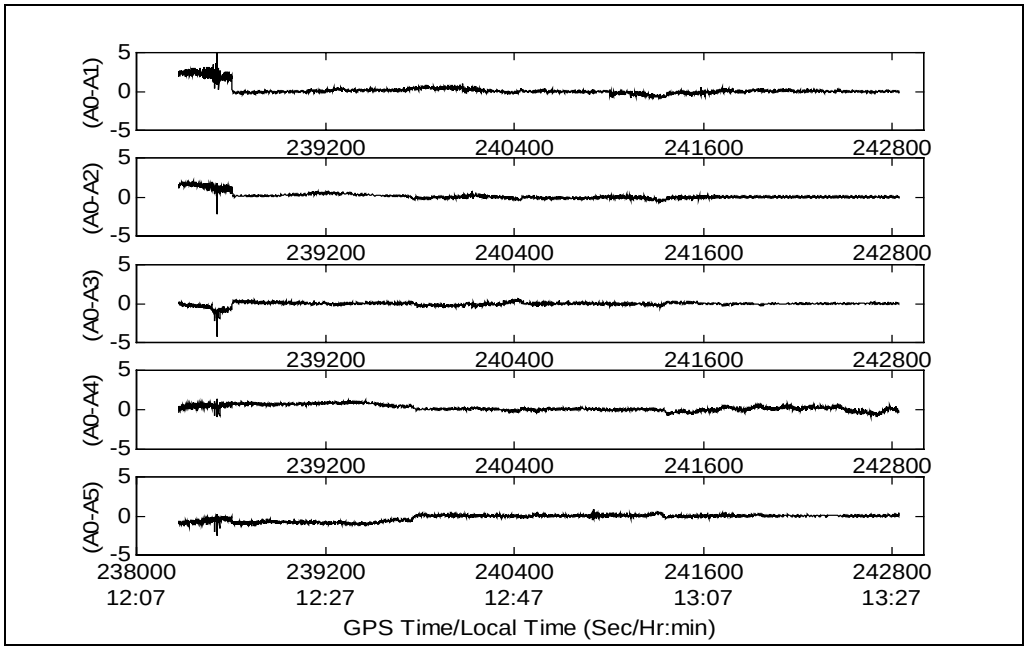

Figure 7.39: Adjusted single differenced residual carrier phase after multipath correction for SV 21 on August 25 (Y-axis in cm; A0-A*n* denotes single difference between antennas 0 and *n*)

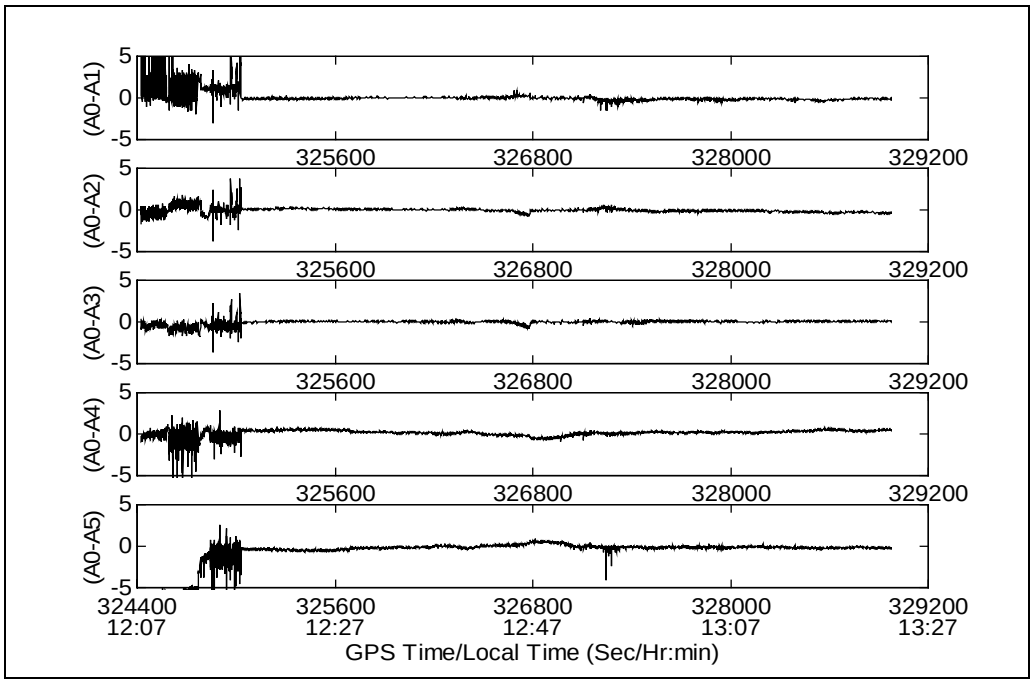

Figure 7.40: Adjusted single differenced residual carrier phase after multipath correction for SV 21 on August 26 (Y-axis in cm; A0-A*n* denotes single difference between antennas 0 and *n*)

Figures 7.41 and 7.42 show the single differenced residual before and after applying the multipath mitigation technique for satellite 31 on August 25. These results are in agreement with SV 21.

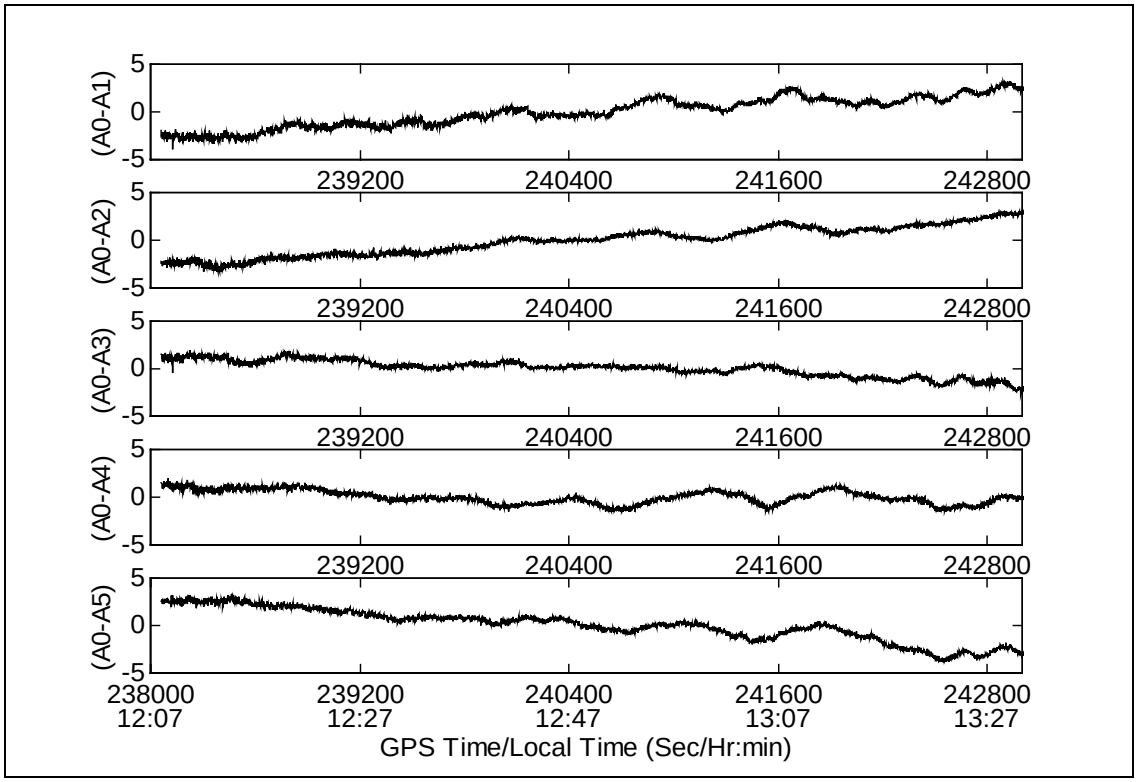

Figure 7.41: Adjusted single differenced residual carrier phase errors before multipath correction for SV 31 on August 25 (Y-axis in cm; A0-A*n* denotes single difference between antennas 0 and *n*)

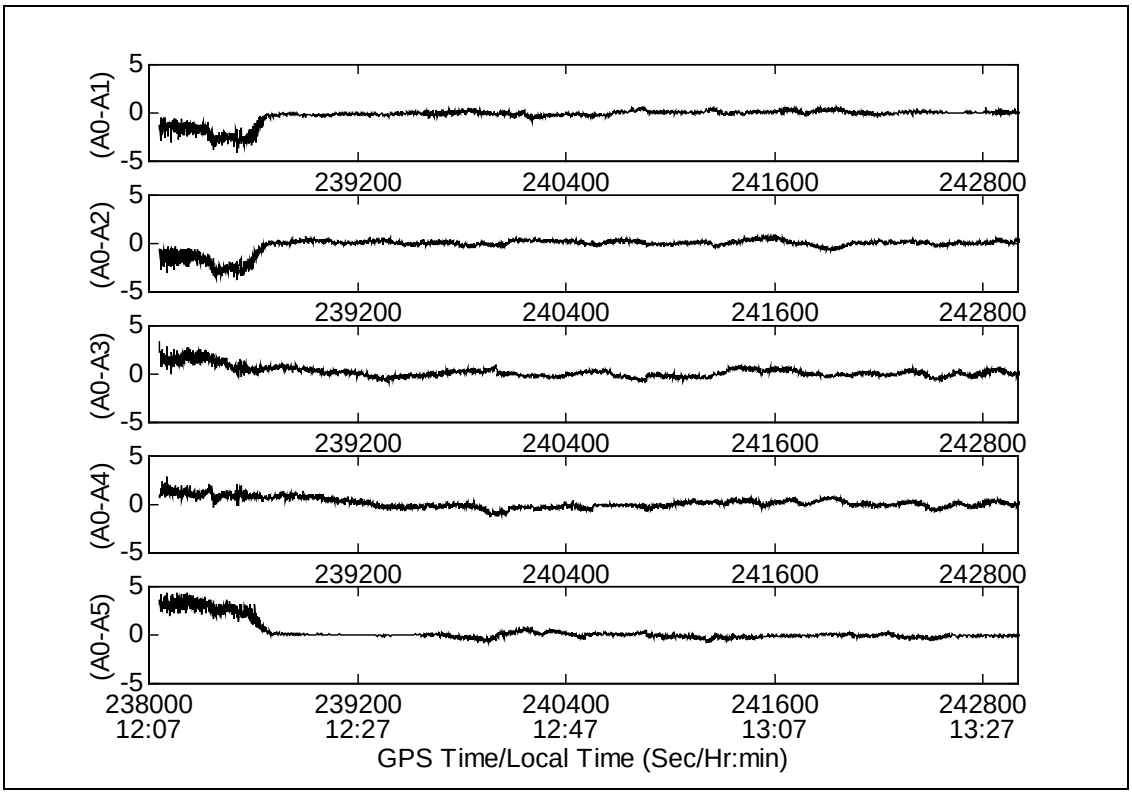

Figure 7.42: Adjusted single differenced residual carrier phase errors after multipath correction for SV 31 on August 25 (Y-axis in cm; A0-A*n* denotes single difference between antennas 0 and *n*)

This method was applied to other satellites available during the data collection period and the improvement is observed in all cases. Table 7.5 gives an overview of statistics before and after multipath mitigation for data collected on August 25, and Table 7.6 gives the corresponding values for data collected on August 26. These statistics were compiled from approximately 4000 samples, (excluding the convergence period), and were averaged over all the antennas.

The RMS values of the multipath-corrected measured phase differences are significantly lower than the values before correction. On average, there was a 73% improvement, which clearly demonstrates the effectiveness of this method to mitigate carrier phase multipath in this environment.

Table 7.5: Carrier phase residuals before and after applying the multipath mitigation technique for data collected on August 25

SV ID	August 25				
	Before correction		After Correction		Improvement
	Mean (cm)	RMS (cm)	Mean (cm)	RMS (cm)	%
17	0.14	1.77	0.00	0.40	77.4
21	0.01	1.26	0.02	0.30	76.2
23	-0.19	1.70	0.26	0.59	65.3
31	0.02	1.30	0.04	0.28	78.5

Table 7.6: Carrier phase residuals before and after applying the multipath mitigation technique for data collected on August 26

SV ID	August 26				
	Before correction		After correction		Improvement
	Mean (cm)	RMS (cm)	Mean (cm)	RMS (cm)	%
17	0.08	1.68	0.01	0.37	78.0
21	-0.08	1.28	-0.01	0.23	82.0
23	-0.17	1.67	0.26	0.67	60.0
31	0.00	1.26	0.03	0.46	63.5

7.6.1.2 Double Difference Residual Test

Procedure

The adjusted single difference residual carrier range measurements (described by Equation 7.8) for a particular satellite were input to the multipath mitigating filter to estimate the parameters of the composite multipath signal. The process and measurement noise were selected based on the factors described in section 7.5.1 and are as follows:

$$Q_{\alpha_1} = 10^{-5}\ s^{-1} \tag{7.14a}$$

$$Q_{\gamma_{01}} = 1.0x10^{-2}\ rad^2/s \tag{7.14b}$$

$$Q_{\theta_1} = 10^{-6}\ rad^2/s \tag{7.14c}$$

$$Q_{\varphi_1} = 10^{-6}\ rad^2/s \tag{7.14d}$$

$$R_{\Delta\Phi_{0i}} = 10^{-4}\ m^2 \tag{7.15}$$

After the parameters were estimated by the filter, the multipath errors in the phase measurements at each antenna were estimated as described in Chapter 6.

The carrier phase multipath errors were isolated using the technique described in Section 7.3.2. The double differenced residuals were determined at each antenna in the multi-antenna assembly with respect to the user antenna and between the base and another satellite. Assuming that the user antenna site has negligible multipath, the residual double differenced phase measurements contain the single difference multipath between the base satellite and another satellite in the antenna assembly. This was deemed the *measured multipath* error.

After the multipath parameters are estimated by the filter, the multipath errors at each antenna in the multi-antenna assembly for a particular satellite can be computed. The single difference of the estimated multipath between the base satellite and another satellite at an antenna in the multi-antenna assembly was determined and deemed as the *estimated multipath* error. Estimated multipath errors were removed from the raw measurements to obtain multipath-reduced, adjusted double differenced phase residuals. Statistics were computed for these double differenced phase residuals before and after multipath mitigation, and were compared to evaluate the performance of this technique. Figure 7.43 shows a flowchart of this procedure.

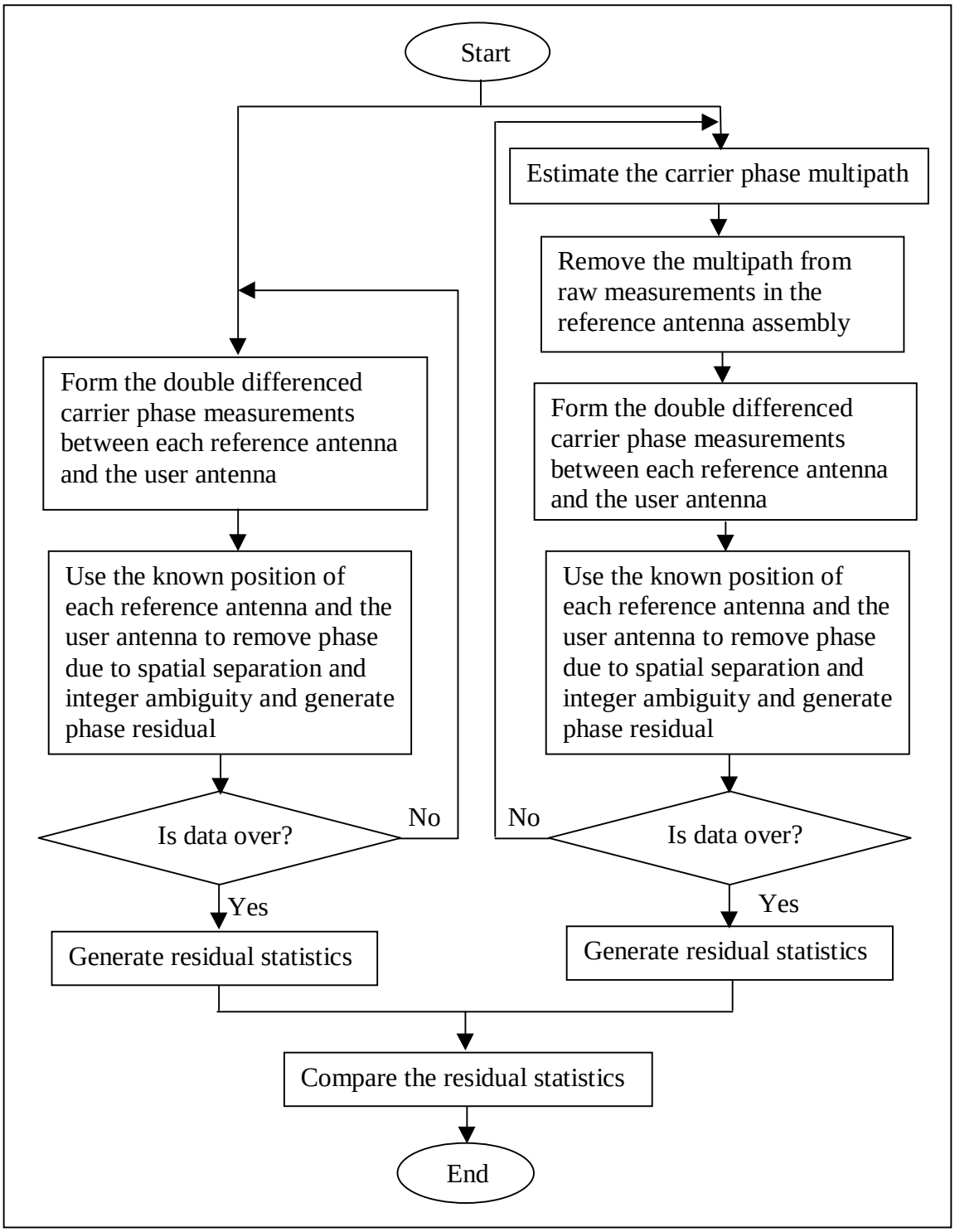

Figure 7.43: Flowchart of evaluating the performance of the multipath mitigation algorithm using double differenced carrier phase measurements

Analysis of results

This analysis was performed on the adjusted double differenced phase residuals between each antenna in the antenna array and the user antenna, with and without multipath correction, using data collected on October 20. Single differenced phase residuals for each antenna pair were derived for satellite 31. This is a low elevation (23°-35°) satellite, and likely to be more affected by multipath. The phase residuals are shown in Figure 7.44. The residuals contain low to medium frequency oscillations, with variable amplitude due to reflections from all the reflectors in the environment. It also contains high frequency phase noise.

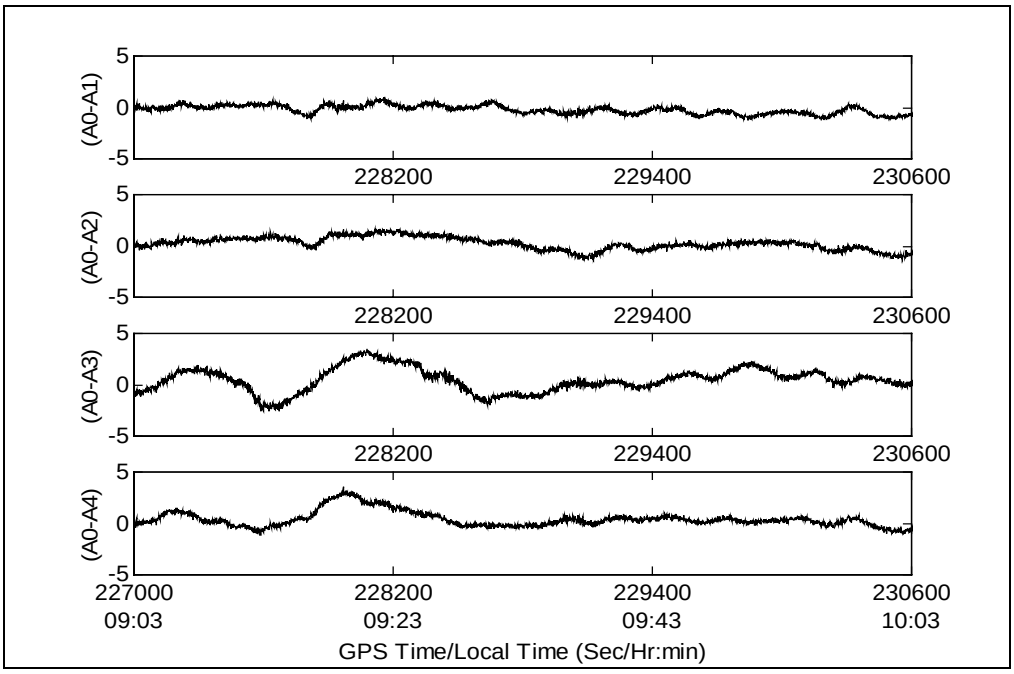

Figure 7.44: Single differenced residual carrier phase error for SV 31 on October 20, 1998 (Y-axis units in cm; A0-A*n* denotes single difference between antennas 0 and *n*)

Figure 7.45 shows the estimated parameters of the composite reflected signal for this satellite as determined by the filter. As expected, the parameters vary with time to track many reflections from the environment. The reflected signal phase changes, which causes positive and negative multipath errors. The reflected signal phase, and thereby the

multipath error at other antennas, were computed from the estimated parameters as described in Chapter 6. Estimated parameters for other satellites had similar characteristics.

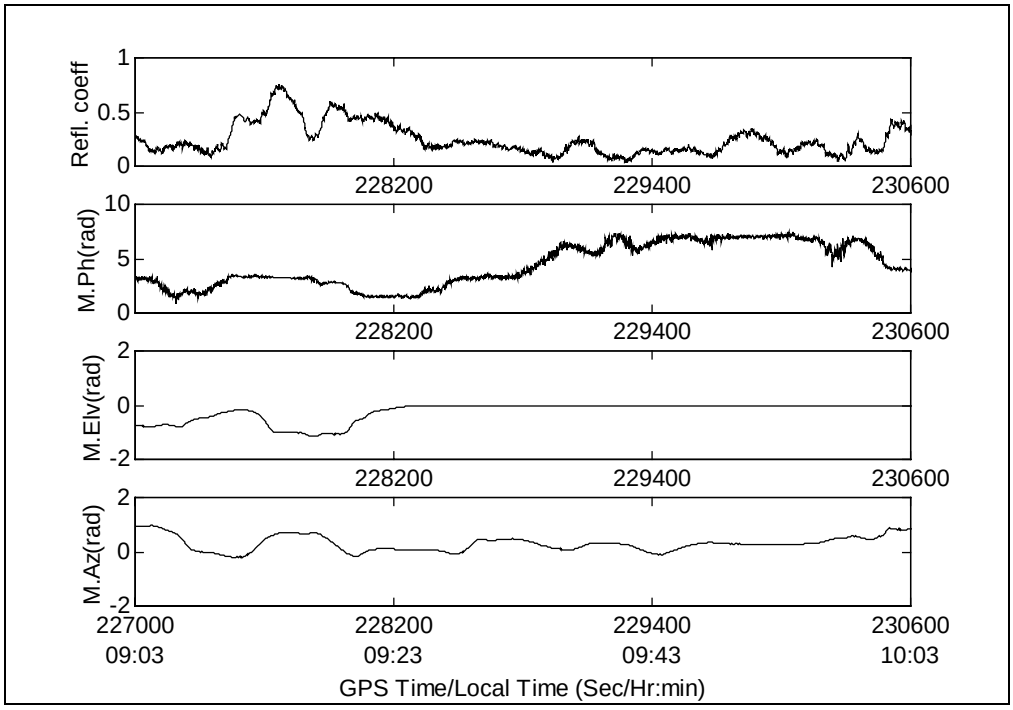

Figure 7.45: Estimated composite reflected signal parameters for SV 31 on October 20

Satellite 23, being the highest elevation (86°-60°) satellite, was used as the base satellite for double differencing. Multipath was also estimated for this satellite at each antenna in the array using the same procedure as for satellite 31. Differences in multipath errors between satellites 23 and 31 in each antenna were computed, and are shown in Figure 7.46 using a dark shaded line (*estimated multipath*). Also, in the same figure, double differenced carrier phase residuals between the user and each antenna in the multi-antenna array are shown using a light shaded line (*measured multipath*). If the multipath in the user antenna was zero, then, ideally, the estimated and measured multipath signals would coincide. In the present case, the user antenna was in an open environment, and should therefore have limited multipath. From the figure, it can be seen that the estimated multipath closely follows the measured multipath.

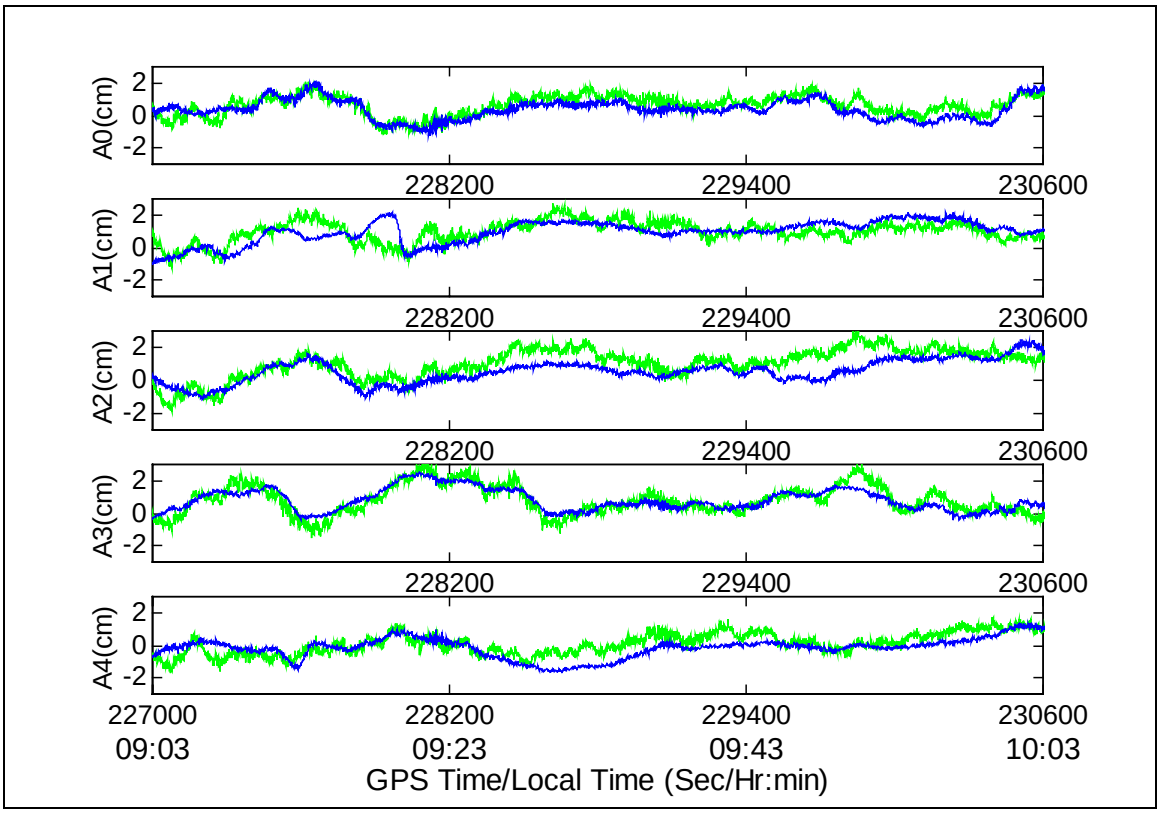

Figure 7.46: Measured multipath (light shade) and estimated multipath (dark shade) for SV 31. (A0…A*n* denote Antenna 0….*n*)

Multipath errors were estimated in other low elevation satellites, and compared with their measured values. Figures 7.47, 7.48 and 7.49 show the estimated and measured multipath for satellites 1, 9 and 17 respectively. In these cases, also, the estimated values closely follow the measured values.

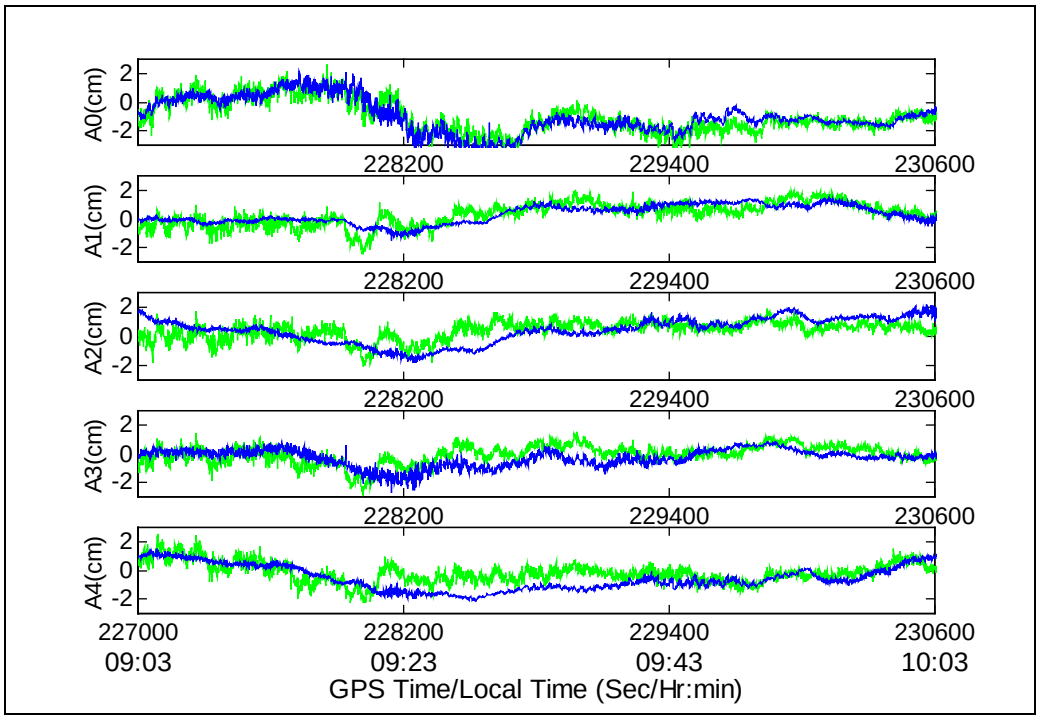

Figure 7.47: Measured multipath (light shade) and estimated multipath (dark shade) for SV 1. (A0…A*n* denote Antenna 0….*n*)

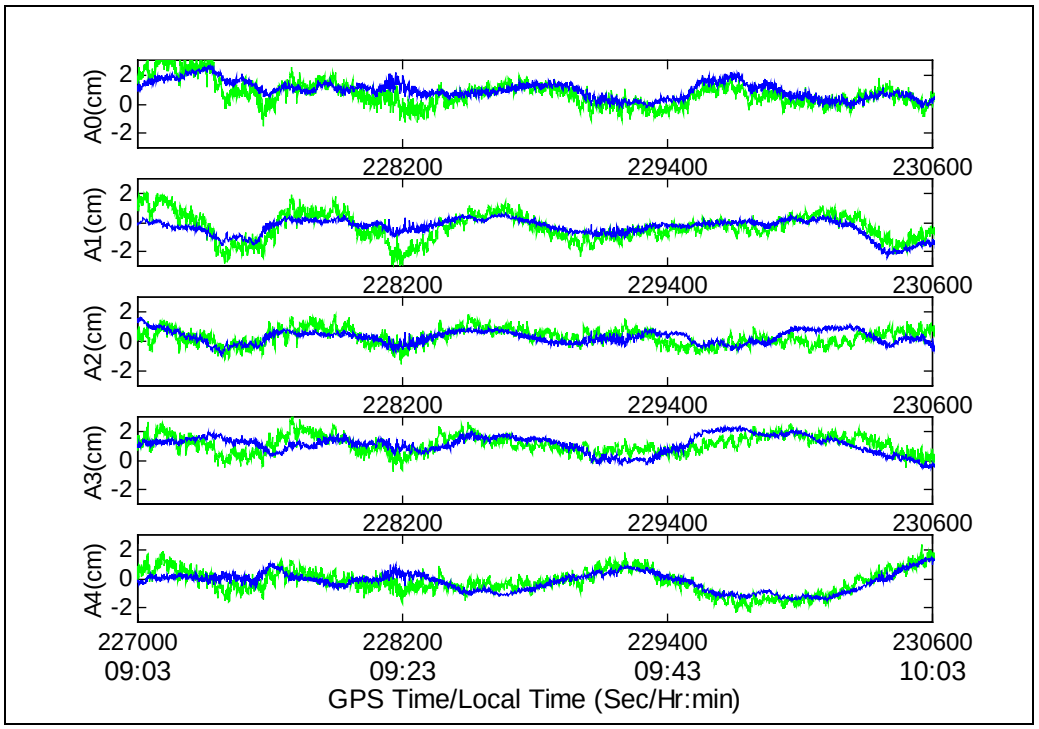

Figure 7.48: Measured multipath (light shade) and estimated multipath (dark shade) for SV 9. (A0…A*n* denote Antenna 0….*n*)

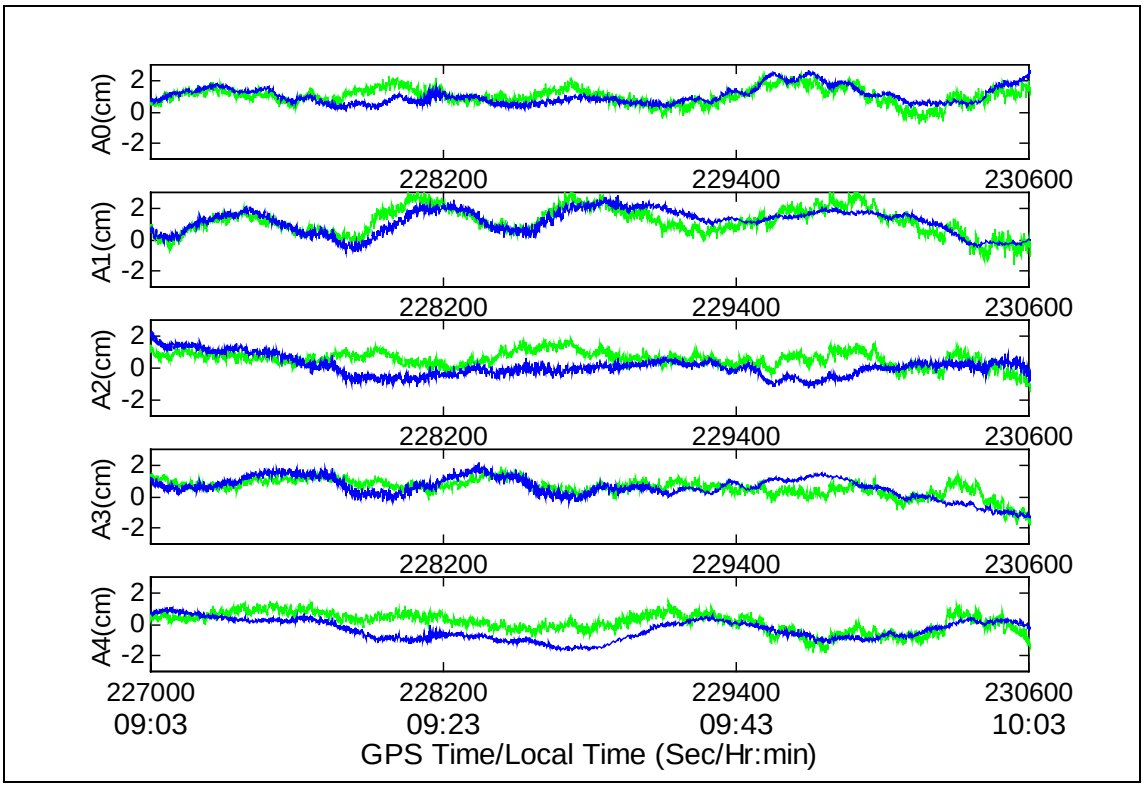

Figure 7.49: Measured multipath (light shade) and estimated multipath (dark shade) for SV 17. (A0…A*n* denote Antenna 0….*n*)

Multipath errors for satellites 1, 9, 17, 23 and 31 in each antenna in the assembly were estimated and removed from the raw data. The double differenced carrier phase measurements between the user and the antennas in the assembly were recomputed using the corrected measurements. Figure 7.50 shows the residuals before and after correction. As is evident from the figure, the corrected residuals have lower oscillations.

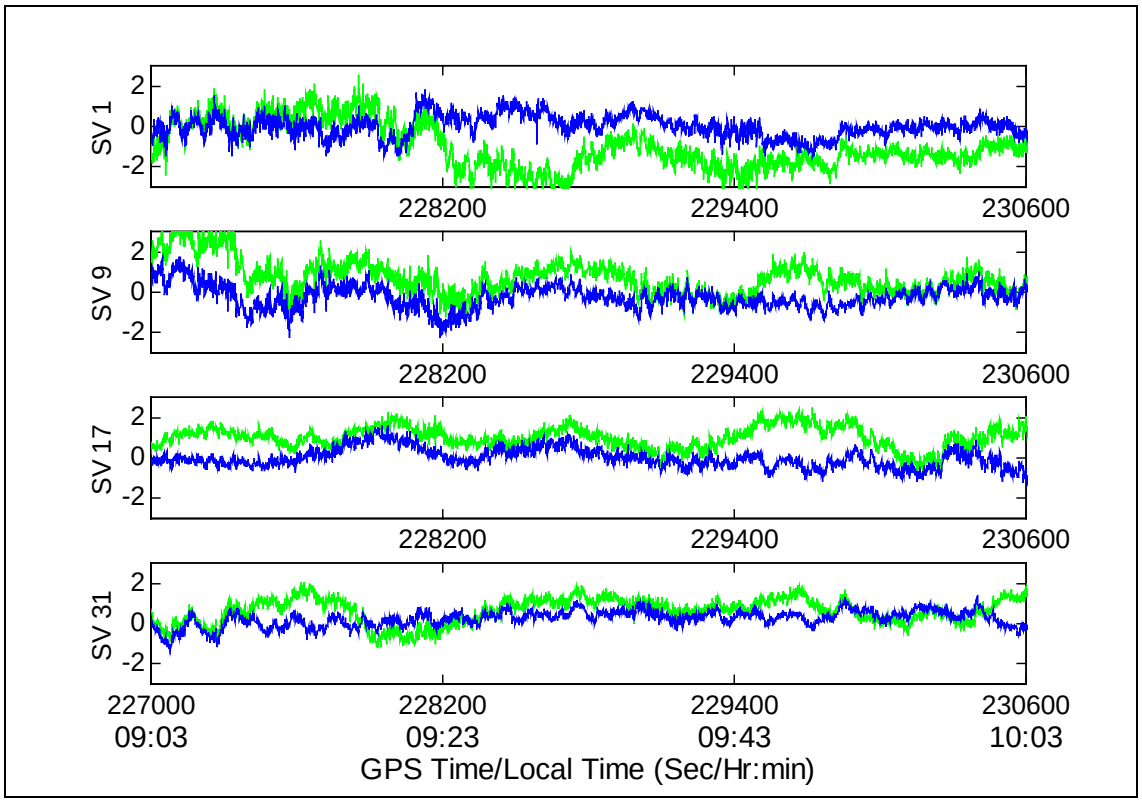

Figure 7.50: Double differenced carrier phase residuals before (light shade) and after (dark shade) correction for Antenna 0. (Y-axis in cm)

Table 7.7 gives the residual statistics before and after multipath correction for the low elevation satellites. There were small mean values in the measured multipath, which may have occurred due to a receiver line bias or an insufficient accuracy estimate in the inter-antenna geometry computation in the antenna array. These were removed from the measured multipath, as carrier phase multipath has a zero mean. Therefore, the statistics are generated for the standard deviation of the errors, rather than their RMS values. The statistics were compiled from a one hour data sample.

It can be observed that this method is quite effective in a high multipath environment; it decreases the RMS values of the residuals up to 52%. An average of 15% improvement of multipath error was observed for all satellites in all antennas. However, when the magnitude of multipath is low, or there is a high frequency component, this method is not

as effective. In some cases, it deteriorates slightly, (e.g. Antennas 2 and 3 for satellite 1 in the table), although the absolute values of the residuals are still quite small (around 0.6 cm).

Table 7.7: Statistics of double differenced carrier phase measurement residuals before and after multipath correction

SV No. (Elevation)	Ant. No.	Before Correction (cm)	After Correction (cm)	Improvement (%)
SV 1 (14°-42°)	A0	1.14	0.55	51.6
	A1	0.80	0.53	33.3
	A2	0.62	0.69	-10.9
	A3	0.65	0.65	-00.6
	A4	0.70	0.70	-00.1
SV 9 (13°-27°)	A0	0.86	0.58	32.9
	A1	0.93	0.71	24.1
	A2	0.54	0.56	-03.6
	A3	0.61	0.65	-05.5
	A4	0.81	0.54	33.2
SV 17 (48°-21°)	A0	0.53	0.47	10.8
	A1	0.86	0.53	38.4
	A2	0.47	0.52	-17.0
	A3	0.53	0.54	-02.1
	A4	0.60	0.61	-01.2
SV 31 (23°-35°)	A0	0.62	0.40	36.4
	A1	0.65	0.65	01.0
	A2	0.89	0.62	29.9
	A3	0.89	0.44	48.2
	A4	0.65	0.56	13.1

It should be noted that in the table the user antenna is assumed to have no multipath, which is realistically impossible. Therefore, the actual improvement using this technique is likely to be higher than the reported values. This is one of the reasons for the percentage of improvement to be lower than the corresponding percentage of improvement for the code multipath as shown in Table 7.2. Another cause for the reduction in the percentage of improvement is that in this case, the carrier phase noise grows (due to double differencing) which eclipses the degree of the performance improvement using this technique.

7.6.2 Analysis of results in position domain

The proposed multipath mitigation technique estimates multipath error in the phase measurements. The multipath-reduced measurements, when used by the user, should then improve the differential position accuracy of the user antenna. Therefore, it is important to analyze the user position accuracy before and after multipath correction at the reference antenna assembly.

Procedure

A baseline test was carried out to analyze the impact in the user position accuracy when using corrected carrier phase measurements from the multi-antenna system. The estimated multipath errors for each satellite in each antenna in the antenna assembly were removed from the phase measurements. The position of the user was then computed in differential mode, first with the uncorrected carrier phase measurements from the reference station, and later using the multipath-corrected measurements from the reference station. Ambiguities were fixed to their integer values and independent positions were generated at 1 Hz (i.e. in 'kinematic mode') A few satellites, which were not available for the entire duration of the experiment, were not used in this analysis. The University of Calgary's Semikin^{TM} software (Cannon, 1993) was used to compute the differential position. A comparison between the position errors with and without corrections indicated the achievable improvement in the user position using such a system. Figure 7.51 shows a flowchart of this procedure.

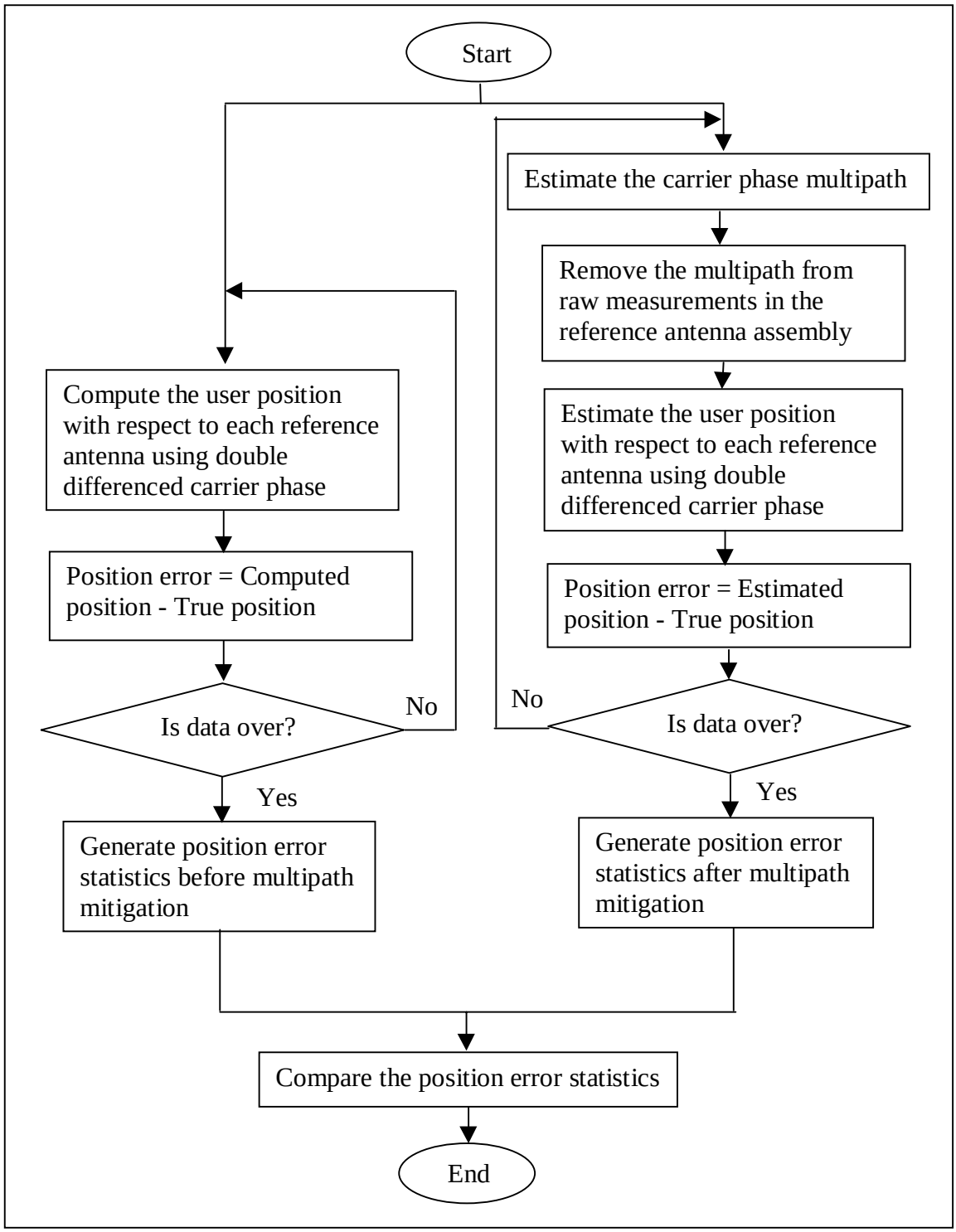

Figure 7.51: Flowchart of evaluating the performance of the carrier phase multipath mitigation algorithm in the position domain

Analysis of Results

The user position was computed using double differenced carrier phase measurements. The position error time series before multipath correction is shown in Figure 7.52 using a shaded light line. Positions were then recomputed using corrected measurements, and the corresponding errors are shown in the same figure using a dark line. It can be observed that the position errors using corrected measurements have smaller magnitudes.

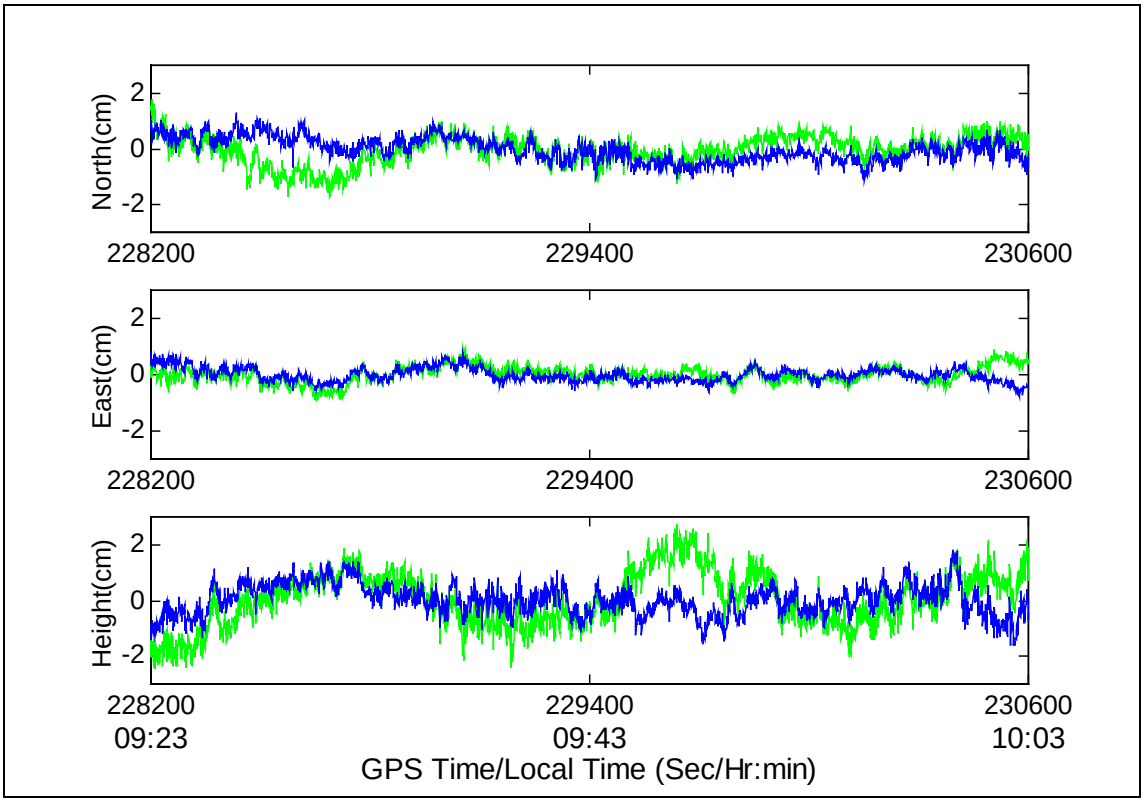

Figure 7.52: Position error in Antenna 0 before (light shade) and after (dark shade) multipath correction of carrier phase measurements

This analysis was repeated using each antenna in the multi-antenna system as the reference (monitor), and the statistics are shown in Table 7.8.

Table 7.8: User position error for ambiguity-fixed carrier before and after multipath correction

Antenna No.		Before Correction (cm)	After Correction (cm)	Improvement (%)	3D Improvement (%)
A0	Lat	0.60	0.45	25.0	36.1
	Lon	0.29	0.25	13.8	
	Hgt	1.00	0.57	43.0	
A1	Lat	0.54	0.40	25.9	34.8
	Lon	0.31	0.42	-35.5	
	Hgt	1.13	0.61	46.0	
A2	Lat	0.43	0.53	-23.3	-03.1
	Lon	0.40	0.38	05.0	
	Hgt	0.82	0.81	01.2	
A3	Lat	0.47	0.49	-04.2	12.7
	Lon	0.34	0.29	14.7	
	Hgt	1.04	0.87	16.3	
A4	Lat	0.39	0.48	-23.1	37.4
	Lon	0.31	0.25	19.3	
	Hgt	1.31	0.69	47.3	

Using this technique, up to a 37% improvement in 3D position was obtained without removing the effect of phase noise. The average improvement over five antennas was around 24%. Antenna 2 showed a slight negative improvement as the residuals slightly deteriorated in this case (although the absolute error is quite small). Overall, an improvement in position accuracy is observed using this technique.

There are several reasons for the position improvement percentage to be smaller compared to the residual improvement percentage. They are; a) the position is computed

from all the available measurements and the percentage of improvement in all the measurements were not of the same degree, and b) the amount of noise in the double differenced carrier phase is quite high, which reduced the percentage of improvement in position accuracy. If the carrier phase noise is removed from the residuals and the statistics of the multipath error before and after multipath mitigation are computed, the percentage of improvement is likely to be much higher.

From Tables 7.2 to 7.7 it can be seen that the proposed technique is quite effective in removing code and carrier multipath effects. This was verified in the measurement domain as well as in the position domain. It can also be seen that the higher the multipath in the antenna, the better the multipath reduction and the higher the position accuracy improvement. This is a desirable quality, as a low elevation satellite causes high multipath error, and is a major problem in achieving high differential position accuracy. The proposed multipath mitigation technique is more suitable under such circumstances.

CHAPTER 8

CONCLUSIONS AND RECOMMENDATIONS

8.1 Introduction

The research has two major components: In the first part of the research, GPS receiver code and carrier tracking loop discriminator function responses were analyzed in the presence of multipath signals. The characteristics of multipath errors were shown in terms of the mean, standard deviation, pattern and overall envelope through simulations for various types of discriminator functions. The influences of the antenna-satellite and antenna-reflector geometry on multipath frequency were analyzed by forming relationships among them. The spatial correlation property of multipath within a small area was investigated in detail through analysis and simulations.

The second part of the research consisted of developing an algorithm to mitigate code and carrier multipath errors using a multi-antenna system. An Extended Kalman Filter was derived and implemented, which uses the single differenced code, carrier or the ratios of SNR measurements between two closely-spaced antennas and estimate various multipath and geometric parameters. It is then possible to estimate the code and the carrier multipath errors from those parameters. The algorithm was first tested using simulated multipath errors. After successful mitigation of the simulated multipath, the algorithm was applied on field data. A multi-antenna array consisting of six closely-spaced antennas was developed to test the multipath mitigation algorithm. NovAtel Beeline^{TM} receivers were used for data collection. Experiments were carried out on the roof of the Engineering building at the University of Calgary. The multipath mitigation algorithm was used on the data and the technique was found to be effective in mitigating code and carrier multipath errors in static receivers.

8.2 Conclusions

The following conclusions can be drawn from the findings of the research:

1. Code multipath error characteristics were extensively studied by analyzing various code discriminator functions in a receiver in the presence of multiapth signal. They were also verified using numerous simulations and found to be consistent with the finding of various other researchers. Some of the confirmed results are:

    a) The multipath error envelope is a function of, i) the reflection coefficient, ii) correlator spacing, and iii) chip width.
    b) The theoretical absolute maximum values of multipath error is equal to half the correlator spacing.
    c) Short delay ($\tau_1 \leq 15$ m) multipath causes almost the same amount of errors for correlators with any spacing between 0.1 and 1 chip.
    d) Multipath signals with delays higher than the theoretical limit (450 m for 1 chip spacing and 315 m for 0.1 chip spacing for C/A code) can also introduce multipath errors. This is because of, a) the trailing-off response of the discriminator due to the bandwidth limitation, and b) non-zero correlation values of C/A code for misalignment higher than 1 chip. Bandwidth limitation for small correlator spacing can cause multipath errors higher than the theoretical limit.
    e) Multipath error has a non-zero mean value for both coherent and non-coherent types of discriminator which can reach up to several tens of metres for correlators with 1 chip spacing and up to several metres for correlators with 0.1 chip spacing for strong multipath signals.

2. Carrier phase multipath error characteristics were also studied and verified using theory and numerous simulations. Some of the confirmed results are:

a) The multipath error envelope is a function of, i) the reflection coefficient, ii) correlator spacing, and iii) carrier wavelength.
b) The multipath phases at which the multipath errors reach the maximum and minimum values depend upon the reflection coefficient.
c) The theoretical absolute maximum multipath error is one-forth the carrier wavelength.
d) Multipath errors are largely unaffected by the type of discriminator used for the code tracking (i.e., coherent vs. non-coherent).
e) The multipath error amplitude (in radians) is the same for GPS L1 and L2 carriers. But the multipath error in the L2 carrier has higher amplitude than that of the L1 carrier when expressed in units of distance (metres, for example).
f) The L1 carrier has higher frequency multipath compared to L2, such that, they look random at a particular instant, but have a definite phase relationship when observed over a time span.

3. Multipath errors on code, carrier and SNR have synergistic relationships as they all can be expressed by a set of parameters, namely, the reflection coefficient, multipath delay (or correlation ratio) and multipath phase. If those parameters are known accurately, it is then possible to compute all these errors. These relationships also allow the combination of code, carrier and SNR measurements to estimate multipath parameters and thereby multipath errors in the code and carrier.

4. Multipath error is influenced by antenna-satellite and antenna-reflector geometry. Assuming that the multipath phase is only due to the differential path delay, the multipath error frequency for a stationary antenna-reflector combination is directly proportional to the distance between the antenna and the reflector, the rate of change of satellite elevation and azimuth, and is inversely proportional to the signal wavelength. A close-by reflector generally causes low frequency multipath, while a far away reflector causes high frequency multipath. It is also a function of the antenna-reflector, and line-of-sight, vectors.

5. In a receiver, code multipath errors generally have more high frequency components than carrier multipath errors, especially if a wide-spacing correlator is used for code tracking. This is because, for the code multipath error, far away reflectors produce higher amplitude multipath errors for a wide spacing correlator and almost the same amplitude multipath errors for a narrow spacing correlator, (see the code multipath error envelope). Whereas, for the carrier multipath error, far away reflectors produce low amplitude multipath errors (see the carrier multipath error envelope). As the far away reflectors produce high frequency multipath errors and code multipath has dominant components due to far away reflectors, the code multipath error is likely to have stronger high frequency error components compared to the carrier multipath. As a result, the correlation time of the code multipath error is smaller than that of the carrier multipath error.

6. Single difference code and carrier multiapth errors between two closely-spaced antennas can be expressed in terms of multipath parameters. Assuming the reflection coefficient and the correlation ratio (or multipath delay) to be the same for both the antennas, the multipath phase would be different in those antennas. The multipath phase in one antenna can be expressed in terms of multipath phase in another antenna (unknown), the direction of the reflected signal (unknown) and the geometry between the antennas (known). That way, the multipath phase in antennas configured in a cluster can be expressed in terms of only three unknowns, namely, the multipath phase in one of the antennas, as well as the elevation and the azimuth of the reflected signal.

7. Code multipath error was isolated using the code minus carrier technique and compensated for the ionospheric delay using a second order polynomial curve-fitting. The error in a moderate multipath environment was found to have amplitudes up to 4 metres and a correlation time of 2-3 minutes. It was found to have a day-to-day repeatability of 70%-90% for various satellites.

8. A multipath mitigation technique was developed which uses measurements from multiple antennas in close proximity. The technique was used to mitigate code multipath error using field data collected in a moderate multipath environment. The multipath mitigation technique removed the code multipath error up to 73% (average 22%) in the measurement domain. The improvement may not be significant when the multiapth error is quite small in the measurements. Generally, the higher the multipath error, the larger the improvement.

9. The differential code position accuracy was improved by up to 51% (average 21%) when multipath-mitigated measurements were used instead of uncorrected measurements with non-smoothed code. The corresponding improvement for differential positioning using carrier-smoothed code was found to be 52% (average 23%). The position accuracy improvement percentage was smaller than the measurement residual improvement percentage due to two reasons: a) the multipath errors in measurements in the user antenna was not mitigated, though used for position computation, and b) the position was computed from all the available measurements and the percentage of improvement in all the measurements were not of the same degree.

10. Carrier phase multipath error could not be isolated and was observed through the double differenced carrier phase residuals between the reference and the user antennas (with the user position fixed to its truth value), and two satellites. The error in a moderate multipath environment was found to have amplitudes up to 3 cm and a correlation time of 5-6 minutes. The carrier multipath error was found to have a repeatability of about 70%.

11. A technique was developed to mitigate carrier phase multipath error using multiple closely-spaced antennas. Tests were carried out with field data collected in a moderate multipath environment. The multipath mitigation technique on average

reduces the single differenced residuals (between antennas) by about 73%. Furthermore, it removes the multipath error up to 52% (average 15%) in the double differenced carrier phase residuals. The improvement may not be significant when the multipath error is quite small in the measurements. Generally, the higher the multipath error, the larger the improvement. One reason for the multipath error reduction percentage in the double differenced residuals being smaller than the corresponding values for code is that, here, the multipath errors in measurements in the user antenna were not removed, but used in the calculations (i.e. in the double differenced carrier phase residuals).

12. The differential carrier phase position accuracy was improved by up to 37% (average 24%) when multipath-mitigated measurements were used instead of un-corrected measurements. The position improvement percentage is smaller compared to the measurement- improvement percentage as the position was computed from all the available measurements and the percentage of improvement in all the measurements were not of the same degree. Furthermore, if the effect of carrier phase noise is isolated and removed, the percentage of improvement would be higher.

13. The proposed technique works well in a multi-reflector environment, estimating the code and carrier multiapth errors using the code, carrier and SNR measurements, as shown through simulations. However, with field data, the technique was used to estimate code multipath from code measurements and carrier multipath from carrier measurements. Code and carrier measurements could not be combined, as the code multipath model is only for the short delay multipath, whereas the carrier multipath model is for both the short and long delay multipath. Furthermore, the SNR measurements could not be incorporated, as the antenna gain pattern variations, which directly affect the SNR, could not be compensated. The technique was evaluated using field data for GPS C/A code and L1 carrier. This, however, is a generic technique and is valid for any other direct sequence spread spectrum communication receivers employing PRN codes for signal spreading.

8.3 Recommendations

1. One of the major limitations of the test setup was non-uniformity of the antenna gain pattern. If an integrated antenna assembly consisting of multiple antenna elements, preferably on the same substrate, can be built, the antenna gain pattern of each element in the assembly will be identical and uniform in all directions. It will then be possible to use the SNR information in the mitigation filter. Furthermore, that will make true the assumption that the reflection coefficient is the same at each antenna in the multi-antenna assembly and is likely to improve the effectiveness of this technique significantly. Furthermore, in that case the antenna elements can be placed closer to each other, causing higher correlation of the multipath errors. That however increases the antenna coupling and likely to deform the antenna gain patterns.

2. Even in a multi-antenna system, such as the one used in this research, the antenna gain patterns can be calibrated in an anachoic chamber and used to compensate measured data. The effectiveness of this calibration and compensation method bears some doubts, as the gain compensation on the reflected signal coming from various directions would be a problem. But, if an integrated antenna assembly is not available, this is probably the only way to compensate for the antenna gain pattern variation and non-uniformity, to improve the performance using this technique.

3. The SNR information from the receiver could not be used as the SNR levels in different receivers were found to be different and varying with time, even after the effects of multipath were removed from the SNR measurements. This problem may be solved once the antenna gain pattern non-uniformity is corrected. Incorporation of SNR information in the estimation process is likely to improve the performance of the technique, and therefore recommended for further investigation.

4. The code multipath error equation was formulated only for the short delay multipath, as long delay multipath errors can be mitigated using existing correlator based

techniques. Multipath error formulation and mitigation of long delay multipath is a logical extension of this technique and needs further research.

5. The current technique does not use L2 measurements for multipath error estimation. This was not an issue, as the receivers used in the reference antenna array did not have L2 tracking capability. It is possible to incorporate L2 measurements in the estimation filter as well. In that case, however, L1 and L2 measurements would be correlated. As a result, even though the number of measurements would be doubled, the benefit would not be increased by the same proportion. Further experiments may be carried out with receivers having L1-L2 capabilities in a multi-antenna system, and use L2 measurements along with L1 measurements to improve the estimation accuracy.

6. The mitigation algorithm assumes that the antennas in the antenna assembly are placed on a local horizontal surface. This might have limitations in terms of sensitivities under certain antenna-reflector geometry. This method may be further extended for an antenna assembly, which has antennas on a vertical plane as well.

7. The current algorithm is quite sensitive to the chosen values of the process noise for the state dynamic models. The situation may be improved by redundant measurements. This is an important area that needs further investigations.

8. Reliability algorithms to reject bad measurements or outliers should be incorporated. The algorithm currently uses stored measurement data to estimate multipath errors in a sequential post-mission processing mode. However, the algorithm is not restricted to batch processing and there is no inherent latency required. Therefore, this method has potential to be used in real time. Experiments should be carried out in real time multipath error estimation in various applications, such as use of two such multi-antenna systems for spacecraft attitude determination.

9. Finally, the system can be tested in various multipath environments, to have a more elaborate performance evaluation. It can further be extended to GLONASS or other similar types of spread spectrum systems.

APPENDIX A

DOT-PRODUCT DISCRIMINATOR FUNCTION RESPONSE IN THE PRESENCE OF A MULTIPATH SIGNAL

A.1 Single Reflector Case

The dot-product discriminator function in the presence of a multipath signal is given by Equation 5.7b:

$$\begin{aligned} D_{nm} = & \sum_{i=0}^{1} \alpha_i R(\hat{\tau}_c - \tau_i)\cos(\gamma_i - \hat{\gamma}_c)\left\{\begin{array}{l} \sum_{i=0}^{1} \alpha_i R(\hat{\tau}_c - \tau_i + T_d)\cos(\gamma_i - \hat{\gamma}_c) \\ -\sum_{i=0}^{1} \alpha_i R(\hat{\tau}_c - \tau_i - T_d)\cos(\gamma_i - \hat{\gamma}_c) \end{array}\right\} \\ & + \sum_{i=0}^{1} \alpha_i R(\hat{\tau}_c - \tau_i)\sin(\gamma_i - \hat{\gamma}_c)\left\{\begin{array}{l} \sum_{i=0}^{1} \alpha_i R(\hat{\tau}_c - \tau_i + T_d)\sin(\gamma_i - \hat{\gamma}_c) \\ -\sum_{i=0}^{1} \alpha_i R(\hat{\tau}_c - \tau_i - T_d)\sin(\gamma_i - \hat{\gamma}_c) \end{array}\right\} \end{aligned} \tag{A.1}$$

Expanding Equation A.1 gives:

$$\begin{aligned} D_{nm} = & \left\{R(\hat{\tau}_c - \tau_0)\cos(\gamma_0 - \hat{\gamma}_c) + \alpha_1 R(\hat{\tau}_c - \tau_1)\cos(\gamma_1 - \hat{\gamma}_c)\right\} \\ & \left\{\begin{array}{l} \left\{R(\hat{\tau}_c - \tau_0 + T_d) - R(\hat{\tau}_c - \tau_0 - T_d)\right\}\cos(\gamma_0 - \hat{\gamma}_c) \\ +\alpha_1\left\{R(\hat{\tau}_c - \tau_1 + T_d) - R(\hat{\tau}_c - \tau_1 - T_d)\right\}\cos(\gamma_1 - \hat{\gamma}_c) \end{array}\right\} + \\ & \left\{R(\hat{\tau}_c - \tau_0)\sin(\gamma_0 - \hat{\gamma}_c) + \alpha_1 R(\hat{\tau}_c - \tau_1)\sin(\gamma_1 - \hat{\gamma}_c)\right\} \\ & \left\{\begin{array}{l} \left\{R(\hat{\tau}_c - \tau_0 + T_d) - R(\hat{\tau}_c - \tau_0 - T_d)\right\}\sin(\gamma_0 - \hat{\gamma}_c) \\ +\alpha_1\left\{R(\hat{\tau}_c - \tau_1 + T_d) - R(\hat{\tau}_c - \tau_1 - T_d)\right\}\sin(\gamma_1 - \hat{\gamma}_c) \end{array}\right\} \end{aligned} \tag{A.2}$$

If Equation A.2 is equated to zero, and $\tau_0 = 0$, then the resultant value of $\hat{\tau}_c$ is the multipath error. Now further expanding Equation A.2:

$$\begin{aligned} D_{nm} = {} & R(\hat{\tau}_c - \tau_0)\{R(\hat{\tau}_c - \tau_0 + T_d) - R(\hat{\tau}_c - \tau_0 - T_d)\}\cos^2(\gamma_0 - \hat{\gamma}_c) + \\ & \alpha_1^2 R(\hat{\tau}_c - \tau_1)\{R(\hat{\tau}_c - \tau_1 + T_d) - R(\hat{\tau}_c - \tau_1 - T_d)\}\cos^2(\gamma_1 - \hat{\gamma}_c) + \\ & \alpha_1 R(\hat{\tau}_c - \tau_0)\{R(\hat{\tau}_c - \tau_1 + T_d) - R(\hat{\tau}_c - \tau_1 - T_d)\}\cos(\gamma_0 - \hat{\gamma}_c)\cos(\gamma_1 - \hat{\gamma}_c) + \\ & \alpha_1 (\hat{\tau}_c - \tau_1)\{R(\hat{\tau}_c - \tau_0 + T_d) - R(\hat{\tau}_c - \tau_0 - T_d)\}\cos(\gamma_0 - \hat{\gamma}_c)\cos(\gamma_1 - \hat{\gamma}_c) + \\ & R(\hat{\tau}_c - \tau_0)\{R(\hat{\tau}_c - \tau_0 + T_d) - R(\hat{\tau}_c - \tau_0 - T_d)\}\sin^2(\gamma_0 - \hat{\gamma}_c) + \\ & \alpha_1^2 R(\hat{\tau}_c - \tau_1)\{R(\hat{\tau}_c - \tau_1 + T_d) - R(\hat{\tau}_c - \tau_1 - T_d)\}\sin^2(\gamma_1 - \hat{\gamma}_c) + \\ & \alpha_1 R(\hat{\tau}_c - \tau_0)\{R(\hat{\tau}_c - \tau_1 + T_d) - R(\hat{\tau}_c - \tau_1 - T_d)\}\sin(\gamma_0 - \hat{\gamma}_c)\sin(\gamma_1 - \hat{\gamma}_c) + \\ & \alpha_1 (\hat{\tau}_c - \tau_1)\{R(\hat{\tau}_c - \tau_0 + T_d) - R(\hat{\tau}_c - \tau_0 - T_d)\}\sin(\gamma_0 - \hat{\gamma}_c)\sin(\gamma_1 - \hat{\gamma}_c) \end{aligned} \tag{A.3}$$

$$\begin{aligned} D_{nm} = {} & R(\hat{\tau}_c - \tau_0)\{R(\hat{\tau}_c - \tau_0 + T_d) - R(\hat{\tau}_c - \tau_0 - T_d)\} + \\ & \alpha_1^2 R(\hat{\tau}_c - \tau_1)\{R(\hat{\tau}_c - \tau_1 + T_d) - R(\hat{\tau}_c - \tau_1 - T_d)\} + \\ & \alpha_1 \begin{Bmatrix} R(\hat{\tau}_c - \tau_0)\{R(\hat{\tau}_c - \tau_1 + T_d) - R(\hat{\tau}_c - \tau_1 - T_d)\} + \\ R(\hat{\tau}_c - \tau_1)\{R(\hat{\tau}_c - \tau_0 + T_d) - R(\hat{\tau}_c - \tau_0 - T_d)\} \end{Bmatrix} \cos(\gamma_0 - \gamma_1) \end{aligned} \tag{A.4}$$

This is the expression given in Equation 5.7c.

A.2 Multiple Reflectors Case

In the multi-reflector case, the upper limit of the summation in Equation A.1 will be equal to the number of reflectors in the environment. Assuming three reflectors in the environment, Equation A.1 may be expanded to give the following expression:

$$
\begin{aligned}
D_{nm} = &\left\{\begin{matrix} R(\hat{\tau}_c-\tau_0)\cos(\gamma_0-\hat{\gamma}_c)+\alpha_1 R(\hat{\tau}_c-\tau_1)\cos(\gamma_1-\hat{\gamma}_c) \\ +\alpha_2 R(\hat{\tau}_c-\tau_2)\cos(\gamma_2-\hat{\gamma}_c)+\alpha_3 R(\hat{\tau}_c-\tau_3)\cos(\gamma_3-\hat{\gamma}_c)\end{matrix}\right\} \\
&\left\{\begin{matrix} \{R(\hat{\tau}_c-\tau_0+T_d)-R(\hat{\tau}_c-\tau_0-T_d)\}\cos(\gamma_0-\hat{\gamma}_c) \\ +\alpha_1\{R(\hat{\tau}_c-\tau_1+T_d)-R(\hat{\tau}_c-\tau_1-T_d)\}\cos(\gamma_1-\hat{\gamma}_c) \\ +\alpha_2\{R(\hat{\tau}_c-\tau_2+T_d)-R(\hat{\tau}_c-\tau_2-T_d)\}\cos(\gamma_2-\hat{\gamma}_c) \\ +\alpha_3\{R(\hat{\tau}_c-\tau_3+T_d)-R(\hat{\tau}_c-\tau_3-T_d)\}\cos(\gamma_3-\hat{\gamma}_c)\end{matrix}\right\}+ \\
&\left\{\begin{matrix} R(\hat{\tau}_c-\tau_0)\sin(\gamma_0-\hat{\gamma}_c)+\alpha_1 R(\hat{\tau}_c-\tau_1)\sin(\gamma_1-\hat{\gamma}_c) \\ +\alpha_2 R(\hat{\tau}_c-\tau_2)\sin(\gamma_2-\hat{\gamma}_c)+\alpha_3 R(\hat{\tau}_c-\tau_3)\sin(\gamma_3-\hat{\gamma}_c)\end{matrix}\right\} \\
&\left\{\begin{matrix} \{R(\hat{\tau}_c-\tau_0+T_d)-R(\hat{\tau}_c-\tau_0-T_d)\}\sin(\gamma_0-\hat{\gamma}_c) \\ +\alpha_1\{R(\hat{\tau}_c-\tau_1+T_d)-R(\hat{\tau}_c-\tau_1-T_d)\}\sin(\gamma_1-\hat{\gamma}_c) \\ +\alpha_2\{R(\hat{\tau}_c-\tau_2+T_d)-R(\hat{\tau}_c-\tau_2-T_d)\}\sin(\gamma_2-\hat{\gamma}_c) \\ +\alpha_3\{R(\hat{\tau}_c-\tau_3+T_d)-R(\hat{\tau}_c-\tau_3-T_d)\}\sin(\gamma_3-\hat{\gamma}_c)\end{matrix}\right\}
\end{aligned}
\qquad \text{(A.5)}
$$

If Equation A.5 is equated to zero, and $\tau_0 = 0$, then the resultant value of $\hat{\tau}_c$ is the multipath error. Now further expanding Equation A.5:

$$
\begin{aligned}
D_{nm} = {} & R(\hat{\tau}_c-\tau_0)\{R(\hat{\tau}_c-\tau_0+T_d)-R(\hat{\tau}_c-\tau_0-T_d)\}\cos^2(\gamma_0-\hat{\gamma}_c)+ \\
& \alpha_1^2 R(\hat{\tau}_c-\tau_1)\{R(\hat{\tau}_c-\tau_1+T_d)-R(\hat{\tau}_c-\tau_1-T_d)\}\cos^2(\gamma_1-\hat{\gamma}_c)+ \\
& \alpha_2^2 R(\hat{\tau}_c-\tau_2)\{R(\hat{\tau}_c-\tau_2+T_d)-R(\hat{\tau}_c-\tau_2-T_d)\}\cos^2(\gamma_2-\hat{\gamma}_c)+ \\
& \alpha_3^2 R(\hat{\tau}_c-\tau_3)\{R(\hat{\tau}_c-\tau_3+T_d)-R(\hat{\tau}_c-\tau_3-T_d)\}\cos^2(\gamma_3-\hat{\gamma}_c)+ \\
& \alpha_1 R(\hat{\tau}_c-\tau_0)\{R(\hat{\tau}_c-\tau_1+T_d)-R(\hat{\tau}_c-\tau_1-T_d)\}\cos(\gamma_0-\hat{\gamma}_c)\cos(\gamma_1-\hat{\gamma}_c)+ \\
& \alpha_2 R(\hat{\tau}_c-\tau_0)\{R(\hat{\tau}_c-\tau_2+T_d)-R(\hat{\tau}_c-\tau_2-T_d)\}\cos(\gamma_0-\hat{\gamma}_c)\cos(\gamma_2-\hat{\gamma}_c)+ \\
& \alpha_3 R(\hat{\tau}_c-\tau_0)\{R(\hat{\tau}_c-\tau_3+T_d)-R(\hat{\tau}_c-\tau_3-T_d)\}\cos(\gamma_0-\hat{\gamma}_c)\cos(\gamma_3-\hat{\gamma}_c)+ \\
& \alpha_1 R(\hat{\tau}_c-\tau_1)\{R(\hat{\tau}_c-\tau_0+T_d)-R(\hat{\tau}_c-\tau_0-T_d)\}\cos(\gamma_0-\hat{\gamma}_c)\cos(\gamma_1-\hat{\gamma}_c)+ \\
& \alpha_2 R(\hat{\tau}_c-\tau_2)\{R(\hat{\tau}_c-\tau_0+T_d)-R(\hat{\tau}_c-\tau_0-T_d)\}\cos(\gamma_0-\hat{\gamma}_c)\cos(\gamma_2-\hat{\gamma}_c)+ \\
& \alpha_3 R(\hat{\tau}_c-\tau_3)\{R(\hat{\tau}_c-\tau_0+T_d)-R(\hat{\tau}_c-\tau_0-T_d)\}\cos(\gamma_0-\hat{\gamma}_c)\cos(\gamma_3-\hat{\gamma}_c)+ \\
& \alpha_1\alpha_2 R(\hat{\tau}_c-\tau_1)\{R(\hat{\tau}_c-\tau_2+T_d)-R(\hat{\tau}_c-\tau_2-T_d)\}\cos(\gamma_1-\hat{\gamma}_c)\cos(\gamma_2-\hat{\gamma}_c)+ \\
& \alpha_1\alpha_3 R(\hat{\tau}_c-\tau_1)\{R(\hat{\tau}_c-\tau_3+T_d)-R(\hat{\tau}_c-\tau_3-T_d)\}\cos(\gamma_1-\hat{\gamma}_c)\cos(\gamma_3-\hat{\gamma}_c)+ \\
& \alpha_1\alpha_2 R(\hat{\tau}_c-\tau_2)\{R(\hat{\tau}_c-\tau_1+T_d)-R(\hat{\tau}_c-\tau_1-T_d)\}\cos(\gamma_1-\hat{\gamma}_c)\cos(\gamma_2-\hat{\gamma}_c)+ \\
& \alpha_1\alpha_3 R(\hat{\tau}_c-\tau_3)\{R(\hat{\tau}_c-\tau_1+T_d)-R(\hat{\tau}_c-\tau_1-T_d)\}\cos(\gamma_1-\hat{\gamma}_c)\cos(\gamma_3-\hat{\gamma}_c)+ \\
& \alpha_2\alpha_3 R(\hat{\tau}_c-\tau_2)\{R(\hat{\tau}_c-\tau_3+T_d)-R(\hat{\tau}_c-\tau_3-T_d)\}\cos(\gamma_2-\hat{\gamma}_c)\cos(\gamma_3-\hat{\gamma}_c)+ \\
& \alpha_2\alpha_3 R(\hat{\tau}_c-\tau_3)\{R(\hat{\tau}_c-\tau_2+T_d)-R(\hat{\tau}_c-\tau_2-T_d)\}\cos(\gamma_2-\hat{\gamma}_c)\cos(\gamma_3-\hat{\gamma}_c)+
\end{aligned}
$$

$$
\begin{aligned}
&R(\hat{\tau}_c-\tau_0)\{R(\hat{\tau}_c-\tau_0+T_d)-R(\hat{\tau}_c-\tau_0-T_d)\}\sin^2(\gamma_0-\hat{\gamma}_c)+\\
&\alpha_1^2R(\hat{\tau}_c-\tau_1)\{R(\hat{\tau}_c-\tau_1+T_d)-R(\hat{\tau}_c-\tau_1-T_d)\}\sin^2(\gamma_1-\hat{\gamma}_c)+\\
&\alpha_2^2R(\hat{\tau}_c-\tau_2)\{R(\hat{\tau}_c-\tau_2+T_d)-R(\hat{\tau}_c-\tau_2-T_d)\}\sin^2(\gamma_2-\hat{\gamma}_c)+\\
&\alpha_3^2R(\hat{\tau}_c-\tau_3)\{R(\hat{\tau}_c-\tau_3+T_d)-R(\hat{\tau}_c-\tau_3-T_d)\}\sin^2(\gamma_3-\hat{\gamma}_c)+\\
&\alpha_1R(\hat{\tau}_c-\tau_0)\{R(\hat{\tau}_c-\tau_1+T_d)-R(\hat{\tau}_c-\tau_1-T_d)\}\sin(\gamma_0-\hat{\gamma}_c)\sin(\gamma_1-\hat{\gamma}_c)+\\
&\alpha_2R(\hat{\tau}_c-\tau_0)\{R(\hat{\tau}_c-\tau_2+T_d)-R(\hat{\tau}_c-\tau_2-T_d)\}\sin(\gamma_0-\hat{\gamma}_c)\sin(\gamma_2-\hat{\gamma}_c)+\\
&\alpha_3R(\hat{\tau}_c-\tau_0)\{R(\hat{\tau}_c-\tau_3+T_d)-R(\hat{\tau}_c-\tau_3-T_d)\}\sin(\gamma_0-\hat{\gamma}_c)\sin(\gamma_3-\hat{\gamma}_c)+\\
&\alpha_1R(\hat{\tau}_c-\tau_1)\{R(\hat{\tau}_c-\tau_0+T_d)-R(\hat{\tau}_c-\tau_0-T_d)\}\sin(\gamma_0-\hat{\gamma}_c)\sin(\gamma_1-\hat{\gamma}_c)+\\
&\alpha_2R(\hat{\tau}_c-\tau_2)\{R(\hat{\tau}_c-\tau_0+T_d)-R(\hat{\tau}_c-\tau_0-T_d)\}\sin(\gamma_0-\hat{\gamma}_c)\sin(\gamma_2-\hat{\gamma}_c)+\\
&\alpha_3R(\hat{\tau}_c-\tau_3)\{R(\hat{\tau}_c-\tau_0+T_d)-R(\hat{\tau}_c-\tau_0-T_d)\}\sin(\gamma_0-\hat{\gamma}_c)\sin(\gamma_3-\hat{\gamma}_c)+\\
&\alpha_1\alpha_2R(\hat{\tau}_c-\tau_1)\{R(\hat{\tau}_c-\tau_2+T_d)-R(\hat{\tau}_c-\tau_2-T_d)\}\sin(\gamma_1-\hat{\gamma}_c)\sin(\gamma_2-\hat{\gamma}_c)+\\
&\alpha_1\alpha_3R(\hat{\tau}_c-\tau_1)\{R(\hat{\tau}_c-\tau_3+T_d)-R(\hat{\tau}_c-\tau_3-T_d)\}\sin(\gamma_1-\hat{\gamma}_c)\sin(\gamma_3-\hat{\gamma}_c)+\\
&\alpha_1\alpha_2R(\hat{\tau}_c-\tau_2)\{R(\hat{\tau}_c-\tau_1+T_d)-R(\hat{\tau}_c-\tau_1-T_d)\}\sin(\gamma_1-\hat{\gamma}_c)\sin(\gamma_2-\hat{\gamma}_c)+\\
&\alpha_1\alpha_3R(\hat{\tau}_c-\tau_3)\{R(\hat{\tau}_c-\tau_1+T_d)-R(\hat{\tau}_c-\tau_1-T_d)\}\sin(\gamma_1-\hat{\gamma}_c)\sin(\gamma_3-\hat{\gamma}_c)+\\
&\alpha_2\alpha_3R(\hat{\tau}_c-\tau_2)\{R(\hat{\tau}_c-\tau_3+T_d)-R(\hat{\tau}_c-\tau_3-T_d)\}\sin(\gamma_2-\hat{\gamma}_c)\sin(\gamma_3-\hat{\gamma}_c)+\\
&\alpha_2\alpha_3R(\hat{\tau}_c-\tau_3)\{R(\hat{\tau}_c-\tau_2+T_d)-R(\hat{\tau}_c-\tau_2-T_d)\}\sin(\gamma_2-\hat{\gamma}_c)\sin(\gamma_3-\hat{\gamma}_c)
\end{aligned}
\tag{A.6}
$$

Equation A.6 can be rewritten as:

$$
\begin{aligned}
D_{nm} = {} & R(\hat{\tau}_c - \tau_0)\{R(\hat{\tau}_c - \tau_0 + T_d) - R(\hat{\tau}_c - \tau_0 - T_d)\} + \\
& \alpha_1^2 R(\hat{\tau}_c - \tau_1)\{R(\hat{\tau}_c - \tau_1 + T_d) - R(\hat{\tau}_c - \tau_1 - T_d)\} + \\
& \alpha_2^2 R(\hat{\tau}_c - \tau_2)\{R(\hat{\tau}_c - \tau_2 + T_d) - R(\hat{\tau}_c - \tau_2 - T_d)\} + \\
& \alpha_3^2 R(\hat{\tau}_c - \tau_3)\{R(\hat{\tau}_c - \tau_3 + T_d) - R(\hat{\tau}_c - \tau_3 - T_d)\} + \\
& \alpha_1 R(\hat{\tau}_c - \tau_0)\{R(\hat{\tau}_c - \tau_1 + T_d) - R(\hat{\tau}_c - \tau_1 - T_d)\}\cos(\gamma_0 - \gamma_1) + \\
& \alpha_2 R(\hat{\tau}_c - \tau_0)\{R(\hat{\tau}_c - \tau_2 + T_d) - R(\hat{\tau}_c - \tau_2 - T_d)\}\cos(\gamma_0 - \gamma_2) + \\
& \alpha_3 R(\hat{\tau}_c - \tau_0)\{R(\hat{\tau}_c - \tau_3 + T_d) - R(\hat{\tau}_c - \tau_3 - T_d)\}\cos(\gamma_0 - \gamma_3) + \\
& \alpha_1 R(\hat{\tau}_c - \tau_1)\{R(\hat{\tau}_c - \tau_0 + T_d) - R(\hat{\tau}_c - \tau_0 - T_d)\}\cos(\gamma_0 - \gamma_1) + \\
& \alpha_2 R(\hat{\tau}_c - \tau_2)\{R(\hat{\tau}_c - \tau_0 + T_d) - R(\hat{\tau}_c - \tau_0 - T_d)\}\cos(\gamma_0 - \gamma_2) + \\
& \alpha_3 R(\hat{\tau}_c - \tau_3)\{R(\hat{\tau}_c - \tau_0 + T_d) - R(\hat{\tau}_c - \tau_0 - T_d)\}\cos(\gamma_0 - \gamma_3) + \\
& \alpha_1\alpha_2 R(\hat{\tau}_c - \tau_1)\{R(\hat{\tau}_c - \tau_2 + T_d) - R(\hat{\tau}_c - \tau_2 - T_d)\}\cos(\gamma_1 - \gamma_2) + \\
& \alpha_1\alpha_3 R(\hat{\tau}_c - \tau_1)\{R(\hat{\tau}_c - \tau_3 + T_d) - R(\hat{\tau}_c - \tau_3 - T_d)\}\cos(\gamma_1 - \gamma_3) + \\
& \alpha_1\alpha_2 R(\hat{\tau}_c - \tau_2)\{R(\hat{\tau}_c - \tau_1 + T_d) - R(\hat{\tau}_c - \tau_1 - T_d)\}\cos(\gamma_1 - \gamma_2) + \\
& \alpha_1\alpha_3 R(\hat{\tau}_c - \tau_3)\{R(\hat{\tau}_c - \tau_1 + T_d) - R(\hat{\tau}_c - \tau_1 - T_d)\}\cos(\gamma_1 - \gamma_3) + \\
& \alpha_2\alpha_3 R(\hat{\tau}_c - \tau_2)\{R(\hat{\tau}_c - \tau_3 + T_d) - R(\hat{\tau}_c - \tau_3 - T_d)\}\cos(\gamma_2 - \gamma_3) + \\
& \alpha_2\alpha_3 R(\hat{\tau}_c - \tau_3)\{R(\hat{\tau}_c - \tau_2 + T_d) - R(\hat{\tau}_c - \tau_2 - T_d)\}\cos(\gamma_2 - \gamma_3)
\end{aligned}
\tag{A.7}
$$

Equation A.7 was used for simulating the code multipath error due to multiple reflectors in the environment.

APPENDIX B

CARRIER LOCK LOOP DISCRIMINATOR FUNCTION RESPONSE IN THE PRESENCE OF A MULTIPATH SIGNAL

A carrier lock loop discriminator function in the presence of a multipath signal is given by Equation 5.8:

$$D_r = \arctan\left(\frac{R(\hat{\tau}_c - \tau_0)\sin(\gamma_0 - \hat{\gamma}_c) + \alpha_1 R(\hat{\tau}_c - \tau_1)\sin(\gamma_1 - \hat{\gamma}_c)}{R(\hat{\tau}_c - \tau_0)\cos(\gamma_0 - \hat{\gamma}_c) + \alpha_1 R(\hat{\tau}_c - \tau_1)\cos(\gamma_1 - \hat{\gamma}_c)} \right) \quad \text{(B.1)}$$

The carrier lock loop tries to minimize the discriminator function. The left-hand side of Equation B.1 becomes zero, when the numerator of the argument of the 'arctan' function becomes zero. Therefore, at steady state,

$$R(\hat{\tau}_c - \tau_0)\sin(\gamma_0 - \hat{\gamma}_c) + \alpha_1 R(\hat{\tau}_c - \tau_1)\sin(\gamma_1 - \hat{\gamma}_c) = 0 \quad \text{(B.2)}$$

Assuming $\gamma_0 = 0$, the carrier phase multipath error is $\Delta\Psi = \hat{\gamma}_c - \gamma_0 = \hat{\gamma}_c$. Furthermore, assuming $\tau_0 = 0$, and by expanding Equation B.2 the following is obtained:

$$R(\hat{\tau}_c)\sin(-\hat{\gamma}_c) + \alpha_1 R(\hat{\tau}_c - \tau_1)\{\sin\gamma_1\cos\hat{\gamma}_c - \cos\gamma_1\sin\hat{\gamma}_c\} = 0 \quad \text{(B.3)}$$

$$\Rightarrow \sin(\hat{\gamma}_c)\{-R(\hat{\tau}_c) - \alpha_1 R(\hat{\tau}_c - \tau_1)\cos\gamma_1\} + \cos\hat{\gamma}_c\{\alpha_1 R(\hat{\tau}_c - \tau_1)\sin\gamma_1\} = 0 \quad \text{(B.4)}$$

$$\tan(\hat{\gamma}_c) = \frac{\alpha_1 R(\hat{\tau}_c - \tau_1)\sin\gamma_1}{R(\hat{\tau}_c) + \alpha_1 R(\hat{\tau}_c - \tau_1)\cos\gamma_1} \quad \text{(B.5)}$$

$$\Rightarrow \hat{\gamma}_c = \arctan\left\{ \frac{\alpha_1 R(\hat{\tau}_c - \tau_1)\sin\gamma_1}{R(\hat{\tau}_c) + \alpha_1 R(\hat{\tau}_c - \tau_1)\cos\gamma_1} \right\} = \Delta\Psi \quad \text{(B.6)}$$

This is the expression given in Equation 5.9. Following the same procedure, the carrier phase multipath due to multiple (for example 3) reflectors is given by:

$$\Delta\Psi = \arctan\left\{ \frac{\alpha_1 R(\hat{\tau}_c - \tau_1)\sin\gamma_1 + \alpha_2 R(\hat{\tau}_c - \tau_2)\sin\gamma_2 + \alpha_3 R(\hat{\tau}_c - \tau_3)\sin\gamma_3}{R(\hat{\tau}_c) + \alpha_1 R(\hat{\tau}_c - \tau_1)\cos\gamma_1 + \alpha_2 R(\hat{\tau}_c - \tau_2)\cos\gamma_2 + \alpha_3 R(\hat{\tau}_c - \tau_3)\cos\gamma_3} \right\} \quad \text{(B.7)}$$

APPENDIX C

MULTIPATH PHASES FOR THE MAXIMA AND MINIMA OF THE CARRIER PHASE MULTIPATH ERROR

The carrier phase multipath error is given by Equation 5.9:

$$\Delta\Psi = \arctan\left(\frac{\alpha_1 R(\hat{\tau}_c - \tau_1)\sin\gamma_1}{R(\hat{\tau}_c) + \alpha_1 R(\hat{\tau}_c - \tau_1)\cos\gamma_1} \right) \tag{C.1}$$

To compute the multipath phase (γ_1) at which the multipath error ($\Delta\Psi$) reaches the extreme values, (maxima and minima), the multipath error expression given by Equation C.1 is to be differentiated with respect to the multipath phase. Then the multipath phases, at which the differentiated multipath error ($\frac{\delta\Delta\Psi}{\delta\gamma_1}$) is equal to zero, correspond to the maxima or minima of the multipath error.

Differentiating Equation C.1 with respect to γ_1 and equating to zero:

$$\frac{\delta\Delta\Psi}{\delta\gamma_1} = \frac{\left\{ \begin{array}{l} \{R(\hat{\tau}_c) + \alpha_1 R(\hat{\tau}_c - \tau_1)\cos\gamma_1\}\{\alpha_1 R(\hat{\tau}_c - \tau_1)\cos\gamma_1\} \\ + \{\alpha_1 R(\hat{\tau}_c - \tau_1)\sin\gamma_1\}\{\alpha_1 R(\hat{\tau}_c - \tau_1)\sin\gamma_1\} \end{array} \right\}}{\{\alpha_1 R(\hat{\tau}_c - \tau_1)\sin\gamma_1\}^2 + \{R(\hat{\tau}_c) + \alpha_1 R(\hat{\tau}_c - \tau_1)\cos\gamma_1\}^2} = 0 \tag{C.2}$$

$$\Rightarrow \frac{\delta\Delta\Psi}{\delta\gamma_1} = \frac{\left\{ \begin{array}{l} \alpha_1 R(\hat{\tau}_c) R(\hat{\tau}_c - \tau_1)\cos\gamma_1 + \\ \alpha_1^2 R^2(\hat{\tau}_c - \tau_1)\cos^2\gamma_1 + + \alpha_1^2 R^2(\hat{\tau}_c - \tau_1)\sin^2\gamma_1 \end{array} \right\}}{\{\alpha_1 R(\hat{\tau}_c - \tau_1)\sin\gamma_1\}^2 + \{R(\hat{\tau}_c) + \alpha_1 R(\hat{\tau}_c - \tau_1)\cos\gamma_1\}^2} = 0 \tag{C.3}$$

$$\frac{\delta\Delta\Psi}{\delta\gamma_1} = \frac{\left\{ \alpha_1 R(\hat{\tau}_c) R(\hat{\tau}_c - \tau_1)\cos\gamma_1 + \alpha_1^2 R^2(\hat{\tau}_c - \tau_1) \right\}}{\{\alpha_1 R(\hat{\tau}_c - \tau_1)\sin\gamma_1\}^2 + \{R(\hat{\tau}_c) + \alpha_1 R(\hat{\tau}_c - \tau_1)\cos\gamma_1\}^2} = 0 \tag{C.4}$$

The denominator in the above expression is the sum of two squared values and is therefore always positive or zero. However, for all values of γ_1, the denominator is non-zero (except for an unrealistic set of α_1, τ_1, and γ_1 values). Therefore, the numerator must be equal to zero. This results in the following expression:

$$\left\{\alpha_1 R(\hat{\tau}_c)R(\hat{\tau}_c - \tau_1)\cos\gamma_1 + \alpha_1^2 R^2(\hat{\tau}_c - \tau_1)\right\} = 0 \tag{C.5}$$

$$\Rightarrow \left\{R(\hat{\tau}_c)\cos\gamma_1 + \alpha_1 R(\hat{\tau}_c - \tau_1)\right\} = 0 \tag{C.6}$$

$$\Rightarrow \gamma_1 = \cos^{-1}\left\{-\frac{\alpha_1 R(\hat{\tau}_c - \tau_1)}{R(\hat{\tau}_c)}\right\} \text{ or } \gamma_1 = 2\pi - \cos^{-1}\left\{-\frac{\alpha_1 R(\hat{\tau}_c - \tau_1)}{R(\hat{\tau}_c)}\right\} \tag{C.7}$$

In the first expression for multipath phase in Equation C.7, the argument of arc cosine is always negative (assuming that the reflection coefficient is positive). Then the corresponding multipath phase always lies in the second quadrant (i.e., $\frac{\pi}{2} > \gamma_1 \geq \pi$). Then, the second expression for the multipath phase in Equation C.7 corresponds to the multipath phase in the third quadrant (i.e., $\pi > \gamma_1 \geq \frac{3\pi}{2}$). Furthermore, it is evident from the expressions in Equation C.7 is that, for a weak reflection, (i.e. α_1 close to zero), the extreme values occur close to 90 and 270 degrees of the multipath phase. But, for a strong reflection, (i.e. α_1 close to one), the extreme values occur close to 180 degrees of the multipath phase.

APPENDIX D

RELATIONSHIP AMONG REFLECTION COEFFICIENT, CORRELATION RATIO AND SIGNAL TO NOISE RATIO

The average signal power measured from the in-phase and quadrature-phase arms of a GPS receiver is given by Equation 5.12:

$$P = R^2(\hat{\tau}_c)\left(1 + \alpha_1^2\alpha'^2 + 2\alpha_1\alpha'\cos\gamma_1\right) \tag{D.1}$$

The maximum and minimum values of the power depend upon the multipath phase. The power is maximum, when the multipath phase is zero (in-phase) and the minimum when the multipath phase is 180 degrees (out-of-phase). Therefore,

$$P_{max} = R^2(\hat{\tau}_c)\left(1 + \alpha_1^2\alpha'^2 + 2\alpha_1\alpha'\right) = R^2(\hat{\tau}_c)(1 + \alpha_1\alpha')^2 \text{ and} \tag{D.2}$$

$$P_{min} = R^2(\hat{\tau}_c)\left(1 + \alpha_1^2\alpha'^2 - 2\alpha_1\alpha'\right) = R^2(\hat{\tau}_c)(1 - \alpha_1\alpha')^2 \tag{D.3}$$

The carrier to noise ratio, C/N_0 is given by:

$$C/N_0 = 20\log\left(\frac{P}{N_0}\right) \tag{D.4}$$

where,

P is the signal power (W), and

N_0 is the noise power spectral density (W/Hz).

This is a popular way of representing SNR in GPS, as the signal power is limited within a bandwidth, but the noise power depends upon the bandwidth of the GPS receiver front-end.

Then,

$$\frac{P}{N_0} = 10^{\left(\frac{C/N_0}{20}\right)} \tag{D.5}$$

Therefore, the maximum and minimum values of the SNR are,

$$\frac{P_{max}}{N_0} = 10^{\left(\frac{(C/N_0)_{max}}{20}\right)} \tag{D.6}$$

and

$$\frac{P_{min}}{N_0} = 10^{\left(\frac{(C/N_0)_{min}}{20}\right)} \tag{D.7}$$

By dividing Equation D.6 by Equation D.7,

$$\frac{P_{max}}{P_{min}} = \frac{10^{\left(\frac{(C/N_0)_{max}}{20}\right)}}{10^{\left(\frac{(C/N_0)_{min}}{20}\right)}} = R \tag{D.8}$$

Combining Equations D.2, D.3 and D.8, the following expression is obtained:

$$\frac{P_{max}}{P_{min}} = \frac{R^2(\hat{\tau}_c)(1+\alpha_1\alpha')^2}{R^2(\hat{\tau}_c)(1-\alpha_1\alpha')^2} = R \tag{D.9}$$

$$\frac{(1+\alpha_1\alpha')}{(1-\alpha_1\alpha')} = \sqrt{R} \tag{D.10}$$

$$\alpha_1\alpha' = \frac{\sqrt{R}-1}{\sqrt{R}+1} \tag{D.11}$$

This is the expression used in Equation 5.14.

APPENDIX E

COMPUTATION OF MULTIPATH DELAY FROM A GEOMETRICAL PERSPECTIVE

The differential path delay of the multipath signal with respect to the direct signal can be obtained from a geometrical perspective as shown in Figure E.1. The figure is similar to Figure 5.23, except that only one antenna and a single reflector case is considered here. This is one of the two scenarios that represent all the possible scenarios of the antenna-reflector geometry.

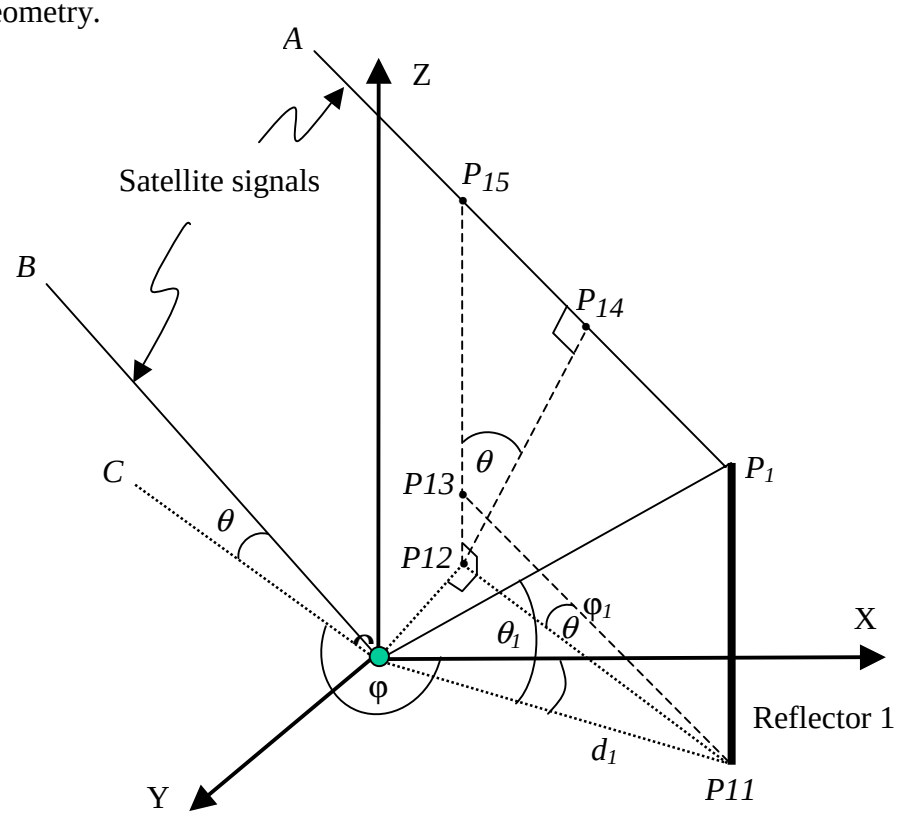

Figure E.1: Direct and reflected signals at an antenna to compute the differential path delay from a geometrical perspective

In Figure E.1, the direct and reflected signals arrive at the antenna at point O. P1 is the point of reflection and P11 is its footprint on the XY plane. The solid lines in the figure

are GPS signals. The dotted lines are on the XY plane and the dashed lines are either slant or vertical. The dotted and dashed lines are drawn for the purpose of analysis only. They are described as follows:

1. Draw a dotted line (OP12) perpendicular to the projection of the direct signal to the antenna on the XY plane (CO).
2. Draw a dotted line (P11P12), which is a projection of the direct signal to the reflector on the XY plane (AP1). This intersects the line drawn in step 1 at point P12.
3. Draw a dashed line (P11P13) from P11 with an elevation angle of the direct signal and in the same vertical plane on which the direct signal to the reflector lie.
4. Draw a dashed line (P12P15) from point P12 and perpendicular to the XY plane. This intersects the line drawn in step 3 at P13. This also intersects the direct signal to the reflector at point P15. Then P15P1 and P13P11 are parallel and of equal length.
5. Draw a dashed line (P12P14) from point P12, which intersects the direct signal to the reflector at point P14 orthogonally.

From the figure it can be observed that the plane containing the points O, P12 and P14 is a wavefront of the direct signal. Therefore, at any point on this plane, the signal will have the same phase. Then the reflected signal relative path delay (or the multipath delay) is equal to P14P1+P1O .

Now, from the paralleolgram P11P13P15P1,

$$P15P1 = P13P11$$

$$= \frac{|P12P11|}{\cos\theta} \qquad \text{(E.1)}$$

From the triangle P11OP12,

$$\angle OP12P11 = 90° \qquad \text{(E.2)}$$

$$\angle P11OP12 = \varphi_1-(\varphi+90) \qquad \text{(E.3)}$$

$$OP11 = d_1 \qquad \text{(E.4)}$$

Then,

$$P12P11 = OP11 \sin(\angle P11OP12)$$
$$= d_1 \sin(\varphi_1 - (\varphi + 90))$$
$$= d_1 \cos(\varphi - \varphi_1) \quad \text{(E.5)}$$

Therefore, from E.1 and E.5, $P15P1 = \dfrac{d_1 \cos(\varphi - \varphi_1)}{\cos\theta}$ (E.6)

Now, in the triangle P12P15P14

$$\angle P15P14P12 = 90° \quad \text{(E.7)}$$
$$\angle P14P12P15 = \theta \quad \text{(E.8)}$$
$$P12P15 = P12P13 + P13P15$$
$$= P12P13 + P11P1$$
$$= P11P12 \tan\theta + d_1 \tan\theta_1$$
$$= d_1 \cos(\varphi - \varphi_1)\tan\theta + d_1 \tan\theta_1 \quad \text{(E.9)}$$

Therefore,

$$P15P14 = P12P15 \sin\theta$$
$$= \{d_1 \cos(\varphi - \varphi_1)\tan\theta + d_1 \tan\theta_1\}\sin\theta \quad \text{(E.10)}$$

Therefore, the differential path delay

$$P14P1 + P1O = P15P1 - P15P14 + P1O$$
$$= \frac{d_1 \cos(\varphi - \varphi 1)}{\cos\theta} - \left(d_1 \cos(\varphi - \varphi 1)\tan\theta + d_1 \tan\theta_1\right)\sin\theta + \frac{d_1}{\cos\theta_1}$$
$$= \frac{d_1 \cos(\varphi - \varphi 1)}{\cos\theta} - \frac{d_1 \cos(\varphi - \varphi 1)\sin^2\theta}{\cos\theta} - d_1 \tan\theta_1 \sin\theta + \frac{d_1}{\cos\theta_1}$$
$$= d_1\left\{\frac{1}{\cos\theta_1} - \tan\theta_1 \sin\theta - \cos\theta\cos(\varphi - \varphi_1)\right\} \quad \text{(E.11)}$$

The same result is obtained for the second reflector shown in Figure 5.23.

APPENDIX F

MULTIPATH MITIGATION MODEL FOR A COHERENT DISCRIMINATOR

F.1 Multipath Mitigation Model

The coherent discriminator function is given by Equation 5.7 and reproduced here for further analysis:

$$D_{cm} = R_{EL}(\tau_e)\cos(\gamma_0 - \hat{\gamma}_c) + \alpha_1 R_{EL}(\tau_e - \tau_1)\cos(\gamma_1 - \hat{\gamma}_c) \quad \text{(F.1)}$$

Assuming γ_0 to be zero, $\hat{\gamma}_c$ is the carrier phase multipath error and $\gamma_{01} = \gamma_1 - \gamma_0 = \gamma_1$ is the multipath phase. Furthermore, as a simplification, assuming that the multipath is due to weak reflectors, the carrier phase multipath error is small and can be assumed to be zero. Then Equation F.1 reduces to the following:

$$D_{cm} = R_{EL}(\tau_e) + \alpha_1 R_{EL}(\tau_e - \tau_1)\cos\gamma_{01} \quad \text{(F.2)}$$

For a nearby dominant reflector ($0<\tau_1<T_d$), substituting the correlation symbol 'R_{EL}' by its value in Figure 4.4 (in the code tracking error range of $-T_d$ and T_d) and then equating it to zero, the following is obtained,

$$D_{cm} = \left\{-2\frac{\hat{\tau}_c}{T}\right\} + \alpha_1\left\{-2\frac{\hat{\tau}_c - \tau_1}{T}\right\}\cos\gamma_{01} = 0 \quad \text{(F.3)}$$

In Equation F.3, τ_1 is the multipath delay, which may be expressed in terms of α' such that $\tau_1 = (1-\alpha')T$. Then from Equation F.3, the code multipath error can be written as:

$$\hat{\tau}_c = \frac{\alpha_1 T(1-\alpha')\cos\gamma_{01}}{1+\alpha_1\cos\gamma_{01}} \quad \text{(F.4)}$$

Equation F.4 is a simplified closed form expression for the code multipath error in a coherent discriminator due to short delay multipath under the assumptions discussed above.

By neglecting the effect of the antenna gain pattern, and assuming that the reflected signal strength is the same at each antenna, the difference in the code multipath error at two closely-spaced antennas in the antenna array is then given by,

$$\begin{aligned}\Delta\tau_{0,i} &= \hat{\tau}_{c0} - \hat{\tau}_{ci} \\ &= \frac{T(1-\alpha')(\cos\gamma_{01} - \cos\gamma_{i1})}{1 + \alpha_1\cos\gamma_{01} + \alpha_1\cos\gamma_{i1} + \alpha_1^2\cos\gamma_{01}\cos\gamma_{i1}}\end{aligned} \tag{F.5}$$

Equation F.5 relates the single difference code multipath error at two closely-spaced antennas in terms of the reflection coefficient, correlation ratio and reflected signal relative phases. This is equivalent to the expression given in Equation 6.6 for a dot-product discriminator.

Following the procedure described in Section 6.3 and 6.4, an Extended Kalman Filter can be developed to estimate multipath and geometric parameters. The design matrix of the filter is similar to the expression given in Equation 6.23, except that the elements of the first *m-1* rows are to be replaced by the following expressions:

$$\frac{\delta\Delta\tau_{0,i}}{\delta\alpha_1} = \frac{1}{b_i^2}\left(b_i\frac{\delta a_i}{\delta\alpha_1} - a_i\frac{\delta b_i}{\delta\alpha_1}\right) \tag{F.6}$$

$$\frac{\delta\Delta\tau_{0,i}}{\delta\alpha'} = \frac{1}{b_i^2}\left(b_i\frac{\delta a_i}{\delta\alpha'} - a_i\frac{\delta b_i}{\delta\alpha'}\right) \tag{F.7}$$

$$\frac{\delta\Delta\tau_{0,i}}{\delta\gamma_{01}} = \frac{1}{b_i^2}\left(b_i\frac{\delta a_i}{\delta\gamma_{01}} - a_i\frac{\delta b_i}{\delta\gamma_{01}}\right) \tag{F.8}$$

$$\frac{\delta\Delta\tau_{0,i}}{\delta\theta_1} = \frac{1}{b_i^2}\left(b_i \frac{\delta a_i}{\delta\theta_1} - a_i \frac{\delta b_i}{\delta\theta_1} \right) \tag{F.9}$$

$$\frac{\delta\Delta\tau_{0,i}}{\delta\varphi_1} = \frac{1}{b_i^2}\left(b_i \frac{\delta a_i}{\delta\varphi_1} - a_i \frac{\delta b_i}{\delta\varphi_1} \right) \tag{F.10}$$

where,

a_i is the numerator of Equation F.5

b_i is the denominator of Equation F.5

$$\frac{\delta a_i}{\delta\alpha_1} = T(1-\alpha')(\cos\gamma_{01} - \cos\gamma_{i1}) \tag{F.11}$$

$$\frac{\delta a_i}{\delta\alpha'} = \alpha_1 T(\cos\gamma_{i1} - \cos\gamma_{01}) \tag{F.12}$$

$$\frac{\delta a_i}{\delta\gamma_{01}} = \alpha_1 T(1-\alpha')(-\sin\gamma_{01} + \sin\gamma_{i1}) \tag{F.13}$$

$$\frac{\delta a_i}{\delta\theta_1} = \alpha_1 T(1-\alpha')\sin\gamma_{i1}\frac{\delta\gamma_{i1}}{\delta\theta_1} \tag{F.14}$$

$$\frac{\delta a_i}{\delta\varphi_1} = \alpha_1 T(1-\alpha')\sin\gamma_{i1}\frac{\delta\gamma_{i1}}{\delta\varphi_1} \tag{F.15}$$

$$\frac{\delta b_i}{\delta\alpha_1} = \cos\gamma_{01} + \cos\gamma_{i1} + 2\alpha_1\cos\gamma_{01}\cos\gamma_{i1} \tag{F.16}$$

$$\frac{\delta b_i}{\delta\alpha'} = 0 \tag{F.17}$$

$$\frac{\delta b_i}{\delta\gamma_{01}} = -\alpha_1\sin\gamma_{01} - \alpha_1\sin\gamma_{i1} - \alpha_1^2\cos\gamma_{01}\sin\gamma_{i1} - \alpha_1^2\sin\gamma_{01}\cos\gamma_{i1} \tag{F.18}$$

$$\frac{\delta b_i}{\delta\theta_1} = (-\alpha_1\sin\gamma_{i1} - \alpha_1^2\cos\gamma_{01}\sin\gamma_{i1})\frac{\delta\gamma_{i1}}{\delta\theta_1} \tag{F.19}$$

$$\frac{\delta b_i}{\delta\varphi_1} = (-\alpha_1\sin\gamma_{i1} - \alpha_1^2\cos\gamma_{01}\sin\gamma_{i1})\frac{\delta\gamma_{i1}}{\delta\varphi_1} \tag{F.20}$$

F.2 Multipath Mitigation Results

Code multipath error was mitigated using the model described above for the data collected on October 20, 1998. The same procedure was followed as described in Chapter 7, except that the design matrix was replaced by the elements described above.

Figures F.1 shows the estimated multipath errors using this technique in a shaded dark line, and the measured multipath errors in a shaded light line for the low elevation satellites (SVs 1, 9, 17 and 31) during the experiment at antenna 0. It can be observed that the estimated multipath closely follows the measured multipath errors. Similar improvements were observed at other antennas as well. Statistics were generated for the improvement achievable by using this model. It was found that the multipath error was reduced up to 65% by using this technique. On average there was an approximately 20% improvement, over all the low elevation satellites and all the antennas. This shows that the code multipath error can be estimated using a coherent code discriminator model as well.

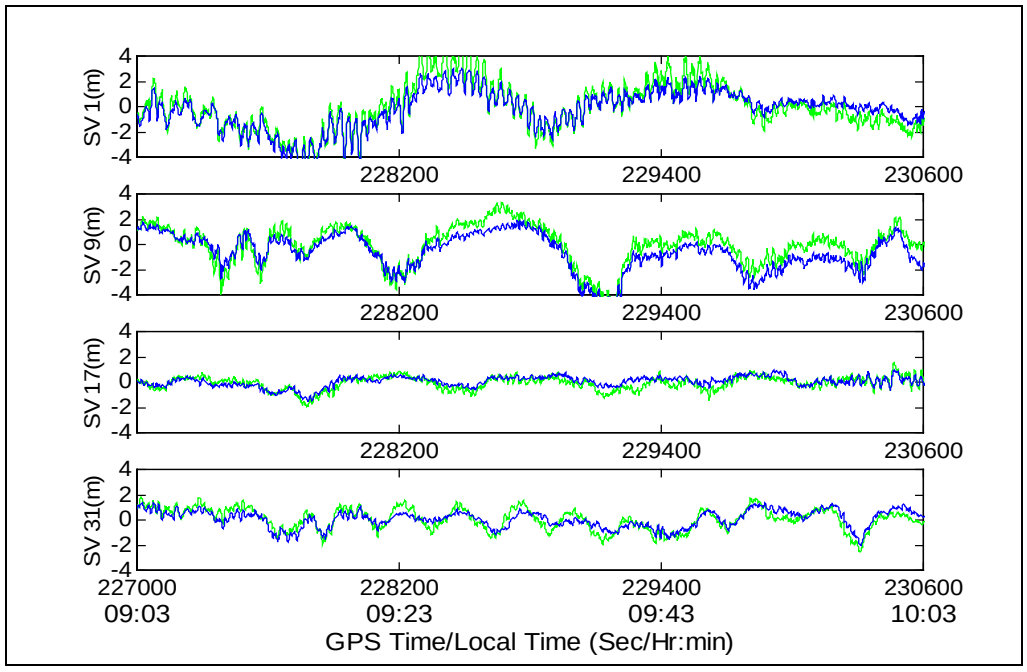

Figure F.1: Measured multipath (light shade) and estimated multipath (dark shade) for low elevation satellites at antenna 0

APPENDIX G

MULTIPATH ESTIMATION FROM THE SNR OF A SINGLE ANTENNA

The possibility of estimating carrier phase multipath errors from SNR information in a single antenna was explored. As the SNR information is readily available from a receiver, and is influenced by multipath in a way that can be expressed in terms of a closed form relationship (Equation 5.12), a simple method may be devised to estimate the multipath parameters from the SNR measurements.

Equation 5.12 is reproduced here for further analysis:

$$P = R^2(\hat{\tau}_c)\left(1 + \alpha_1^2\alpha'^2 + 2\alpha_1\alpha'\cos\gamma_1\right) \tag{G.1}$$

In a receiver, the SNR is expressed in terms of $\frac{C}{N_0}$. Therefore,

$$20\log\frac{P}{N_0} = \frac{C}{N_0} \tag{G.2}$$

$$P = N_0 10^{\frac{\left(\frac{C}{N_0}\right)}{20}} = R^2(\hat{\tau}_c)\left(1 + \alpha_1^2\alpha'^2 + 2\alpha_1\alpha'\cos\gamma_1\right) \tag{G.3}$$

$$10^{\frac{\frac{C}{N_0}}{20}} = \frac{R^2(\hat{\tau}_c)\left(1 + \alpha_1^2\alpha'^2 + 2\alpha_1\alpha'\cos\gamma_1\right)}{N_0} \tag{G.4}$$

$$10^{\frac{\frac{C}{N_0}}{20}} = K_1\left(1 + \alpha''^2 + 2\alpha''\cos\gamma_1\right) = z \tag{G.5}$$

where, K_1 equal to $\frac{R^2(\hat{\tau}_c)}{N_0}$, α'' = modified reflection coefficient = $\alpha_1\alpha'$, and z is the observable.

A Kalman filter may be devised with the state vector as follows:

$$x = [K_1,\ \alpha'',\ \gamma_1]^T \tag{G.6}$$

Then the design matrix is given by the following expression:

$$H = \left[\frac{\delta z}{\delta K_1} \quad \frac{\delta z}{\delta \alpha''} \quad \frac{\delta z}{\delta \gamma_1} \right] \tag{G.7}$$

where

$$\frac{\delta z}{\delta K_1} = 1 + \alpha''^2 + 2\alpha'' \cos\gamma_1 \tag{G.8}$$

$$\frac{\delta z}{\delta \alpha''} = 2K_1(\alpha'' + \cos\gamma_1) \tag{G.9}$$

$$\frac{\delta z}{\delta \gamma_1} = -2K_1\alpha'' \sin\gamma_1 \tag{G.10}$$

A simulation was performed, wherein multipath corrupted SNR was used as input in a Kalman filter described above. Figure G.1 shows the SNR, estimated multipath phase, as well as true and estimated carrier phase multipath errors. It is evident that the estimated multipath error does not match the true multipath error. The cause for the mismatch can be analyzed from the estimated multipath phase. It can be seen that the multipath phase oscillates approximately between zero and π radians (i.e. first and second quadrant). In reality however, the multipath phase can take values between zero and 2π (i.e. all quadrants). As, the estimated multipath phase does not take a value between π and 2π (i.e. third and fourth quadrant), the estimated multipath error does have negative values. Instead, the negative values have a mirror image with respect to the time axis. This can also be explained from Equation G.1, which relates SNR with multipath parameters. It can be observed that the SNR is related to the multipath phase by a cosine function. But a cosine function has the same value for an angle in the first or fourth quadrant (i.e. γ_1 or $-\gamma_1$). This is also true for an angle in the second or the third quadrant (i.e. $180°-\gamma_1$ or $180°+\gamma_1$). That means, from the cosine value alone, it is not possible to distinguish

whether the angle (multipath phase) lies in the first and second quadrant or fourth and third quadrant. This problem was also encountered when this multipath mitigation model was used to estimate multipath using field data. The quadrant ambiguity of the multipath phase defeats this approach of multipath error estimation.

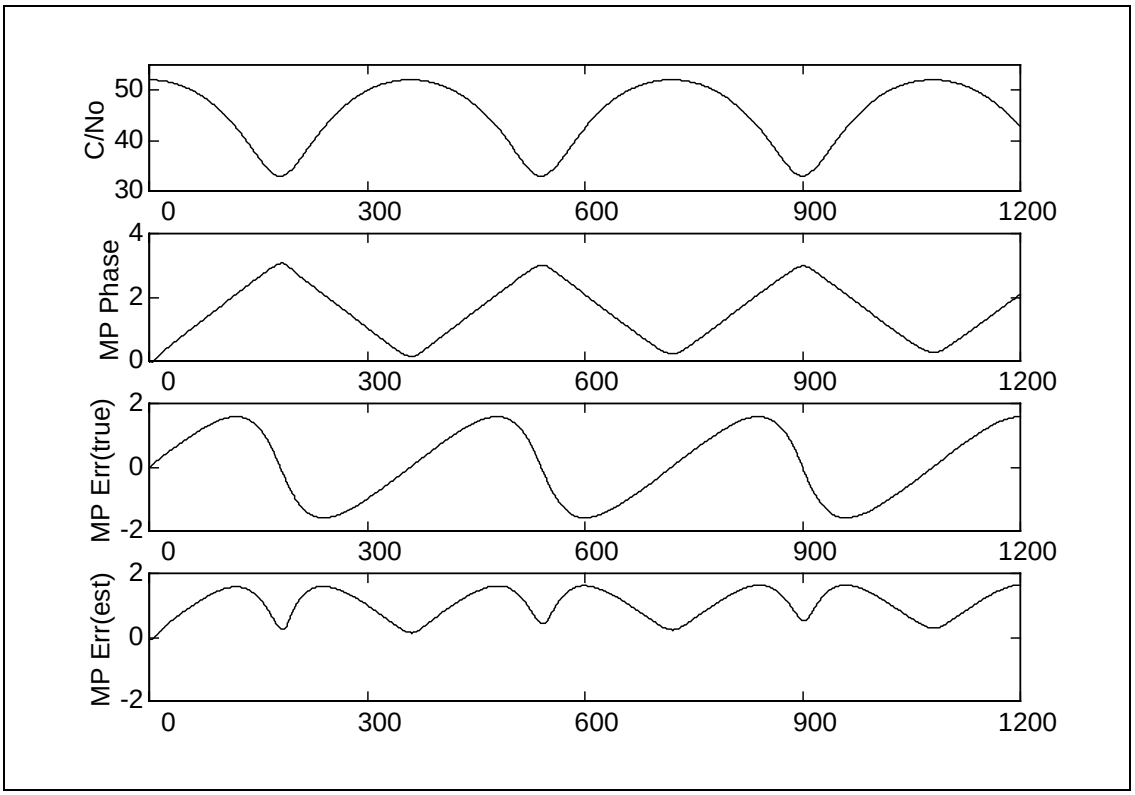

Figure G.1: Multipath estimation from SNR. The units for C/N0, Multipath Phase, Multipath Error (true) and Multipath Error (est) are dB-Hz, radian, cm and cm respectively

APPENDIX H
CODE MULTIPATH ESTIMATION FROM CODE-MINUS-CARRIER MEASUREMENTS

The code multipath error can be isolated by using the code-minus-carrier technique described in Chapter 7. One limitation of this technique is that it can not be used in real time, as the estimation of ionospheric error using a curve fit method is a batch process and requires stored data. Here, a technique is explored, wherein the code multipath error is estimated from the code-minus-carrier measurements (without ionospheric error compensation), which has potential to be used in real time. Some of the drawbacks of this technique are also described.

The code-minus-carrier observable is given by Equation 7.1 and reproduced here for further analysis:

$$P - \Phi = 2d_{ion} - \lambda N + \varepsilon_{Mp} - \varepsilon_{M\varphi} + \varepsilon_{p} - \varepsilon_{\varphi} \tag{H.1}$$

From Equation H.1, it can be seen that the code-minus-carrier contains a) ambiguity error, which is a constant bias, in absence of a cycle slip, b) ionospheric error, which is of a slow varying nature, c) code multipath error, which is of a medium to fast varying nature, and d) other small errors due to the receiver code noise and carrier phase multipath and noise.

Therefore, the code-minus-carrier observations can be used as measurements in a Kalman filter, which has the following state variables:

$$x = \begin{bmatrix} x1 \\ x2 \\ x3 \end{bmatrix} = \begin{bmatrix} \text{bias due to ambiguity} \\ \text{ionosphere error} \\ \text{multipath error} \end{bmatrix} \tag{H.2}$$

A first-order Gauss-Markov process was used as the state dynamic model for each of the state variables. However, the time constant used for each state variable was different. A very high time constant (1 hour) was used for the ambiguity state variable. Medium (30 minutes) and low time (one minute) constants were used for the ionospheric and multipath errors respectively. Figure H.1 shows the estimate of various state variables using this model for satellite 9 using the data collected on October 20, 1998.

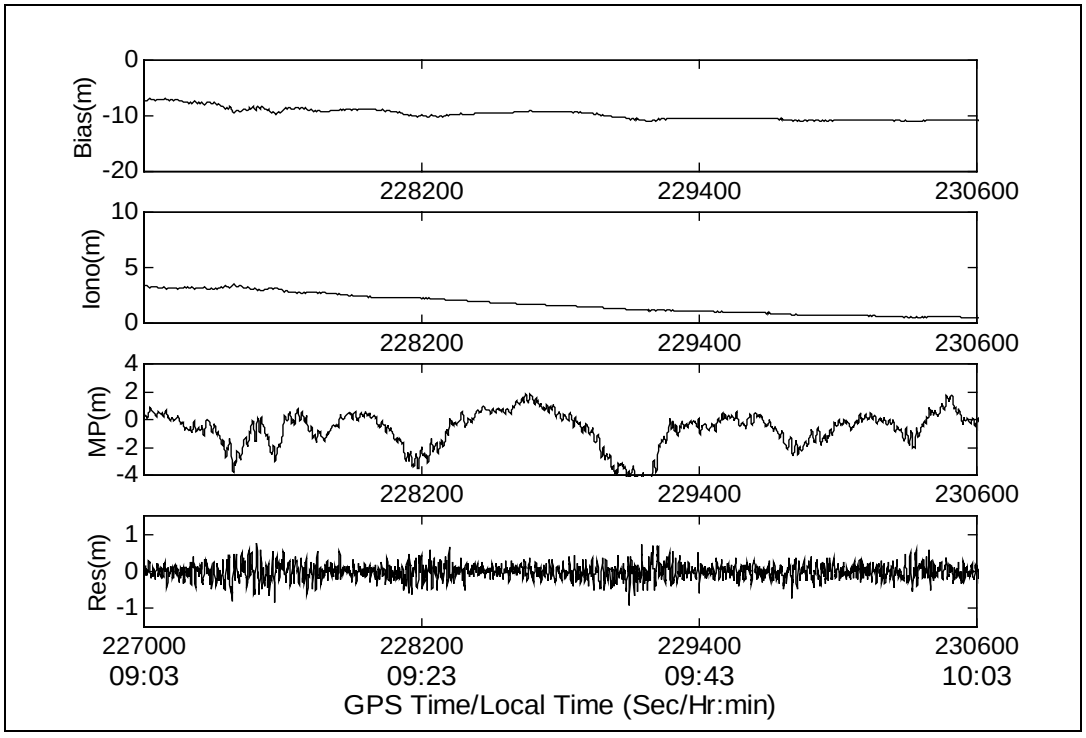

Figure H.1: Estimates of a) bias, b) ionospheric error, c) multipath error, and d) residuals using code-minus-carrier measurements in a Kalman filter

It is evident from the figure that the bias value takes some time to settle and thereafter remains nearly constant. The ionospheric error slowly decreases during the experimental period. The multipath error has a lot of oscillations and the residual is nearly white.

The estimated multipath error was compared with its true value obtained by the code-minus-carrier (and ionospheric error compensated) technique described in Chapter 7. Figure H.2 shows the true code multipath error in a light shaded line and the estimated

multipath error in a dark shaded line at antenna 0 for the low elevation satellites during the experiment. It is clear from the figure that the estimated multipath errors closely follow their true values.

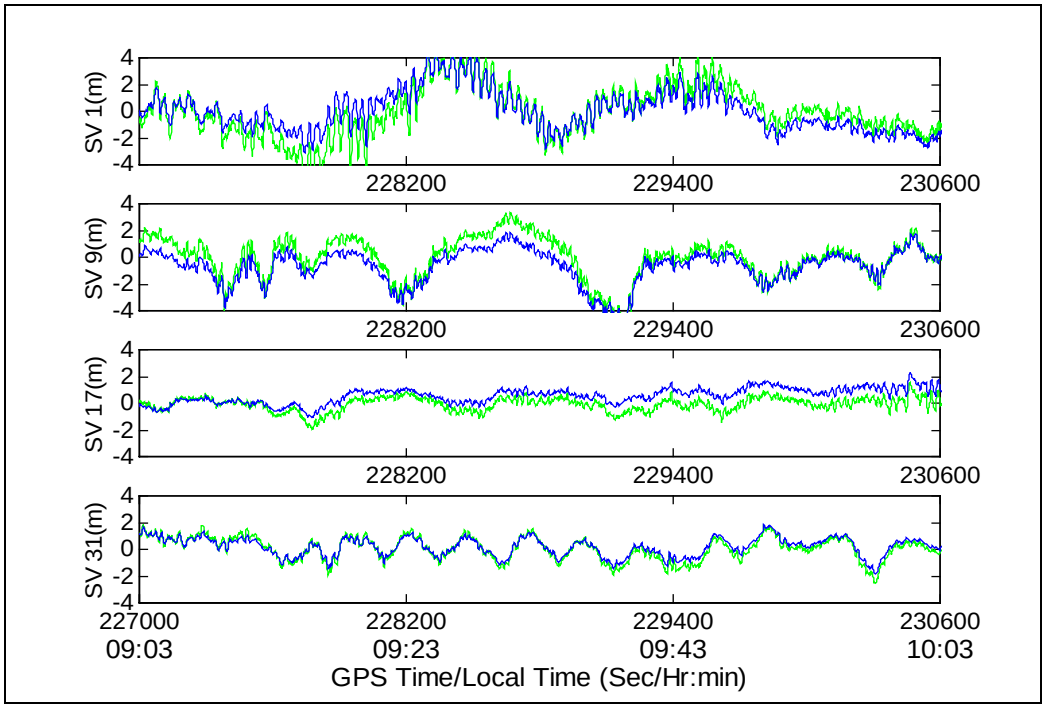

Figure H.2: Measured (light shade) and estimated multipath (dark shade) for low elevation satellites at antenna 0

Figures H.3 shows the measured and estimated multipath errors for the low elevation satellites at antenna 1. From the figure it is clear that the estimated multipath closely follows the measured multipath. This was observed at other antennas as well. Code multipath error was reduced by up to 70% using this technique.

However, this method has several drawbacks. The choice of time constants depends upon the multipath environment. This is equivalent to computing the frequency components of the measurement and rejecting the frequencies outside the desired band. This method requires a long time to settle as the bias and ionospheric errors have large time constants. Furthermore, very low frequency multipath errors may be interpreted as ionospheric

errors and removed during the estimation process. Additionally, the mean code multipath error is removed as a bias estimate during the estimation process.

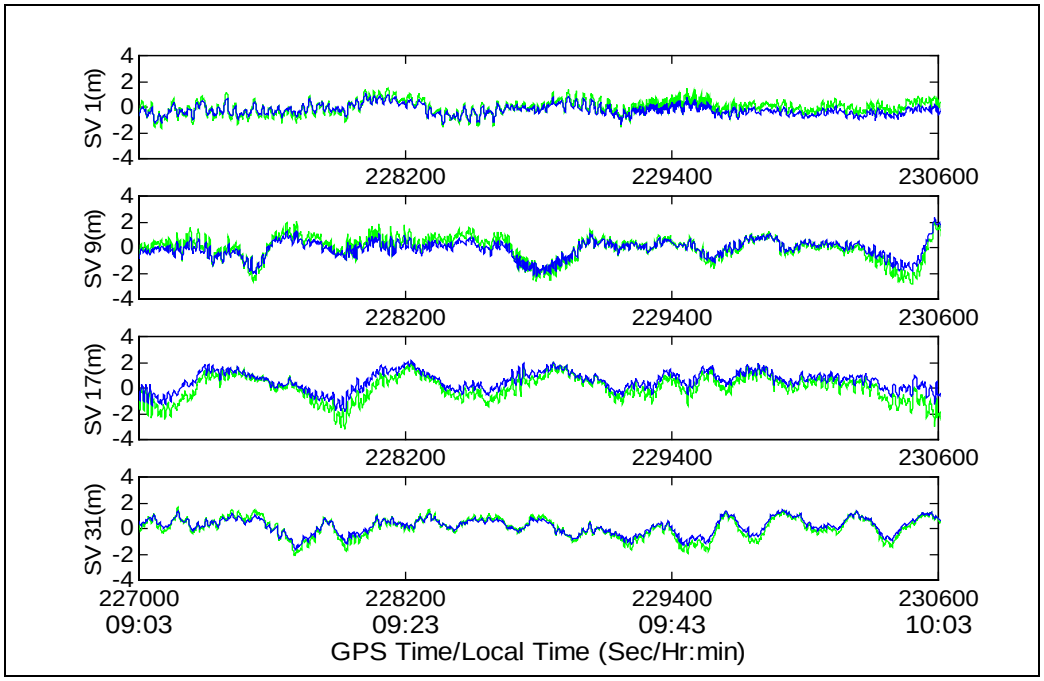

Figure H.3: Measured (light shade) and estimated multipath (dark shade) for low elevation satellites at antenna 1

REFERENCES

Accord (1993), *Requirement Specification for a GPS Receiver, Revision 1.2*, Accord Software and Systems Pvt. Ltd., June, Bangalore, India, 68 pp.

Aparicio, M., P. Brodie, L. Doyle, J. Rajan and P. Torrione (1996), GPS Satellite and Payload, *Global Positioning System: Theory and Applications, Vol. I*, ed. B.W. Parkinson and J.J. Spilker Jr., American Institute of Aeronautics and Astronautics, Inc., Washington DC, pp. 209-244.

Armor, J. (1999), Navstar Global Positioning System, *Proceedings of ION National Technical Meeting*, San Diego, January 25-27, pp. 7-10.

Axelrad, P., C.J. Comp and P.F. MacDoran (1996), SNR Based Multipath Error Correction for GPS Differential Phase, *IEEE Transaction on Aerospace & Electronic Systems*, **32**, 2, April, pp. 650-660.

Bartholomew, C. A. (1980), Satellite Signal Standards, *Global Positioning System, Papers published in Navigation, Vol. I,* Institute of Navigation, pp. 21-28.

Bartone, C. and F. van Graas (1998), Airport Pseudolites for Local Area Augmentation, *Proceedings of IEEE PLANS*, Palm Springs, April 20-23, pp. 479-486.

Becker, D., K.H. Thiel and P. Hartl (1994), A special Method of Managing Multipath Effects, *Proceedings of ION GPS-94*, Salt Lake City, September 20-23, pp. 157-163.

Beckmann, P. and A. Spizzichino (1963), *The Scattering of Electromagnetic Waves from Rough Surfaces*, Pergamon Press, Oxford, 503 pp.

BeeLine (1998), *GPSCard User Manual, Revision 1*, NovAtel Inc, Calgary, Alberta, Canada, 115 pp.

Black, H.D. and A. Eisner (1984), Correcting Satellite Doppler Data for Tropospheric Effects, *Journal of Geophysical Research*, **89**.

Braasch, M.S. (1995), Isolation of GPS Multipath and Receiver Tracking Errors, *NAVIGATION: Journal of The Institute of Navigation*, **41**, 4, pp. 415-434.

Braasch, M.S. (1996a), Multipath Effects, *Global Positioning Systems: Theory and Applications, Vol. I*, ed. B.W. Parkinson and J.J. Spilker Jr., American Institute of Aeronautics and Astronautics, Washington DC, pp. 547-568.

Braasch, M.S. (1996b), GPS Multipath Model Validation, *Proceedings of IEEE PLANS-96*, Atlanta, April 22-26, pp. 672-678.

Braasch, M.S. (1997), Autocorrelation Sidelobe Considerations in the Characterization of Multipath Errors, *IEEE Transactions on Aerospace and Electronic Systems*, **33**, 1, January, pp. 290-295.

Braasch, M.S. (1998), *Viewgraphs of the lecture presented at the University of Calgary*, Calgary, Alberta, Canada, July 8, 73 pp.

Braasch, M.S. and F. van Graas (1991), Guidance Accuracy Considerations for Real time GPS Interferometry, *Proceedings of ION GPS-91*, Albuquerque, September 9-13, pp. 373-386.

Breeuwer, E. (1991), *Modeling and Measuring GPS Multipath Effects, Master's Thesis*, Faculty of Electrical Engineering, Delft University of Technology, Delft, The Netherlands, January, 117 pp.

Brown, R.G. and P.Y.C. Hwang (1992), *Introduction to Random Signals and Applied Kalman Filtering, Second Edition*, John Wiley & Sons Inc., 502 pp.

Bruton, A.M. (1997), Kinematic Positioning Using Adaptive Filters and Multiple DGPS Receiver Configurations, *Advances in Positioning and Reference Frames: IAG International Symposium*, **118**, Rio De Janeiro, September 3-9, pp. 325-330.

Cannon, M.E. (1990), High Accuracy GPS Semikinematic Positioning: Modeling and Results, *NAVIGATION: Journal of the Institute of Navigation*, **37**, 1, pp. 53-64.

Cannon, M.E. (1993), *Semikin™ Operating Manual, Ver. 2.0*, Department of Geomatics Engineering, The University of Calgary, Calgary, Alberta, Canada, March, 12 pp.

Cannon, M.E. and G. Lachapelle (1992), Analysis of a High-Performance C/A-Code GPS Receiver in Kinematic Mode, *NAVIGATION: Journal of The Institute of Navigation*, **39**, 3, pp. 285-300.

Cannon, M.E. and G. Lachapelle (1997), *C³NAV™ Operating Manual, Ver. 1.3*, Department of Geomatics Engineering, The University of Calgary, Calgary, Canada, January, 17 pp.

CANSPACE (2000), *Latest GPS Constellation Status Website*, Canadian Space Geodesy Forum, University of New Brunswick, Fredericton, New Brunswick.

Comp, C.J. and P. Axelrad (1998), Adaptive SNR-Based Carrier Phase Multipath Mitigation Technique, *IEEE Transactions on Aerospace and Electronic Systems*, **34**, pp. 264-276.

Cohen, C.E. and B.W. Parkinson (1991), Mitigating Multipath Error in GPS based Attitude Determination, *Guidance and Control, Advances in Astronautical Sciences*, **74**, pp. 53-68.

Counselman, C.C. (1998), Array Antennas for DGPS, *Proceedings of IEEE PLANS*, Palm Springs, April 20-23, pp. 352-357.

Cox, D.T., K.W. Shallberg, A. Manz (1999), Definition and Analysis of WAAS Receiver Multipath Envelopes, *Proceedings of ION NTM-99*, San Diego, January 25-27, pp. 827-838.

Dai, D., T. Walter, C.J. Comp, Y.J. Tsai, P.Y. Ko, P. Enge and J.D. Powell (1997), High Integrity Multipath Mitigation Techniques for Ground Reference Stations, *Proceedings of ION GPS-97*, Kansas City, September 16-19, pp. 593-604.

Easton, R. L. (1980), The Navigation Technology Program, *Global Positioning System, Papers published in Navigation, Vol. I*, Institute of Navigation, pp. 15-20.

Efratom (1989), *Operation and maintenance manual for FRK (H or L) LN - Low noise rubidium frequency standard, Efratom Division*, Ball Corporation, Irvine, 79 pp.

Falkenberg, W., P. Kielland and G. Lachapelle (1988), GPS Differential Positioning Technologies for Hydrographic Surveying, *Proceedings of IEEE PLANS*, Orlando, December, 310-317.

Fenton, P., B. Falkenberg, T. Ford, K. Ng and A.J. van Dierendonck (1991), Novatel's GPS Receiver: The High Performance OEM Sensor of the Future, *Proceedings of ION GPS-91*, Albuquerque, September 9-13, pp. 49-58.

Ford, T., W. Kunysz, R. Morris, J. Neumann, J. Rooney and T. Smit (1997), Beeline RT20 - a Compact, Medium Precision Positioning System with an Attitude, *Proceedings of ION GPS-97*, Kansas City, September 16-19, pp. 687-695.

Francisco, S. G. (1996), GPS Operational Control Segment, *Global Positioning System: Theory and Applications, Vol. I*, ed. B.W. Parkinson and J.J. Spilker Jr., American Institute of Aeronautics and Astronautics, Inc., Washington, DC, pp. 435-468.

Garin, L., F. van Diggelen and J. Rousseau (1996), Strobe & Edge Correlator Multipath Mitigation for Code, *Proceedings of ION GPS-96*, Kansas City, September 17-20, pp. 657-664.

Garin, L. and J. Rousseau (1997), Enhanced Strobe Correlator Multipath Rejection for Code & Carrier, *Proceedings of ION GPS-97*, Kansas City, September 16-19, pp. 559-568.

GEC Plessy, (1996), GP2021 - *GPS 12 Channel Correlator with Microprocessor Support Functions*, GEC Plessy Semiconductors, July, 59 pp.

Gelb, A. (1979), *Applied Optimal Estimation*, MIT Press, Massachusetts Institute of Technology, Massachusetts, Cambridge, 374 pp.

Georgiadou, Y. and A. Kleusberg (1988), On Carrier Signal Multipath Effects in Relative GPS Positioning, *manuscripta geodatica*, Springer-Verlag, **13**, 3, pp. 172-179.

Hagerman, L.L. (1973), *Effects of Multipath on Coherent and Non-coherent PRN Ranging Receiver, Aerospace Report No. TOR-0073 (3020 – 03) –3*, Development Planning Division, The Aerospace Corporation, 39 pp.

Hatch, R. (1982), The Synergism of GPS Code and Carrier Measurement, *Proceedings of Third International Geodetic Symposium on Satellite Doppler Positioning*, DMA/NGS, Washington DC, pp. 1213-1232.

Haykin, S. (1989), *An Introduction to Analog and Digital Communication*, John Wiley & Sons, Inc., New York, 645 pp.

Hofmann-Wellenhof, B., H. Lichtenegger and J. Collins (1994*), Global Positioning System Theory and Practice, Third revised edition*, Springer-Verlag, New York, 355 pp.

Holmes, J.K. (1982), *Coherent Spread Spectrum Systems*, Krieger Publishing Company, Malabar, Florida, 624 pp.

Hopfield, H.S. (1963), The Effect of Tropospheric Refraction on the Doppler Shift of Satellite Data, *Journal of Geophysical Research*, **68**, 18, pp. 5157-5168.

ICD-GPS-200 (1991), *Interface Control Document*, Navstar GPS, July 3, 115 pp.

Itani, K., K. Hamada and T Hayashi (1996), Development of a Real-time Multipath Monitor and Experimental Results, *Proceedings of ION GPS-96*, Kansas City, September 16-19, pp. 729-733.

Kee, C. and B. W. Parkinson (1994), Calibration of Multipath Errors on GPS Pseudorange Measurements, *Proceedings of ION GPS-94*, Salt Lake City, September 20-23, pp. 353-362.

Klobuchar, J. A. (1987), Ionospheric Time-Delay Algorithm for Single-Frequency GPS Users, *IEEE Transactions on Aerospace and Electronic Systems*, **23**, 3, pp. 325-331.

Klobuchar, J. A. (1996), Ionospheric Effects on GPS, *Global Positioning Systems: Theory and Applications, Vol I*, ed. B.W. Parkinson and J.J. Spilker Jr., American Institute of Aeronautics and Astronautics, Washington DC, pp. 485-516.

Krakiwsky, E.J. (1990), *The Method of Least Square: A Synthesis of Advances, UCGE No. 10003*, Geomatics Engineering, The University of Calgary, Calgary, Alberta, Canada, 115 pp.

Kraus, J.D. and K.R. Carver (1973), *Electromagnetics*, *Second Edition*, McGraw-Hill Book Company, 828 pp.

Lachapelle, G. (1997), *Lecture notes of GPS Theory and applications*, The University of Calgary, Calgary, Alberta, Canada, Fall, 444 pp.

Lachapelle, G., W. Falkenberg, D. Neufeldt and P. Keilland (1989), Marine DGPS Using Code and Carrier in Multipath Environment, *Proceedings of ION GPS-89*, Colorado Springs, September 27-29, pp. 343-347.

Lachapelle, G., A. Bruton, J. Henriksen, M.E. Cannon and C. McMillan (1996), Evaluation of High Performance Multipath Reduction Technologies for Precise DGPS Shipborne Positioning, *The Hydrographic Journal*, **82**, October, pp. 11-17.

Leick, A. (1995), *GPS Satellite Surveying*, *Second Edition*, John Wiley & Sons, Inc., New York, 560 pp.

Leva, J.L., M.U. de Haag and K.V. Dyke (1996), *Performance of Standalone GPS, Understanding GPS Principles and Applications*, ed. D. Kaplan, Artech House, Boston, pp. 237-285.

Lightsey, E.G. (1996), Spacecraft Attitude Determination Using GPS Carrier Phase, *Global Positioning System: Theory and Applications, Vol. II*, ed. B.W. Parkinson and J.J. Spilker, American Institute of Aeronautics and Astronautics, Inc., Washington DC, pp. 461-482.

Mannucci, A.J., B.J. Iijima and B.D. Wilson (1997), Wide Area Ionospheric Delay Corrections under Ionospheric Storm Conditions, *Proceedings of ION National Technical Meeting*, Santa Monica, January.

Maybeck, P.S. (1994), *Stochastic Models, Estimation, and Control, Vol. I*, Navtech, Arlington, 423 pp.

Mikhail, E.M. (1976), *Observations and Least Squares*, IEP-A Dun-Donnelley Publisher, New York, 497 pp.

MiLLennium (1997), *Command Description Manual*, Novatel Inc., Calgary, Alberta, Canada, 255 pp.

Milliken, R.J. and C.J. Zoller (1980), Principle of Operation of the NAVSTAR and System Characteristics, *Global Positioning System, Papers published in Navigation, Institute of Navigation, Vol. I*, pp. 3-14.

Moelker, D. (1997), Multiple Antennas for Advanced GNSS Multipath Mitigation and Multipath Direction Finding, *Proceedings of ION GPS-97*, Kansas City, September 16-19, pp. 541-550.

Mora-Castro, E.J. (1998), Characterization of the Multipath Effects on the GPS Pseudorange and Carrier Phase Measurements, *Proceedings of ION GPS-98*, Nashville, September 15-18, pp. 1065-1074.

Navstar GPS (1995*), Global Positioning System Standard Positioning Service Signal Specification, Second Edition,* June 2, 51 pp.

Parkinson, B.W. (1980), Overview, *Global Positioning System, Papers published in Navigation, Vol. I, Institute of Navigation*, pp. 1-2.

Parkinson, B.W., T. Stansell, R. Beard and K. Gromov (1995), A History of Satellite Navigation, *NAVIGATION: Journal of The Institute of Navigation*, **42**, 1, Special Issue, pp. 109-164.

Parkinson, B.W. and P.K. Enge (1996), Differential GPS, *Global Positioning System: Theory and Applications, Vol. II*, ed. B.W. Parkinson and J.J. Spilker Jr., American Institute of Aeronautics and Astronautics, Inc., Washington DC, pp. 3-50.

Raquet, J. (1998), *Development of a Method for Kinematic GPS Carrier Phase Ambiguity Resolution Using Multiple Reference Receivers, Ph.D. Thesis, UCGE No. 20116,* Department of Geomatics Engineering, The University of Calgary, Calgary, Alberta, Canada.

Raquet, Capt. J. and G. Lachapelle (1996), Determination and Reduction of GPS Reference Station Multipath using Multiple Receivers, *Proceedings of ION GPS-96*, Kansas City, September 17-20, pp. 673-681.

Ray, J.K. (1999), Use of Multiple Antennas to Mitigate Carrier Phase Multipath in Reference Stations, *Proceedings of ION GPS-99*, Nashville, September 14-17 (in press).

Ray, J.K. and M.E. Cannon (1999), Characterization of GPS Carrier Phase Multipath, *Proceedings of ION National Technical Meeting*, San Diego, January 25-27, pp. 243-252.

Ray, J.K., M.E. Cannon and P. Fenton (1999a), Mitigation of Static Carrier Phase Multipath Effects Using Multiple Closely-Spaced Antennas, *NAVIGATION: Journal of The Institute of Navigation,* **46**, 3, Fall, pp. 193-202.

Ray, J. K., M.E. Cannon and P. Fenton (1999b), Code Range and Carrier Phase Multipath Mitigation using SNR, Range and Phase Measurements in a Multi-Antenna System, *Proceedings of ION GPS-99*, Nashville, September 14-17 (in press).

Ray, J. K., O. S. Salychev and M. E. Cannon (1999c), The Modified Wave Estimator as an Alternative to a Kalman Filter for Real time GPS/GLONASS-INS Integration, *Journal of Geodesy*, **73**, 10, Springer-Verlag, pp. 568-576.

Reichert, A. and P. Axelrad (1999), GPS Carrier Phase Multipath Reduction Using SNR Measurements to Characterize and Effective Reflector, *Proceedings of ION GPS-99*, Nashville, September 14-17 (in press).

Saastamoinen, J. (1972), Atmospheric Correction for the Troposphere and Stratosphere in Radio Ranging of Satellites, *Geophysical Monograph 15*, American Geophysical Union, Washington, DC.

Salychev, O. (1998), *Inertial Systems in Navigation and Geophysics*, Bauman MSTU Press, Moscow, 352 pp.

Sennott, J.W. and D. Pietrazewski (1987), Experimental Measurements and Characterization of Ionospheric and Multipath Errors in Differential GPS, *NAVIGATION: Journal of The Institute of Navigation*, **34**, 2, pp. 160-173.

Shenoy, M.R., S. Murali Krishna, N.S. Sudhir, R. Anjan and S. Kiran (1999), NAV2300 – Accord's High Performance Low Cost Receiver Technology with Soft-

Correlator™ and Programmatic Interface, *Proceedings of ION GPS-99*, Nashiville, September 14-17, (in press).

Sleewaegen, J. (1997), Multipath Mitigation, Benefits from using the Signal-to-Noise Ratio, *Proceedings of ION GPS-97*, Kansas City, September 16-19, pp. 531-540.

Skone, S. (1998), *Wide Area Ionosphere Grid Modelling in the Auroral region, Ph.D. Thesis, UCGE No. 20123*, Department of Geomatics Engineering, The University of Calgary, Calgary, Alberta, Canada, December, 198 pp.

Spilker, J.J. Jr. (1996), GPS Signal Structure and Theoretical Performance, *Global Positioning System: Theory and Applications, Vol. I*, ed. B.W. Parkinson and J.J. Spilker Jr., American Institute of Aeronautics and Astronautics, Inc., Washington DC, pp. 57-120.

Spilker, J.J. Jr. and B.W. Parkinson (1996), Overview of GPS Operation and Design, *Global Positioning System: Theory and Applications, Vol. I*, ed. B.W. Parkinson and J.J. Spilker Jr., American Institute of Aeronautics and Astronautics, Inc., Washington DC, pp. 29-56.

Stansell, T.A. and J.E. Maenpa, (1999), *ClearTrak™ GPS Receiver Technology*, Leica Geosystems Inc., Torrance, March, 8 pp.

Townsend, B. and P. Fenton (1994), A Practical Approach to the Reduction of Pseudorange Multipath Errors in a L1 GPS Receiver, *Proceedings of ION GPS-94*, Salt Lake City, September 20-23, pp. 143-148.

Townsend, B., P. Fenton, K. van Dierendonck and R.D.J. van Nee (1995), L1 Carrier Phase Multipath Error Reduction Using MEDLL Technology, *Proceedings of ION GPS-95*, Palm Spring, September 12-15, pp. 1539-1544.

Taub, H. and D. Schilling (1986), *Principles of Communication Systems, Second Edition*, McGraw-Hill Book Company, 759 pp.

Tranquilla, J. and J. Carr (1991), GPS Multipath Field Observations at Land and Water Sites, *NAVIGATION: Journal of the Institute of Navigation*, **37**, 4, pp. 393-414.

van Dierendonck, A.J. (1996), GPS Receivers, *Global Positioning System: Theory and Applications, Vol. I*, ed. B.W. Parkinson and J.J. Spilker Jr., American Institute of Aeronautics and Astronautics, Inc., Washington DC, pp. 329-408.

van Dierendonck, A.J., S.S. Russel, E.R. Kopitzke and M. Birnbaum (1980), The GPS Navigation Message, *Global Positioning System, Papers published in Navigation, Vol. I*, The Institute of Navigation, pp. 55-73.

van Dierendonck, A.J., P. Fenton and T. Ford (1992), Theory and Performance of Narrow Correlator Technology in GPS Receiver, *NAVIGATION: Journal of The Institute of Navigation*, **39**, 3, pp. 265-283.

van Dierendonck, A.J. and M.S. Braasch (1997), Evaluation of GNSS Receiver Correlation Processing Techniques for Multipath and Noise Mitigation, *Proceedings of National Technical Meeting*, Santa Monica, pp. 207-215.

van Graas, F. and M.S. Braasch (1996), Selective Availability, *Global Positioning System: Theory and Applications, Vol. I*, ed. B.W. Parkinson and J.J. Spilker Jr., American Institute of Aeronautics and Astronautics, Inc., Washington DC, pp. 601-622.

van Nee, R.D.J. (1992), Multipath Effects on GPS Code Phase Measurements, *NAVIGATION: Journal of the Institute of Navigation*, **39**, 2, pp. 177-190.

van Nee, R.D.J. (1995), *Multipath and Multi-Transmitter Interference in Spread-Spectrum Communication and Navigation Systems, Ph.D. Thesis*, Delft University Press, The Netherlands, 208 pp.

Ward, P. (1996), Satellite Signal Acquisition and Tracking, *Understanding GPS Principles and Application*s, ed. E.D. Kaplan, Artech House, Boston, pp. 119-208.

Weill, L.R. (1997), Conquering Multipath: The GPS Accuracy Battle, Innovation, *GPS World*, **8**, 4, April, pp. 59-66.

Wells, D.E., N. Beck, D. Delikaraoglou, A. Kkeusberg, E.J. Krakiwsky, G. Lachapelle, R.B. Langley, M. Nakiboglu, K.P. Schwarz, J.M. Tranquilla, P. Vanicek (1987), *Guide to GPS Positioning*, Canadian GPS Associates, Fredericton, N.B.

Zumberge, J.F. and W.I. Bertiger (1996), Ephemeris and Clock Navigation Message Accuracy, *Global Positioning System: Theory and Applications, Vol. I*, ed. B.W. Parkinson and J.J. Spilker Jr., American Institute of Aeronautics and Astronautics, Inc., Washington DC, pp. 585-600